Christine Junior
Daniel Jänsch
Oliver Dingel *Editors*

Energy and Thermal Management, Air Conditioning, Waste Heat Recovery

1st ETA Conference, December 1–2, 2016, Berlin, Germany

automotive engineering iau

Springer

Energy and Thermal Management, Air Conditioning, Waste Heat Recovery

Christine Junior · Daniel Jänsch
Oliver Dingel
Editors

Energy and Thermal Management, Air Conditioning, Waste Heat Recovery

1st ETA Conference,
December 1–2, 2016, Berlin, Germany

Springer

Editors
Christine Junior
Engineer Society Automobile and Traffic
IAV GmbH
Gifhorn
Germany

Oliver Dingel
Engineer Society Automobile and Traffic
IAV GmbH
Chemnitz
Germany

Daniel Jänsch
Engineer Society Automobile and Traffic
IAV GmbH
Berlin
Germany

ISBN 978-3-319-47195-2 ISBN 978-3-319-47196-9 (eBook)
DOI 10.1007/978-3-319-47196-9

Library of Congress Control Number: 2016957477

Printed on acid-free paper

This Springer imprint is published by Springer Nature
The registered company is Springer International Publishing AG
The registered company address is: Gewerbestrasse 11, 6330 Cham, Switzerland

Contents

Thermal Management, Approaches to Optimization

Hybrid-Optimized Engine Cooling Concept

Christoph Käppner(✉), Jörg Fritzsche, Nuria Garrido Gonzalez, and Holger Lange

Volkswagen AG, Wolfsburg, Germany
christoph.kaeppner@volkswagen.de

Abstract. An increasing level of hybridization in modern passenger car powertrains creates new challenges concerning the internal combustion engine. Primarily affected are turbo-/supercharging system, start performance, oil deterioration and exhaust aftertreatment. But thermal management faces new demands and requirements as well. A significantly more frequent intermitting operation mode of the ICU, which even includes frequent instantaneous switching from high load operation to a shut-off engine and vice versa, requires the cooling concept to be capable of suppling full cooling performance independently from engine rpm. Apart from the ICU itself, several peripheral components as e.g. cabin heater and EGR cooler demand an engine-rpm-independent supply of heating or cooling power. Additionally, a rapid warm-up phase after cold start further gains in importance as ICU operation time decreases and number of cold starts increases. A critical target conflict arises between the above mentioned, additional technical requirements on the one hand and an increased cost pressure on the other hand. The later one occurs due to a growing overall complexity of any hybridized powertrain and a therefore increased cost optimization pressure on the ICU and its periphery. This target conflict was solved by developing a cooling system concept combining maximum thermal management functionality, including an electric main water pump, with a highly reduced system complexity, including e.g. the complete abandonment of any active valves.

Keywords: Cooling · Hybrid · ICU · Electrification

1 Motivation and Background

As can be seen in Figs. 1 and 2, the usage of a conventional mechanical coolant pump in an ICU designed for application in hybridized powertrains does result, among other, in two exemplary technical issues. Clutch power and thus thermal waste heat of modern downsized turbo charged engines is significantly less engine-speed-dependent than in former naturaly aspirated engine architectures. As the coolant volume and thus the supplied cooling performance of a fixed-coupled mechanical coolant pump is roughly proportional to the engine speed, this does lead into a design conflict when

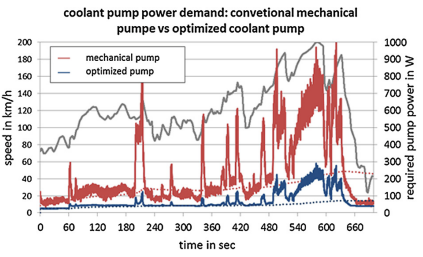

Fig. 1. Coolant pump power demand

C. Junior et al. (eds.), *Energy and Thermal Management, Air Conditioning, Waste Heat Recovery*, DOI 10.1007/978-3-319-47196-9_1

setting the drive ratio. Obtaining sufficient coolant volume flow in the low end torque point requires high pump drive ratios which come along with unnecessarily high pump speed and coolant volume flow at higher engine speeds. Especially in dynamic customer drive cycles, this results in avoidable mechanical losses and decreased engine efficiency.

While this applies to any downsized turbo charged ICU independent from its hybridization level, a second aspect does primarily concern ICUs with strongly intermitting work mode. A damping effect resulting from internal thermal masses creates a phase shift between mechanic clutch power (driver's power demand) and thermal waste heat. This phase shift corresponds with an identical phase shift between mechanical output power and cooling demand. In dynamic drive cycles with rapid transition between high engine load acceleration periods and succeeding deceleration periods, the effect described above generates an engine cooling demand during periods without mechanical power demand. When using an ICU-driven mechanical coolant pump, a running ICU is thus required for driving the pump when otherwise a cycle section could have been run with switched off ICU.

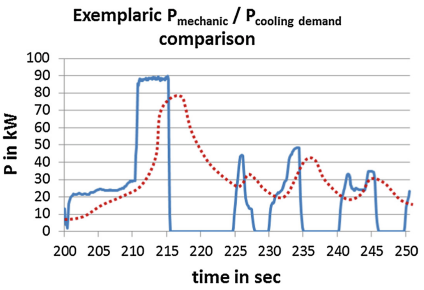

Fig. 2. Phase shift between clutch power and cooling demand (symbolic)

2 Concept and Technical Details

A large collective of system requirements and project goals, of whom some were mentioned above, have been bundled into three central design guidelines:

I Decoupling of cooling performance and engine speed
II High thermal management functionality (split cooling, micro cooling, variable oil cooling, variable engine temperature)
III Decreased system complexity and reduced costs

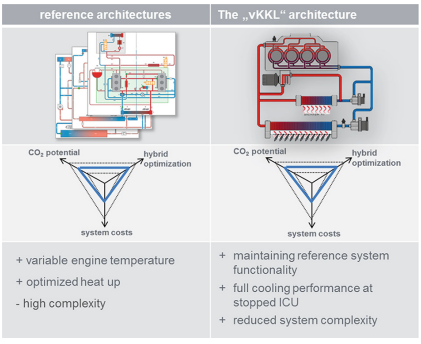

Fig. 3. Architecture comparison

A benchmarking of different technical approaches to fulfil demand number one did provide an electric main coolant pump as best compromise solution. As this technical solution comes along with a significant cost increase in comparison with mechanical pump concepts, a maximum complexity downgrade (demand III) in all attended system parts became immanent. Parallel to that technical simplification, full thermal management functionality, including split cooling and variable engine temperature had to be maintained. To achieve these opposing

goals, the concept of a valve-free two pump cooling system, in the following referred to as the "vKKL", was developed. It was managed, to substitute the significant number of electric valves, auxiliary pumps and further active actuators used in the reference cooling systems by a single additional electric coolant pump of medium power level. Figure 3 shows a simplified comparison between the reference cooling system architectures and the "vKKL" architecture.

In summary, the required number of actuators to provide a total of seven independent thermal management functions were reduced from up to seven independent actuators down two only two (see Fig. 4). Obtaining this level of function integration did demand a complete usage of each component's effective degrees of freedom, including those created by interaction of the two actuators. The technical approach shall be described by the example of two chosen functions.

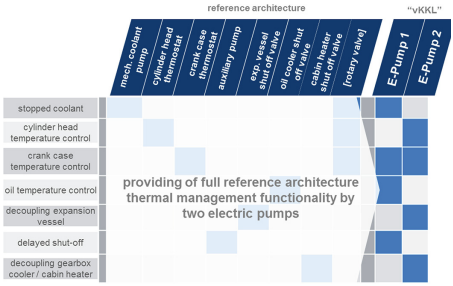

Fig. 4. Function integration

(1) split cooling (independent temperature control for cylinder head and crank case)
(2) cabin heater/gear box cooler shut-off

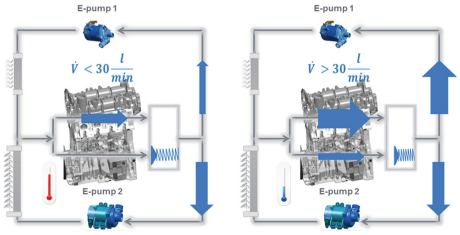

Fig. 5. Crank case temperature control by passive valve

ature. Corresponding to that architecture, pump 1 has significant power reserves in low and medium load engine operation which form a usable further degree of freedom. The system now uses a very simple, passive, pressure difference controlled valve at the crank case outlet to control the crank case outlet temperature independent from the cylinder head outlet temperature (Fig. 6). That passive valve is positioned and designed to be controlled by the coolant pressure drop over the cylinder head. Pump 1 compensates fluctuations in pump 2's

To minimize heat losses and friction, an increased crank case outlet temperature is prefered during low load ICU working points. During regular operation mode with fully heated up powertrain, pump 1 (see Fig. 5) does supply a clutch power proportional base volume flow inside the inner coolant circle. Pump 2 supplies a cooling demand proportional volume flow through the main frontend cooler and thus controls the cylinder head temper-

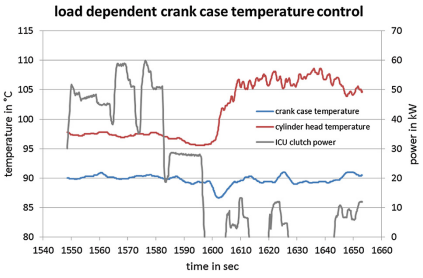

Fig. 6. Measurement data for variable crank case temperature control

volume flow which result from variating cooling demand of the cylinder head by reducing/increasing its own volume flow contrarily and thus stabilizes and controls the overall volume flow through the cylinder head. As the total pressure drop over cylinder head is proportional to the square of the volume flow through the cylinder head, a strategy has been developed to control that pressure drop via pump 1 and therefore control opening and closing of the crank case outlet valve.

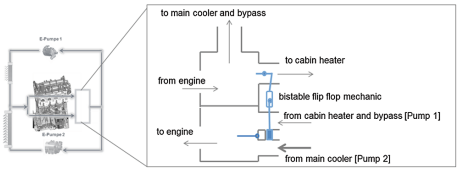

Fig. 7. Cabin heater/oil cooler shut off

The demand to supply an on/off function for the cabin heater, here used as a second function integration example, was added during a project phase when all continuous degrees of freedom of the two actuators had been designated to several functions already and were no longer available. Thus a new approach had to be used. A pulse-like, in its endurance very limited, variation of the volume flow generated by one or both pumps was still available without influence to other system functions like e.g. the crank case temperature control described above. To control a continuous state like the usage (flow) or non-usage (no flow) of the cabin heat exchanger by such a pulse-like variation of the coolant volume flow only, an additional passive component with memory capability was necessary. A robust and cost efficient solution was found in the concept of a passive pressure controlled 2-way flip-flop (bistable) valve. As described in Fig. 7, the valve is capable of opening and closing the cabin heater connection and is switched between these two stable positions by short pressure pulses generated between pump 1 and 2.

3 Design, Application and Test Results

A total of seven cars were equipped with the system of which two were gasoline powered, two were gasoline powered and hybridized, two were diesel powered and one was diesel powered and hybridized. Additionally, the system underwent intense engine

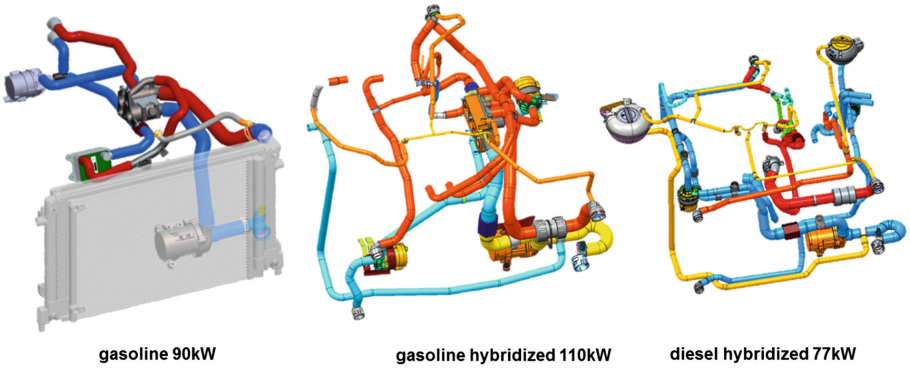

Fig. 8. Overview system concepts for gasoline/diesel

test bench operation. The ICU power range of all cars lay between 77 kW and 110 kW. Owing to this variety, three main system designs were developed differing in number of integrated cooling system components (e.g. w or w/o EGR cooler) and total cooling performance. Therefore, a choice of possible pumps was benchmarked against each other. The following pump types represent the systems with highest relevance in regard of test fleet usage: For usage as pump 1 (base volume flow), KSPG CWA 50 and CWA100, Continental EWP 110W and Bosch PCE-XL (among others) were tested. As pump 2 (main cooler), KSPG CWA200, KSPG CWA200.1 and KSPG CWA400 were used. Figure 8 shows a comparison of system designs for the application gasoline, hybridized gasoline and hybridized diesel.

All systems underwent a test program focused on the following key aspects:

(1) Mass production compatible filling procedure and minimum residual air
(2) Fulfillment of all cooling performance requirements including (among others) v_{max} at > 45 °C, Towne Pass, Großglockner and stop&go, of which some were checked via conditioned dynameter tests.
(3) CO_2 benefit via hydraulic efficiency gains
(4) CO_2 benefit via thermal efficiency gains
(5) Temperature control quality in regard of thermal shock minimization
(6) General robustness and reliability

As described earlier, the used tool chain consists of simulation (primary 1-D), engine test bench tests, car dynameter test bench tests and car road-tests. In the following figures, representative test results are summarized to give a general overview.

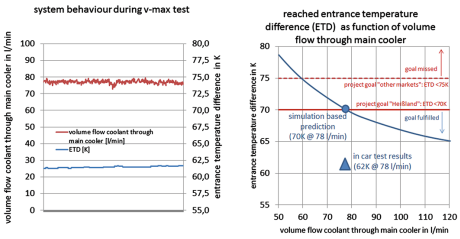

Fig. 9. Test results v_{max} tests for 90 kW gasoline

Figure 9 represents the system behavior during a maximum load, maximum velocity test scenario. Investigated key figure is the entrance temperature difference (ETD) which describes the delta temperature between coolant temperature at main cooler inlet (equaling engine temperature) and air temperature at main cooler inlet. In case of multi-layer cooler packs, e.g. including LT-cooler and AC-condenser, ambient air temperature is used instead of air temperature at main cooler inlet. Simplified, the ETD describes how close the engine temperature can be kept to ambient temperature. Design goal was an ETD below 70 K. For a maximum ambient temperature of 45 °C, this corresponds with a maximum engine temperature during the v_{max} test of 115 °C. The system outperformed the design goal and proved a maximum ETD of only 62 K, which, again for an ambient temperature of 45 °C, corresponds with a maximum engine temperature of 107 °C.

Figure 10 summarizes the efficiency gains resulting from hydraulic and thermal loss reduction. As all reference systems used mechanical pumps with fixed crank shaft to pump transmission ratio, engine working points exist for which the supplied coolant volume flow exceeds the required optimum volume flow, resulting in unnecessarily high hydraulic power demand. An additional benefit of the vKKL concept is that lower

working point's base volume flow demand is primarily supplied by the smaller pump 1 which thus is able to provide these smaller volume flow demands with significantly higher hydraulic efficiency than larger mechanical pumps and larger single-electric pumps are able to. Apart from (1) its cost efficiency due to high function integration and (2) its improved fail save reliability, this does represent a third significant advantage in comparison to earlier competitor solutions combining a single electric pump with a conventional cooling cycle concept including active valves.

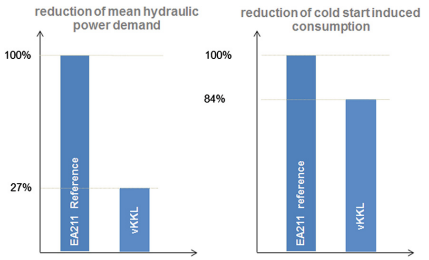

Fig. 10. Loss reduction in NEDC @20 °C

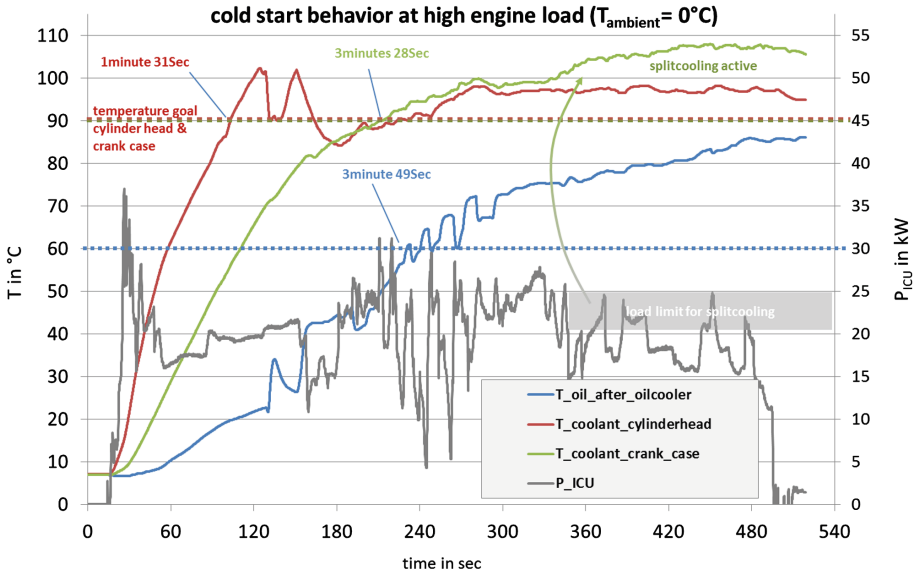

Fig. 11. Warm up performance at hybrid typical high load start scenario

Finally, Fig. 11 gives an example of the system warm up performance during high load start scenarios. As described in Sect. 1, an optimization of this ICU operation scenario was a key focus of project, as it is of increasing relevance for any ICU which is part of hybridized and especially plug-in hybridized powertrains. Defining a completed warm-up phase by reaching a cylinder head temperature of 90 °C, the warm up phase was reduced to less than two minutes (1 min and 31 s). Using the more ambitious definition of reaching a crank case temperature of 90 °C and an oil temperature above 60 °C, a reduction of the warm up phase down to still less than four minutes was achieved. Last but not least, Fig. 11 also gives a good impression of how an increase of crank case temperature via activated split cooling was achieved, when at second 330, the mean ICU clutch power drops below 25 kW.

Analytical Description of Thermal Control Circuits in Vehicles

Alexander Herzog(✉), Carolina Pelka, and Frank Skorupa

IAV GmbH, Rockwellstraße 16, 38518 Gifhorn, Germany
dr.alexander.herzog@iav.de

Abstract. Strict emission standards together with the desire for high efficiency and low fuel consumption necessitate an accurate manipulation of the state variables in the air system of modern combustion engine vehicles. As far as thermal management is concerned, we observe a trend towards on-demand temperature control. The possibilities for such an approach are limited for direct heat exchanging devices, as the efficiency of the thermal transfer is essentially dictated by the vehicle speed. For this reason, indirect heat exchangers are increasingly employed. Such systems allow to implement smart control strategies via appropriate actuators like pumps or valves. This permits to adjust the local temperatures in a wide range, as the efficiency of the heat exchanging device is largely independent of the current driving situation.

On the other hand, robust control strategies usually require the knowledge of the relevant state variables of the system under consideration. Here the desire to minimize the number of sensors follows from economic reasons. However, due to the limited computing power of common automotive CPUs, the possibility to apply numerical methods are also very restricted. From this viewpoint an analytical method to describe the thermal control circuit is desirable. In this paper we outline such an approach. The composition of the cooling fluid may influence the performance of the temperature control system. As the coolant mixture varies for different vehicles and climatic zones, this dependency should be taken into account. Thus, assuming a binary mixture of water and ethylene glycol, we formulate our model for arbitrary volume concentrations.

Our model is based on the method of the so-called dimensionless temperature change, which may be utilized both for single heat-exchangers as well as for entire thermal control circuits. In the latter case, as it turns out, the dimensionless temperature change of the overall system can analytically be traced back to the ones of the individual heat exchangers, which constitute the thermal control circuit. The physical properties of the cooling medium are discussed in detail, where the heat transfer between the working fluid and the cooling medium is described within the frameworks of fluid dynamics. Furthermore, we determine the number of temperature sensors needed for the presented method.

We exemplify the model's validity by means of a thermal control circuit of the indirect charge air cooling device of two different Diesel engine vehicles. Finally, possible generalizations and applications of the model are discussed.

Keywords: Thermal control circuits · Heat exchange · Fluid dynamics

C. Junior et al. (eds.), *Energy and Thermal Management, Air Conditioning, Waste Heat Recovery*,
DOI 10.1007/978-3-319-47196-9_2

1 Introduction

Recent years have witnessed considerable progress of thermal management systems. Being considered as one of the cornerstones on the route to improved efficiencies and reduced pollutant and greenhouse gas emissions, the developments inter alia span from constructive optimizations of heat exchanging devices and actuators [1, 2] over waste heat recovery [3, 4] to on-demand temperature control strategies [5–8]. The latter topic is essentially facilitated by an increased automation level of the utilized actuators like pumps and valves and bears the prospect not only to realize improvements as far as fuel consumption and tailpipe emissions are concerned, but also in the light of driving comfort and dynamic response. A prominent example for novel concepts in this respect is given e.g. by low temperature charge air cooling, where the working fluid is cooled below ambient temperature [7, 8].

However, alongside the advantages induced by an increased automation level within thermal management systems, they also involve higher complexity, such that the utilized control strategy has to be chosen diligently to provide both performance and stability. Among the various possible approaches, model-based control strategies usually meet these demands, and, in addition offer benefits concerning calibration efforts with the opportunity to minimize the number of cost-intensive sensors. Consequently numerous studies and attempts have been put forward in this direction. For instance in Refs. [9, 10] the coolant flow control for an electric water pump in combination with an intelligent thermostat valve has been investigated. This has been followed by detailed studies on nonlinear control approaches based on the physical model of the thermal management system [11, 12].

Given the aforementioned benefits of model-based control strategies, a severe obstacle for the capability of series production of such algorithms is posed by the limited computing power of common automotive CPUs. This usually requires an analytical description of the systems at hand. In the general case this constitutes a formidable task. As an exception we mention the realization of a model predictive real time controller for an engine cooling system of a truck [13]. Another example for an analytical formulation of a cooling system suited for automotive CPU applications is given by a steady-state model for a simple thermal control circuit, as discussed in Ref. [14]. This model has been formulated for an equimolar mixture of ethylene glycol and water. The validity of the approach has been demonstrated for the indirect charge air cooling device of a Diesel engine vehicle. However, taking the concept of a model-based control strategy seriously and bearing in mind that different vehicle types may contain differing volume concentrations c of ethylene glycol,[1] a model describing the thermal control device should take this dependency explicitly into account. Based on this motivation the present article is concerned with the generalization of the model given in Ref. [14] to arbitrary $c \in [0, 1]$. We give a detailed account of the relevant state variables of the fluids involved in the thermal exchange processes to formulate a closed steady-state model for both the individual heat exchangers as well as the overall temperature control circuit. Our approach is based on the method of the dimensionless temperature change (DTC),

[1] The same applies for vehicles in different climatic zones.

which may be utilized for an individual heat exchanger (HE) on the one hand. As it turns out however, an analogous formulation of the overall temperature control circuit under consideration is also possible. We find, that the DTC of the overall system can analytically be traced back to the DTCs of the individual HEs. From this finding we determine the minimum number of temperature signals which have to be provided externally[2] in order to run the presented method. Furthermore, we discuss the physical properties of the cooling medium in detail. Finally, the results drawn from our theoretical approach are discussed in comparison to experimental data obtained from the indirect charge air cooling circuit of two different Diesel engine vehicles.

The paper is organized as follows: In Sect. 2, we discuss the system under consideration and give a brief summary on the method used in Ref. [14] in terms of the present notation. From this, we will see that the closed analytical formulation of the system is induced by the theoretical description of the HEs constituting the thermal control circuit. The approach is based on the representation of the DTCs of the individual HEs by means of the heat capacity flows of the fluids. This task, involving approaches from similitude theory, will be undertaken in Sect. 3. For an automotive application of the model, we have to trace back the heat capacity flows to quantities available to the CPU of the vehicle. This shall be discussed in Sect. 4. Besides well-established formulations for the intake system and the air flow at the front-end of the vehicle, we give a theoretical account on the cooling section. Here the dependency of the cooling fluid properties on the concentration comes into play. The discussion of the experimental setup and details about the calibration of the model are given in Sect. 5. Section 6 gives a comparison of measurements and results obtained from the model. We summarize our findings and give an outline for future research and development perspectives in Sect. 7. The appendix contains details of the cooling fluid properties utilized in Sect. 4 to obtain the coolant heat capacity flow.

2 Formal Description of the Considered Thermal Control System Within the Method of Dimensionless Temperature Change

Apart from the aforementioned steady-state description, throughout the paper the following assumptions concerning the considered system are made:

1. Thermal losses and conversion of internal fluid energies into work as well as phase transitions of the fluids are neglected.
2. The fluids solely occur as single phase.
3. Hoses and pipes are treated as ideal heat insulators, such that lost or gained heat at these elements are not taken into account.

We note, that these assumptions are identical to those made in Ref. [14].

The system under consideration is displayed in Fig. 1, where we have depicted two coupled HEs which are indicated due to the indices 1 and 2. In HE1 two media

[2] E.g. by sensor information or independent models.

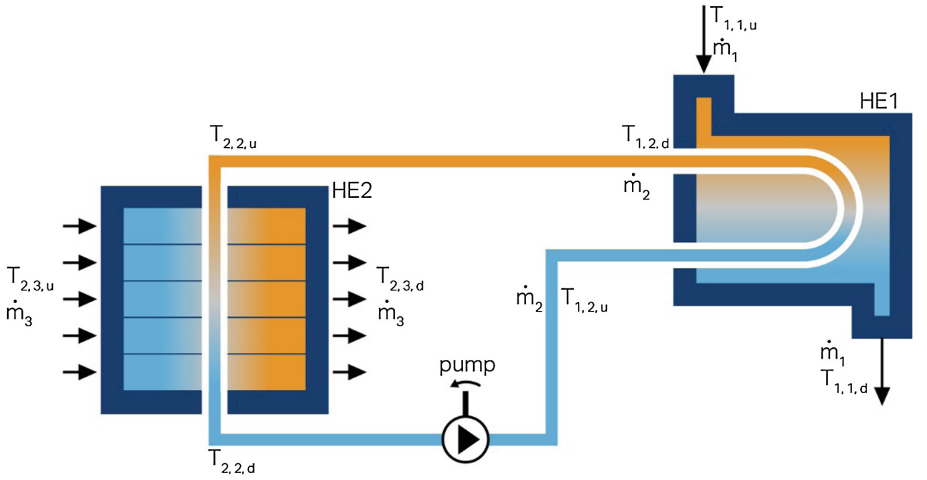

Fig. 1. System under consideration: the pump circulates the cooling medium represented by the mass flow $\dot{m}_2$. Thus, enthalpy is extracted from the working fluid mass flow $\dot{m}_1$ in the heat exchanger HE1. The transferred heat decreases the working fluid temperature from $T_{1,1,u}$ to $T_{1,1,d}$ while it heats up the cooling medium from $T_{1,2,u}$ to $T_{1,2,d}$. The dissipated heat is transferred to the ambience in the heat exchanger HE2 where the air flow $\dot{m}_3$ is warmed up from $T_{2,3,u}$ to $T_{2,3,d}$ at the expense of the coolant enthalpy, thus decreasing the cooling medium temperature from $T_{2,2,u}$ to $T_{2,2,d}$.

described by their respective mass flows $\dot{m}_1$ and $\dot{m}_2$ are in thermal contact, where the latter is circulated through the circuit by an electrical pump upstream to HE1. The thermal contact between the fluids given via $\dot{m}_2$ and $\dot{m}_3$ is facilitated in HE2. For the automotive application we have in mind, HE1 represents a specific heat exchanging device at or around the engine compartment (e.g. a charge air or an exhaust gas cooler) and HE2 serves as the cooler at the front-end of the vehicle transferring the dissipated heat to the ambience. Albeit the chosen display of the individual HEs hints at the actual geometries of the respective devices under consideration, the discussion put forward in this section is valid in general and does not depend on the specific construction of the elements. The temperatures at the respective in- and outlets of the HEs are written as $T_{j,l,q}$, where the index $j \in \{1; 2\}$ represents the HE and $l \in \{1; 2; 3\}$ gives the fluid where 1 is attributed to the working fluid, 2 to the coolant, and 3 to the air mass flow induced by the fan and the head wind. Finally, $q \in \{u; d\}$ determines the position respective to the HE j, where u denotes upstream and d downstream to the device in question.

Mind that assumption 3 implies that

$$T_{1,2,{}^{u}_{d}} = T_{2,2,{}^{d}_{u}}, \tag{1}$$

such that out of the initially eight temperatures, six remain to be determined. In order to simplify the notation, we perform a commensurate shift in the subscripts according to $\{j; l\} = \{1,1; 1,2; 2,3\} \rightarrow \{m\}\ \{1; 2; 3\}$. Then we may rewrite the temperatures as $T_{m,}$

$_q$, where m now refers to the respective fluid the same way as l, the difference being however, that we have fixed the indexing such that for $m = 2$, the second subscript in the transformed notation refers to the notation of HE1. Thus, in summary, together with Eq. (1), we have $T_{1,q} = T_{1,1,q}$, $T_{2,q} = T_{1,2,q}$, and $T_{3,q} = T_{2,3,q}$. Throughout the paper we assume $T_{1,u} \geq T_{2,u} \geq T_{3,u}$.

In order to model the system represented by Fig. 1, we intend to proceed via the so-called method of DTC [14, 15]. This quantity, referred to as P_i with $i \in \{1; 2\}$, for the HEs shown in Fig. 1, serves as a measure for the efficiency of a heat exchanger. Although the DTC of a HE can be represented both for heating the cooler fluid as well as for cooling the warmer fluid, here we confine ourselves to a formulation where it is given in terms of the latter context. Thus we define it as the ratio of the temperature difference $\Delta T_i = (-1)^{i+1}(T_{i,u} - T_{i,d})$ achieved through the heat exchanging process and the maximum temperature difference being available between the two fluids in thermal contact. For instance, for HE1 this amounts to the temperature difference between the working fluid and the cooling medium upstream to the HE. Within our present notation, we then end up at

$$P_i = (-1)^{i+1} \frac{T_{i,u} - T_{i,d}}{\lambda_i T_{i,u} + (1 - \lambda_i) T_{i,d} - T_{i+1,u}}, \tag{2}$$

where we have defined $\lambda_i = (1 - (-1)^i)/2 \in \{0; 1\}$.

The idea of our approach is to express P_i by means of the heat capacity flows Γ_i and Γ_{i+1} with

$$\Gamma_m = c_{p,m} \dot{m}_m, m \in \{i; i+1\}, \tag{3}$$

i.e.

$$P_i = P_i[\Gamma_i, \Gamma_{i+1}]. \tag{4}$$

Here the specific heat capacity $c_{p,m} = c_{p,m}(T_m)$ is given as a function of the average temperature $T_m := (T_{m,u} + T_{m,d})/2$ at the HE. If furthermore the specific heat capacities $c_{p,m}$ and the mass flows $\dot{m}_m$ can be modelled by analytical means, then, substituting Eq. (4) into Eq. (2), the resulting expression can explicitly be solved for any of the temperatures appearing in Eq. (2), given that the other two temperatures are known.[3] Finally, $T_{i+1,d}$, not appearing in Eq. (2), is determined from the enthalpy balance of the HE, thus reading

$$T_{i+1,d} = T_{i+1,u} - (-1)^i \frac{\Gamma_i}{\Gamma_{i+1}} (T_{i,u} - T_{i,d}). \tag{5}$$

Hence, the knowledge of the DTC by means of the heat capacity flows together with two temperature signals up- or downstream to the HE enables us to calculate the respective other two temperatures at the device [15].

[3] E.g. due to values measured by a sensor or given by an independent model.

Generalizing this approach, the overall thermal control circuit depicted in Fig. 1 may effectively be viewed as an overall HE. For this reason we may also define a DTC P_{TCC} corresponding to the entire system as

$$P_{TCC} := \frac{T_{1,u} - T_{1,d}}{T_{1,u} - T_{3,u}}. \tag{6}$$

As it turns out, this expression can be traced back to the DTCs of the HEs constituting the thermal control circuit [14, 15]. This yields

$$P_{TCC} = \frac{\Gamma_2 P_1 P_2}{\Gamma_2 P_2 + \Gamma_1 P_1 (1 - P_2)}. \tag{7}$$

We conclude, that if a representation as given in Eq. (4) can be found for both HEs, we will end up at $P_{TCC} = P_{TCC}[\Gamma_1, \Gamma_2, \Gamma_3]$ with no additional effort at all. Again, from the knowledge of P_{TCC} by means of Eqs. (6) and (7) can be solved for any of the appearing temperatures, given that the other two temperatures are known. The remaining relevant temperatures in the system, not occurring in Eq. (6), may then be determined from local DTC relationships and enthalpy balances.

Summarizing, we conclude, that if we succeed in expressing P_i by means of Eq. (4), and in turn may trace back the heat capacity flows to quantities available to the CPU of the vehicle, the overall cooling system is described in an analytically closed form, given that two temperature signals in the system are known. Therefore, we shall proceed to investigate the DTCs of the individual HEs in more detail in what follows. The description of the heat capacity flows by means of quantities accessible to the CPU shall be postponed to the subsequent section.

3 Models for the Heat Exchangers

3.1 Dimensionless Temperature Changes

In order to model the overall thermal control circuit we have to express the DTCs of HE1 and HE2 by means of the heat capacity flows of the media involved in the heat exchanging processes. The details of the thermal exchange depend on the overall heat transfer coefficient k_i and the heat transfer area A_i of the respective HE. Within the present model these quantities exclusively enter in product form, such that they can be combined as an effective thermal conductibility γ_i as

$$\gamma_i := k_i A_i. \tag{8}$$

Moreover, the explicit form of a HE's DTC depends on its actual topology. Here we assume, the topologies displayed in Fig. 1. Therefore, HE1 exhibits one shell-side with two tube-side passes. The DTC of such a device has been discussed in Refs. [16, 17] and according to our notation reads

$$P_1 = \frac{2}{1 + \frac{\Gamma_1}{\Gamma_2} + \sqrt{1 + \left(\frac{\Gamma_1}{\Gamma_2}\right)^2 + \frac{2\Gamma_1}{\Gamma_2}(2\varepsilon - 1)}\coth\left[\frac{\gamma_1\sqrt{1 + \left(\frac{\Gamma_1}{\Gamma_2}\right)^2 + \frac{2\Gamma_1}{\Gamma_2}(2\varepsilon-1)}}{2\Gamma_1}\right]}, \tag{9}$$

where ε takes account of differences between the two passes, due to distinctions in the effective heat transfer areas and heat transfer coefficients [15].

The topology of HE2 shown in Fig. 1 resembles a cross-flow HE where the fluids are laterally mixed on both sides. For such a device the DTC reads [18]

$$P_2 = 1 - \exp\left[\frac{\Gamma_3}{\Gamma_2}\left(\mathrm{e}^{-\frac{\gamma_2}{\Gamma_3}} - 1\right)\right]. \tag{10}$$

Thus, apart from the heat capacity flows, the dependency of P_i on the effective thermal conductibility has to be taken into account for both HEs. As we will see however, γ_i can be traced back to Γ_i and Γ_{i+1}, thus

$$\gamma_i = \gamma_i[\Gamma_i, \Gamma_{\mathrm{i}+1}]. \tag{11}$$

This shall be discussed in the following subsection.

3.2 Thermal Conductibility

From the theory of heat transfer it is known that the overall thermal resistivity, being the reciprocal value of the respective thermal conductibility, is given by the sum of the individual thermal resistivities of the materials facilitating the thermal contact. Thus, for $i \in \{1, 2\}$ we have

$$\frac{1}{\gamma_i} = \frac{1}{\alpha_i A_i} + \frac{\delta}{\lambda A_{\mathrm{M}}} + \frac{1}{\alpha_{\mathrm{i}+1} A_{\mathrm{i}+1}}, \tag{12}$$

The heat transfer coefficient of the fluid $m \in \{i; i+1\}$ transmitted through the area A_m is given by α_m. The material properties of the HE have been taken account of by the thickness δ, the area A_M and the thermal conductivity λ. Assuming $A_i = A_{i+1} = A_{\mathrm{M}}$ throughout what follows, a crude estimation of typical heat transfer coefficients reveals that the thermal resistivity of both fluids does exceed the one of the HE material by at least two orders of magnitude. Therefore, it seems permissible to neglect this term. Furthermore, as is well-known, the heat transfer coefficient α_m can be reformulated by means of the respective Nusselt number Nu_m via

$$\alpha_m = \frac{\lambda_m \mathrm{Nu}_m}{L}, \tag{13}$$

where $\lambda_m = \lambda_m(T_m)$ describes the heat conductivity of the fluid m and L is a characteristic length of the device.

On the other hand the Nusselt number of a fluid can be expressed by the corresponding Reynolds and Prandtl number. For our present purposes we write the Reynolds number as

$$\mathrm{Re}_m = \frac{L}{A_m c_{p,m} \eta_m} \Gamma_m, \tag{14}$$

with the dynamic viscosity $\eta_m = \eta_m(T_m)$. The Prandtl number is given by

$$\mathrm{Pr}_m = \frac{\eta_m c_{p,m}}{\lambda_m}. \tag{15}$$

In the present context, the heat conductivity λ_m, the specific heat capacity $c_{p,m}$ and the dynamic viscosity η_m can be regarded as mere functions of the average temperature T_m. Thus, the heat transfer coefficient can, combining Eqs. (13)–(15), be separated into a product of a function of the average temperature $\widetilde{g}(T_m)$ and a function of the heat capacity flow $f(\Gamma_m)$.

For thermal exchange problems it is quite common in automotive applications to assume a power-law relation between Nu_m, Re_m and Pr_m [19]. From this the heat transfer coefficient α_m may be cast into the form

$$\alpha_m = \Gamma_m^{n_m} \widetilde{g}(T_m). \tag{16}$$

where the function $\widetilde{g}(T_m)$ does only weakly depend on the average temperature and may thus be approximated by the constant g_m. Furthermore, we assume a universal exponent n_m for the two media which are in thermal contact through the HE under consideration. Taking this into account we finally end up at a three parameter theory for the thermal conductibility of the HE, which has to be fitted to given experimental data. We stress that the thermal conductibility is a quantity which is essentially induced by convection. Therefore γ_i turns out to be a strictly increasing, yet saturating function of Γ_i and Γ_{i+1}.

Once the aforementioned three parameters are determined, the DTC of each HE is solely given by means of the heat capacity flows of the respective fluids (c.f. Eqs. (9) and (10)). In the next section, we will investigate these quantities in more detail.

4 Model for the Heat Capacity Flows

The heat capacity flow of the fluid m is given by Eq. (3). Thus, for each medium we have to determine both the specific heat capacity and the respective mass flow.

4.1 Heat Capacity Flow for the Intake Air and the Head Wind

The mass flow $\dot{m}_1$ of the working fluid is given by the sum of the mass flow of fresh air $\dot{m}_{1,\mathrm{F}}$ and the mass flow of recirculated exhaust gas $\dot{m}_{1,\mathrm{EGR}}$ streaming through HE1.

Usually the mass flow of fresh air is measured by an airflow sensor. The recirculated mass flow can be modelled by a one-dimensional mass flow balance [20]. As far as the head wind is concerned, the corresponding mass flow can be determined as a function of the vehicle velocity and the rotational speed of the fan at the front-end. A correction due to the state variables of the ambience is taken into account.

We model the specific heat capacity of air in the relevant temperature regime according to

$$c_{p,A} = \begin{cases} c_{p,A,0} & \forall T_A < 293,15K \\ c_{p,A,1(T_A)} & \forall T_A \geq 293,15K' \end{cases} \tag{17}$$

where $c_{p,A,0}$ is a constant and $c_{p,A,1}(T_\mathrm{A})$ is given by a second order polynomial of the local air temperature T_A. This expression is used both for the determination of the specific heat capacity of the head wind and the fresh air share in the working fluid. For the latter, however, we also have to take into account that the specific heat capacity of the recirculated exhaust gas may differ significantly from $c_{p,\mathrm{A}}$. To this end, we formulate the specific heat capacity $c_{p,1}$ of the gas flowing through HE1 on the footing of energy conservation

$$c_{p,1} = c_{p,A}(1 - r_{EGR}) + r_{EGR}c_{p,EGR}, \tag{18}$$

where the recirculated exhaust gas rate $r_{EGR} = \dot{m}_{1,EGR}/\dot{m}_1$ has been used.

In the present context we assume the exhaust gas to consist of air, water, and carbon dioxide. The specific heat capacity of the recirculated exhaust gas may then be determined in analogy to Eq. (18) where we assume the water- and carbon dioxide-rates to be constant within the exhaust gas. They are fitted to vehicle measurements.

The temperature dependence of the isobaric specific heat capacity of carbon dioxide is approximated to linear order in the given temperature range. The specific heat capacity of liquid water is discussed in the appendix, whereas for water vapor a constant value may be assumed.

Thus the heat capacity flow of the intake gas is determined.

4.2 Heat Capacity Flow for the Coolant

We model the coolant mass flow through a pipe segment in the cooling circuit by means of the Hagen-Poiseuille equation [21]:

$$\dot{m}_2\left(c, T_{2,u}, r\right) = C\varrho_2\left(c, T_{2,u}\right)\frac{\Delta p\left(c, T_{2,u}, r\right)}{\eta_2\left(c, T_{2,u}\right)}. \tag{19}$$

Both the dynamic viscosity η_2 as well as the density ϱ_2 of the coolant exhibit a dependence on volume concentration c and temperature $T_{2,u}$.[4] The pressure drop Δp in the considered pipe segment does also depend on these quantities. Here, in addition, the rotational speed of the pump n_P comes into play. We define $r := n_P/n_{P,max}$ as the rotational speed normalized to the respective maximum value $n_{P,max}$. Finally, C takes account of the geometry of the segment.

For a discussion of the dynamic viscosity and the density of the fluid, we refer the reader to the appendix. Apart from this, we have to model the pressure drop in the pipe segment by means of $x, T_{2,u}$, and r. For an incompressible fluid we find

$$\Delta p\big(c, T_{2,u}, r\big) = \varrho\big(c, T_{2,u}\big) a(c, r). \tag{20}$$

Here the acceleration a induced by the pump is assumed to depend on c and r. An explicit temperature dependence is excluded as can be justified by means of vehicle measurements. We write $a(c, r) = a_\xi(c) a_\zeta(r)$ where we put $a_\xi(r) = r^2 + \xi r^3$ and $a_\zeta(c) = 1 + \zeta_1 c + \zeta_2 c^2$. The parameters ξ, ζ_1, and ζ_2 are fitted to vehicle measurements.

Being a generic property of the cooling medium the specific heat capacity of the coolant is discussed in the appendix. Thus the heat capacity flow of the cooling medium is determined as a function of $c, T_{2,u}$, and r.

5 Experimental Details and Calibration

The predictions of our model shall be compared to experimental data obtained from two charged Diesel engine vehicles referred to as V1 and V2 henceforth. Both test carriers have a displacement of two liters and the rated power outputs are given by 140 and 110 kW respectively. The system under consideration consists of the thermal control circuit of the indirect charge air cooling device of V1 and V2.

All parameters required to describe the properties of the cooling mixture, as discussed in the appendix, have been calibrated on the basis of the respective data sheets of the cooling medium. Here we briefly summarize our findings in this respect. The density of water and ethylene glycol can be modelled by a three and a two-parameter theory respectively. By the conservation of mass the interpolated density for the coolant mixture is then given by a mere linear combination with respect to the volume concentration of the densities of the respective pure agents. The dynamic viscosity is given by a three-parameter theory for the respective pure fluids and the interpolation can be taken account of by a two-parameter model. Contrary to this, the interpolation for the specific heat capacity of the coolant mixture is determined from the conservation of energy and does hence not require any free parameters. However, in order to give a satisfying account of this quantity, for the pure components, the PDDS equation, taking the lowest four orders into account, is used [15]. Finally, the heat conductivity of water can be approximated by a second order polynomial, whereas this property can be

[4] We have chosen a pipe segment in the inlet flow because temperature effects are much more crucial here due to the exponential temperature behavior of the viscosity (c.f. the appendix).

captured by a linear approximation for ethylene glycol. The interpolation for the mixture is well-described by a two-parameter interpolation. In total we thus utilize mutually independent models for the properties of the pure agents with up to four parameters. The interpolation for the coolant mixture, if not restricted by mass- or energy conservation may then be obtained by independent two-parameter models.

In order to calibrate our mass flow model, a measuring device, combining a volume flow and a temperature sensor, has been installed in the cooling circuits. The parameters are fitted to vehicle measurements where the rotational speed of the pump is varied for different volume concentrations under numerous ambient conditions. As suggested by the model, we do not observe any temperature dependence for a (c.f. Eq. (20)). Thus, together with the fitting process for the specific heat capacity of the working fluid outlined in Subsect. 4.1, the heat capacity flows of all media involved within the model are at our disposal.

Finally, the calibration of the models for the individual heat exchangers can be executed. To this end the test carriers were equipped with temperature sensors up- and downstream to the respective charge air coolers for the two media in thermal contact. A further temperature sensor has been installed upstream to the cooler at the front-end on the head wind side. In a multi-stage fitting procedure, taking both the DTCs of the individual HEs as well as the overall DTC of the integral cooling device into account, the three free parameters of each $\gamma_i, i \in \{1;2\}$, introduced in Subsect. 3.2, were determined. This final step completes the calibration of the model.

6 Results

In this section we compare the results predicted from the calibrated model with vehicle measurements. Within this report the DTC has served as the central quantity when discussing individual HEs and the overall thermal control system. The quality of the described method depends crucially on the possibility to represent the individual DTCs (c.f. Eq. (2)) by means of the respective heat capacity flows as given by Eqs. (9) and (10). In Figs. 2 and 3 the DTCs of the charge air coolers of the investigated test vehicles are exemplified. For V1 a comparison between experiment and theory is displayed in Fig. 2. The surface illustrates a connected envelope of our model for P_1 as a function of the normalized heat capacity flows $\Gamma_1/\Gamma_{1,max}$ for the intake gas and $\Gamma_2/\Gamma_{2,max}$ for the cooling medium. Here $\Gamma_{m,max}$ gives the maximum value observed for the heat capacity flow of the fluid m. The model is to be compared to the respective measure points shown in the plot, where test series were recorded for pure water, pure ethylene glycol and a mixture with $c = 0.6$. Overall we find good agreement between theory and experiment. As predicted by the model, P_1 does not explicitly depend on the volume concentration. Instead this dependency comes into play implicitly, as Γ_2 is a function of c. Note in particular the tendency of an increased cooling fluid heat capacity flow with decreasing volume concentration. This is of course essentially induced both by the lower viscosity resulting from the smaller content of ethylene glycol and the high specific heat capacity of water. We furthermore observe that the DTC of the charge air cooler is a monotonically increasing function of Γ_2. The physical picture behind this finding is intuitively clear: The bigger the heat capacity flow of the coolant,

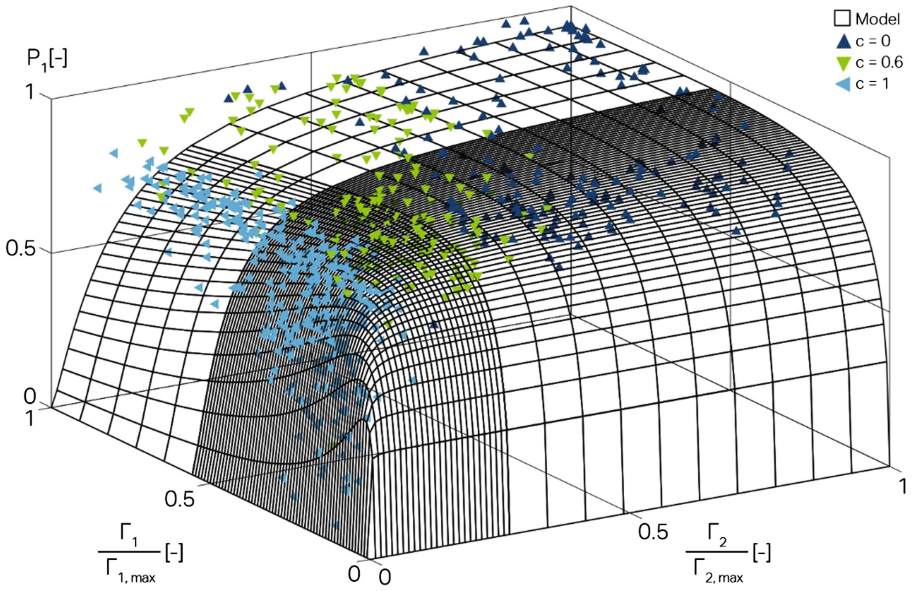

Fig. 2. Dimensionless temperature change as a function of the normalized heat capacity flows of intake air and cooling fluid for the charge air cooler of the Diesel engine vehicle with 140 kW rated power output. A comparison between our model (surface) and experimental data (symbols) for the pure agents as a well as for a mixture with 60 % volume concentration in ethylene glycol is displayed.

be it due to an increased mass flow or specific heat capacity, the higher the performance of the heat exchanging process. Due to the pronounced nonlinearity of P_1, the gradient along an increasing heat capacity flow is very steep for small Γ_2 and falls off rapidly for $\Gamma_2/\Gamma_{2,max} \gg \Gamma_1/\Gamma_{1,max}$ such that the DTC saturates in this regime.

Applying the simple picture utilized to explain the tendency of increasing P_1 with increasing Γ_2 suggests that an inverse behavior should be observed along the heat capacity flow of the intake air, i.e. the DTC should diminish with growing Γ_1. This indeed is observed for sufficiently high values of Γ_1. However, we find, that along Γ_1 the DTC of the charge air cooler does not monotonically decrease. Instead we have

$$\lim_{\Gamma 1 \to 0} P_1(\Gamma_1, \Gamma_2) = 0. \tag{21}$$

Consequently for $\Gamma_1 \ll \Gamma_{1,max}$ we find

$$\frac{\partial P_1}{\partial \Gamma_1} > 0. \tag{22}$$

This is due to the fact that the effective heat conductibility γ_1 monotonically increases with increasing heat capacity flow, as the heat transfer processes are facilitated by convective means (c.f. Sect. 3.2). Therefore, starting from small Γ_1, we find a

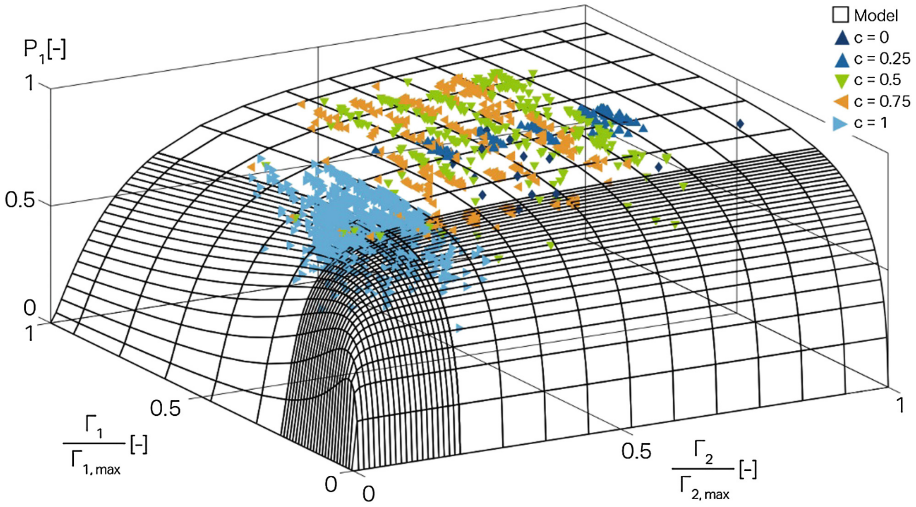

Fig. 3. Dimensionless temperature change as a function of the normalized heat capacity flows of intake air and cooling fluid for the charge air cooler of the Diesel engine vehicle with 110 kW rated power output. A comparison between our model (surface) and experimental data (symbols) for various volume concentrations is displayed.

steep positive slope in the DTC of the HE. Along Γ_1 the DTC runs through a maximum for fixed Γ_2 from which the aforementioned decrease of P_1 for increasing Γ_1 is observed. The maximum occurs in the region, where the thermal conductibility is close to saturation, i.e. for values where an increase in Γ_1 does not lead to a significant increase in γ_1 which could compensate the greater amount of heat to be transferred away from the intake air.

Turning to V2 (c.f. Fig. 3) all these findings are confirmed. The experimental values displayed by the measure points for various volume concentrations as indicated in the plot are in good accordance with the theoretical predictions, again shown as a connected envelope.

In Fig. 4, the analytically closed model for the DTC of the integral cooling system (c.f. Eq. (7)) of V1 is compared to the respective measure points. Here merely points which correspond to a given value of the heat capacity flow of the head wind allow for a significant comparison. The chosen data corresponds to a vehicle velocity of 120.5 ± 0.5 km/h with an inactive fan. The experimental results are to be compared with the surface shown in Fig. 4. As for the individual HEs the DTC of the overall cooling circuit is well-described within our model. We have checked that this is also true for other values of the head wind heat capacity flow.

Along increasing Γ_2 we find that the DTC of the thermal system is monotonically increasing, where a saturation effect is observed for sufficiently high Γ_2. Unlike for the individual HE such a behavior is not necessarily fulfilled for the overall system. As Γ_2

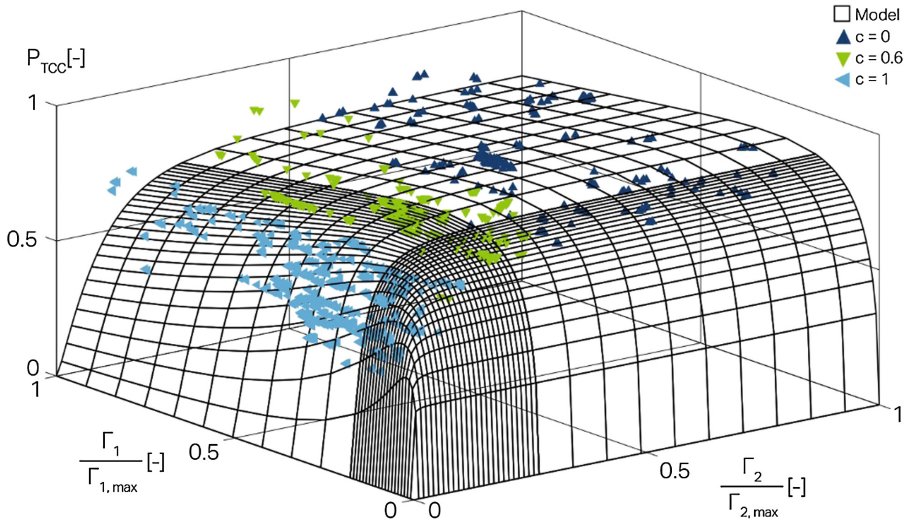

Fig. 4. Dimensionless temperature change for the overall thermal control system as a function of the normalized heat capacity flows of intake air and cooling fluid for the Diesel engine vehicle with 140 kW rated power output. The displayed data corresponds to a constant heat capacity flow of the head wind at a vehicle speed of 120.5 ± 0.5 km/h with inactive fan. A comparison between our model (surface) and experimental data (symbols) for various volume concentrations is displayed.

has respectively opposing impacts on P_1 and P_2,[5] there may exist operating points, with $\partial P_{TCC}/\partial \Gamma_2 < 0$. However, such a behavior has not been observed for the two test vehicles under consideration.

Contrarily, along the intake air heat capacity flow P_{TCC} runs through a maximum value for any fixed Γ_2 and falls of towards higher Γ_1. This behavior clearly resembles our findings for P_1. As P_2 does not depend on the heat capacity flow of the intake air, this effect already studied for the DTC of the charge air cooler remains pronounced for the overall system. Finally, we want to stress, that P_{TCC} increases with increasing Γ_3. This is of course due to the fact, that P_2 turns out to increase with increasing Γ_3. This effect is clearly attributed to the circumstance, that the heat transfer from the cooling medium to the ambience necessitates a sufficiently high heat capacity flow due to the head wind.

Figure 5 contains a representation of the DTC of the overall charge air cooling system for V2. Here Γ_3 corresponds to a vehicle velocity of 98 ± 2 km/h with an inactive fan. As for the other test car we find good agreement between the measured data (symbols) and the surface calculated from the model. The findings discussed for Fig. 4 are reproduced for this vehicle.

For both test cars we find the tendency that a decreased volume concentration c leads to an increased coolant heat capacity flow due to viscosity and specific heat capacity effects. This results in slight but significant differences in the absolute values of the DTC for the thermal control circuit. These slight differences may however have a

[5] I.e. P_1 increases with increasing Γ_2, whereas P_2 decreases in that case.

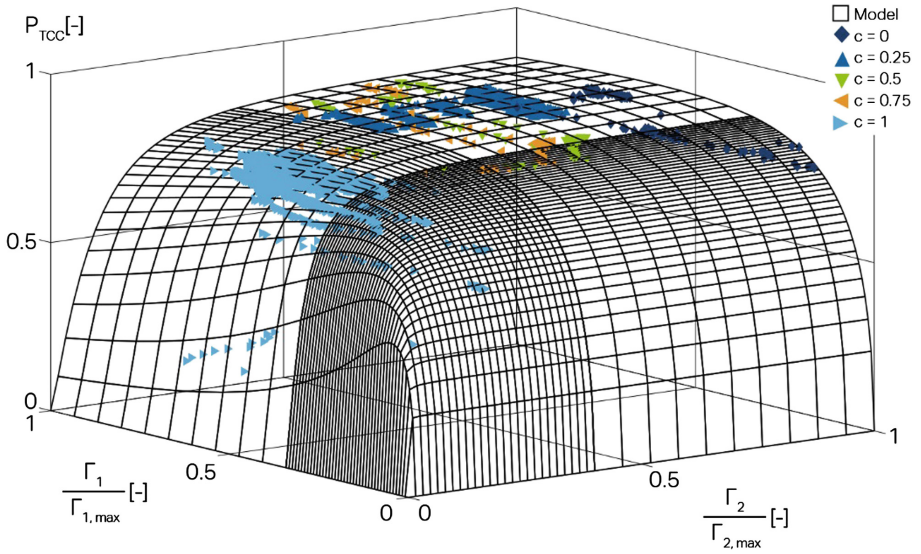

Fig. 5. Dimensionless temperature change for the overall thermal control system as a function of the normalized heat capacity flows of intake air and cooling fluid for the Diesel engine vehicle with 110 kW rated power output. The displayed data corresponds to a constant heat capacity flow of the head wind at a vehicle speed of 98 ± 2 km/h with inactive fan. A comparison between our model (surface) and experimental data (symbols) for various volume concentrations of ethylene glycol is displayed.

distinct effect on the respective fluid temperatures as P_{TCC} occurs in combination with large absolute temperatures or temperature differences. Moreover, this has an impact on the model for Γ_2 and underlines the importance to take the adequate volume concentration into account, when model-based applications like diagnostics and control are utilized for series production.

Finally we want to apply the presented method to model the temperature downstream to the charge air cooler of the two vehicles. To this end we rewrite Eq. (6) as

$$T_{1,d} = T_{1,u} - P_{TCC}[\Gamma_1, \Gamma_2, \Gamma_3]\left(T_{1,u} - T_{3,u}\right), \tag{23}$$

where $T_{1,u}$ and $T_{3,u}$ are provided by sensor signals. In Fig. 6 representative results from this approach (solid lines) are compared with experimental data (dotted lines) drawn from measurements performed for V1. Here the volume concentrations $c = 0$, $c = 0.6$, and $c = 1$ have been investigated (c.f. Fig. 6(a), (b) and (c) respectively). For confidential reasons a constant reference temperature $T_{1,d,\mathrm{Ref}}$ has been subtracted from the absolute value of $T_{1,d}$. The left inset shown in Fig. 6(a) displays the corresponding signal for the temperature upstream to the charge air cooler also shifted by a constant reference temperature $T_{1,u,\mathrm{Ref}}$. The normalized heat capacity flow of the intake air is depicted in the right inset of Fig. 6(a). Both insets underline that the measurements mostly resemble dynamical driving situations. Albeit the presented model is based on a

steady-state formulation, the results drawn from the model do agree well with the experimental data for $c = 0$. The same may be said for $c = 0.6$ and $c = 1$ displayed in Figs. 6(b) and (c) respectively. Here also experimental data of the shifted intake air temperature downstream to the charge air cooler is compared to the corresponding values obtained from our model. These measurements also do represent dynamical driving situations. Taking all measurements into account, we find that the mean absolute deviation

$$\delta T_{1,d} := \frac{\sum_{q=1}^{q_{max}} \left| T_{1,d,mod} - T_{1,d,meas} \right|}{q_{max}}$$

between model and experiment is given by 4.17K for this vehicle. Here we have averaged the absolute values of the deviation between theory and experiment, respectively given by $T_{1,d,mod}$ and $T_{1,d,meas}$ over the overall number q_{max} of recorded time slots.

For V2 the shifted charge air temperature as given by our model is compared to experimental data in Fig. 7. The corresponding volume concentrations are $c = 0$ (c.f. Fig. 7(a)), $c = 0.5$ (c.f. Fig. 7(b)), and $c = 1$ (c.f. Fig. 7(c)). Again for $c = 0$ the transient nature of the underlying driving situation is clearly displayed by the supplemented insets. Summarizing, we find that the predictions from our model correlate well with the measurement data, albeit the accuracy is a little reduced in comparison to V1. This is also reflected in the mean absolute deviation for this vehicle which is given by $\delta T_{1,d} = 4.7$K. However, these deviations should be compared to those obtained in Ref. [14], where a mean absolute deviation of 5K was given for a test vehicle with a strictly equimolar mixture of ethylene glycol and water. We stress that restricting the range of application of the volume concentration allows a more accurate calibration of the model parameters. From this a further reduction of the mean absolute deviation between measurement and model data would result. Taking into account that the presented model is sufficiently simple to be run on an automotive CPU, the approach exhibits an overall satisfying accuracy. Finally, we like to point out, that the model interpolates smoothly as a function of c.

Having determined $T_{1,d}$, the coolant temperature up- and downstream to the charge air cooler can be obtained by means of the DTC of the individual HEs and local enthalpy balances. Figure 8 shows a representative comparison between the model values (solid line) of the coolant temperature and corresponding experimental data (dotted line). In Fig. 8(a) the cooling fluid temperature $T_{2,u}$ upstream to the charge air cooler is displayed, where again a constant reference temperature $T_{2,u,Ref}$ has been subtracted from both data sets. Due to error propagation, the accuracy of the modeled coolant temperature is a little reduced in comparison to $T_{1,d}$. However, the model may still serve as a quantitative estimation for the coolant temperature upstream to the charge air cooler. Here the test vehicle with 110 kW rated power output has been used with a volume concentration of $c = 0.25$. Again the measurement resembles dynamic driving situations. The corresponding measurement for the coolant temperature downstream to the charge air cooler is depicted in Fig. 8(b). We observe good agreement between theory and experiment, such that the model for instance may be utilized to detect critical temperatures in the charge air cooler outlet.

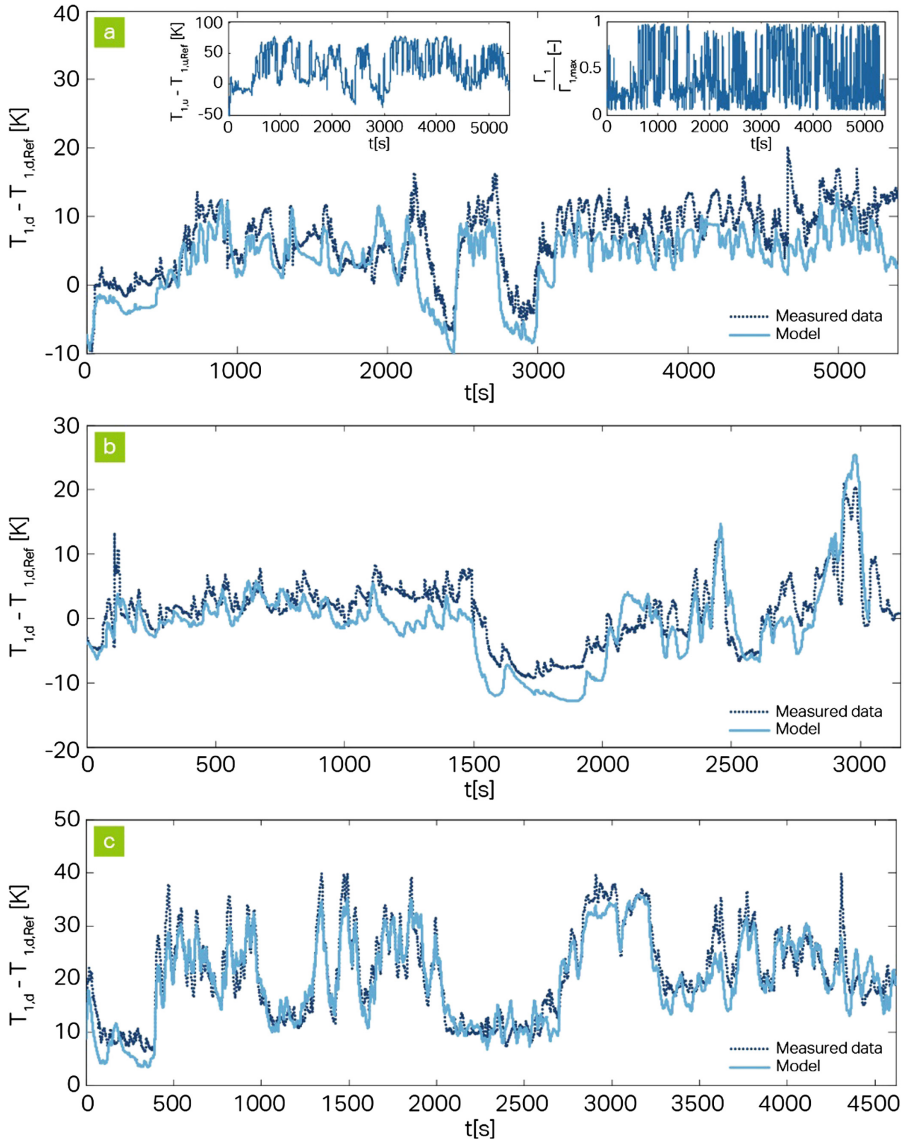

Fig. 6. Comparison between experimental data (dotted line) and predictions of the calibrated model (solid line) for several volume concentrations of ethylene glycol. The intake air temperature downstream to the charge air cooler of the vehicle with lower rated power output is shown. (a) Pure water: In order to illustrate the transient nature of the driving situations, the left inset displays the respective intake air temperature upstream to the charge air cooler. In the right inset the corresponding intake air heat capacity flow is depicted. (b) 60 % volume concentration of ethylene glycol. (c) Pure ethylene glycol

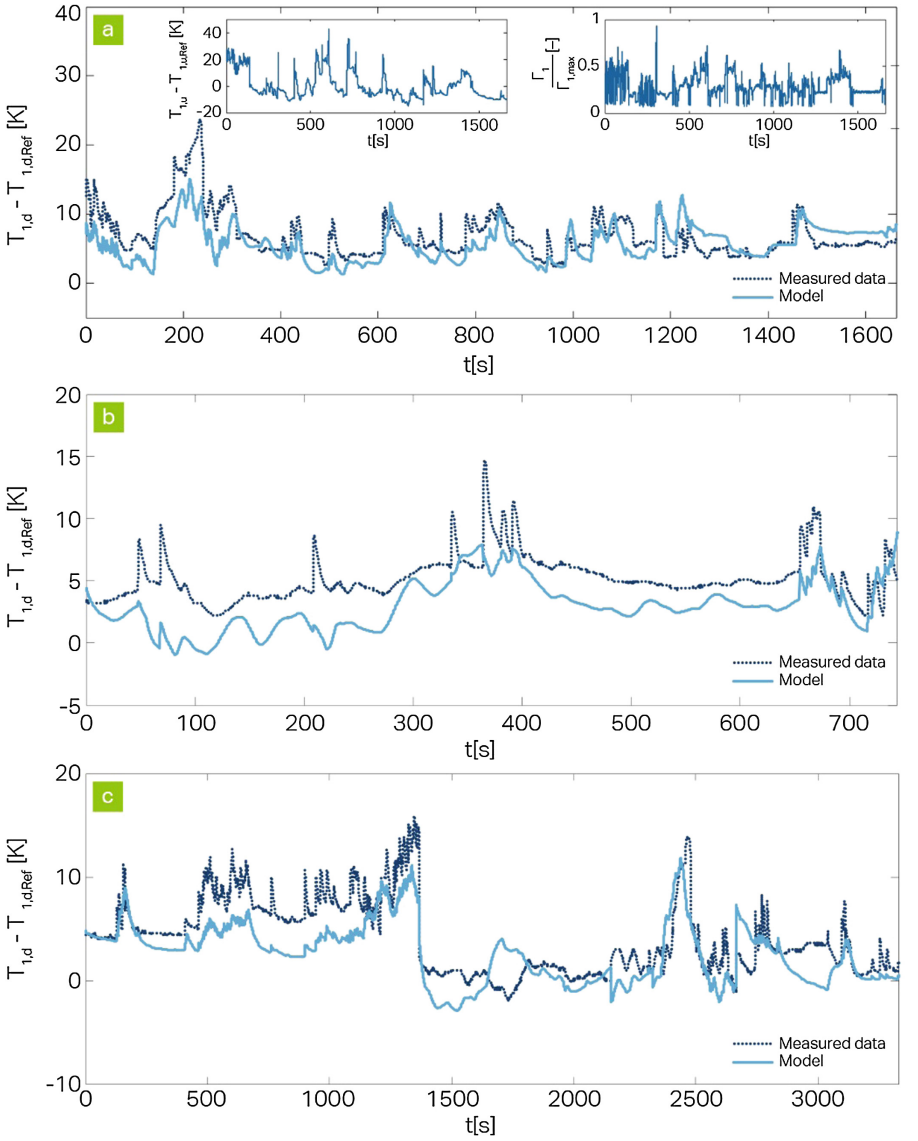

Fig. 7. Comparison between experimental data (dotted line) and predictions of the calibrated model (solid line) for several volume concentrations of ethylene glycol. The intake air temperature downstream to the charge air cooler of the vehicle with 110 kW rated power output is shown. (a) Pure water: In order to illustrate the transient nature of the driving situation the left inset displays the respective intake air temperature upstream to the charge air cooler. In the right inset the corresponding intake air heat capacity flow is depicted. (b) 50 % volume concentration of ethylene glycol. (c) Pure ethylene glycol.

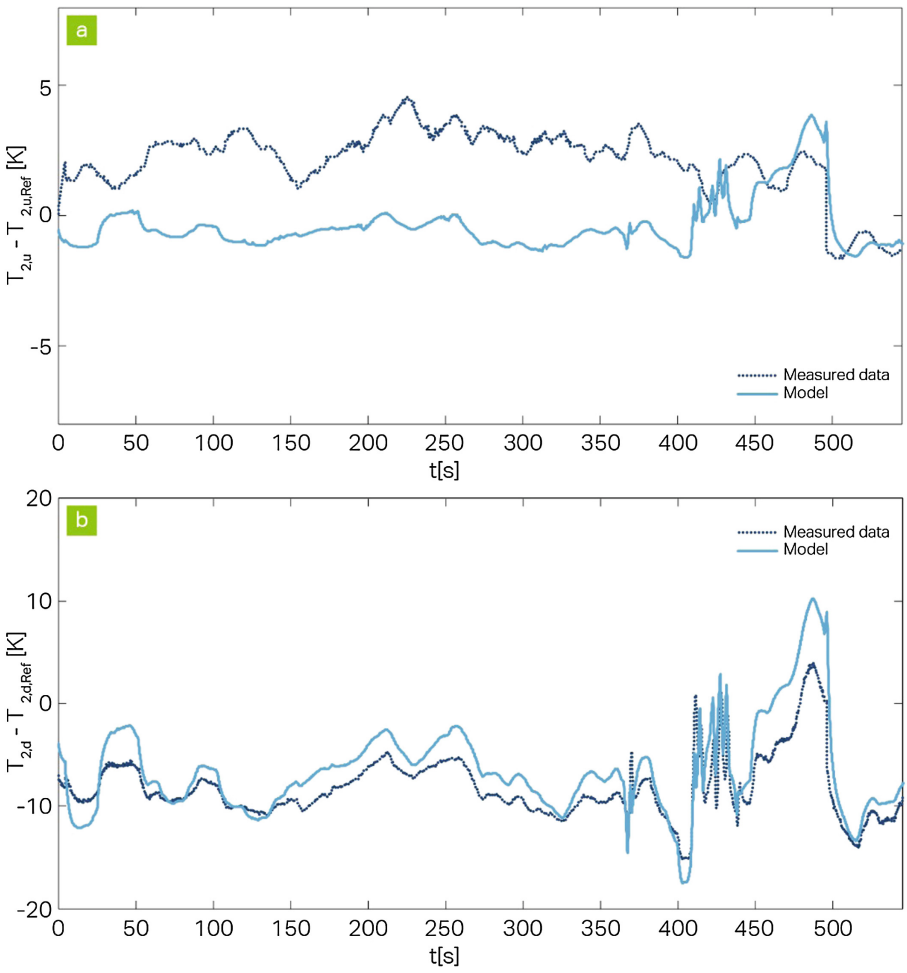

Fig. 8. Comparison between theoretical (solid line) and experimental (dotted line) values for the cooling fluid temperature in the vehicle with 110 kW rated power output. Here, a mixture with an ethylene glycol volume concentration of 25 % has been used. (a) Coolant temperature upstream to the charge air cooler. (b) Coolant temperature downstream to the charge air cooler.

7 Summary and Outlook

In this paper we have investigated a simple temperature control circuit which consists of a heat exchanger in the air intake or exhaust gas system of a vehicle with a combustion engine. We have argued that the growing automation level of the actuating elements in thermal management systems bears good prospects to realize advantages concerning tailpipe emissions and fuel consumption. Driving comfort and transient response may also be improved by thermal on-demand control strategies. Among the latter, model-based concepts offer advantages as far as control stability and calibration

efforts are concerned. In this spirit, formulating the thermal control circuit by analytical means, the volume concentration of ethylene glycol should be treated as a model parameter, as different vehicle types and vehicles in different climatic zones exhibit different cooling fluid mixtures. A theoretical approach taking this dependency explicitly into account has been discussed in this paper, where the full range between pure water and pure ethylene glycol has been covered. The model is based on the method of dimensionless temperature change. This quantity can be defined both for individual heat exchangers as well as for the overall temperature control circuit and may be interpreted as the efficiency of the heat exchanging device under consideration. The dimensionless temperature change of the overall circuit can be traced back to the ones of the individual heat exchangers (c.f. Eq. (7)). Thus, if the dimensionless temperature changes of the individual heat exchangers can be expressed by quantities available to the CPU of the vehicle, the considered overall temperature control system may by described by analytical means without any additional calibration effort at all. The representation of the individual dimensionless temperature changes by means of the fluid heat capacity flows was discussed on the basis of heat transfer and similitude theory. Provided that two temperature signals of the overall system are known from sensor information or from an independent model, the remaining four non-trivial temperatures can be determined with the presented method.

The fluid properties were described in the framework of well-established phenomenological models. Here the dependency of the volume concentration of ethylene glycol in the coolant mixture comes explicitly into play. In general, the cooling medium properties are discussed in terms of the pure agents (i.e. water and ethylene glycol). For an arbitrary volume concentration interpolation models are used. In particular, we find that the individual dimensionless temperature changes do not explicitly depend on the volume concentration. Instead, this dependency merely enters implicitly by means of the cooling fluid properties. To our satisfaction, this theoretical prediction is confirmed by experiment.

Summarizing, the presented approach consists of various mutually independent models for the fluid properties, the thermal conductibilities, and the dimensionless temperature changes of the individual heat exchangers. Each model is expressed by means of elementary functions such that the suggested approach is suited for automotive CPU applications.

We have applied our model to the indirect charge air cooling devices of two Diesel engine vehicles with different rated power outputs. Using the ambient temperature and the intake air temperature upstream to the charge air cooler as reference information, we have utilized the dimensionless temperature change of the overall temperature control circuit to determine the charge air temperature. A comparison to experimental data exhibits good accordance between model and measurement. In particular, not only the steady-state but also the transient behavior of the thermal system is captured within our model. For both test vehicles, we have exemplified the quality of our model for three distinct volume concentrations of ethylene glycol. Overall we find a mean absolute deviation between measurement and model of 4.17 and 4.7K for the charge air temperature of the higher and lower rated power output vehicle respectively. We have checked, that the model interpolates correctly between the individual ethylene glycol volume concentrations. We stress that the model has been calibrated for the whole

range of volume concentration between zero and one. Limiting this region during the calibration process naturally restricts the applicability of the model. However, this restriction on the other hand comes with a benefit regarding model accuracy.

Moreover, utilizing the dimensionless temperature changes for the individual heat exchangers as well as enthalpy balances, the coolant temperature up- and downstream to the respective charge air cooler were determined. A comparison between theory and experiment reveals satisfying agreement. For instance, the model may be applied to detect critical temperatures in the cooling circuit.

The presented model has been motivated on the footing of model-based automotive applications such as control or diagnosis with the application of heat exchanging devices in the intake air or exhaust gas system. The approach may be utilized to minimize the number of temperature sensors within a temperature control device resembling the system discussed in this report. However, the overall temperature control systems of vehicle engines are more complex than the simple cooling circuit we have addressed here. Therefore, a generalization of the approach outlined in this paper is highly desirable. Of course with an increased complexity of the system not only the theoretical description will be more involved. Also the treatment of the temperature control problem is much more demanding in that case, as different components may have different and even mutually excluding requirements. Also in this case, model-based decision making and control may help to further reduce pollutant emissions or to improve the efficiency of combustion engines.

A Appendix: Properties of the Coolant Mixture

Throughout the paper, the importance of the volume concentration c of ethylene glycol has been stressed. In this appendix we want to give a detailed account on the properties of the mixture as a function of c. To this end we discuss the respective properties of the pure substances respectively in a first step.[6] The resulting models are then interpolated as a function of the volume concentration of ethylene glycol c. Throughout this appendix our models for the fluid properties are compared to experimental data given in a data sheet of the coolant producer.

Note that strictly speaking an additive rule for the individual volumes does not apply. However, effects stemming from this circumstance turn out to be negligible and are therefore ignored within our investigations.

In general, the interpolation used to describe a fluid property $y(T_{2,q})$ by means of the respective properties of the pure components $y_{C_2H_6O_2}(T_{2,q})$ and $y_{H_2O}(T_{2,q})$ is realized by the interpolating functions $h_y(c, T_{2,q})$ and $\overline{h}_y(c, T_{2,q})$ such that

$$y(T_{2,q}) = h_y(c, T_{2,q}) y_{C_2H_6O_2}(T_{2,q}) + \overline{h}_y(c, T_{2,q}) y_{H_2O}(T_{2,q}), \tag{24}$$

[6] Although for the properties of water there exist accurate models [22], here we want to use simplified relations, as these are more suited for automotive CPU usage.

where the limiting cases $c = 0$ and $c = 1$ require $h_y(0, T_{2,q}) = \overline{h}_y(1, T_{2,q}) = 0$ and $h_y(1, T_{2,q}) = \overline{h}_y(0, T_{2,q}) = 1$. For our purposes we write

$$h_y(c, T_{2,q}) = ce^{a_y(1-c)/T_{2,q}}, \tag{25}$$

and

$$\overline{h}_y(c, T_{2,q}) = (1-c)e^{\overline{a}_y c/T_{2,q}}, \tag{26}$$

with the coefficients a_y and $\overline{a}_y$, which have to be determined from experimental data or restrictions due to conservation laws.

A.1 Density

Generally, we approximate the temperature dependence of the density by means of a power series, where in the case of water, we restrict ourselves to quadratic order. For ethylene glycol, a linear approximation is sufficient for our purposes. From the conservation of mass, the density of the mixture within our approach is given by (c.f. Eqs. (25) and (26)) $a_y = \overline{a}_y = 0$, viz.

$$\varrho(c, T_{2,q}) = c\varrho_{C_2H_6O_2}(\mathrm{T}_{2,q}) + (1-c)\varrho_{H_2O}(\mathrm{T}_{2,q}). \tag{27}$$

Here ϱ_X is the density of the component X. A comparison to experimental data reveals, that our model exhibits a maximum relative error of below 2.5 % in the temperature region between 250 and 390K[7].

A.2 Dynamic Viscosity

The dynamic viscosity η_X for the pure component X is described within a generalized phenomenological approach due to Raman [14, 15, 23] via

$$\eta_X = A_X e^{E_X(\mathrm{T_X})/(k_B T_X)}, \tag{28}$$

where k_B gives the Boltzmann constant and T_X resembles the temperature of the pure component X. The coefficients $E_{X,0}$ and $E_{X,2}$ appearing in the energy functional $E_X(T_X) = E_{X,0} + E_{X,2}T_X^2$, and the prefactor A_X are determined from a fit to the data sheet.

For the interpolation, we observe, that a higher accuracy is achieved if we use the natural logarithm of the dynamic viscosity instead of setting $y = \eta$ in Eq. (24). Then determining the interpolation coefficients, we find $a_\eta, \overline{a}_\eta \ll T_{2,q}$, such that within the

[7] Given that the liquid phase exists for the considered volume concentration of ethylene glycol.

Eqs. (25) and (26) the exponential functions may be expanded to linear order. From this, we obtain

$$\eta\left(T_{2,q}\right) = \eta_{C_2H_6O_2}^{c(1+a_\eta(1-c)/T_{2,q})}\left(T_{2,q}\right)\eta_{H_2O}^{(1-c)(1+\overline{a}_\eta c/T_{2,q})}\left(T_{2,q}\right). \tag{29}$$

Comparing our model to experimental data, we find that in the aforementioned temperature region the maximum relative error is given by 1.8 %.

A.3 Specific Heat Capacity

The specific heat capacities of the pure components are given by means of the PPDS equation [15], where for the present purpose an approximation up to quadratic order terms in the reduced temperature $\tau_X = 1 - T_X/T_{X,crit}$ is sufficient, both for ethylene glycol and for water. Here $T_{X,crit}$ is given by the critical temperature of the component X.

As far as the interpolation is concerned, from the conservation of energy, we observe, that consistency requires to set $y = \varrho c_p$, with $a_{\varrho c_p} = \overline{a}_{\varrho c_p} = 0$. Thus we arrive at

$$c_p\left(c, T_{2,q}\right) = \frac{\varrho_{C_2H_6O_2}\left(T_{2,q}\right)}{\varrho\left(c, T_{2,q}\right)} c \;\; c_{p,C_2H_6O_2}\left(T_{2,q}\right) + \frac{\varrho_{H_2O}\left(T_{2,q}\right)}{\varrho\left(c, T_{2,q}\right)}(1-c) \;\; c_{p,H_2O}\left(T_{2,q}\right). \tag{30}$$

Utilizing this approach, we are able to model the specific heat capacity of the fluid within the fore cited temperature region and with a maximum relative error below 5.9 %.

A.4 Heat Conductivity

The heat conductivity λ_{H_2O} for water is described by means of a second order polynomial in temperature. For ethylene glycol a linear approximation is sufficient. For the interpolation function we set $y = \lambda$ and fit a_λ and $\overline{a}_\lambda$ to experimental data. The latter turn out to be in the same order of magnitude as temperatures relevant for our purposes, such that further simplifications by means of power series expansions cannot be put forward. Our model gives a satisfactory accuracy with a maximum relative error of below 6 %.

References

1. Zähr, J., Füssel, U., Ulrich, H.-J., Türpe, M., Ebert M., Weinbruch, S.: Anwendbarkeit von Benetzungsversuchen für verschiedene Metalle (Applicability of wetting trials for different metals). METALL **62**(10), 611 (2008)
2. Hawksworth, D.K., Sekulic, D.P., Yu, C.-N., Fu H., Westergard, R.G.J.: A mechanistic study of aluminium controlled atmosphere brazing processes. In: VTMS, p. 107 (2015)

3. Li, B., Akdogan, V., Li, Y., Yan, Y., Li, J., Wang, J.: A novel and efficient thermoelectric-generating (TEG) system of energy harvesting from exhaust gases of passenger vehicles. In: VTMS, p. 397 (2015)
4. Gotovskiy, M.A., Grinman, M.I., Formin, V.I., Aref'ev, V.K., Grigor'ev, A.A.: Use of combined steam-water and organic rankine cycles for achieving better efficiency of gas turbine units and internal combustion engines. Thermal Eng. **3**, 236 (2012)
5. Banzhaf, M., Hendrix, D., Schmidt, M.: Ecological advances in engine cooling. ATZ Worldwide **9**, 28 (2001)
6. Edwards, S., Müller, R., Feldhaus, G., Finkeldei, T., Neubauer, M.: The reduction of CO2 emissions from a turbocharged DI gasoline engine through optimised cooling system control. MTZ Worldwide **1**, 12 (2008)
7. Guhr, C., Zellbeck, H.: Turbocharging with low temperature charge air cooling and EGR. MTZ Worldwide **10**, 44 (2012)
8. Kadunic, S., Baar, R., Scherer, F., Zegenhagen, T., Ziegler, F.: Heat2Cool-Engine Operation at Charge Air Cooling below Ambient Temperature. 22. Aachen Colloquim (2013)
9. Wagner, J.R., Ghone, M., Dawson, D., Marotta, E.E.: Coolant Flow Control Strategies for Automotive Thermal Management Systems, SAE paper no. 2002-01-0713 (2002)
10. Wagner, J.R., Srinivasan, V., Dwason, D.M., Marotta, E.E.: Smart Thermostat and Coolant Pump Control for Engine Thermal Systems, SAE paper no. 2003-01-0272 (2003)
11. Setlur, P., Wagner, J.R., Dawson, D.M., Marotta, E.E.: An advanced engine thermal management system: nonlinear control and test. IEEE/ASME Trans. Mechatron. **10**(2), 210 (2005)
12. Salah, M.H., Mitchell, T.H., Wagner, J.R., Dawson, M.D.: Nonlinear-control strategy for advanced vehicle thermal-management systems. IEEE Trans. Veh. Tech. **57**(1), 127 (2008)
13. Khodabakhshian, M., Feng, L., Wikander, J.: Predictive control of the engine cooling system for fuel efficiency improvement. In: IEEE International Conference on Automation Science and Engineering (CASE), p. 61 (2014)
14. Herzog, A., Skorupa, F., Meinecke, R., Frase, R.: Thermal management in the air intake system of combustion engines. MTZ Worldwide **5**, 24 (2014)
15. VDI Heat Atlas, 2nd edn. p. 34 ff., Springer, Heidelberg (2010)
16. Roetzel, W., Spang, B.: Analytisches Verfahren zur thermischen Berechnung mehrgängiger Rohrbündelwärmeübertrager, Fortschr.-Ber. VDI, vol. 19(18). VDI-Verlag, Düsseldorf (1987)
17. Rötzel, W., Spang, B.: Thermal calculation of multipass shell and tube heat exchangers. Chem. Eng. Res. Des. **67**, 115 (1989)
18. Smith, D.M.: Mean temperature difference in cross flow. Engineering **138**(479), 606 (1934)
19. Pflaum, W., Mollenhauer, K.: Wärmeübergang in der Verbrennungskraftmaschine. Heat Transfer in the Combustion Engine. Springer, New York (1977)
20. Heuck, M.: Modellgestütztes Luftsystem-Management für einen Pkw-Dieselmotor mit Hoch- und Niederdruck-Abgasrückführsystemen, Dissertation (2009)
21. Landau, L., Lifshitz, E.M.: Fluid Mechanics. Course of Theoretical Physics, vol. 6, 3rd edn. Pergamon Press Ltd. (1966)
22. The International Association for the Properties of Water and Steam: Revised Release on the IAPWS Formulation 1995 for the Thermodynamic Properties of Ordinary Water Substance for General and Scientific Use (2014)
23. Raman, C.V.: A theory of the viscosity of liquids. Nature **111**, 532 (1923)

Waste Heat Utilization, Rankine Cycle

High-Throughput Screening of ORC Fluids for Mobile Applications

Markus Preißinger[1(✉)], Johannes Schwöbel[2], Andreas Klamt[2], and Dieter Brüggemann[1]

[1] Chair of Engineering Thermodynamics and Transport Processes (LTTT), Center of Energy Technology (ZET), University of Bayreuth, Bayreuth, Germany
zet@uni-bayreuth.de
[2] COSMOlogic GmbH & Co. KG, Leverkusen, Germany

Abstract. Although huge effort has been invested in research and development of Organic Rankine Cycle (ORC) systems for mobile applications, it was not possible so far to identify a working fluid which covers nearly all of the requirements defined by OEMs and component suppliers. Therefore, the intention of this work was the identification of a so-called "superfluid" by screening the complete chemical space of more than 72 million chemical substances given by the PubChem© database. For this purpose, a fast simulation tool (DetailSimORC) was programmed in Matlab®. The thermodynamic properties were gained by the COSMOtherm software with a combination of the COSMO-RS theory and a cubic equation of state. The subsequent evaluation was based on a scoring system taking into account constructional aspects (e.g. minimum pressure level), safety issues (e.g. flammability) and regulatory requirements (e.g. ozone depletion potential, ODP) in addition to the thermodynamic performance. The results revealed that a conflict occurs between optimal thermodynamic performance and safety issues. Fluids showing a high net power output and low ODP are often highly flammable, whereas well-performing non-flammable working fluids have drawbacks concerning environmental and toxico-logical issues. Keeping these conflicting priorities in mind, it is possible to select a set of diverse best-ranked fluids for further investigation: the alcohol ethanol, the linear siloxane hexamethyldisiloxane, as well as the refrigerant R-152 (1,2-difluoroethane).

Keywords: Organic Rankine Cycle · Mobile sector · COSMO-RS · Scoring system · PubChem · Screening

1 Introduction

The mobile sector is driven by legislation and economics to reduce fuel consumption constantly. To meet future targets on fuel savings in heavy duty truck, passenger cars and the marine sector, waste heat recovery by means of Organic Rankine Cycle has gained increased interest in the last years. A crucial aspect for the efficiency and, therefore, for the profitability of such systems is the working fluid. Mostly, common databases for thermodynamic properties of organic fluids like RefProp® are applied

C. Junior et al. (eds.), *Energy and Thermal Management, Air Conditioning, Waste Heat Recovery*,
DOI 10.1007/978-3-319-47196-9_3

with the goal of identifying a suitable working fluid. However, results of a number of publications as well as two research projects of the Research Association of Combustion Engines (FVV) eV revealed that among the investigated fluids no fluid meets nearly all requirements set by OEMs and component supplier. Therefore, this projects deals with the search for an ideal fluid based on a highly innovative methodology: High-Throughput-Screening of potential working fluids using a combination of Computational Chemistry and thermodynamic process simulations. The goal of the project was nothing less than finding an ideal fluid for the exhaust gas usage in mobile applications by screening the complete chemical space defined by the PubChem database that covers around 72 million chemical substances at the moment. Possible advantages of such a fluid could be:

- higher net power output and, therefore, higher CO_2-reduction
- lower costs and reduced weight and size of the Rankine-system
- lower additional costs for condensation/cooling of the working fluid

To find the ideal fluid, a simulation tool in Matlab is programmed and combined with thermodynamic properties from COSMOtherm to ensure that the complete chemical space given by the PubChem database can be investigated. This work summarizes the main methods and results; more information can be found in a previous publication [1].

2 Theory and Methods

2.1 Organic Rankine Cycle

Although the mobile sector summarizes three different applications, namely heavy duty trucks, passenger cars and the marine sector, thermodynamically only two cases have to be distinguished: internal combustion engines using heat from exhaust gas recirculation (EGR) and the ones just using heat downstream of exhaust gas aftertreatment (EGA). The layout for cases including EGR is displayed in Fig. 1.

Boundary conditions for the simulation of all cares are selected according to discussions in the working committee of the research project. Furthermore, the working committee provided heat source characteristics based on real engine operation points. Based on these assumption, the simulation tool “DetailSimORC” is programmed within the simulation environment Matlab®. DetailSimORC is based on steady state simulations and the principle of conservation of energy. Radiation losses in the heat exchangers as well as pressure drops in the cycle are neglected. Figure 2 shows a simplified flow chart.

2.2 Computational Chemistry Methods (COSMOtherm)

The quantum chemically based Conductor-like Screening Model for Realistic Solvation (COSMO-RS) is a rather general method for predicting the chemical potentials of almost arbitrary molecules in almost any dense pure or mixed liquid. This chemical potential difference can be transformed into properties such as vapor pressures, activities or solubilities. In general, COSMO-RS is composed of two fundamental steps:

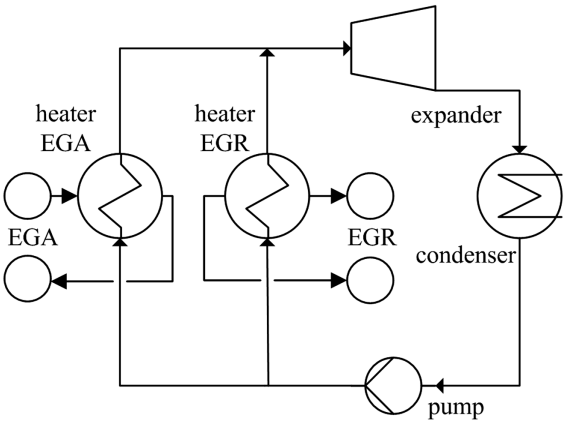

Fig. 1. Layout of Organic Rankine Cycle with exhaust gas recirculation

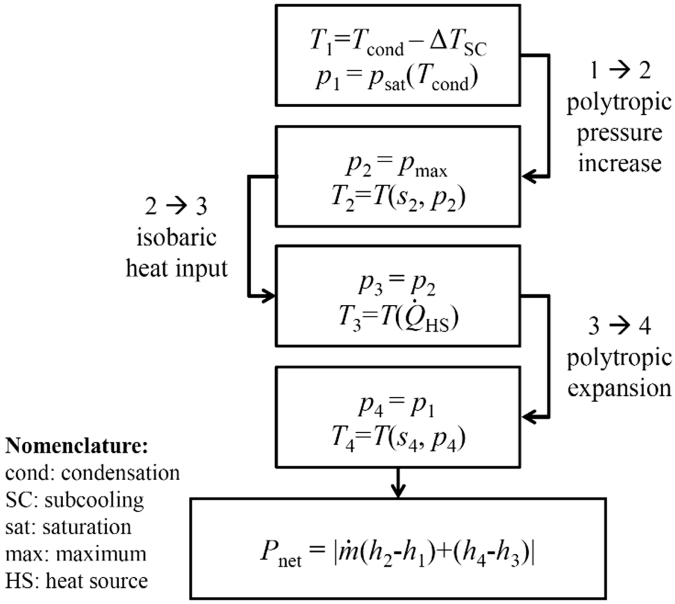

Fig. 2. Simplified flow chart of DetailSimORC

At first, quantum chemical calculations have to be performed for all compounds of interest. In these calculations a virtual conductor embedding the molecule is taken into account by the continuum solvation model COSMO [2]. In the second step of COSMO-RS, the statistical thermodynamics of the molecular interactions, this polarization charge density is used for the quantification of the interaction energy of pairs of surface segments. As most important molecular interaction modes, electrostatics and hydrogen bonding are taken into account in this way.

The classic COSMO-RS theory is based on the assumption of incompressible liquids and ideal gases. The ORC process, however, uses temperatures and pressures up to the critical point. In this range of application, the treatment of both liquid phase compressibility and real gas behaviour is essential. In order to extend the applicability range of COSMO-RS, the theory is combined with the Patel-Teja equation of state within this study [3].

The ORC fluid screening requires a preferably diverse chemical structure dataset. Here, the PubChem database has been chosen as the largest inventory publically available. In an automatized workflow, the molecular structures are fetched from the database, quantum chemical calculations are initiated for appropriate compounds and the thermodynamic properties are predicted via the COSMOtherm software, as depicted in Fig. 3. DetailSimORC simulations are then performed for a filtered set according to suitable thermodynamic properties for the ORC process (critical temperatures, vapor pressures…) as described above.

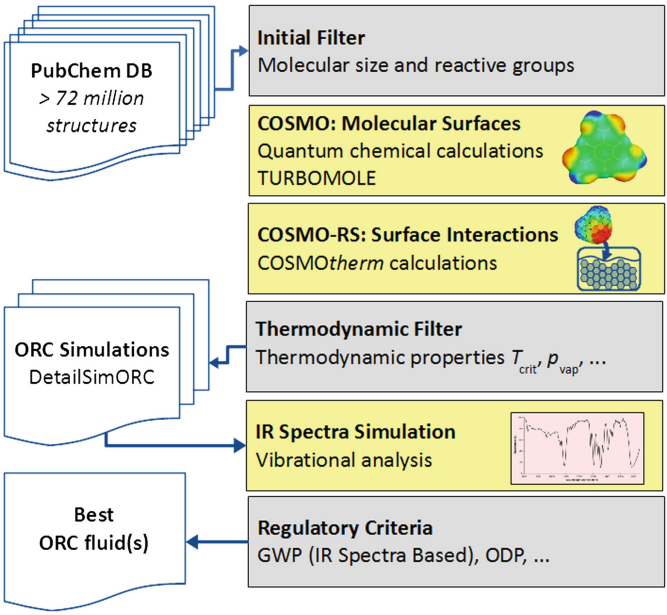

Fig. 3. Schema of the PubChem database screening by COSMOtherm calculations and DetailSimORC simulations

3 Results and Discussion

In total, 3,175 working fluids are simulated in DetailSimORC based on accurate thermodynamic properties from COSMOtherm (TZVPD-FINE level, see also Preißinger et al. [1]). Each working fluid is considered for two different applications (heavy

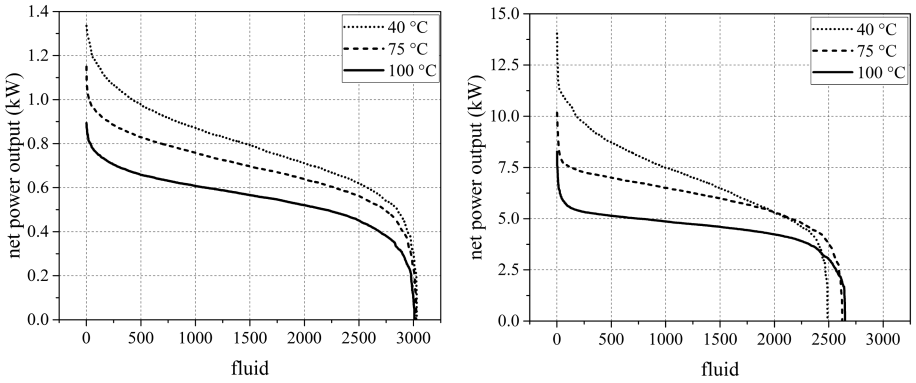

Fig. 4. Net power output for various working fluids depending on condensation temperature for application passenger car (left) and heavy duty truck (right)

duty truck, passenger car) and three different condensation temperatures (40 °C, 75 °C, 100 °C).

Figure 4 shows the expected decreasing net power output with increased condensation temperature. Furthermore, a steep increase in net power output for the best 50 working fluids is observed.

It is obvious that several working fluids reach high net power output. In a next step an overall evaluation by summing up the ranking of each fluid within each of the six cases. An ideal working fluid would come up with an overall scoring of 6 (being ranked on 1st place for all six cases), the least efficient working fluid would lead to a value of 19050 (begin last ranked for all six cases). It can be seen that the working fluid with the best overall ranking is acetaldehyde with an overall score of 27. This shows that the methodology of combining a fast simulation environment with computational chemistry is an effective way to find ideal working fluids from a thermodynamic point of view.

However, based on security aspects like flammability, autoignition temperature and the formation of highly explosive peroxides, acetaldehyde cannot be applied under real world conditions. Therefore, a more comprehensive evaluation method is developed which takes into account constructional aspects, safety issues, regulatory parameters and thermodynamic efficiency.

Constructional aspects include minimum and maximum pressure, maximum temperature, heat flux in the condenser and pressure ratio in the expansion unit. Flammability, mutagenicity, carcinogenicity, acute toxicity and aquatic toxicity are investigated among other as safety issues. Regulatory parameters include global warming potential GWP, ozone depletion potential ODP, freezing point as well as structure analysis concerning e.g. reactive substructures and stability analysis by autoignition temperature. The overall results reveal that a conflict occurs between optimal thermodynamic performance and safety issues. Fluids with high net power output and low ODP are often highly flammable, whereas well-performing non-flammable working fluids have drawbacks concerning environmental and toxicological issues.

Nevertheless, a set of diverse best-ranked working fluids can be selected for further investigation. Ethanol combines high thermodynamic efficiency in different cases with a

lack of special toxicological or ecotoxicological issues. Hexamethyldisiloxane is especially attractive for high condensation temperatures (above 100 °C). R-152 is a synthetic refrigerant that combines an excellent net power output with reasonable constructional parameters. Alternatively, 1-propanol and cyclopentane are well-performing in a specific range of boundary conditions, whereas 1-propanol should be favored for high condensation temperature, cyclopentane for low ones.

4 Summary and Outlook

The complete PubChem database with more than 72 million chemical substances were screened to find an ideal working fluid for Organic Rankine Cycle in mobile applications like heavy duty trucks, passenger cars and the marine sector. The main results can be summarized as follows:

- Based on different filter criteria the set of suitable working fluids can be brought down to 3,175 chemical substances.
- Acetaldehyde can be identified as a thermodynamic "superfluid", however, it cannot be applied in real world conditions due to security aspects.
- A scoring system has been implemented to allow for a holistic evaluation of ORC working fluids based on thermodynamic, constructional, safety and regulatory aspects.
- Screening the complete chemical space of the PubChem database leads to well-performing and unconventional working fluids partly not known so far.
- A diverse set of best-ranked working fluids including alcohols (ethanol), refrigerants (R-152) as well as siloxanes (hexamethyldisiloxane) is suggested.

In a next step, the selected working fluids should be tested in small-scale test rigs and demonstration units. Furthermore, dynamic simulations are necessary to give more information about the behavior of the working fluids under typical operating conditions.

Acknowledgment. This work was financed by the Research Association of Combustion Engines (FVV) eV under project number 1155. The financial support is gratefully acknowledged by the authors.

References

1. Preißinger, M., Schwöbel, J., Klamt, A., Brüggemann, D.: Ideales fluid für rankine (fluid-design). In: FVV Herbsttagung, Forschungsvereinigung Verbrennungskraftmaschinen e.V., R572 (2015)
2. Klamt, A., Schüürmann, G.: COSMO: a new approach to dielectric screening in solvents with explicit expressions for the screening energy and its gradient. J. Chem. Soc. Perkin Trans. **2** (1993), 799–805 (2003)
3. Patel, N.C., Teja, A.S.: A new cubic equation of state for fluids and fluid mixtures. Chem. Eng. Sci. **37**, 463–473 (1982)

Assessment of Evaporators Used in Waste Heat Recovery Rankine Cycle Based Systems for Heavy Duty Truck Application

Vincent Grelet(✉) and Pierre Tipner

Tenneco GmbH, Clean Air Europe, Luitpoldstr. 83, 67480 Edenkoben, Germany
{vgrelet,ptipner}@tenneco.com

1 Introduction

Since the beginning of internal combustion engine development, engineers tackle the problem of losses into the exhaust gases. The gases exiting the combustion chamber are hot and pressurized. Recovering a part of the energy contained in those gases could be beneficial for the ICE efficiency.

In the seventies, the turbocharger, which was the first recovery system introduced in a vehicle, started to be widely used in the automotive industry (Ronan and Abernathy 1979). Its operation is pretty simple and well adapted to diesel engines. It is composed of two parts: a turbine expanding the pressurized gases and turning the expansion work into mechanical one. This turbine is mechanically linked to a compressor which increases the pressure of fresh air entering into the combustion chamber. Its introduction allowed manufacturers to reduce engine size, pollutant emissions and fuel consumption over the last decades.

Recently, new technologies such as turbocompounding, thermoelectric generators and thermodynamic bottoming cycles have been developed by engine makers (Saidur et al. 2012).

Turbocompounding has attracted a lot of interest in the automotive industry and especially for commercial vehicles during the last decade (Aghaali and Ångström 2015). When aircraft were propelled with piston engines (i.e. between the thirties and the fifties), the manufacturers established first turbocompound as fuel savings technology. It was well adapted due to the long hours of operation at constant load and the high expansion ratios at low ambient pressure obtained at cruise altitude. Later, with the massive introduction of turbines as aircraft propeller, the technology became obsolete but found applications in marine engines. Since then, the technology is mounted on ship and modern vessels engines can achieved total efficiency greater than 50 % (Hiereth et al. 2007). The first interest of road vehicle manufacturers about the technology dates back in the eighties. In 1991, Scania became the first original equipment manufacturer (OEM) to commercialize a turbocompounded engine. Since, more and more commercial vehicles have been released with the use of a turbocompound and various configurations have been developed (Aghaali and Ångström 2015).

Heat recovery systems are also strategic for OEM's (Saidur et al. 2012). Thermoelectric generators (TEG's) are one promising technology mainly due to

C. Junior et al. (eds.), *Energy and Thermal Management, Air Conditioning, Waste Heat Recovery*,
DOI 10.1007/978-3-319-47196-9_4

their apparent simplicity. TEG are based on the Seebeck effect and the properties of some materials which when they are subjected to a temperature difference at the joints, produce a potential difference in the joint circuit. This is called the thermo-current and thermo-electromotive force. Even if the phenomenon is well known, intensive researches are ongoing on the material properties to find the suitable materials for commercial vehicles and passenger cars (LeBlanc 2014).

Waste heat recovery systems (WHRS) based on thermodynamic bottoming cycles have attracted a high interest over the last ten years. Various bottoming cycles have been analyzed and compared from a thermodynamic principle point of view over the last years. Between Rankine, Brayton and Ericsson cycles, heat recovering devices based on the Rankine cycle result to be the most adapted system to the long haul truck application.

2 Rankine Process

An efficient way to recover the low grade waste heat from the internal combustion engine is the Rankine cycle (Stobart and Weerasinghe 2006). It uses the same principle than most of heat engines found in power generation plants and allows to convert heat into mechanical work. Different to the classical Rankine cycle which uses water as working fluid, the organic Rankine cycle (ORC) is referencing to carbon based media.

The Rankine cycle has been discovered by William John Macquorn Rankine and is based on the Carnot cycle. Instead of the two isothermal transformations, the ideal Rankine cycle is composed of two isobaric and two isentropic state changes.

- The pressure of the fluid in liquid state is increased by the pump work up to the evaporating pressure ($1 \rightarrow 2$) consuming power $\dot{W}_{f_{in}}$.
- The pressurized working fluid is pre-heated, vaporized and superheated ($2 \rightarrow 3c$) by recovering heat transfer rate $\dot{Q}_{f_{in}}$ from the heat source.
- The superheated vapor expands from evaporating pressure to condensing pressure ($3c \rightarrow 4$) in an expansion device creating mechanical power on the expander shaft $\dot{W}_{f_{out}}$.
- The expanded vapor condenses ($4 \rightarrow 1$) through a condenser (linked to the heat sink) releasing heat flow rate $\dot{Q}_{f_{out}}$.

Ideally the Rankine cycle operates closely to the Carnot cycle due to the isothermal phase change occurring during evaporation and condensation process. In reality, the Rankine cycle used in waste heat recovery system differs from the ideal Rankine cycle due to the irreversibilities in the different components. The main sources of irreversibility are:

- Losses during compression and expansion due to friction, leakages, etc.
- Pressure drops in the heat exchangers and pipings due to friction.
- Heat losses to the ambient due ton non adiabatic components.
- Irreversibilities due to finite temperature differences in heat exchangers.

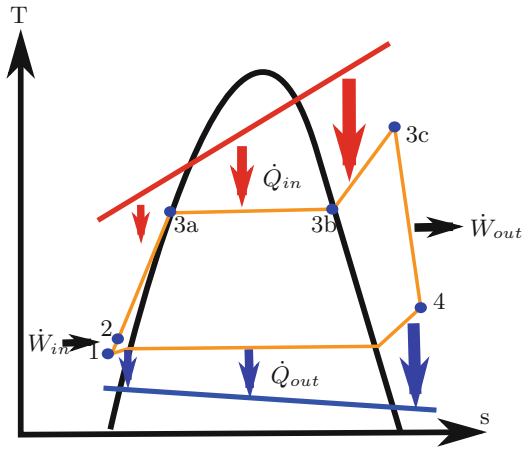

Fig. 1. Temperature-entropy diagram of the ideal Rankine cycle

A classical representation of the Rankine cycle is done through its associated temperature entropy (T-s) diagram shown in Fig. 1. This one is practical since it gives a rough estimation of the cycle efficiency. The highest efficiency is obtained when the cycle looks like a rectangle on the T-s diagram. Indeed, the more rectangular, the closer from the Carnot cycle. In reality, a net output power maximization is preferred which is not always in line with an efficiency maximization.

3 System Overview

Rankine cycle based WHR systems consist in using a Rankine cycle to recover waste heat from the internal combustion engine. Nowadays vehicles are powered with reciprocating internal combustion engines where engine efficiency and fuel consumption are more and more prioritized in the overall vehicle's performance evaluation.

In the early seventies, during the first oil shock, first developments have been done in the field of Rankine bottoming cycle. The most advanced project was certainly the ThermoElectron project reported in (Doyle and Kramer 1979), where a prototype has been built and tested on road during a year. A Mack 676 diesel engine has been compounded with an ORC, recovering heat from the exhaust gases. Road tests have demonstrated up to 15 % fuel efficiency improvement and a drop in noxious emissions equal to the gain in efficiency. As the oil prices came back to their pre-crisis level after 1980, fuel efficiency became less important for truck manufacturers. As a consequence, the need for such technology was null and the program was canceled.

No work is reported until the early nineties, where the Iraqi invasion of Koweit created a rapid raise in petrol price. Some companies restart to investigate the Rankine cycle as solution to reduce the fuel consumption. The most interesting

project during this time frame is the work reported in (Oomori 1993) applying the Rankine cycle to a passenger car. The engine was acting as a boiler and the traditional engine cooling system was turned into an evaporative cooling system. This was done to simplify the Rankine system and remove the needs of an external evaporator. Results indicate a fuel economy of 3 % under normal operating conditions.

Until the beginning of 21st century, no major research nor development activities have been reported. Since then, all major actors of the automotive industry have demonstrated an interest for this technology: AVL (Teng et al. 2007), BMW (Freymann et al. 2008), Cummins (Dickson et al. 2014), Honda (Ibaraki et al. 2007), Volvo trucks (Espinosa 2011) and many other. Several demonstrators are today running around the globe and proving that the technology could lead to a large benefit in fuel consumption. Since 2010, the US Department Of Energy (DOE) is funding the Supertruck program which aims to develop and demonstrate an engine with at least 50 % brake thermal efficiency (BTE). Four companies were at that time selected to participate to this program: Cummins, Detroit Diesel, Navistar and Volvo. In 2015, first press release about the result were impressive (Daimler Trucks North Amercia 2015). Fuel savings of more than 10L/100 km were announced wherein WHRS contribution was evaluated to about 1.5 L/100 km.

If the system has proven itself to be efficient to decrease the fuel consumption, it is not yet cost effective for mass production. Recent studies have identified tailpipe evaporator as a cost stopper since it could represent more than a third of the total system price. If this components has been widely studied and optimized recently (Karellas et al. 2012), no global optimization of that latter has been proposed.

4 Evaporator Concepts and Design Optimization

Due to vehicle implementation constraints numerous investigations have been done on the plate evaporator (Latz et al. 2015) which can offer high performance in a limited volume since it is made of a plate stack (meaning the heat transfer area can be obtained by an increase in height and not in length) but other concepts can be found such as shell and tube and double tube (DT) evaporator (Ambros and Fezer 2014).

The aim of this study is to compare the three different concepts from a performance point of view but also from their ability to decrease total system cost and make the system more profitable for the end user. Plate and fin (PF), shell and tube (ST) and double tube concepts are designed, modeled and simulated on some typical heavy duty engine operating points. Then the manufacturability is assessed based on some assumptions regarding the manufacturing process (brazing, welding, ...) and actual material prices. Using a simple top to bottom approach on current heavy duty market the three different concepts are ranked on their ability to make the system cost effective. Figure 2 shows an overview of the double tube and plate and fins evaporator concepts whereas the shell and tube can be seen as a DT without any internal gas flow.

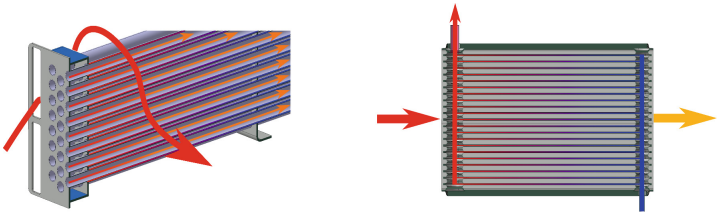

Fig. 2. Overview of the investigated evaporator concept: DT (left) and PF (right)

Performance comparison of each concept is based on two indicators: the heat exchange efficiency calculated according to (Legros et al. 2014) and a new non dimensional number taking into account as well the heat flow rate transferred to the working fluid as the evaporator weight and volume, the exhaust gas back-pressure and working fluid mass flow. That performance index PI is equal to:

$$PI = \frac{\dot{Q}_f^{\frac{3}{2}} \ \dot{m}_f^{\frac{1}{2}}}{\Delta P_g^{\frac{1}{2}} \ M^{\frac{3}{2}} \ V^{\frac{1}{2}} \ g^2}, \tag{1}$$

where $\dot{Q}_f$ is the recovered heat flow rate by the working fluid, $\dot{m}_f$ is the working fluid mass flow rate, ΔP_g is the exhaust gas backpressure, M is the evaporator mass, V is the evaporator volume and g the gravity constant. It is shown that the introduced non dimensional number allows to better evaluate and compare the different evaporator types.

Then starting from some assumptions concerning the manufacturing process and material prices a cost is evaluated and the specific projected cost SPC (ratio of projected cost on heat flow rate recovered) is calculated for the three evaporator concepts. The SPC is calculated according to:

$$SPC = \frac{C_{ev}}{\dot{Q}_{f,d}}, \tag{2}$$

where C_{ev} is the cost of the considered evaporator ($ev = plate, shell, DT$) and $\dot{Q}_{f,d}$ corresponds to the heat flow rate recovered on the design point.

4.1 Evaporator Modeling

In order to properly assess the evaporator performance, a detailed model is built using a well known commercial simulation environment in the automotive industry: GT Power. The model using modified literature correlations to predict the heat transfer and pressure drop in both working and transfer media. This model is using a finite volume approach where the number of discretization is chosen to ensure a good trade off between model performance and simulation time. The implicit solver is then resolving mass, energy and momentum conservation principle in each discrete volume in order to calculate the fluid properties at the outlet of the cell.

4.2 Design Constraints

The evaporator design are here submitted to both performance and packaging constraints to fairly compare the three investigated concepts. These latter are listed below:

- Maximum exhaust gas pressure drop shall remain below 50 mbar.
- Maximum working medium pressure drop shall remain below 1500 mbar.
- Heat exchanger core length shall be lower than 600 mm.
- Heat exchanger weight shall be lower than 40 kg.

4.3 Performance Assessment

First of all, the engine operating point on which the evaporator is designed is selected as being the most representative of a long haul truck usage. The 13 L heavy duty engine is tested on the European stationary cycle (ESC) on which the engine operating point used for design of the evaporator is selected. Indeed, following a simple approach for vehicle modeling, the required engine power to pull a mass of 33 tons (corresponding to 75 % of the maximum gross vehicle weight rating in Europe) is calculated. This power corresponds to the traction force needed to drive a vehicle with the following parameters over a flat road at a speed of 80 km/h:

- Frontal area: 7.5 m^2
- Drag coefficient: 0.78
- Tire rolling resistance coefficient: 8 kg/metric tons
- Driveline efficiency: 0.85
- Mechanical accessory consumption: 7.5 kW

Figure 3 shows the exhaust mass flow rate and temperature on the 13 operating points of the ESC. Among the 13 tested engine operating points the number 5 is further referred as design point.

Then the evaporator concepts are optimized on the design operating point with the objective to maximize the heat flow rate recovered by the working fluid. In order to do so, a complete design study is performed in order to check on the influence of the different design parameters. The design parameters of each concept are listed below:

- Double tube:
  - Tube diameters (internal and external)
  - Tube pattern
  - Tube length
- Plate and fins:
  - Plate dimensions
  - Fins (working fluid and exhaust side)
  - Passage height

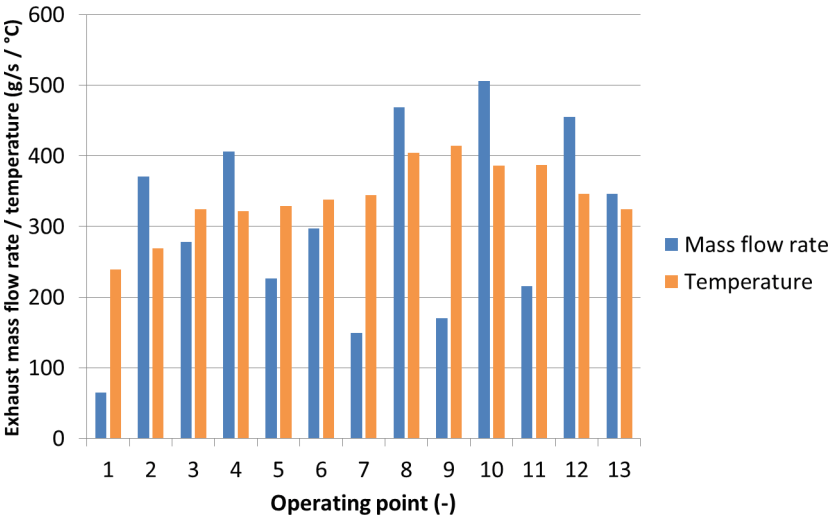

Fig. 3. Exhaust mass flow rate and temperature over ESC

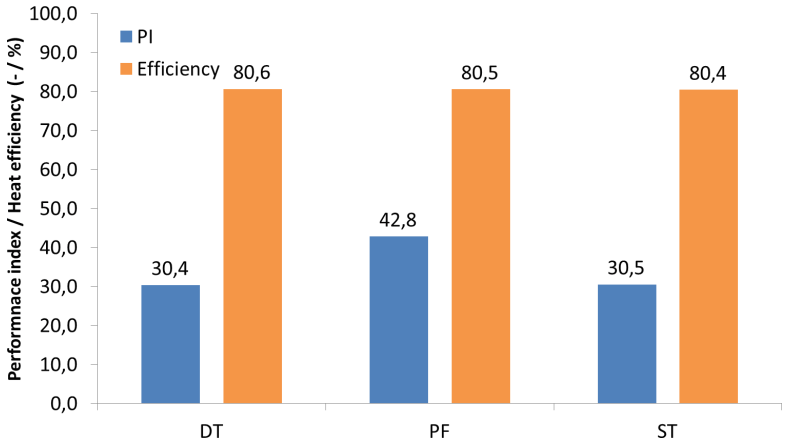

Fig. 4. Performance index and heat exchange efficiency

– Shell and tube:
  - Tube diameter
  - Tube pattern
  - Tube length

After solving the optimization problem the performance index and the heat exchange efficiency can be plotted for each evaporator concept (see Fig. 4).

As it can be seen on Fig. 4, the heat exchange efficiency are more or less the same for each concept. Indeed, this indicator does not take into account any packaging data nor other performance figures than the heat exchanged

(Legros et al. 2014). The new introduced performance index (Eq. (1)), shows difference from concept to concept since it includes as well packaging and backpressure data. The plate and fins concept shows the higher PI due to the compactness of such evaporator. In addition, it is possible to ensure a good trade off between exchanged heat flow rate and exhaust gas pressure drop by selecting appropriate fins on both side. Concerning the DT and ST concepts, it can be seen that the PI is in the same range. This is due to the fact that, in the DT concept, the low backpressure achieved by the optimized concept is balanced by the higher weight (and vice-versa for the ST) due to the concentric tubes. In conclusion, it is shown that no real optimized concept exists but the evaporator design results from a compromise between performance, installation requirements and costs.

5 Economical Estimation

Once the evaporators design are frozen, the specific projected cost for each concept is evaluated. First some assumptions are made concerning the production volume, the materials and manufacturing process. Then using the SPC for each concept is calculated and put into balance with some additional operating cost due to the increase in exhaust backpressure and weight induced by the evaporator.

5.1 Assumptions

Below are listed the assumptions used to calculate the specific projected cost.

- Double tube:
  - Production volume: 15000 pieces per year
  - Material: Stainless steel
  - Manufacturing process: welding
- Plate and fins:
  - Production volume: 15000 pieces per year
  - Material: Stainless steel
  - Manufacturing process: brazing
- Shell and tube:
  - Production volume: 15000 pieces per year
  - Material: Stainless steel
  - Manufacturing process: welding

5.2 Specific Projected Cost Calculation

Using internal material and supplier database, the material cost is first assessed for each concept. Then, using the manufacturing process assumed for DT, PF and ST, the specific projected cost is calculated for the three previously designed evaporators. For sake of confidentiality, the SPC is normalized over a base ten with the double tube as reference.

As it can be seen on Fig. 5 the specific projected cost can not be correlated to the evaporator weight. Indeed, the use of fins and the assumed manufacturing

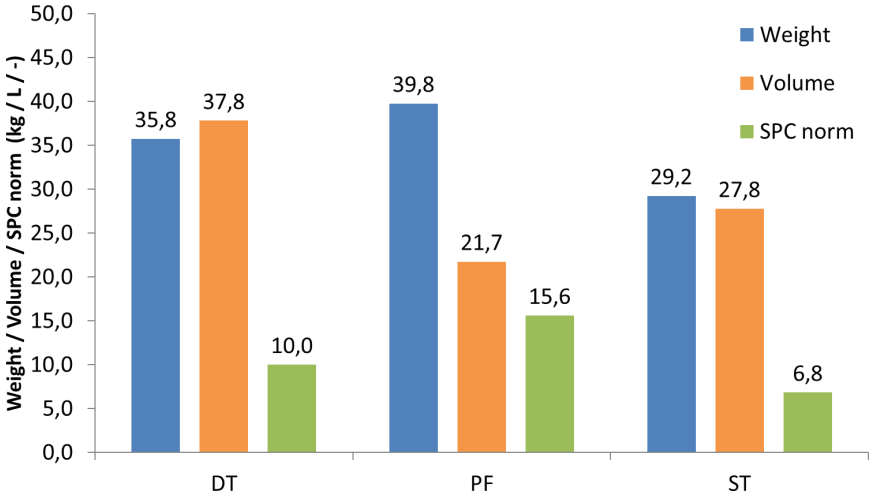

Fig. 5. Weight, Volume and SPC for each concept

process for the plate and fins concept result into a higher SPC. From this analysis, the ST evaporator concept seems more favorable from an economic perspective. This shall obviously be put into perspective with other aspects such as the additional consumption due to the increase in exhaust line backpressure and in weight.

Using an engine model built in GT Power the relation between fuel consumption and exhaust line backpressure can be drawn (see Fig. 6).

In addition, the relation between additional weight and fuel consumption is calculated using the official tool for greenhouse gas (GHG) emissions and fuel efficiency performance of heavy duty vehicle released by the environmental protection agency (EPA) in the frame of the future GHG Phase 2 standards in the United States (EPA 2016). This tool assessed the additional fuel consumption to 7.10^{-4} l/100 km/kg. Using those two data the influence of each concept over the fuel consumption can be calculated. Figure 7, shows the contribution of both weight and additional exhaust line backpressure to the increase in fuel consumption due to the installation of the evaporator. If the weight contribution can be considered as negligible, one should pay attention to the backpressure contribution since that latter can represent up to 0.58 % for the ST concept.

When calculating the yearly cost associated to those contribution (assuming 100000 Km a year and a fuel price of 1€/l), the following figures can be calculated (see Table 1):

These numbers shall be interpreted with attention since they do not reflect the additional benefit due to the complete Rankine cycle based exhaust heat recovery system but only the fuel consumption increase due to the evaporator installation.

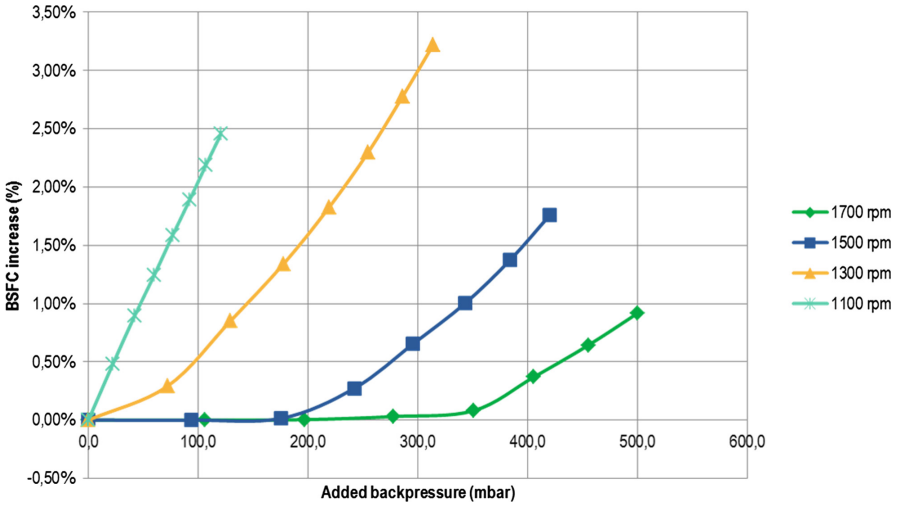

Fig. 6. Relation between additional backpressure and BSFC for various engine speed

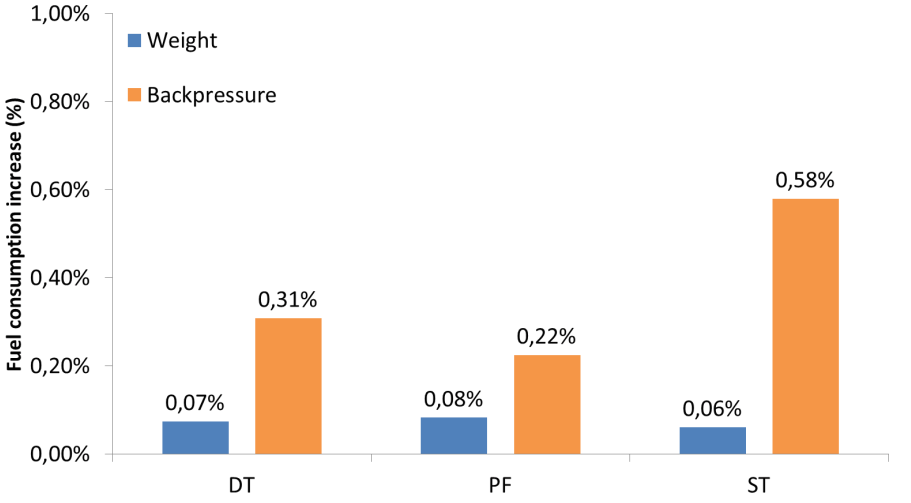

Fig. 7. Weight and backpressure contribution to the additional fuel consumption

Table 1. Additional operating cost due to the evaporator installation

Concept		DT	PF	ST
Additional operating cost due to weight increase	€	35.79	39.80	29.27
Additional operating cost due to backpressure increase	€	149.55	109.04	281.33

6 Conclusion and Next Steps

This work brings a first step concerning cost evaluation of evaporators used in Rankine cycle based exhaust heat recovery systems. By means of the newly introduced performance index, the superiority in terms of performance of the plate and fins concept is shown. Although the DT shall bring some advantages in terms of heat transfer area, it is shown that similar PI can be achieved with a ST evaporator. However this number shall be analyzed carefully since it assumes that every of its components are on the same level. Indeed, it is shown that backpressure and weight added to the exhaust line by the evaporator result into higher operating cost but other PI components are not analyzed here (e.g. mileage reduction due to fuel tank removal in order to integrate the evaporator).

The specific projected cost of the three studied concepts is also calculated in order to rank these latter between them. It is shown that SPC and weight can not be correlated since manufacturing and composing elements of the evaporator takes an important place in that calculation. Nevertheless, when calculating the additional operating cost induced by each concept it becomes clear that the SPC shall integrate more quantity in order to take into account the increase in operating cost due to the evaporator integration in the vehicle.

Next study should focus in defining new indicators that could be used to compare evaporators on a more global basis. A thermo-economic optimization shall also be done in order to understand the trade off between performance and SPC.

Acknowledgements. The authors gratefully acknowledge Tenneco GmbH for their support, F. Terres, M. Glas, M. Miersch and V. Brennion for their contribution and help during this study and the reviewing phase.

References

Aghaali, H., Ångström, H.-E.: A review of turbocompounding as a waste heat recovery system for internal combustion engines. Renew. Sustain. Energy Rev. **49**, 813–824 (2015)

Ambros, P., Fezer, A.: Twin round tube evaporator for waste heat recovery. MTZ Worldwide eMag. **75**(1), 36–39 (2014)

Daimler Trucks North America, Freightliner supertruck presentation (2015)

Dickson, J., Ellis, M., Rousseau, T., Smith, J.: Validation and design of heavy vehicle cooling system with waste heat recovery condenser. SAE Int. J. Commercial Veh. **7**, 458–467 (2014)

Doyle, E., DiNanno, L., Kramer, S.: Installation of a diesel-organic rankine compound engine in a class 8 truck for a single-vehicle test. In: SAE Technical Paper, number 790646, SAE International (1979)

EPA, Greenhouse Gas Emissions Model (GEM) for Medium- and Heavy-Duty Vehicle Compliance (2016)

Espinosa, N.: Contribution to the study of waste heat recovery systems on commercial truck diesel engines. Ph.D thesis, University of Liege, National Polytechnic Institute of Lorraine (2011)

Freymann, R., Strobl, W., Obieglo, A.: The turbosteamer: a system introducing the principle of cogeneration in automotive applications. MTZ Worldwide **69**(5), 20–27 (2008)

Hiereth, H., Drexl, K., Prenninger, P.: Charging the Internal Combustion Engine. Springer, Heidelberg (2007)

Ibaraki, S., Endo, T., Kojima, Y., Takahashi, K., Baba, T., Kawajiri, S.: Study of efficient on-board waste heat recovery system using rankine cycle. Rev. Automot. Eng. **28**(3), 307–313 (2007)

Karellas, S., Schuster, A., Leontaritis, A.-D.: Influence of supercritical ORC parameters on plate heat exchanger design. Appl. Thermal Eng. **33–34**, 70–76 (2012)

Latz, G., Erlandsson, O., Skare, T., Contet, A., Andersson, S., Munch, K.: Water-based rankine cycle waste heat recovery systems for engines: challenges and opportunities. In: 3rd International Seminar on ORC Power Systems (ORC15) (2015)

LeBlanc, S.: Thermoelectric generators: linking material properties and systems engineering for waste heat recovery applications. Sustain. Mater. Technol. **1–2**, 26–35 (2014)

Legros, A., Guillaume, L., Diny, M., Zaïdi, H., Lemort, V.: Experimental investigations of the valorization of the exhaust waste heat of a gasoline engine based on a rankine cycle (2014)

Oomori, H., Ogino, S.: Waste heat recovery of passenger car using a combination of rankine bottoming cycle and evaporative cooling system. In: SAE Technical Paper, number 930880, SAE International (1993)

Ronan, L., Abernathy, W.: The development and introduction of the automotive turbocharger: A case of innovation in response to fuel economy regulation. Technical report (1979)

Saidur, R., Rezaei, M., Muzammil, W., Hassan, M., Paria, S., Hasanuzzaman, M.: Technologies to recover exhaust heat from internal combustion engines. Renew. Sustain. Energy Rev. **16**(8), 5649–5659 (2012)

Stobart, R., Weerasinghe, R.: Heat recovery and bottoming cycles for si and ci engines - aperspective. In: SAE Technical Paper, SAE International (2006)

Teng, H., Regner, G., Cowland, C.: Waste heat recovery of heavy-duty diesel engines by organic rankine cycle part I: Hybrid energy system of diesel and rankine engines. In: SAE Technical Paper, SAE International (2007)

Integration of a Piston Expander for Exhaust Heat Recovery in a Long Haul Truck

Rémi Daccord(✉), Julien Melis, Antoine Darmedru, Edouard Davin, Antoine Debaise, Brice Mandard, Alexandre Bouillot, Stéphane Watts, and Xavier Durand

Exoès, Gradignan, France
remi.daccord@exoes.com

Abstract. Nearly 30 percent of the fuel energy in an internal combustion engine is lost as waste heat in the form of hot exhaust gases. Nowadays it seems clear that the heavy duty manufacturers will implement bottoming Rankine cycles to recover the exhaust heat on their long haul trucks in the 2020s as an answer to future stringent regulations and the still increasing customer pressure for reductions in operating costs.

The Exoès Company has developed a swashplate expander working with ethanol or refrigerant vapors for Rankine cycles that would provide 3 to 5 % fuel economy on heavy duties. The design of a swashplate piston expander has been carried out. A prototype has been built as well as a test bench that can reproduce the hot source and cold sink available in a truck. The performance tests of the prototype took place in 2015. A refined 1D Matlab physical model has been coded and calibrated to point out the different efficiency losses. A first feedback loop improved the general prototype design to increase efficiency, lower the weight and better the packaging so that the prototype is ready to be integrated and tested in a demonstration truck.

In this paper, we present the expander technology, the test results, the expander model and its calibration. The performances of the expander will be assessed as well as the detailed losses repartition. The choices made for the integration in the vehicle will be detailed. To conclude the paper, a dynamic simulation on a driving cycle will explain how the expander optimization is done.

Keywords: Exhaust heat recovery · Heavy duty vehicles · Piston expander · Tests · Simulation · Demonstration truck · Dynamic modeling

1 Introduction

Up to now, the focus has been cast on regulating local pollutants emitted by internal combustion engine (ICE). However, future regulations will also target CO_2 emissions and thus fuel consumption. While today the best efficiency of a modern ICE remains below $\sim$ 42 % (Fig. 1), electrification of ancillaries and hybridization would be too expensive to meet regulation thresholds on long haul trucks compared to air drag reduction and waste heat recovery (WHR). Given the fact that heavy commercial vehicles (HCVs) aerodynamic is mostly constrained by regulation and also depends on trailer manufacturers, WHR appears as essential in the future innovation panel of truck OEMs.

C. Junior et al. (eds.), *Energy and Thermal Management, Air Conditioning, Waste Heat Recovery*,
DOI 10.1007/978-3-319-47196-9_5

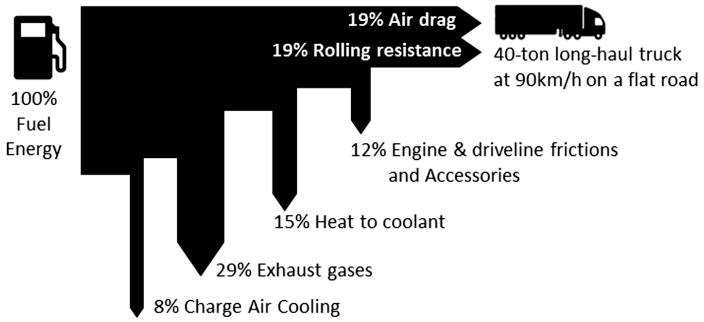

Fig. 1. Sankey diagram - energy repartition on a HCV [1]

2 Rankine Cycles for WHR

Among several technologies for WHR, Rankine cycles (RCs) seem promising to win the competition regarding their efficiency, cost and maturity. The key components of a RC are shown hereafter (Fig. 2).

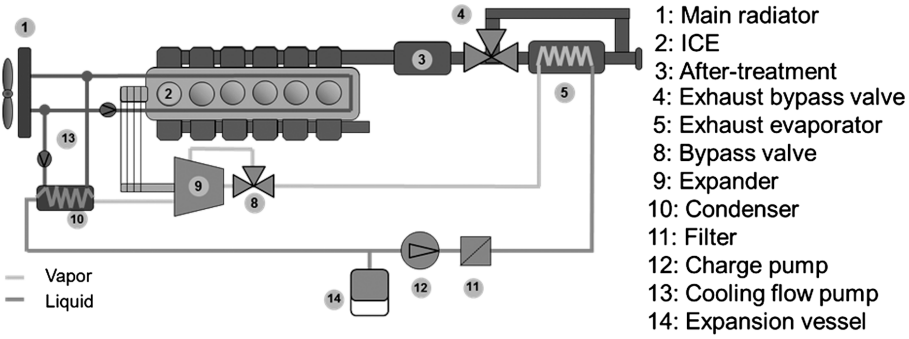

Fig. 2. Typical layout of a bottoming RC on a HCV exhaust line

In this paper, options are taken *a priori*. The working fluid of the RC is an ethanol-based mixture. The expander developed by the Exoès Company is a piston type which is mechanically linked to the ICE re-injecting its torque to spare fuel. We deliberately decided to use the existing ICE cooling loop to avoid an additional front radiator and to be more versatile.

3 The Expander

3.1 Expander Technology

The expander, called EVE-T, is built around three double acting crosshead pistons arranged around a swash plate (Fig. 3). More details can be found in a previous paper [2].

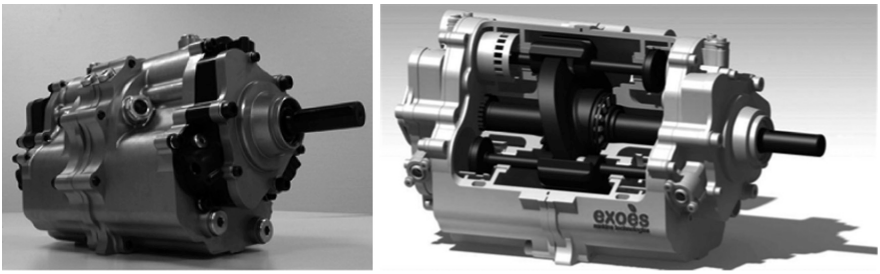

Fig. 3. EVE-T expander swashplate technology

A Matlab 1D model was coded and calibrated [2]. This model showed a good accuracy (Fig. 4) to assess the expander efficiency, calculated as follow:

$$\eta_{is} = \frac{\dot{W}_{shaft}}{\dot{M}.(1 - OCR).(h_{in} - h(P_{out}, s_{in}) + (\frac{\dot{M}.OCR}{\rho_{oil}}).(P_{in} - P_{out})} \quad (1)$$

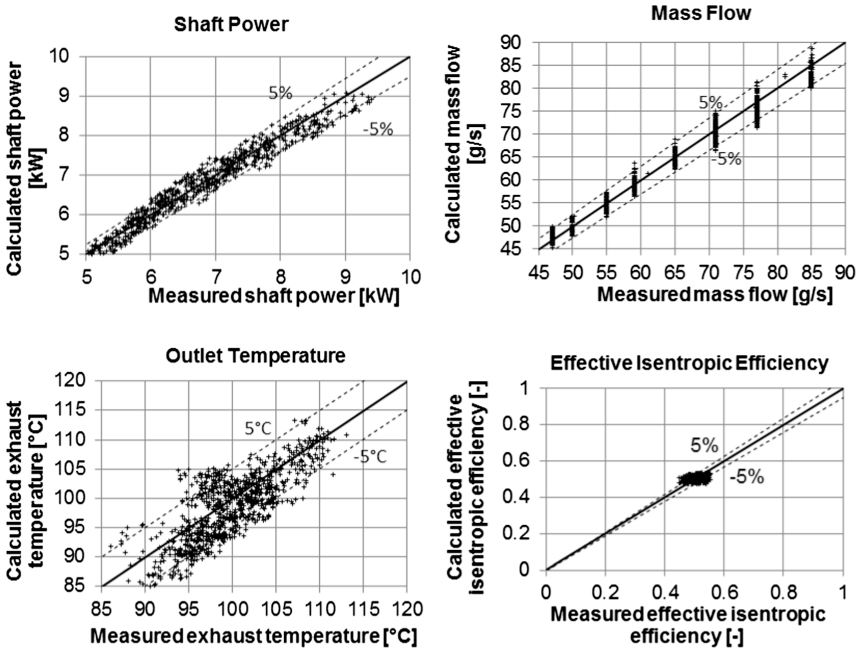

Fig. 4. Matlad 1D model calibration results (996 measure points)

3.2 Expander Losses Analysis

The model enabled to assess the origins of the major losses. In Fig. 5, the impact of each loss is plotted against the pressure ratio. One can see that the expander suffers from friction and internal transfers. The heat transfer is for a large proportion due to the cooling of the inlet vapor by a sort of internal thermal short-circuit between hot inlet and cold outlet. Regarding the friction, the Fig. 6 details that piston rings and sliding shoes on the plate are responsible for most of it, but still the mechanical efficiency in cruise point remains above 90 %. On this first generation of expander, the driver to improve efficiency was then to reduce the internal heat transfers.

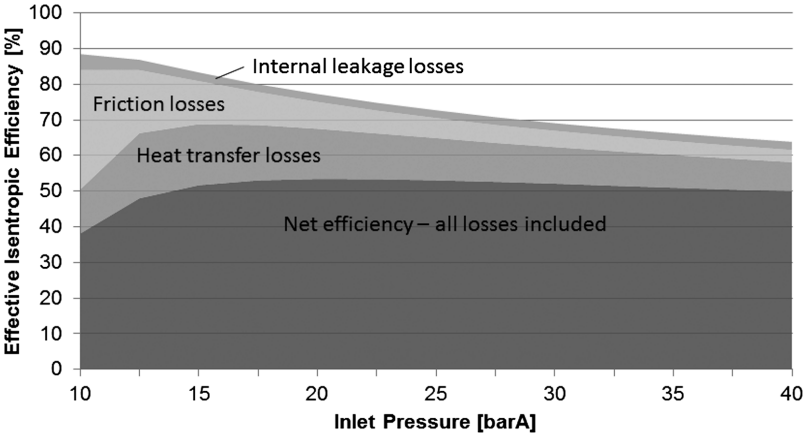

Fig. 5. Losses distribution in the expander EVE-T Speed = 2,400 rpm – Pout = 1 bar – Superheat = 20°C

4 Expander Integration in a Truck

4.1 Mechanical Coupling

In order to prove the technology, it was decided to implement it in a demonstration truck. The development of the coupling to the ICE was carried out for that purpose. The connection of the expander is preferably located at the back of the engine on one of the available power-take-off because the front side of the engine is always overcrowded and it would add more weight on the front axle which is detrimental to the trailer filling load capability. Given the fact that the best location of the expander in a RC is to be at the highest point above the condenser and the evaporator, we decided to use a belt, as shown in Fig. 7, to raise the expander and place it where space is available below the cabin.

The expander is linked to the evaporator through a bypass valve. In order to accommodate easily the components in the truck it has been decided to attach this valve on the expander itself which should anticipate the future development with a bypass valve integrated into the expander.

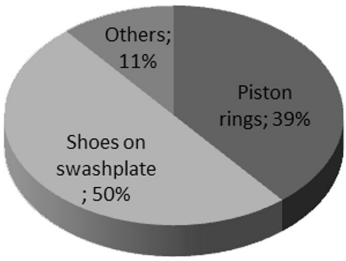

Fig. 6. Friction losses repartition in the expander EVE-T. Speed = 2,400 rpm – Pin = 25 bar – Pout = 1 bar – Superheat = 20°C. Total friction losses = 579 W

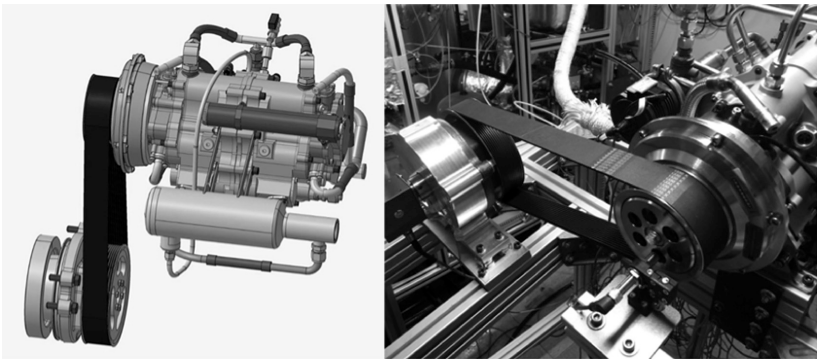

Fig. 7. Coupling 3D model and its associated tests rig

Even though the expander can start by itself when high pressure vapor is sent to its inlet, it has been decided for this first application to use an electromagnetic clutch instead of a freewheel to actively disconnect the expander from the engine. Indeed, the disconnection is required especially at start when the RC is cold. To prevent air to penetrate the system, the Rankine loop is filled with liquid ethanol to insure a positive pressure balance to the ambient. No expander can spin flooded with liquid when the driver starts the ICE. Instead a heat-up period is needed to prepare the vapor that would drain the liquid out and warm the expander. According to the truck load, this heat-up phase can last from 3 to 20 min (Fig. 8). During this phase the vapor is bypassed and sent to the expander crankcase. Once a temperature threshold is overpassed in the expander, then the valve is commuted to expander inlet and the clutch is activated.

4.2 Expander Efficiency Optimization on Operating Ranges

To anticipate the expander behavior on the truck, a dynamic model on Simulink has been built in-house and is based on the work of these two papers [3, 4]. The four main components have been coded: a volumetric pump, a finite volume model of the evaporator, a polynomial model of our expander, a model of a vapor volume to modify

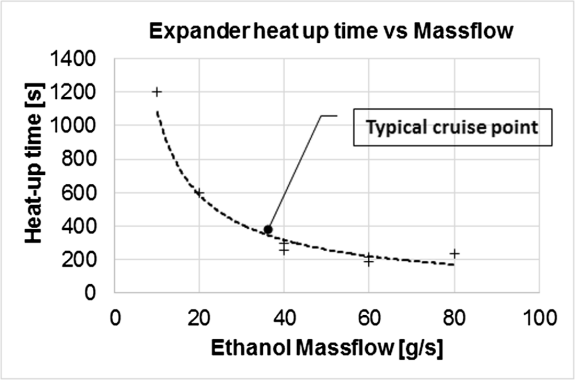

Fig. 8. Heat-up time of the expander EVE-T

the system evaporating pressure and a finite volume model of the condenser. The cooling temperature is set constant for this simulation.

Public data of a "rolling hills" driving cycle [5] (Fig. 9) were used. This cycle is showing quite slow transients. So a simple PI controller with variable parameters was used to control the superheating by adjusting the pump speed (Fig. 10). For highly transient behavior, it is clear that a better controller should be set up.

What interests us in this paper is the expander boundaries range. Unlike the speed and the outlet pressure, the inlet pressure and the massflow are fluctuating a lot (Fig. 11). Assuming constant speed and constant outlet pressure, a simple linear relation can be asserted between the massflow and the shaft power of the expander, and

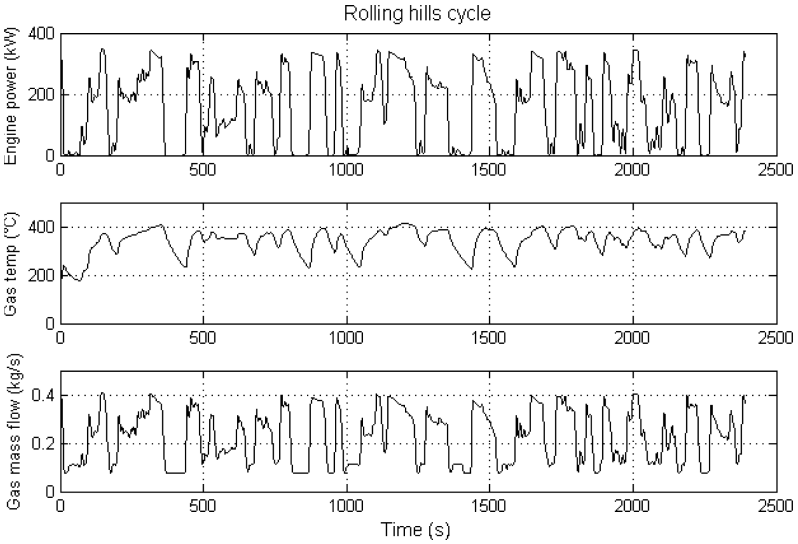

Fig. 9. "Rolling hills" driving cycle [5]

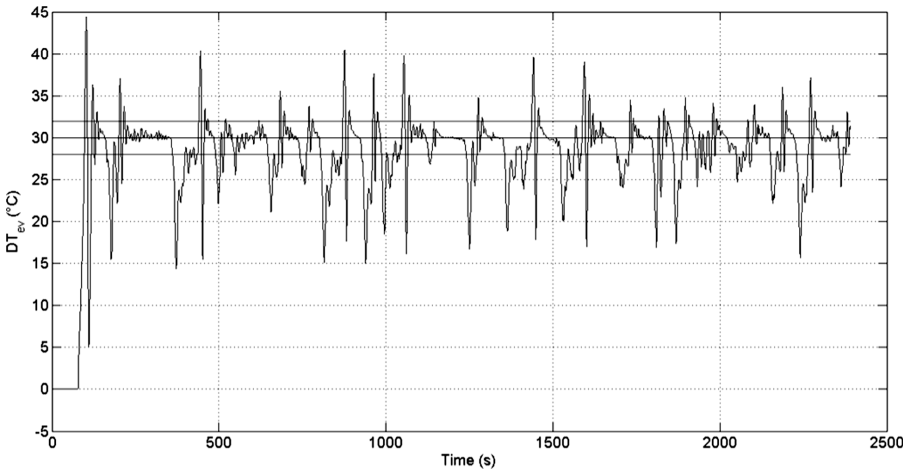

Fig. 10. Superheating control through simple PI control with variable parameters

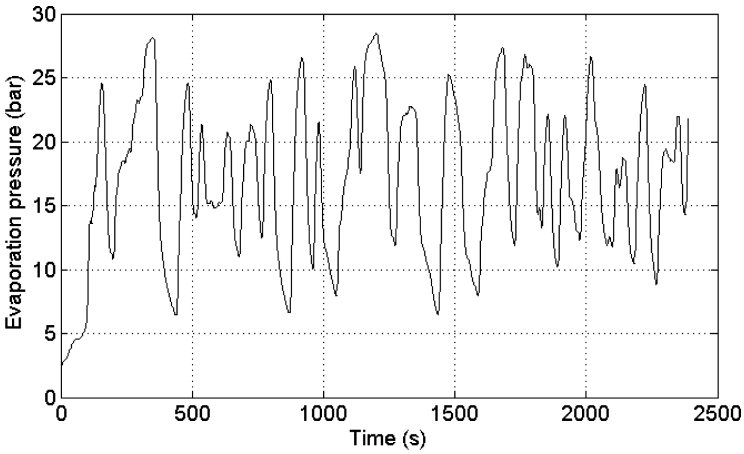

Fig. 11. Inlet pressure variation range over the driving cycle

the massflow and the inlet pressure. Then we can only consider one variable to assess if the expander is well suited for the truck application and assess whether it is used in its nominal massflow range at maximal efficiency or not.

In case the expander is not used in its appropriate range, there are possibilities to tune it and to adjust it to the application. Our designers can play on the valve timing and the dead volume (volume at the top dead center) (Fig. 12) in order to modify the relation between inlet pressure and massflow and to set the expander maximal efficiency on a different point.

In Fig. 13, we can see the impact of an increase of the dead volume: Increasing the dead volume tends to increase the massflow consumed by the expander at a given inlet

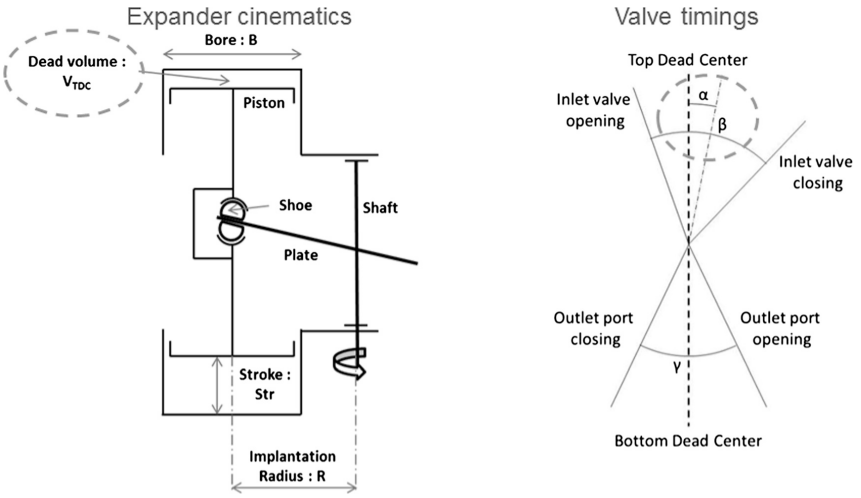

Fig. 12. Adjustable parameters of the expander

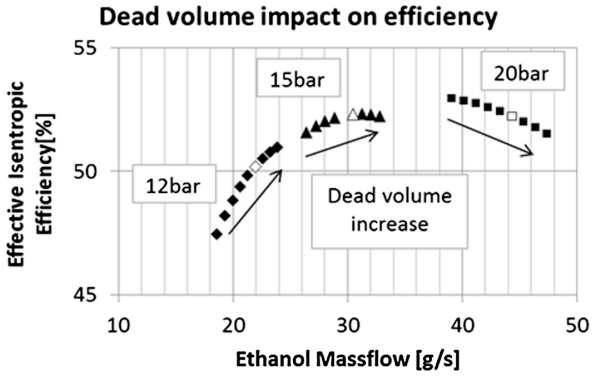

Fig. 13. Impact of a dead volume increase on the relation between inlet pressure and massflow

pressure. It means that in average in the driving cycle, the evaporating pressure will be lower.

However the optimization process of the expander is not straight forward and cannot be done apart from the rest of the components. For example a change in the mean evaporating pressure, will change the optimal massflow that the evaporator can evaporate and will change the pump consumption. The fuel savings depend on the joint work of these 3 components. It is then necessary to run again the dynamic model to compare different expander configuration and chose the best one that optimize the net power of the RC (Fig. 14).

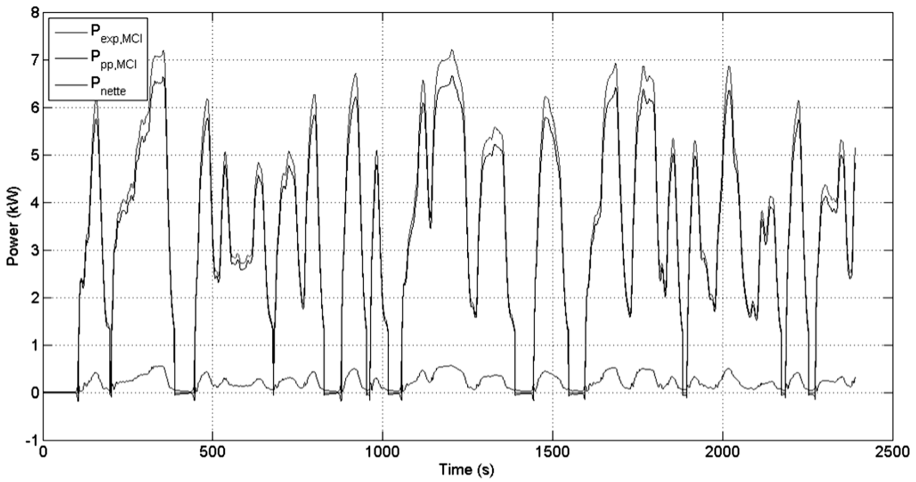

Fig. 14. Power variation during the driving cycle: expander, pump and net power (= expander minus pump power)

5 Conclusion

A new expander prototype has been presented that shows promising results, proving that piston expanders are a flexible and robust technology perfectly suited for the vehicle exhaust heat recovery. This expander has been optimized to enhance the fuel economy not only on stationary conditions but also on transient driving cycles. Though the potential of WHR is clear, the technology has to prove the business, durability and safety cases to be widely spread in the next decade.

1 Nomenclature, Subscripts and Abbreviations

h specific enthalpy [J.kg−1]

$\dot{M}$ flow [kg/s]

P pressure [bar]

s specific entropy [J.T−1.kg−1]

T temperature [K]

$\dot{W}$ work [kW]

η efficiency

ρ density [kg.m3]

HCV heavy commercial vehicle

OCR Oil Circulating Rate (%mass)

ICE internal combustion engine

RC Rankine cycle

WHR waste heat recovery

in relative to the expander inlet

is isentropic

out relative to the expander outlet

oil relative to lubricant

References

1. Espinosa, N., Lejeune, M.: Rankine system for long haul trucks application. SIA powertrain–Renault trucks plant (2014)
2. Daccord, R., Mélis, J., Darmedru, A., Debaise, A., Kientz, T., Davin, E.: A piston expander for exhaust heat recovery on heavy commercial vehicles. In: FISITA World Automotive Congress, F2016-ESYE-012 (2016)
3. Feru, E.: Auto-calibration for efficient diesel engines with a waste heat recovery system. Ph.D. thesis, TNO Nederlands (2015)
4. Grelet, V.: Rankine cycle based waste heat recovery system applied to heavy duty vehicles: topological optimization and model based control. Ph.D. thesis, Lyon University and Liège University (2016)
5. Luong, D.: Modeling, estimation, and control of waste heat recovery systems. Ph.D. thesis, Univeristy of California (2013)

Air-Conditioning, Thermal Comfort

Energy-Efficient Climate Control in Electric Vehicles Through Innovative Sensor Technology and Novel Methods for Thermal Comfort Evaluation

Henning Metzmacher(✉), Daniel Wölki, Carolin Schmidt, Jérôme Frisch, and Christoph van Treeck

Institute of Energy Efficiency and Sustainable Building (E3D), RWTH Aachen University, Aachen, Germany
metzmacher@e3d.rwth-aachen.de

Abstract. The increasing emission of greenhouse gases caused by a growing global rate of motorization contributes substantially to global warming and climate change. Germany aims to cut CO2 emission by 80% by the end of 2050 (BMWi 2012). In order to reach this goal, the transportation sector has to make a significant contribution. The required energy for engines in electric vehicles can be harvested from regenerative energy sources, therefore offering an opportunity for the reduction of greenhouse gas emissions. This work introduces a system for intelligent thermal management and energy-efficient climate control in electric vehicles adopting a sensor-based evaluation of individual thermal comfort of each passenger. By deriving individual measures for each person, the overall vehicle air conditioning system operates at much lower energy levels, which results in a drastic reduction of energy consumption and hence an increase in the driving range of the vehicle.

In order to evaluate the individual thermal comfort of each passenger, novel and innovative sensor technology is used. The paper presents a method for fusing temperature and humidity sensor information as well as different types of optical and thermal infrared sensors, proposing a structured approach to merge and evaluate the acquired data. The system itself consists of four consecutive sub-processes. Initially, camera-based sensors recognize the gestures and infrared signature of each passenger. Seat mounted heat and moisture sensors detect zonal microclimates at the interface between the seat surface and a person, thus completing the overall picture. In a subsequent step, this information is merged and pre-processed using a central software abstraction layer. The processed information is passed to high-level mathematical models in order to generate an accurate evaluation of the overall and local thermal condition of each passenger including the thermal physiology. Finally, individual control variables for local climate control are computed and sent to the vehicle's air condition system. Furthermore, each passenger has the opportunity to give feedback on its individual thermal comfort level, which is subsequently used to individualize the prediction model for each passenger.

Keywords: Human thermal comfort · Sensor fusion · Face detection · Pose detection · Thermography · Intelligent climate control · Model predictive control

C. Junior et al. (eds.), *Energy and Thermal Management, Air Conditioning, Waste Heat Recovery*,
DOI 10.1007/978-3-319-47196-9_6

1 Introduction

Modern passenger transportation greatly relies on air-conditioning in order to keep the vehicle cabin at a healthy and comfortable indoor temperature. Car manufacturers adapt automatic air conditioning systems in order to create a microclimate inside the enclosed area, based on temperature sensor data and human preference. Unfortunately, vehicle air-conditioning is still very much a low-granularity process, lacking a real-time in-depth analysis of the cabin. Therefore, many passenger's needs as well as potential energy-saving opportunities are left unobserved. The energy used for air conditioning negatively impacts the fuel consumption in conventional combustion engine cars although the issue is much more significant in electric vehicles where it can cut the driving range by as much as 50% (Schmidt 2015). In order to overcome the still challenging issues of driving range and limited power storage of electric drives, it is mandatory to find ways to reduce a vehicle's energy consumption. In this regard, the use of intelligent conditioning systems is a promising endeavor. In order to find potential opportunities to save energy a much better representation of the passenger's physiological and subjective state is required. Additionally, advanced actuators like movable outlets as well as enhanced control of air flow in the vehicle need to be computationally controllable so that precise measures are possible. Real-time analysis of the passenger's thermal state requires a high sensor-density, which comes along with a well thought out objective function that makes the person's subjective state tangible.

Several studies have been performed in the past to narrow down influencing factors of human thermal comfort. The latter is usually determined on the base of energy balance calculations that involve a person's metabolic heat production, its thermal insulation as well as physical parameters such as air velocity, relative humidity, air and radiant temperatures (ANSI/ASHRAE 2013). However, those models were mainly designed to predict thermal comfort at steady state conditions near thermal neutrality and are mainly applicable in buildings, where dynamic and highly asymmetric ambient conditions rarely occur. In vehicles, however, such ambient scenarios are always present and require the use of much more sophisticated comfort prediction models that are capable to break down the overall thermal comfort prediction to the level of individual body sectors and further taking into account the thermal history of the individual. In this context, various empirical models exist that predict the overall thermal comfort based on a set of intrinsic and extrinsic parameters by proposing body sector specific unit-less comfort indices (Zhang 2003; Nilsson 2003). Even though these models are well-known, their comfort predictions show limitations for body areas that are in contact with solid objects such as the seat surface or the steering wheel. In order to overcome those weaknesses, (Schmidt 2015) developed a new thermal comfort model that combines Zhang's fuzzy logic approach with Fanger's energy-balance calculations (Fanger 1970) which was extended for the contact area.

The system developed in this work is required to continuously adjust air-condition so that a neutral thermal comfort state is maintained for each passenger. In order to effectively reduce the energy consumption of the vehicle's HVAC system, the presented approach needs to find a way to diminish energy consumption while conditioning local body zones in such a way that the required individual overall thermal comfort level for

each person in the vehicle is guaranteed. The introduced research platform involves several distinct steps ranging across hardware and software platforms.

1. Available sensor data is gathered and integrated so that it is available in a coherent format with respect to time scale and comparability. Data integration also accounts for possible history based analysis that requires a temporary or persistent storage of the available information. This step requires a robust hardware-abstraction layer as it deals with low-level input from various data sources.
2. Computational models are used to evaluate the fused data. While in the current research phase, these models can range from integrated transformations to completely separated software packages, it can be assumed that for product ready solutions a far more monolithic software solution is applicable.
3. User feedback adding subjective information to the data pool is regarded as additional sensor data that functions as a last step of a process cycle that feeds back corrected comfort values to the data analysis. Changes in cabin climate captured by the control system itself are also considered as a form of feedback which in turn is picked up by the sensor for the next iteration.

2 System Overview

This section provides a description of the overall software architecture. See Fig. 1 for a complete outline of the system. The design is chosen to be non-monolithic in the sense that the software is divided into independent components which communicate over a

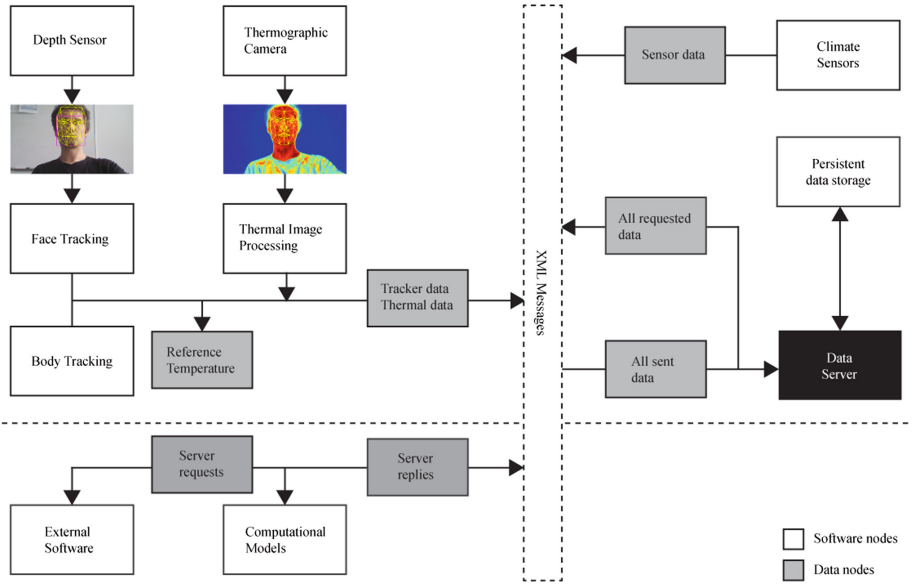

Fig. 1. General outline of the system including software components and data streams. Central to the communication is the data server and the XML syntax which is used by all components.

central data server via XML messages using common TCP/IP networking (see Sect. 2.1). As a research platform, this approach is straightforward since it provides a robust hardware abstraction layer and allows for distribution onto multiple computers. Compiler configurations can be set independently for each component which greatly simplifies the software development process. Software components with direct hardware access are the image processing component (see Sect. 2.2) and the software component responsible for temperature and climate sensors (see Sect. 2.3). A newly developed numerical human model as well as diverse thermal comfort models are used to evaluate a passenger's thermal state as wells as its thermal comfort on the base of the acquired sensor data (see Sect. 2.4).

2.1 Data Server and Communication Protocol

The data server is implemented in JAVA and functions as a communication proxy for all the different software components. The software provides a common HTTP interface for communication over TCP/IP. A customized XML syntax is used for data exchange (see Fig. 2). The syntax is based on a key-value scheme where each value is encapsulated in a "signal" node. The name and signal group are a combined unique identifier for the signal. A software component may simultaneously send and request one or multiple signals in a single XML message. The signal group was added to the syntax in order to identify identical sensors that occur more than once.

```
<?xml version="1.0" encoding="UTF-8" standalone="no" ?>
<data>
    <send>
        <signal>
            <!-- Name of the signal: -->
            <name>T_IR_01</name>
            <!-- Value of the signal: -->
            <value>23.43</value>
            <!-- Group name of the signal: -->
            <signal_group>SEAT_FRONT_LEFT</signal_group>
        </signal>
    </send>
    <request>
        <signal>
        <name>T_AIR_02</name>
        </signal>
    </request>
</data>
```

Fig. 2. Example XML message sent to the data server

XML sensor data is appended to an internal hash map at runtime which in turn can be stored as binary or ASCII files (e.g. CSV) for persistent storage. Additionally, the server provides a data plotting interface as well as a 3D visualization environment for data analysis and to study the behavior of control heuristics.

2.2 Image Processing

Image acquisition and processing is encapsulated in a single software component. The Microsoft Kinect sensor is used as a depth camera capable of face and human pose detection and the FLIR model A35 is used as a thermal imaging device. The software is designed in such a way that each camera is operated in a separate thread sending image matrices to a main thread which then finalizes the processing. Communication with the server is handled by yet another thread. In addition, the software supports frame skipping since the frame rate of each camera system is generally too high for the data rate required by the system. Both cameras are physically mounted on top of each other in a prototypical setup (see Fig. 3).

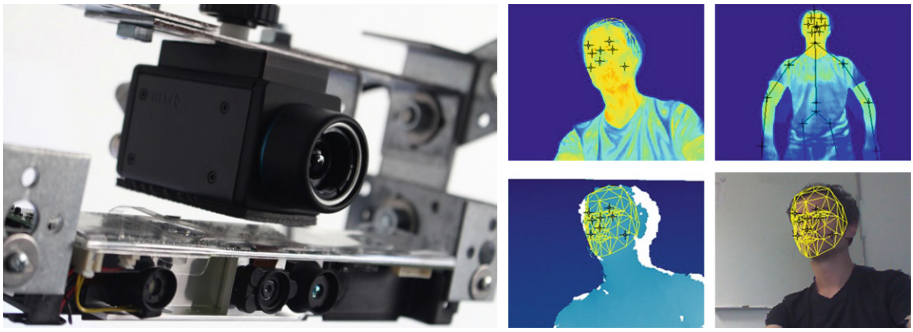

Fig. 3. Thermal camera mounted on top of the Microsoft Kinect sensor. The images on the right show the thermal face tracking (top left), thermal body tracking (top right), depth view (bottom left), color (bottom right).

The image processing and detection pipeline is structured as follows:

Image acquisition. Both camera threads receive images at framerates set by the cameras. As soon as a frame event occurs, the new image is stored for internal processing by the thread before it is sent to the main thread.

Camera calibration/image registration. A calibration procedure for the thermographic camera is included for cases in which the system detects no calibration files for intrinsic and extrinsic camera parameters. It is required because of the physical differences of the camera lenses and the vertical offset (see Fig. 4).

During the calibration procedure, a wooden circle grid is used to estimate intrinsic and extrinsic camera parameters using stereo calibration of the OpenCV library (see Fig. 5) (Rangel 2014). The grid pattern is detected using circular Blob detection and

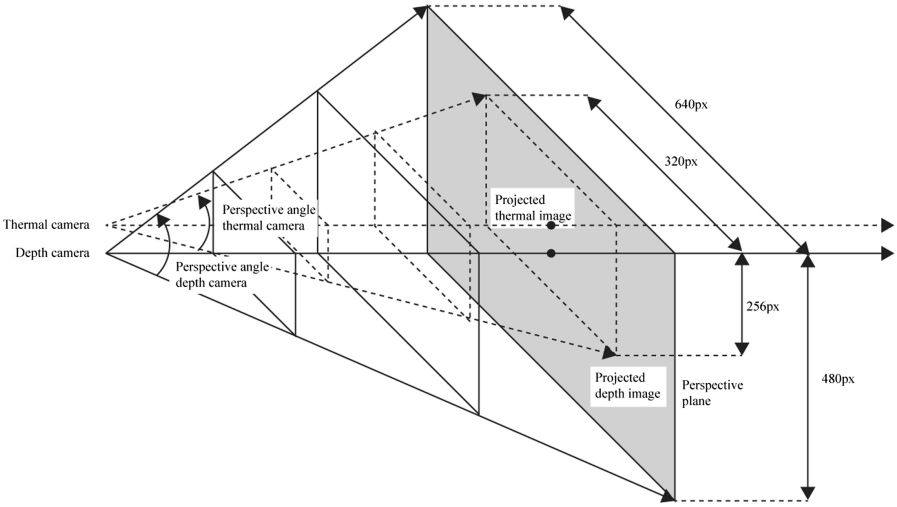

Fig. 4. Perspective projection of the depth sensor and the thermographic camera system. A difference in size and vertical offset is clearly visible. The illustration is not true to scale and does not include lens distortions.

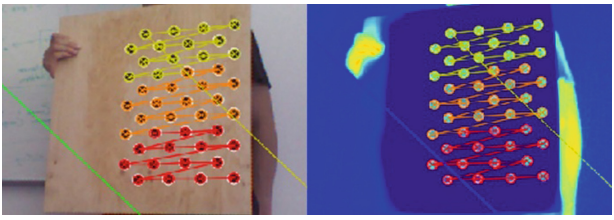

Fig. 5. Calibration pair used for stereo calibration of the Microsoft Kinect sensor and the thermographic camera

used as a perspective reference. Approximately 40 frame pairs are used to finalize the calibration. The estimated camera parameters can then be used to perfectly map the thermal image into the Microsoft Kinect depth image. This results in a single coordinate system, hence points detected in the depth image can be used in the thermal image as well.

Face/pose detection. This step only applies to the Microsoft Kinect sensor. The Microsoft face and pose recognition framework is used to detect and virtually split the body of a passenger into predefined segments (Smolyanskiy et al. 2014; Shotton et al. 2013). An appropriate data structure stores key face and body coordinates which are sent to the main thread. The respective regions are selected according to the requirements of the thermophysiological/thermal comfort models connected to the system.

Reference temperature detection. Two reference temperature sensors covered by black, matt varnish are used for continuously calibrating the temperature measurements

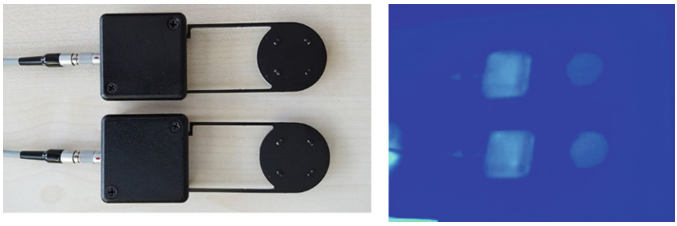

Fig. 6. Reference temperature sensors in a normal photograph and in a thermal image. The reference measurement points are placed on the circular surfaces at the top of the sensors.

of the thermographic camera. The measured temperatures of the sensors are requested from the data server and used in combination with the detected radiation at their position in the thermal image for the calculation of a calibration factor based on the Stefan-Boltzmann law. An emissivity value of $\in = 0.97$ and $\in = 0.99$. is assumed for the reference sensors and human skin, respectively (Fig. 6).

For testing purposes, the temperatures measured by the reference temperature sensors are compared to the detected temperature of the thermographic camera. Corresponding results are depicted in Fig. 7 and show deviations between the recorded data of the two sensor systems. This can be partly explained through image noise generated by the camera sensor. However, the surfaces of the sensors are also slightly more reflective in the infrared spectrum than would be optimal. Due to this reason, changes in the environment can influence the measurement. Figure 8 shows different temperature measurement points at the face region of a person in connection with the performed study. As expected, the upper and lower nose region are slightly below the average face temperature, as a consequence of the heat exchange processes that are related to breathing.

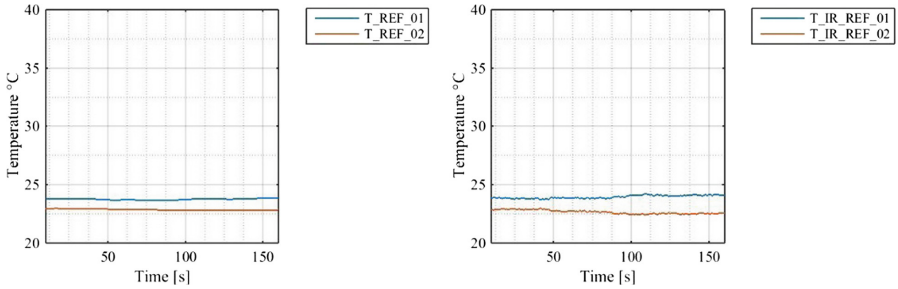

Fig. 7. Sensor temperatures measured by the reference temperature sensors (left) and as seen by the thermal camera (right).

Temperature measurement. Measurement points are given default offsets and can be subsequently assigned to a tracking point from the Microsoft Kinect sensor. The measurement point follows the movement of the tracking point during runtime so that they can be distributed according to the required computational model.

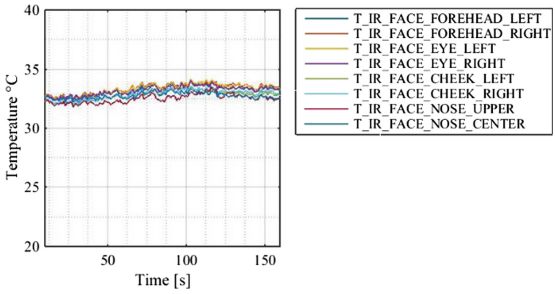

Fig. 8. Face region temperatures measured by the thermal camera while being continuously calibrated with the reference temperature sensors.

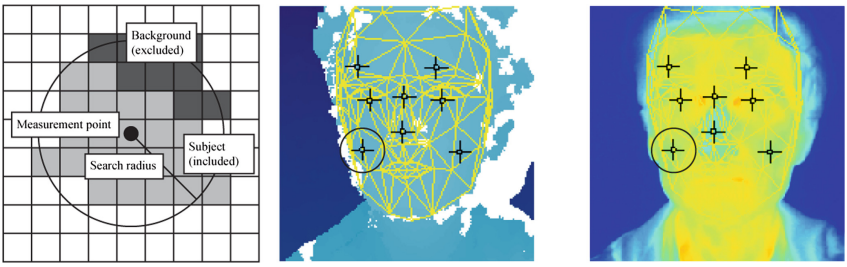

Fig. 9. Tracking point search algorithm and outlier elimination

In this connection, each measurement point has a circular pixel neighborhood with radius r that is used to compute an average temperature in terms of noise reduction. Pixels are masked using the human silhouette which can be detected in a much more robust manner than specific body parts. Hence, measurement points placed in border regions still return accurate results and points outside the silhouette borders are automatically excluded from the measurement (see Fig. 9).

The resulting temperatures from the measurement points are accumulated in a single XML message and sent to the server. The corresponding signal names in the XML message identify the measurement region.

2.3 Temperature and Climate Sensors

Sensors that measure temperature, humidity, air velocity or radiation are currently grouped together into one software component. Similar to the image processing software, sensors belonging to the same hardware driver are accessed in a separate thread. The data is accumulated in a main thread and a combined XML message is sent to the data server.

2.4 Numerical Models

The numerical human model (Wölki et al. 2013) as well as corresponding thermal comfort models were implemented in the equation-based acausal modeling language Modelica. The models were pre-compiled for co-simulation as a Functional Mockup Unit (FMU) according to the Functional Mockup Interface (FMI) standard (Blochwitz et al. 2012). Python's FMI library is used to load the corresponding models and communicate with the data server via the Python HTTP library. The thermophysiological model is a scalable, numerical multi-element model that calculates local skin temperatures of individual body segments as well as the average skin temperature of the entire body. As input parameters, the model requires the local/global values of relative air velocity (v_{air}), relative humidity (r_h) as well as the surface temperatures of the surrounding walls (T_{sf}) and the ambient air (T_a). Furthermore, the model is designed in such a way that skin temperatures can be calculated at segments that are not covered by the sensory input of the system, hence completing the picture for the human thermal comfort calculation. The model itself (Wölki et al. 2013) is based on the work of Tanabe (Tanabe et al. 2002) and Fiala (Fiala et al. 1999; Fiala et al. 2001). In order to determine local and global thermal comfort states, the model described by Schmidt (Schmidt 2016) is used. Functioning as the de-facto objective function for the passenger's comfort state, this model determines the heuristic of the air-conditioning actuators of the system.

3 Climate Control

Based on the vehicle requirement, an appropriate control heuristic for actuators involved in the air-conditioning process has to be derived from the sensory input and model analysis. The system is self-correcting in the sense that it immediately recognizes the effects of changed conditions and adapts accordingly in each iteration. During the course of this work, simulated movable air outlets were used as actuators in order to study the interoperability of the implemented components and to test possible future approaches. The simulation was visualized within the data server software (see Fig. 10).

Fig. 10. Simulated air-conditioning in a vehicle using two movable outlets controlled by the system. Each outlet can rotate 60 degrees along its horizontal and vertical axes.

This 3D interpretation of the system state can also be viewed by the passenger who in turn can give a subjective feedback via a network-compatible device. The feedback is encoded into the XML syntax and interpreted by the data server.

4 Conclusion

In this work, a robust and extendable framework was introduced for the fusion of multi-modal sensor technology that is applicable for real-time human thermal com-fort assessment and energy efficient air-conditioning of passengers. The system pro-vides an open architecture with no direct hardware dependencies and a generic communication layer that allows the user to easily add new components. Moreover, the paper contains a novel approach for inclusion of computational thermal image analysis, based on the combination of thermal/depth camera systems. Thermal comfort predictions for passengers that result from the measured quantities of the physical ambient and simulated thermophysiological reactions are currently in progress.

References

ANSI/ASHRAE. Standard 55-20013, Thermal environmental conditions for human occupancy. American Society of Heating, Refrigerating and Air-Conditioning Engineering, Atlanta, GA (2013)

Blochwitz, T., et al.: Functional mockup interface 2.0: the standard for tool independent exchange of simulation models. In: Proceedings of the 9th International MODELICA Conference, pp. 173–184, 3–5 September 2012

BMWi. Germany's new energy policy. Federal Ministry of Economics and Technology (BMWi), Berlin (2012)

Fanger, P.: Thermal Comfort. Danish Technical Press, Copenhagen (1970)

Fiala, D., Lomas, J., Stohrer, M.: A computer model of human thermoregulation for a wide range of environmental conditions: the passive system. J. Appl. Physiol. **87**, 1957–1972 (1999)

Fiala, D., Lomas, K., Stohrer, M.: Computer prediction of human thermoregulatory and temperature responses to a wide range of environmental conditions. Int. J. Biometeorol. **45**, 143–159 (2001)

Nilsson, H.O.: Comfort climate evaluation with thermal manikin methods and computer simulation models. Indoor Air **13**(1), 28–37 (2003)

Rangel, J., Soldan, S., Kroll, A.: 3D thermal imaging: fusion of thermography and depth cameras. In: International Conference on Quantitative InfraRed Thermography (2014)

Schmidt, C.: Zusammenhang zwischen lokalem und globalem Behaglichkeitsempfinden: Untersuchung des Kombinationseffektes von Sitzheizung und Strahlungswärmeübertragung zur energieeffizienten Fahrzeugklimatisierung. FAT-Schriftenreihe 272 (2015)

Schmidt, C.: Entwicklung eines Modellansatzes zur Bewertung der thermischen Behaglichkeit unter inhomogenen Klimabedingungen (2016)

Shotton, J., et al.: Real-time human pose recognition in parts from single depth images. Commun. ACM **56**, 116–124 (2013)

Smolyanskiy, N., Huitema, C., Liang, L., Anderson, S.E.: Real-time 3D face tracking based on active appearance model constrained by depth data. Image Vis. Comput. **32**, 860–869 (2014)

Tanabe, S., et al.: Evaluation of thermal comfort using combined multi-node thermoregulation (65MN) and radiation models and computation fluid dynamics (CFD). Energy Build. **34**, 637–646 (2002)

Wölki, D., Schmidt, C., van Treeck, C.: Neu-Kalibrierung eines Modells des menschlichen Thermoregulationssystems zur Untersuchung des Einflusses der Physiologie auf das thermische Komfortempfinden. Gebäudetechnik, Innenraumklima: GI **134**(4), 238–251 (2013)

Zhang, H.: Human thermal sensation and comfort in transient and non-uniform thermal environments. Center for the Built Environment (2003)

Concepts for Comfortable Air-Conditioning – Simulation Using a Zonal Cabin Model and a Metrological Evaluation Based on Equivalent Temperature

Sebastian Stratbücker[1(✉)], Sumee Park[1], Arnav Pathak[1], Victor Norrefeldt[1], and Gunnar Grün[1,2]

[1] Fraunhofer-Institut für Bauphysik IBP, Valley, Germany
{sebastian.stratbuecker, gunnar.gruen}@ibp.fraunhofer.de
[2] Technische Hochschule Nürnberg Georg Simon Ohm, Nürnberg, Germany

Abstract. In the design of future electric vehicles, the air conditioning of the passenger compartment is considered as the largest auxiliary consumer. To test new climate control concepts and quantify their effectiveness in terms of user acceptance, energy efficiency and driving range, corresponding methods and tools are needed. This includes the numerical, experimental and subject-supported study regarding human thermal comfort.

New developed zonal models simulate air flow and temperature, surface temperature, pressure and also humidity in a closed environment. Predicting indoor environmental conditions in vehicle cabin is achieved in transient inhomogeneous load cases. With the combination of a radiation model, the long-wave radiation exchange between human and cabin is included in the heat balance equation with a high level of detail.

In order to improve the assessment of the local thermal conditions near the passenger, a climate measurement system (DressMAN 2.0) was developed by the Fraunhofer Institute for Building Physics (IBP). Using dedicated controllers and sensor devices the DressMAN is able to measure equivalent temperature on local segments for evaluation according to DIN EN ISO 14505-2. Based on these methods novel and existing concepts for heating have been tested with subjects in a cabin mock-up. The experiments used simulation-based methods and local climate measurement devices to compare and evaluate different climate control concepts.

Keywords: Vehicle air conditioning · Equivalent temperature sensor · Virtual test environment · Cabin mock-up · Zonal simulation model

1 Introduction

One of the challenges in the development of future electrical vehicle is to achieve an equivalent or higher level of thermal comfort and energy efficiency compared to hybrid vehicles or internal combustion engine driven vehicles. In case of combustion engine driven vehicles the inefficiency of the combustion engine offers an efficient way of

C. Junior et al. (eds.), *Energy and Thermal Management, Air Conditioning, Waste Heat Recovery*,
DOI 10.1007/978-3-319-47196-9_7

conditioning the cabin. The waste heat from the engine could be used to heat-up the cabin and the mechanical drive from the engine could be used to drive the air-conditioning system. On the other hand in case of an electrical vehicle the efficient electric motors generate hardly any waste heat to heat-up the cabin. The mechanical drive to run the compressor is not available in an electric vehicle although the air conditioning system compressor can be powered electrically - but powering a conventional air conditioning compressor (3–5 kW) is not the most energy efficient way of climatizing, e.g. when a typical electrical vehicle consumes only 120 Wh/km [1]. Thus the use of conventional air-conditioning systems will inevitably lead to a reduction of the driving range, especially under cold outdoor conditions.

One of the solutions is the targeted use of local and close to the body climate control measures, which make it possible to increase the subjective feeling of passengers comfort. These measures should be distinguished through a direct effectiveness on the climate comfort with minimal energy consumption. The local (close to body) climate control concepts considering the human body energy balance and thermal regulation mechanism have an effect on the local and global temperature sensation and feeling of comfort.

In order to assess this potential of local climate control concept, both indoor environmental measurements and numerical evaluation methods were investigated. Subsequently four different types of local climate control measures have been examined in a vehicle mock-up and the evaluated results from measurements and numerical methods were compared to subject responses with respect to local thermal sensation and comfort perception.

2 Methodology

2.1 Comfort Measurement Using Equivalent Temperature

To determine the thermal comfort in vehicles, individual parameters of the cabin such as air temperature, air velocity and thermal radiation are often measured to detect the effect of changes in the climate design of the vehicle. Different manifestations of individual parameters can have adverse effects on each other, so that overall assessment of thermal comfort is not feasible. It would therefore be desirable to provide a measuring method by which the resulting effect of all climate parameters can be read from a single integral value. Because of the thermal inhomogeneity in a passenger compartment, for example, due to hot surfaces or strong incident airflow, locally different conditions have to be considered and identified.

The essential technical measurable parameters for assessing the expected thermal sensation of humans are in this case convection (depends on air temperature and air velocity) long wave radiation (depends on temperature of enclosed surfaces and the geometry of enclosure) and an impingement of short wave radiation due to sunlight. To research and evaluate indoor climate so called thermal manikins are utilized. Besides being expensive to procure and maintain, these manikins cannot be configured flexibly to yield a higher measurement resolution for critical zones.

As part of a research project, a comfort sensor has been developed which enables the measurement of equivalent temperatures (see Fig. 1) [2]. The equivalent temperature defined in DIN EN ISO 14505-2 [3] summarizes variables like air temperature, air velocity and thermal radiation, which determine thermal comfort, into one climate index. With the equivalent temperature as climate index, thermal environmental conditions can be described with only one numerical value, which allows a comparative evaluation of different climate scenarios. This applies even if the effects of the various individual parameters are compensated or enhanced. It is assumed that the same equivalent temperature values yield the same effect on humans with respect to the dry heat exchange between body surface and its surroundings.

Fig. 1. Equivalent temperature sensor and system software of DressMAN 2.0

A novel equivalent temperature sensor has been developed by the Fraunhofer IBP and integrated to the DressMAN 2.0 system. Measured local equivalent temperatures can be linked to comfort ratings in accordance with DIN EN ISO14505-2. To be able to detect also locally prevailing factors influencing the thermal sensation, commercially available sensors for air temperature and air velocity are provided.

2.2 Numerical Evaluation Based on Zonal Cabin Models and Manikin Models

For capturing the impact of various climate measures on humans, a computational analysis was conducted parallel to the empirical studies. To avoid long computation times of computational fluid dynamics (CFD), the VEPZO model (VElocity Propagating ZOnal Model) is implemented in Modelica [4]. The zonal modelling approach is an intermediate approach between CFD and a single node modeling. The zonal models provide a better resolution of airflow distribution in an enclosure than the perfectly mixed air volume of nodal models. A VEPZO model typically subdivides a room into 10^1-10^2 zones. In the zones, the conservation of mass and enthalpy are implemented. The VEPZO model is using the airflow velocity as a property of a zone and a viscous loss model in order to better match the physics of airflows. This allows a rapid prediction of local temperature distributions considering the location and intensity of heat sources and air vents. As an extension of the VEPZO model, the RADZO model has

been developed which is able to calculate the heat radiation on the zonal grid [5]. In addition, the Thermal Model Generation Tool has been developed to automatically build up a VEPZO model, thermal enclosure models and a RADZO model from a CAD geometry export. Space boundaries are subdivided into small areas in accordance with the zonal grid [6].

Zonal simulations predict the effect of cooling or heating surfaces on the air temperature distribution as well as their radiation effect. Local measures, such as radiant heating surfaces, can be evaluated for their energy efficiency as well as their influence on passenger comfort.

For evaluating the thermal comfort in a vehicle, geometric models of the cabin surroundings and of the human body are needed. For this purpose, a vehicle mock-up was modelled for zonal simulation. In addition, a virtual manikin with ten body segments was implemented in the thermal vehicle model to numerically predict the thermal comfort. The view factors of local body segments were determined for the surrounding cabin and for all body segments involved in radiant heat exchange. The view factors determine the thermal influence of temperatures enclosing inner surfaces on the manikin and thus serve alongside the surface temperature and emissivity of the surrounding surfaces as an output variable for calculating the radiation heat exchange between the local body segments and the environment.

While the view factors strongly affect the radiative heat exchange, the convective heat transfer coefficient of the local body segments together with the local air temperature determine the convective heat exchange. The coefficients were determined in this study as a function of the air velocity at the ventilation outlets through CFD and segmentally transferred to the zonal model (Fig. 2).

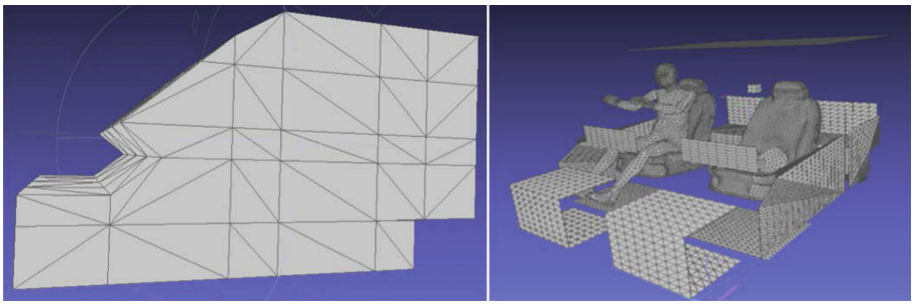

Fig. 2. Zonal geometry and virtual manikin with heating segments in the cabin mock-up model

3 Experimental Study in a Vehicle Mock-up

3.1 Vehicle Mock-up

The vehicle mock-up at Fraunhofer IBP is generic mock-up made of wood and plexiglas, thus enabling a vendor neutral form with defined geometry and a high level of flexibility in the creation of new surface heating and cooling systems. Thus, both the heating of the cabin via electrical heating foils, as well as the cooling of the cabin via a

secondary refrigerant circuit are possible. For the control system, the internal surfaces were divided into 11 different segments like door, floor, roof, footwell, dashboard, etc. The volumetric air flow rate can be varied in four stages. The ventilation air is exhausted from two openings in the rear shelf.

In the passenger compartment, two conventional vehicle seats are installed in beige fabric. A seat heater with flexible control of heat flow or the contact surface temperature was fabricated.

A total of 37 PT100 sensors were installed in the interior for measurement of air and surface temperatures. In addition, six sensors were attached to the outer surfaces of the mock-up. In support, the air velocities in the vehicle cabin and the heat flow on the seat were measured. The climate measuring system DressMAN 2.0 is used for the measurements of temporary cabin climate states.

3.2 Test Design for Experimental Study

In test conditions with subjects, the different climate measures were implemented with different proportions to convective-heating, radiation-heating and seat heating in the vehicle mock-up and evaluated energetically and climatically. In all test cases, an equivalent cabin climate was targeted to make the resulting energy consumption and comfort evaluation comparable. Five climate measures with different proportions to convective, radiative and seat heating were evaluated energetically and climatically in several test runs (Fig. 3). The reference cabin climate was an acceptable climate for the driver in winter, which means that the subjects on the driver's seat should assess the indoor climate in the vehicle cabin between a bit cool to neutral and rate it as acceptable.

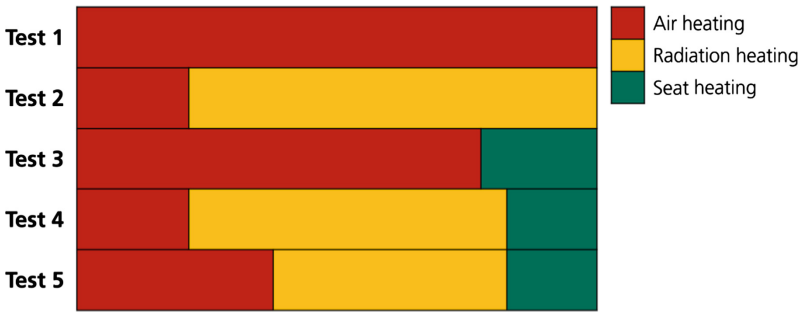

Fig. 3. Schematic representation of the proportions of different heating systems used in the test design, Test 1: reference system

3.3 Execution of the Tests in the Vehicle Mock-up

The experiments were conducted over a five days period in the vehicle mock-up at the Fraunhofer IBP in Holzkirchen. Every day a different climate control measure was tested. The outer boundary condition of the vehicle mock-up for all tests was held

constant at 7 °C. For stable indoor climate conditions, the climate chamber and the vehicle mock-up were conditioned four hours before the tests started. For the study, 10 to 12 people between 25 and 32 years of age participated. The proportion of women was 25%. On all tests, the same participants attended to better asses the difference in the boundary conditions.

The participants were wearing individual but the same clothing in five trials according to the instructions on the clothing insulation value (about 1.0 clo). They stayed for 20 min for acclimatization in a room. There was only one person in the vehicle mock-up per trial. In order to have the activity level of a participant similar to the activity level of driving (1.2 met, 70 W/m^2), the participants had to steer in a driving simulator. Subsequently, the participants evaluated the indoor climate by means of electronic questionnaires, in which the complete thermal sensation, the overall comfort, the local feeling as well as the local discomfort were requested.

4 Results

4.1 Evaluation Using DressMAN 2.0 Measurement

Figure 5 shows the results of the DressMAN 2.0 measurement on all local body segments. For comparison, the air temperature measurements are shown for two height levels in degrees Celsius during the experiments in the cabin mock-up (Fig. 4).

The air temperature varied within 2 K at 0.1 m during test 2, which suggests a variable boundary condition and correspondingly different thermal perceptions within one experiment. In exception to test 2, the other four studies showed stable thermal boundary conditions in all trials. The thermal evaluation of the subjects can thus be compared well with one another and a further analysis with mean values is possible, while the mean value of test 2 should be considered carefully.

The temperature variation of test 2 during the experiment impacts also the subject comfort evaluation. The overall thermal sensation votes of test 2 varied from slightly cool to slightly warm in the range of two scale points, while other tests showed mainly variation of only one scale point. According to the comfort assessments, the condition in Test 5 with a combination of air-, radiation- and seat heating system yields the highest satisfaction of subjects (Fig. 5).

While the air temperature reaches the required 21 °C at 1.1 m in test 1 (air heating), the equivalent temperature is shown at almost all body segments below 20 ° C, which indicates increased air velocity and thus increased convective heat loss. In particular, the equivalent temperature in the footwell is exceeding largely the temperature range, at least 22.3 °C are recommended in DIN EN ISO 14505-2 (see Fig. 6).

If the temperature profile in the vehicle mock-up is taken into account during convective heating, the set temperature should not be 21 °C at 1.1 m but above 24 °C in order to meet the required temperature in the footwell. The air heating systems (Test 1 and Test 3) show few variations between local segments as opposed to radiant heaters (Test 2, 4, 5), where the left hand and the foot-well are much warmer than the other body segments due to the asymmetrical panel heating (left door and foot well).

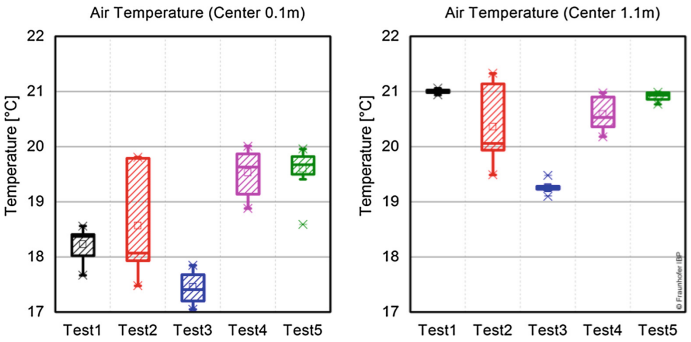

Fig. 4. Box plot of the room air temperature in the middle of the vehicle mock-up in five trials at a height of 0.1 m and 1.1 m (large box with strips: 25%–75% range, small box within large box: mean value).

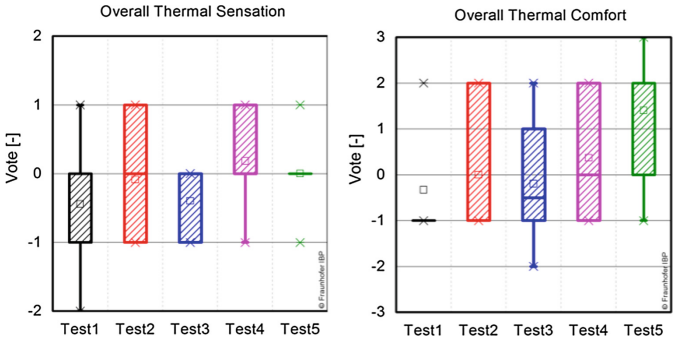

Fig. 5. Subject assessment: overall thermal sensation (1: slightly warm, 0: neutral, −1: slightly cool); overall thermal comfort (3: satisfied, −3; dissatisfied)

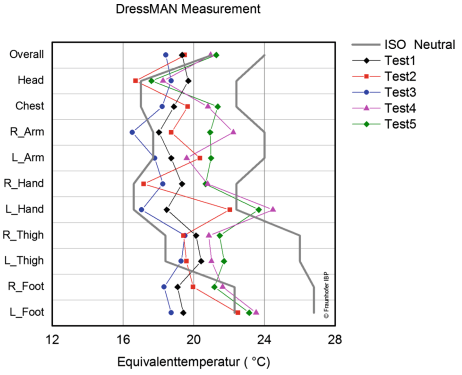

Fig. 6. Local thermal sensation of the five climate control concepts using the DressMAN 2.0 measurement; ISO neutral: Comfortable area according to DIN EN ISO 14505-2.

The total equivalent temperature, which in this study is area-weighted by local equivalent temperatures, meets the requirement of DIN EN ISO 14505-2 only for test 5, whereby test 4 misses the requirement only closely. No measurement was performed on the seat and back during the DressMAN measurement. Therefore, the examined local position varies from the participant's question.

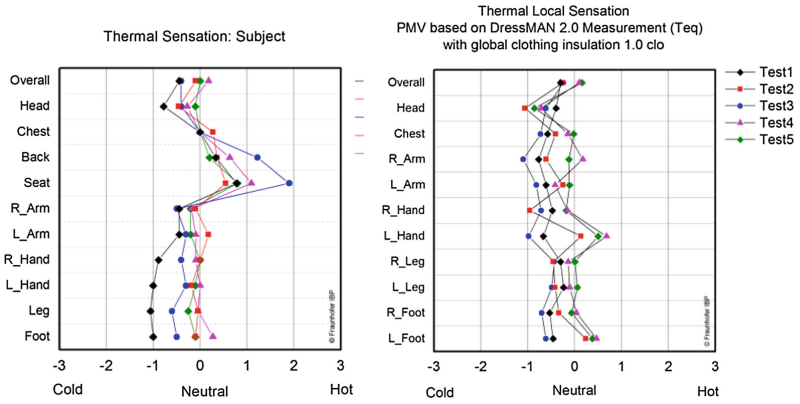

Fig. 7. Local thermal sensation of the five air-conditioning concepts based on the subject's evaluation and local PMV calculation from the equivalent temperature of DressMAN measurements with global clothing insulation values

4.2 Comparison of Subject Responses with Numerical Models and Measurements

Figures 6 and 7 show the local thermal sensation in five tests with different evaluation methods; subject evaluation, evaluation using DressMAN 2.0 measurement and numerical evaluation.

Since the DIN EN ISO 14505-2 does not provide a quantitative evaluation option but only a qualitative evaluation (comfortable or not), the results of the measurement (equivalent temperature) of DressMAN 2.0 were transferred to a predicted mean vote (PMV) calculation based on local heat exchange and quantified. There was a strong influence of the local clothing insulation values on the local heat balance. The uncovered parts of the body, such as the head and hands, are rated very cold, while the body parts with high insulation values such as the chest and back are rated slightly warm in all the tests.

In order to reduce the influence of local clothing insulation values, evaluations with uniform clothing insulation values of 1.0 clo were carried out. This resulted in a reduced variation between local segments. The contact heat transfer between the seat and manikin was additionally taken into account for all evaluations. If the driver's seat (0.26 clo) is taken into account for the clothing insulation value, which would be correct for the heat balance evaluation according to the literature in [7, 8], all ratings are moved by 0.4 in the direction of the warm area in the right figure of Fig. 8.

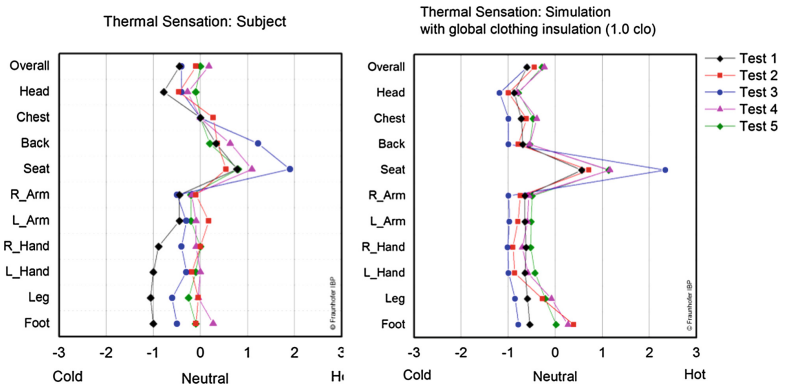

Fig. 8. Local thermal sensation of the five air-conditioning concepts based on the subject's evaluation and Thermal local sensation of the five air-conditioning concepts according to the numerical evaluation.

According to the subject evaluations, the climate control measures dominated by air heating (Test 1 and Test 3) show a strong difference in the leg area compared to other solutions. In Test 1, the leg area, hands and head are rated "slightly cool". Interestingly, in Test 3, where a strong seat heating is used and the air temperature is almost 2 K and the equivalent temperature 1 K lower than in Test 1, all local segments are judged to be a bit warmer than in Test 1. The radiant heating of the footwell and that of the left door in test 2, 4 and 5 has a significant effect on the leg area as desired.

Regardless of the application of the seat heating, the seat contact surfaces and the back have always been rated as slightly warm or warm. These results are reproducible because the questionnaires were only carried out after 20 min and thus the strong heat loss from the body to the seat through heat conduction faded. If the proportion of the air heating is increased compared to the radiant heating, the evaluation in the head area (test 5 compared to test 2) improves. The evaluation in the upper body area hardly differed in all experiments; especially the chest was always rated as "neutral".

Comparing all evaluations, the DressMAN measurements show better agreement with subject responses than the simulation result. All PMV ratings based on the heat balance calculation and the DressMAN measurement show a slight deviation of 0.2 on the ASHRAE scale [9] (7-point scale from cold (−3) to hot (+3)) compared to subject questionnaires. The simulation always evaluates a little cooler from 0.2 to 0.4 points on the ASHRAE scale. The deviations are more prevalent in trials with radiant heating than in trials with air heating.

Although the difference of thermal evaluation between individual participants was not high, being −0.4 to 0.2 on the ASHRAE scale, the simulation model was still able to predict the order of thermal sensation votes of the test boundary conditions. A 0.1 ASHRAE scale difference correlates to approx. 0.5 K operative temperature difference by near to neutral (neither cold nor warm) indoor environment with normal indoor winter clothing (1.0 clo). The local equivalent temperature measurements as well as the thermal computational simulation seem to be well suited for the evaluation of the cabin environment even for local measures close to the body (Fig. 9).

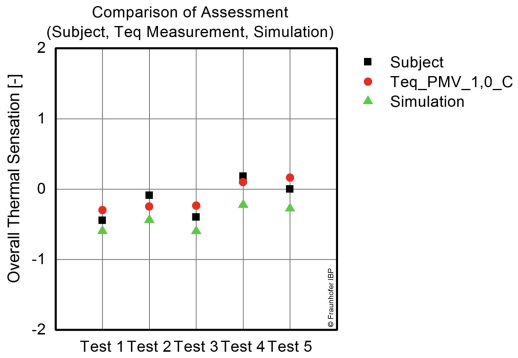

Fig. 9. Comparison of evaluation methods for thermal overall temperature sensation (Test: Thermal, average overall feeling of participants, Teq_PMV_C: PMV calculation based on DressMAN measurement taking into account the heat flow on the seat).

4.3 Evaluation of Energy Demand

Since the measured energy consumption of the vehicle mock-up in the air heating system was strongly dependent on the efficiency of the fan and the thermal perceptions were not identical in all experiments, the energy efficiency between test variants was evaluated by the simulation.

According to the simulation results Fig. 10, the reference system (pure air heating, test 1) consumes more energy compared to other climate control concepts in order to achieve similar thermal sensation. A seat heating (test 3) will effectively reduce the energy requirement, if real subjects' local perception is ignored and only the heat balance of the manikin is considered. Although the conduction heating is most effective for the heat balance of a human, a powerful seat heating like test 3 will cause high local discomfort in real tests. The powerful radiant heating and weak air heating (test 2) is

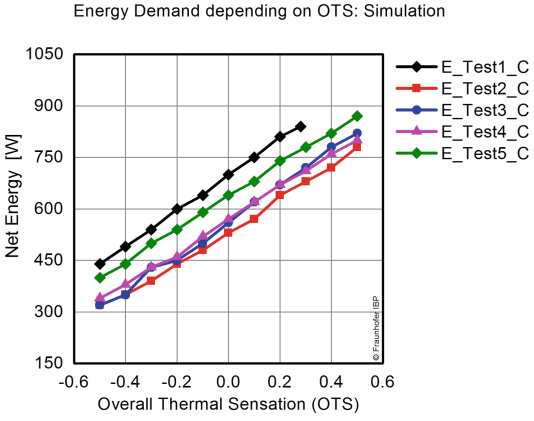

Fig. 10. Comparison of energy demand depending on the predicted thermal sensation for different climate control concepts (simulation results)

even more effective than the combination of air and seat heating (test 3). The greater the proportion of radiant heating, the lower the energy demand for the vehicle mock-up is.

According to the results of the numerical evaluation, a climate control concept which is local and close to the body can reduce the net energy demand compared to the pure air heating system. The concept study in test 2 with strong radiant heating showed a 24% lower energy demand, test 5 with air, radiation, and seat heating resulted in a reduction of 9%.

5 Conclusion and Outlook

We investigated the potentials of local climate control concepts in experimental studies. Given detailed evaluations from subjects on local thermal sensation and overall comfort, the ratings are compared with measurements of equivalent temperatures and with numerical results from refined numerical simulation models.

The results of the study show that the local, near-body climate control measures are more energy-efficient and more comfortable than conventional heating systems in the vehicle. For this purpose, the applied assessment methods, namely a local, directed equivalent temperature measurement and the thermal comfort simulations, have a good suitability for the evaluation of cabin climate control systems (also in the case of local and near-body measures).

It can be concluded, that any local discomfort should be avoided for a high comfort in vehicle cabin. In the case of air heating, the foot area represents a discomfort zone, while the head was perceived to be too cold during the air conditioning with a high proportion of radiation. Only a combination of conventional air heating, as well as radiation and seat heating can provide a homogeneous thermal perception (non-homogeneous temperature) in a vehicle cabin and thus high comfort. As already shown in previous studies, it is affirmed that locally warmer climate in the foot region and a colder area in the region of the head of subjects are preferred. The conventional air heating in the vehicle cannot produce such optimal local boundary conditions. Thus a different climate control concept is required for a high degree of comfort. The energetic and cabin climatic evaluation of the local climate control measures in the real vehicle may differ from existing results, since the vehicle mock-up has other insulation and hermetical properties to a real vehicle. Nevertheless, this study shows the potential of the near-body measures in the vehicle as well as the assessment methods of such measures.

With the combination of measurement and simulation data, it is now possible to thoroughly test new architectures for innovative thermal management. The aim is to minimize the risks of design and configuration in vehicle air conditioning at an early stage. After having invested in establishing a virtual test environment, the study showed that costs for developing and testing novel concepts are minimized and evaluation of solutions is less time-consuming.

References

1. U.S. Department Of Energy: The official U.S.goverment source for fuel economy information: EPA Fuel Economy. www.fueleconomy.gov. Accessed 6 October 2016
2. Grün, G., Stratbücker, S., Schwab, R.: Klimamesssystem zur Erfassung der Äquivalent-Temperatur für die Bestimmung des thermischen Komforts: DressMAN 2.0: Entwicklung im Verbundvorhaben E-Komfort. In: Bahn-Klimatechnik 2013, pp. 83–95. Interdisziplinärer Forschungsverbund Bahntechnik, Berlin (2013)
3. Beuth, Berlin: DIN EN ISO 14505-2: 2007: Ergonomie der thermischen Umgebung – Beurteilung der thermischen Umgebung in Fahrzeugen – Teil 2: Bestimmung der Äquivalenttemperatur (ISO 14505-2:2006); Deutsche Fassung EN ISO 14505 2:2006
4. Norrefeldt, V.: VEPZO - Velocity Propagating Zonal Model. A locally refined airflow model for confined spaces to use in optimization applications. Dissertation, Universität Stuttgart/Technische Universität München (2013)
5. Pathak, A., Norrefeldt, V., Grün, G.: Modelling of radiative heat transfer in modelica with a mobile solar radiation model and a view factor model. In: Proceedings of the 9th International MODELICA Conference, 3–5 September 2012, Munich, Germany. Online resource, pp. 271–278. Modelica Association, Linköping (2012)
6. Pathak, A., Norrefeldt, V., Lemouedda, A., Grün, G.: The Modelica thermal model generation tool for automated creation of a coupled airflow, radiation model and wall model in Modelica. In: Proceedings of the 10th International Modelica Conference, pp. 115–124. Modelica Association, Linköping (2014)
7. Nilsson, H.O.: Comfort climate evaluation with thermal manikin methods and computer simulation models. Ph.D. thesis (2004)
8. McCullough, E.A., Jones, B.W., Huck, J.: A Comprehensive data base for estimating clothing insulation. ASHRAE RP-411. Refrigerating and Air-Conditioning Engineers Inc. (1985)
9. Atlanta: American Society of Heating, Refrigerating and Air-Conditioning Engineers, Inc: ANSI/ASHRAE STANDARD 55: 2004: Thermal Environmental Conditions for Human Occupancy

Reduced Climate Control Unit for Individual Interior Comfort

Thomas Wysocki(✉), Christine Junior, and Johannes Ritter

IAV GmbH, Gifhorn, Germany
{Thomas.Wysocki, Christine.Susanne.Junior, Johannes.Ritter}@iav.de

Abstract. The climate control unit is one of the most important interfaces between user and vehicle. As a result of increasing attention in the field of user experience, topics as intuitive handling and customer satisfaction become more and more important for climate control as well. To create a new user concept in an easily comprehensive format the alteration of the operating philosophy to a more intuitive and plausible one is recommended. The presented concept offers the advantage that the customer does not necessarily need to grasp the climate control system or its operating philosophy respectively, but just his own experienced thermal discomfort. With the user's information concerning the discomfort as well as the allocation of these feelings in regard of his body, the climate control improves the interior comfort corresponding to his input.

Keywords: Climate control unit · Interface · User concept · Thermal comfort

1 Challenges for Interior Climate Control

In the course of digitization of passenger cars, as well as other mobility concepts, automatic user recognition and the realization of the passenger's individual preferences play an important role. Thereby, the customer places high demands towards air quality and interior comfort – irrespective to his way of locomotion.

With customer comfort being a growing concern within automotive industries, the climate control unit by now represents one of the most important interfaces between the user and the vehicle. Hereby, the usage concept plays a significant role since it enables the interaction between user and climate control.

However, due to the variety of hard and soft keys and multiple setting options, the interior climate control often cannot be operated simply and intuitionally. This way, the customer can realize simple comfort requests in certain circumstances only by a multitude of operating steps, where the keys have to be pressed singly and one after another. Hereby, the different setting options have to be understood and cognitively processed by the user to perform the desired settings, which implies an increased distractive potential from the actual driving task [1, 2].

Because of the many possibilities of key combinations there is a risk that entries are placed inconsistently and the air conditioning system cannot be handled as desired. If the worst comes to the worst, this may lead to a poor air conditioning result and an

C. Junior et al. (eds.), *Energy and Thermal Management, Air Conditioning, Waste Heat Recovery*,
DOI 10.1007/978-3-319-47196-9_8

unsatisfied customer. As well, the main safety aspect of a good interior climate like support of the user's serenity and relaxation is annihilated [3, 4].

2 User Experience and Control of Thermal Comfort

In the course of individualization and generation of configurable user profiles the attention is increasingly on the so called user experience (UX), which is to be understood as the experience of a user in interaction with a product or system [5]. As a result, topics as intuitive handling, thermal comfort and customer satisfaction become more and more important for climate control as well [6, 7].

Since the subject takes up an important role in building physics for quite some time [8–10], automobile industries now also focusses very strongly on the topic of thermal comfort [11–13]. But while thermal comfort has an important part within theoretical investigations, climate control units as well as the subjacent control and regulation of air conditioning systems are still based on the average interior temperature. In order to better respond to the customer demands and reliably assure real thermal comfort, the transition to the so called felt temperature [14] or a degree of comfort (i.e. the Predicted Mean Vote (PMV) [15]) is advisable.

For use as a control value a continuous calculation of the PMV with a suitable simulation model that can be implemented in the climate control strategy is necessary. The active control by means of the calculated PMV has the advantage that existing climate-controlling actuators can be triggered more effectively. Thus, the PMV control unit can assure the thermal comfort more reliable as a conventional control algorithm and thereby cause a higher customer satisfaction.

3 Inversed Operating Philosophy

The current technology of interior climate control and climate control units require information about the user's desired interior comfort. Usually, these information have to be provided by operating the keys that are displayed at the control unit. This kind of operation and its philosophy is not without problems – as it was already described above – and does not necessarily lead to the desired result.

In order to avoid cognitive overload and prevent the user from these well-known problems, not only the reduction of the number of hard and soft keys but fundamental changes within the operating philosophy are needed. To realize a more intuitive handling of the climate control, the usual operating philosophy is altered and the new philosophy is oriented towards the user's actual state in regard of thermal comfort.

Instead of the desired state and the implicit question "How do you want to feel?", information concerning the user's actual state ("How do you feel?") are necessary to control the air conditioning system and provide the required thermal comfort within the vehicle's compartment. This concept offers the advantage that the customer does not necessarily need to grasp the climate control system or its operating philosophy respectively, but just his own experienced thermal discomfort. After the request of the

user's actual state, a downstream logic or artificial intelligence translates the actual state in a desired state and hands it over towards the climate control.

With the use of the PMV as control value the transition to a new user concept is crucial, so that the user's input required by the system can be reduced drastically. To create a new user concept in an easily comprehensive format the alteration of the operating philosophy to a more intuitive and plausible one is recommended.

4 Reduced Operating Concept

Modern displays are to become more and more important for vehicle cockpits and offer a large design flexibility in regard to new interior concepts [16]. In addition, user relevant information can be provided more clearly and a reduced operating concept can be developed without the need of any hard key. In the development phase of the reduced operating concept, the concept was to be expected to be intuitive and catchy for all ages. Furthermore, a reduction of the input data required from the user was specified, in the new concept only two information are necessary to provide a comfortable interior climate.

The altered operating philosophy should be clearly recognizable throughout the chosen concept and its visualization on the display. To realize these claims, a carefully designed and structured user interface had to be developed. Therefore it was considered to utilize symbols and icons for visualization, which ensures that the climate control can be used by anyone – regardless of age and origin.

The extreme climatic conditions *too hot*, *too cold*, *too drafty* and *too stuffy*, which can occur in the vehicle's compartment under certain ambient parameters, are graphically displayed in a definite way by corresponding icons. For use in the reduced climate control concept these extreme conditions are diametrically arranged in a so

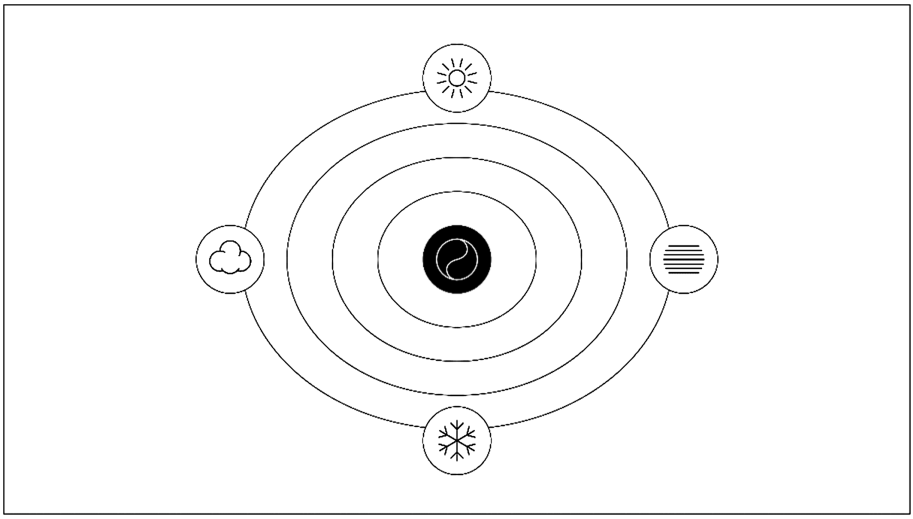

Fig. 1. Depiction of the reduced operating concept

called level of sense-perception, so that the conditions *too hot* and *too cold* as well as *too drafty* and *too stuffy* are lying opposite to each other. Figure 1 depicts the user interface of the reduced operating concept.

In the center of the perception level a symbol is located, which symbolizes the serene and relaxed user and is clearly recognizable by coloring and appearance. With a relocation of this symbol within the level the user can give a response in regard of the question how he feels just in the very moment. During the movement of the symbol its appearance changes accordingly, so that it displays the user a direct feedback concerning the information that was transmitted towards the climate control.

Hereby, the icons located on the rim of the perception level, which symbolize the extreme climate conditions, are of particular significance. As a function of the symbols position within the sensory level a change of size occurs and these icons become smaller and larger. When a user, for example, drags the symbol in the direction of *too cold* and *too drafty*, these icons expand, while the icons representing the conditions *too warm* and *too stuffy* recede into the background or rather disappear as it can be seen in Fig. 2.

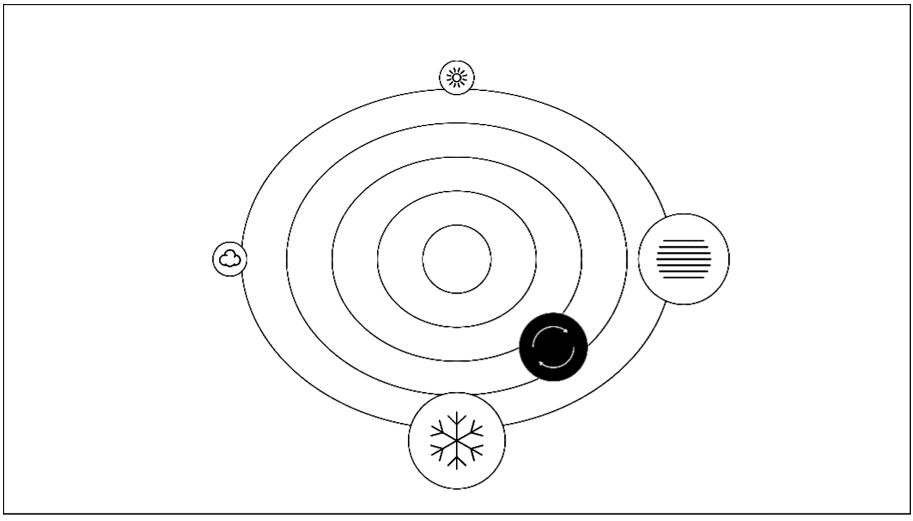

Fig. 2. Entering the actual state

By positioning the symbol between two conditions – e.g. *too cold* and *too drafty* - the user is able to give a feedback concerning the proportion between these conditions. If the conditions *too cold* and *too drafty* both apply equally to the user, the symbol needs to be located central between these conditions and the size of both icons remains even.

If the user needs to differentiate between both states because he feels significantly too cold and only marginally too drafty, the symbols has to be placed between both conditions but much closer to the state *too cold*. As a result, the icon representing the state *too cold* will clearly increase, while the *too drafty* icon decreases (Fig. 3).

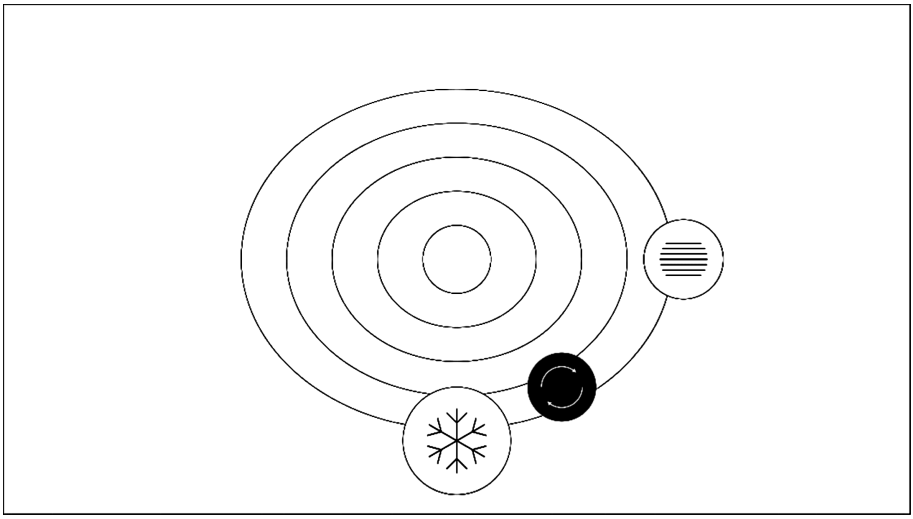

Fig. 3. Differentiation of the actual state

In addition to a statement about the experienced thermal comfort, which is given by the replacement of the symbol, a direct selection of the extreme conditions enables the user to give a feedback about significant discomfort. In this case the symbol automatically moves in the direction of the extreme state and positions itself right on top of the selected icon.

Once the user has entered the information concerning his actual state via the control unit, he is able to verify if his climatic impression refers to a specific region of his body. Therefore, an abstract representation of a human figure is displayed next to the level of perception, which illustrates the user's body.

By tapping on the different areas, a feedback concerning the user's personal perception in regard of his head, torso and legs can be differentiated. In addition, a feedback concerning the overall perception can be given by tapping the rim of the figure. When choosing one of the body regions or the overall perception the chosen region is indicated accordingly, e.g. by changing its color, as it is shown in Fig. 4.

With the information concerning the user's perception as well as the allocation of these feelings in regard of a body region, the climate control is able to adjust the control values air flow, temperature and flap position accordingly to improve the interior comfort corresponding to his input.

In order to give a visual feedback about the adjustment of the control values, the symbol moves back towards the center of the perception level and indicates its current activities during the regulating process with a steadily rotating frame at the rim of the symbol. If the symbol appears in the center again, an optimized interior climate was adjusted due to the underlying logic and the symbol represents once more the serene and relaxed user.

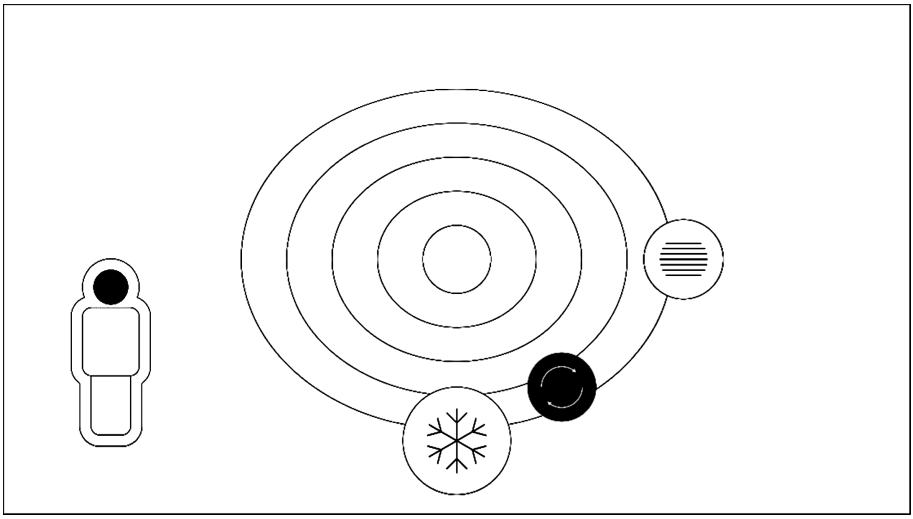

Fig. 4. Selection of a body region

The interaction between the user and the control unit is repetitive and can be repeated as often as required, so that the user can give a feedback concerning his current climate situation until the desired comfort state is finally achieved.

5 Application – Future Scenarios

To further reduce the operating effort of the user, a link between the user concept and an adaptive climate control as well as a recording of the desired settings in an individual user profile is practical. The basic idea is that predefined primary functions are adjusted and saved individually on base of the user's input and thus an individual climate profile is generated over time.

For the application in car sharing services an additional link to an automatic user recognition function, e.g. via smart phone, is imaginable. Thus, the user's individual climate profile can shift from one vehicle to another and is always available as usual – even after changing between vehicles of different brands. A connection to the vehicle's infotainment system also enables the availability of the familiar user interface and the user does not have to switch between different operating concepts anymore.

References

1. Spies, R., Blattner, A., Lange, C., Wohlfarter, M., Bengler, K., Hamberger, W.: Measurement of driver's distraction for an early prove of concepts in automotive industry at the example of the development of a haptic touchpad. In: Jacko, J.A. (ed.) HCI 2011. LNCS, vol. 6762, pp. 125–132. Springer, Heidelberg (2011). doi:10.1007/978-3-642-21605-3_14

2. Vollrath, M., et al.: Ablenkung durch Informations- und Kommunikationssysteme. Forschungsbericht Nr. 26, Gesamtverband der Deutschen Versicherungswirtschaft e. V. (2015)
3. Bubb, H., Bengler, K., Grünen, R.E., Vollrath, M.: Gestaltung der Konditionssicherheit. In: Automobilergonomie. ATZ/MTZ-Fachbuch, pp. 471–523. Springer Fachmedien, Wiesbaden (2015). doi:10.1007/978-3-8348-2297-0_8
4. Arminger, G., Bonne, T.: Einfluss der Witterung auf das Unfallgeschehen im Straßenverkehr. ATZ Automobiltechnische Zeitschrift **101**(9), 675–678 (1999). Jahrgang
5. Wu, L., Li, J., Lei, T.: Design entropy: a new approach for evaluating user experience in user interface design. In: Rebelo, F., Soares, M. (eds.) Advances in Ergonomics in Design. Advances in Intelligent Systems and Computing, vol. 485, pp. 125–132. Springer, Switzerland (2016). doi:10.1007/978-3-319-41983-1_53
6. Spanner-Ulmer, B., Leiber, P.: Fahrer-Fahrzeug-Schnittstelle – Interaktion des Menschen mit dem Produkt. In: Ebel, B., Hofer, M.B. (eds.) Automotive Management, pp. 319–337. Springer, Heidelberg (2014). doi:10.1007/978-3-642-34068-0_22
7. Bubb, H., Vollrath, M., Reinprecht, K., Mayer, E., Körber, M.: Der Mensch als FahrerAutomobilergonomie. In: ATZ/MTZ-Fachbuch, pp. 67–162. Springer Fachmedien, Wiesbaden (2015). doi:10.1007/978-3-8348-2297-0_3
8. Fabbri, K.: A brief history of thermal comfort: from effective temperature to adaptive thermal comfort. In: Indoor Thermal Comfort Perception, pp. 7–23. Springer, Switzerland (2015). doi:10.1007/978-3-319-18651-1_2
9. Willems, W.M., et al.: Raumklima/Behaglichkeit. In: Vieweg Handbuch Bauphysik Teil 1, pp. 356–376. Vieweg & Sohn Verlag, Wiesbaden (2006). doi:10.1007/978-3-8348-9123-5_4
10. Kordjamshidi, M.: House Rating Schemes. Springer, Heidelberg (2011)
11. Lee, D.W.: Impact of a three-dimensional air-conditioning system on thermal comfort: an experimental study. Int. J. Automot. Technol. **16**(3), 411–416 (2015)
12. Konstantinov, M., Wagner, C.: Numerical simulation of the thermal comfort in a model of a passenger car cabin. In: Dillmann, A., Heller, G., Krämer, E., Wagner, C., Breitsamter, C. (eds.) New Results in Numerical and Experimental Fluid Mechanics X. NNFMMD, vol. 132, pp. 383–393. Springer, Heidelberg (2016). doi:10.1007/978-3-319-27279-5_34
13. Thomschke, C., et al.: Bewertung der transienten thermischen Behaglichkeit in einer realen Fahrzeugumgebung. In: Fifth German-Austrian IBPSA Conference (2014)
14. DIN ISO/TS 14505-2, Ergonomie der thermischen Umgebung –Beurteilung der thermischen Umgebung in Fahrzeugen, Teil 2: Bestimmung der Äquivalenttemperatur (ISO 14505-2:2006); Deutsche Fassung EN ISO 14505-2:2006
15. DIN EN ISO 7730, Ergonomie der thermischen Umgebung – Analytische Bestimmung und Interpretation der thermischen Behaglichkeit durch Berechnung des PMV- und des PPD-Indexes und Kriterien der lokalen thermischen Behaglichkeit (ISO 7730:2005); Deutsche Fassung EN ISO 7730:2005
16. Reilhac, P., Moizard, J., Kaiser, F., Hottelart, K.: Cockpitkonzept für das teilautomatisierte Fahren. ATZ - Automobiltechnische Zeitschrift **118**(3), 44–49 (2016). Jahrgang

Thermal Management, Consumption Optimization

Condensation in Exhaust Gas Coolers

Nuria Garrido González(✉)

Volkswagen AG, Wolfsburg, Germany
nuria.garrido.gonzalez@volkswagen.de

Abstract. Exhaust gas recirculation is increasingly being integrated into both diesel and gasoline engines with the focus on reducing emissions or on improving fuel efficiency, respectively. Also the potential in terms of energy of warm exhaust gases is becoming more investigated. These relative new techniques involve the cooling of the exhaust gas and so are bringing some new challenges, since exhaust condensation may occur under certain circumstances. Aim of this paper is to clarify, when this condensation process begins and which exhaust components are likely to be found in condensate.

Keywords: Condensate · Exhaust gas cooling · Dew point · Exhaust heat exchanger

1 Diesel and Gasoline Exhaust Gas: Water Dew Point

Diesel and gasoline fuels are mixtures of hydrocarbons (CxHy) whose combustion with the in the air present oxygen produces primarily carbon dioxide and water vapor.

The first fact affecting the water amount in exhaust is the fuel proportion hydrogen to carbon. Gasoline usually contains hydrocarbons with 4-12 carbon atoms while diesel is heavier and presents typically 12-20 carbon atoms. However both fuels keep approximately the weight proportion 86 % carbon and 14 % hydrogen, [1]. Taking this mass relation into account, a generic hydrocarbon $C_{0.07}H_{0.14}$ is assumed in this study in order to simplify the following analyses.

The second factor having an effect on water quantity is lambda, the air-fuel-ratio, which informs about the air quantity the engine is working with. When lambda takes the value one or higher, fuel disposes of enough oxygen for its complete combustion. Main difference is that with lean mixtures, an air excess is available and oxygen appears on the reaction products side too. Last, rich mixtures provide the mixture with more fuel than possible to burn and so fuel can be found on the products side as well.

$$aC_{0.07}H_{0.14} + b(O_2 + 3.76N_2) \rightarrow cCO_2 + dH_2O + eN_2 + fO_2 + gC_{0.07}H_{0.14}$$

- For $\lambda = 1$ the complete ideal reaction coefficients take following values:

$$\mathrm{a} = 1$$

$$\mathrm{b} = (0.07 \text{ x } 2 + 0.14/2)/2$$

C. Junior et al. (eds.), *Energy and Thermal Management, Air Conditioning, Waste Heat Recovery*,
DOI 10.1007/978-3-319-47196-9_9

$$c = 0.07$$

$$d = 0.14/2$$

$$e = b \text{ x } 3.76$$

$$f = 0$$

$$g = 0$$

This general fuel combustion reaction leads for stoichiometric (λ = 1) conditions to a water vapor concentration at the products side of the equation of approximately 13 % (in volume or mole), the same as for carbon dioxide, whereas the nitrogen concentration achieves up to 74 %. Since gasoline engines usually operate under (nearly) stoichiometric conditions, this 13 % exhaust water vapor concentration can be assigned to them.

- For $\lambda > 1$, lean mixtures, the combustion reaction is described with:

$$a = 1$$

$$b = (0.07 \text{ x } 2 + 0.14/2)/2\lambda$$

$$c = 0.07$$

$$d = 0.14/2$$

$$e = b \text{ x } 3.76$$

$$f = (\lambda - 1)\ b$$

$$g = 0$$

This case can describe the typical operation of diesel engines, which usually run under lean conditions. This deviation decreases the water concentration in the exhaust due to the dilution effect caused by the excess air.

- When $\lambda < 1$, rich mixtures, coefficients take next values:

$$a = 1$$

$$b = (0.07 \text{ x } 2 + 0.14/2)/2\lambda$$

$$c = 0.07\lambda$$

$$d = 0.14/2\lambda$$

$$e = b \text{ x } 3.76$$

$$f = 0$$

$$g = (1 - \lambda)a$$

Nevertheless, it is interesting to note that the produced water quantity per kilogram burnt fuel remains nearly the same, about 1.3 kg, as can be distinguished in Fig. 1. Water coming with the charge air is, in this simplified study, regarded as negligible, since the ambient typical 8-12 g water per kilogram air would maximal lead to less than 180 g in the exhaust per kilogram burnt fuel.

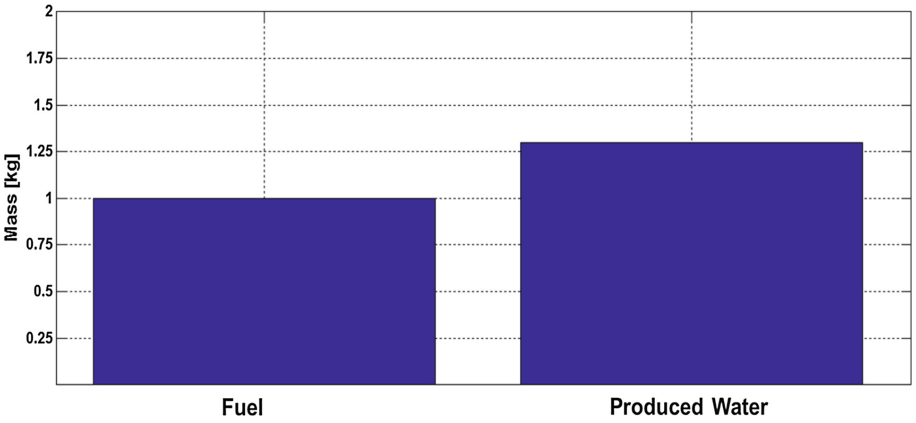

Fig. 1. Water produced by the combustion of 1 kg fuel.

Once the water vapor concentration in exhaust gas is known, the water dew point can, by means of the Dalton law and water saturation curve, be easily derived. The water concentration derived from the combustion reaction results in a water partial pressure which is associated with a saturation temperature. This temperature represents the dew point and is characteristic of each substance.

$$p_{H2O,exhaust} = p_{exhaust} x_{H2O}$$

$$T_{DP} = T_{sat}\left(p_{H2O,exhaust}\right)$$

Higher exhaust pressures imply higher water partial pressures, which correspond to higher saturation temperatures. It means, that exhaust gas coolers working under high pressure are more susceptible to condensation than other heat exchangers operating under low pressure conditions, even when the gas composition is the same. In [2], it was shown, how an increase of 100 mbar in exhaust pressure causes a saturation temperature increment of approximately 2°C.

In Fig. 2, the dependency on air-fuel-ratio for the exposed generic fuel at 1 bar exhaust pressure is described. Under stoichiometric conditions, water vapor represents

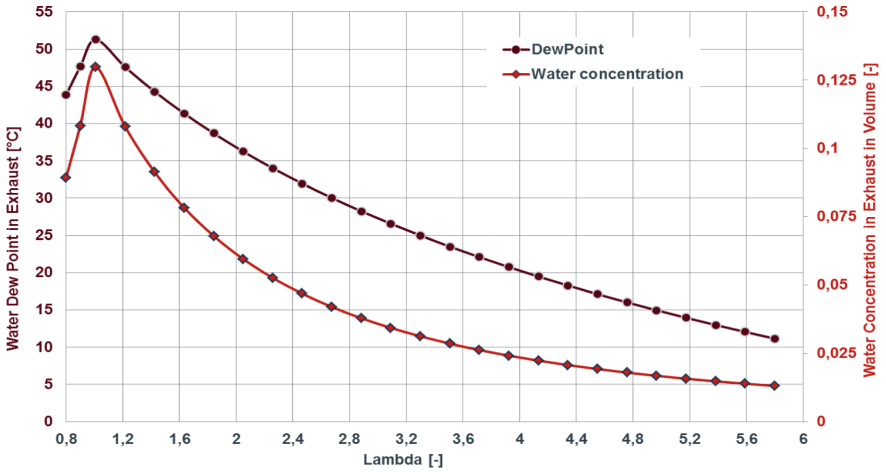

Fig. 2. Water dew point and concentration in the exhaust depending on air-fuel-ratio.

the mentioned 13 % of the exhaust gas and condensation occurs below about 52°C. For mixtures containing two times more air than what for the fuel combustion necessary, $\lambda = 2$, water concentration supposes only 6 % and the dew point decreases down to 36°C. As can be seen, the highest dew point temperatures correspond to stoichiometric conditions, as only there, neither excess of air nor excess fuel occurs and, thus, no dilution. For rich mixtures, the air scarcity disables the complete combustion and residual fuel can be found at the exhaust.

It has to be mentioned, that when using exhaust gas recirculation, the reactors side of the combustion reaction should include those burnt gases in form of water vapor, carbon dioxide as well as an additional nitrogen source. If this recirculation is done keeping lambda invariable, non alteration in the exhaust composition would be seen. On the other side, if this recirculated exhaust gas substitutes part of the excess fresh air and lambda decreases, the effect is a lower water dilution.

2 Condensation Cooling Requirement

To operate an exhaust cooler under condensing conditions brings some technical issues apart from the water removal. The water phase change vapor to liquid releases a huge amount of energy, corresponding to vaporization enthalpy, 2400 kJ per kilogram condensing water have to be removed.

$$\dot{m}_{cool} c_{p_{cool}} (T_{cool,out} - T_{cool,in}) = \dot{m}_{cond} h_{vap} + \dot{m}_{exh} c_{p_{exh}} (T_{exh,in} - T_{exh,out})$$

As soon as the condensation begins, heat removed by the coolant consists of two components: the sensible heat due to the gas cooling and the latent heat coming from the condensing water. Different to the condensation of a pure substance, the partial condensation of water in the exhaust does not occur at constant temperature but

following the saturation curve as the water content decreases. Even though, the contribution of this last mechanism penalizes the cooling part and the cooler efficiency decreases notably.

3 Condensable and Non-condensable Condensate Components

In Sects. 1 and 2, the exhaust gas has been described as a mixture of water vapor, carbon dioxide, nitrogen and residual fuel or oxygen when running below or above stoichiometric conditions, respectively. Along general lines, that consideration was useful and adequate for estimating the water concentration in exhaust and its dew point, because pollutant concentrations in exhaust gas mixtures are negligible compared to the water, carbon dioxide and nitrogen amounts and should not cause significant error. But when analyzing the condensed water quality, those pollutants may affect drastically the condensate quality, even though their presence in exhaust is only marginal.

Figure 3 shows exemplary raw emissions values for diesel and gasoline engines without after treatment. It can be seen that undesired combustion products like particle matter, unburnt hydrocarbons, nitrogen and sulfur oxides or carbon monoxide come into consideration. They occur due to several factors like fuel impurities in the case of sulfur, nitrogen coming with the intake air or uncompleted combustions, among others.

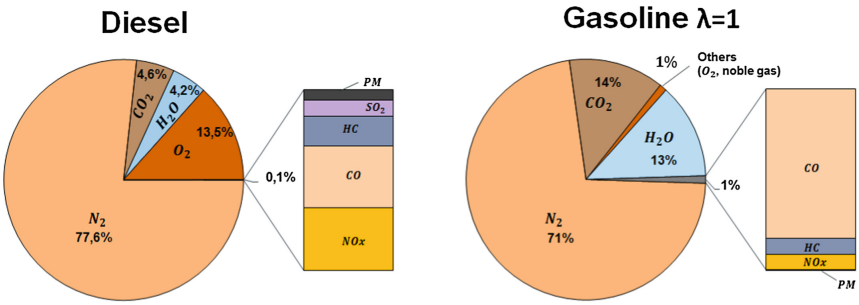

Fig. 3. Exemplary raw emissions values for diesel [3] and gasoline [4] engines (in volume).

It is well known that nitrogen and sulfur oxides build acids in presence of water vapor. These acids and water vapor build binary and ternary systems, whose dew points may strongly diverge from dew point of pure water. Furthermore, the composition of these condensing mixtures depends on condensing temperature. The sulfuric acid-water system has higher dew points than pure water (often above 100°C) and, thus, tends to form the first condensing droplets in exhaust gas coolers. Operation points at temperatures between the sulfuric acid - water and pure water dew points suppose the highest corrosion risk, since the acidic concentration of these droplets is less diluted and could achieve up to 30 %.

In the case of nitrogen oxide, the formation of nitric and nitrous acid – water systems builds less aggressive condensate, thus the dew points of their acid-water systems lie near the pure water dew point. When those systems start to condense at about 50°C, pure water vapor is condensing to a greater extent and causes an acid dilution.

The presence of solids in the exhaust gas stream will favor water droplets condensing upon them and acts so as an activator. Even in the case of gasoline exhaust gas, whose particle size lies in nanometer range, particle may agglomerate in condensate and build larger ones. Particles can also contribute to fouling in parts of the exchanger where condensate tends to collect, when at higher operation temperatures condensate evaporates leaving them behind.

Exhaust after treatment systems can strongly affect the condensate composition. For instance, three way catalyst operating under rich conditions converts carbon monoxide with water into carbon dioxide and hydrogen, as a result of secondary reactions. The latter participates in the nitrogen oxides transformation into ammoniac. These reactions could also take place by stoichiometric operation points, though to a very lesser extent. The described mechanism is responsible for the neutral or even alkaline pH-values of condensates of gasoline engines with three way catalyst. In diesel engines operating with reduction agent after treatment, some of the ammoniac contained in the reduction agent itself may be still present at the exhaust. In contrast to other condensate components, which condense at specific temperatures, ammoniac gas tends to dissolve easily in liquid water.

Aside the above mentioned condensate components, some others like organic acids or hydrochloric acid may be present in condensate too, although in a lower amount than the above described.

4 Condensate Analysis and Corrosiveness

Numerous condensate samples have been collected with a gasoline engine, whose specification is summarized in Table 1.

For the collecting task, a small part of the exhaust gas was derived to a stainless steel heat exchanger placed after the three way catalyst. The exhaust gas was cooled below the pure water dew point. Due to its position, downstream of the after treatment, all collected samples showed neutral to alkaline pH-values, between 6.9 and 8.8.

Table 1. Test engine specification

Configuration	4 Cylinder inline
Displacement	1395 cc
Valves per cylinder	4
Compression ratio	10,5 : 1
Max. Power	90 kW at 5000-6000 rev/min
Max. Torque	200 Nm at 1400-4000 rev/min
Fuel	Gasoline Super ROZ 95
Exhaust gas treatment	3 way catalyst

Probes collected when operating under rich conditions; had the highest pH-values, caused by its higher ammoniac content.

Analysis via ion chromatography of four representative collected samples, regarding stoichiometric conditions (A and B) and rich conditions (C and D), are shown in Fig. 4. Differences between samples A and B or C and D are due to several factors like condensate collecting temperature, engine operation point or three way catalyst state. However, it can be easily distinguished, how condensates collected under stoichiometric conditions present much lower pollutant content.

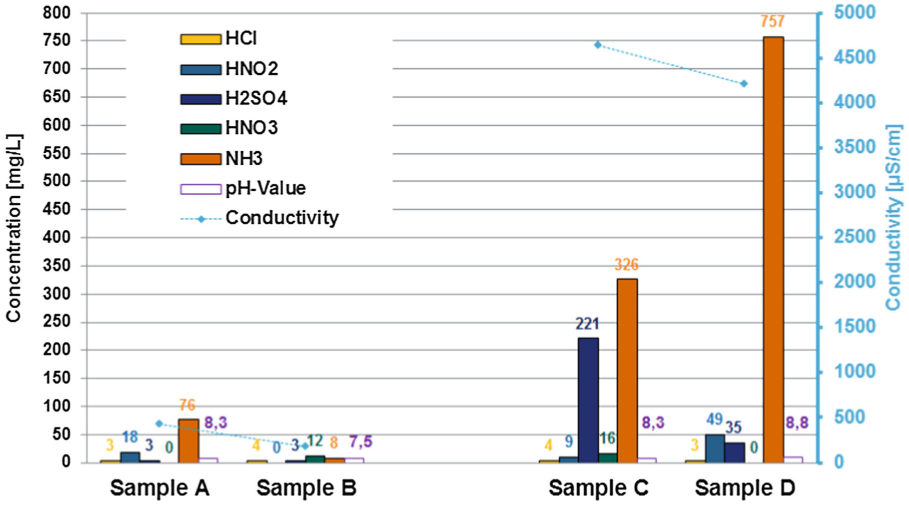

Fig. 4. Ion chromatography condensate analysis.

The above described samples are used to quantify the corrosiveness of condensate at 50°C on stainless steel 1.4301 and on aluminum. For the electrochemical tests, a silver reference electrode, a platina counter electrode as well as the work electrode are partial immersed in an electrolyte solution (condensate). The three electrodes are connected to a potentiostat, Fig. 5.

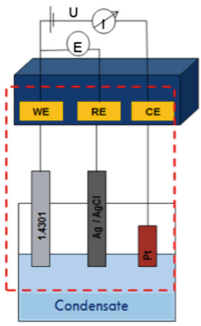

Fig. 5. Polarization cell sketch.

In order to evaluate the corrosion behavior, a constant potential is imposed between the work and the counter electrode for a determined time period and then varied in small increments. Depending on the so established current flows, the corrosion behavior can be estimated, since the current density is a signal of the ion transfer between the studied metal and the condensate. Figure 6 shows the corrosion test results. Stainless steel was tested against samples A and C, corresponding to stoichiometric and rich conditions. Analog, the aluminum electrode corrosion ratio was measured with samples B and D.

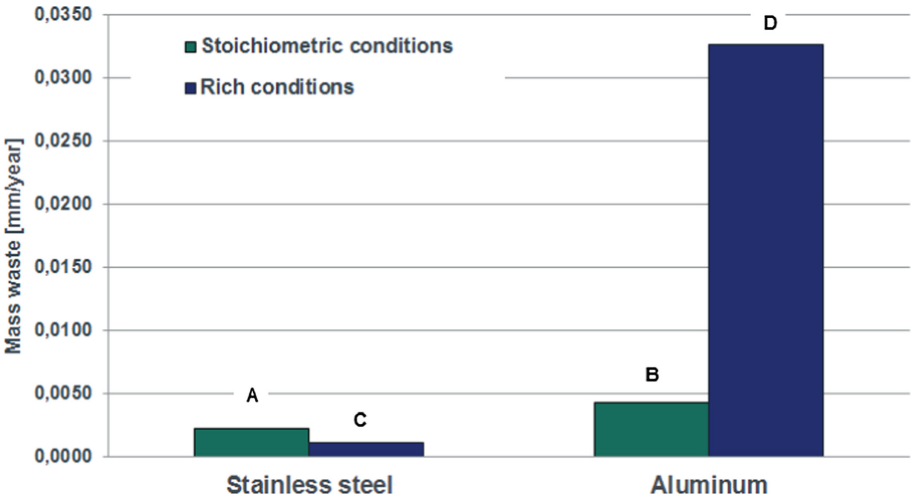

Fig. 6. Corrosion ratio caused by condensate on diverse metals.

It becomes evident at first view that aluminum is significantly more susceptible to be corroded by exhaust gas condensate than stainless steel. Also the high ammoniac and moderate acids concentrations in sample D, with an 8.8 pH-value, derive in a much major aluminum mass waste. On the other side, stainless steel does not show a greater corrosion with condensate collected under rich conditions. Its corrosion rates remain moderated under the condensate light basic conditions.

5 Conclusion and Outlook

Water vapor concentration in exhaust gas has been theoretically investigated at several engine operation points and its dew point has been calculated. The influence of fuel composition, air-fuel-ratio or exhaust pressure on condensation temperature was shown. Typical condensate pollutants have been discussed. Electrochemical tests for estimating the corrosiveness of condensate on stainless steel and on aluminum have been carried out.

Main facts to take into account when operating with exhaust gas cooling are listed below:

1. Even though the water production of about 1.3 kg per kilogram burnt fuel in gasoline and diesel engines is very similar, the water concentrations in the exhaust gas of both engines differ considerably. Gasoline engines, operating near stoichiometric conditions, show the highest water dew point of about 52°C. Diesel engines typically operate with air excess, causing a water dilution effect in the exhaust gas and thus a significantly decreased water dew point.
2. Exhaust gas pressure causes a shift of the water dew point. For the same water concentration in exhaust, higher pressure leads to higher water partial pressure and thus to an increased condensation temperature. Therefore, condensation in high pressure EGR coolers starts earlier than in low pressure heat exchangers.
3. Exhaust gas coolers operation points at temperatures between the sulfuric acid - water system and pure water dew point, suppose the highest corrosion risk, due to the higher acidic concentrations of the first condensing droplets.
4. After treatment systems can in some cases (three way catalyst or reduction systems) shift the condensate pH-value from acid to alkaline. Exhaust gas coolers operating without after treatment can build more corrosive acidic condensate than the neutral/alkaline condensates downstream of the after treatment.
5. For gasoline engines, condensate quality is significantly higher when operating under stoichiometric conditions.
6. Condensate corrosiveness has been tested on stainless steel 1.4301 and aluminum electrodes. Based on the results, stainless steel shows much higher resistance against alkaline/neutral exhaust condensate than aluminum and less susceptibility to air-fuel ratio.

References

1. Bennett, S.: Medium/Heavy Duty Truck Engines, Fuels and Computerized Management Systems. Cengage Learning, Delmar (2015)
2. Roeder, E., Faust, P.-U., Hattingen, U., May, H.: Zum Einfluß der Betriebsbedingungen eines Ottomotors auf die Zusammensetzung des Abgaskondensates, ATZ (1985)
3. Klingenberg, H.: Automobile Exhaust Emission Testing: Measurement of Regulated and Unregulated Exhaust Gas Components, Exhaust Emission Tests. Springer, Heidelberg (1996)
4. Reif, K.: Abgastechnik für Verbrennungsmotoren. Springer, Heidelberg (2015)

Waste Heat Utilization, Thermoelectrics, Heat Storage Systems

Reproducibility and Reliability in Manufacturing New High-Temperature Thermoelectric Modules

Karina Tarantik, Martin Kluge(✉), Kilian Bartholomé, Eugen Geczi, Uwe Vetter, Mark Vergez, and Jan König

Fraunhofer-Institut für Physikalische Messtechnik IPM, Heidenhofstraße 8, 79110 Freiburg, Germany
martin.kluge@ipm.fraunhofer.de

1 The Basics of Thermoelectric Waste Heat Recovery

1.1 Introduction

What is thermoelectrics? [1] - Thermoelectrics refers to the direct conversion of an electrical current flow into a heat flow as well as the heat flow into a current flow – thermoelectrics works in both ways.

The basic principle was already recognized by Thomas Johann Seebeck in 1821. He observed that a compass needle near two different, interconnected metal wires is deflected when the temperatures at the junctions differ, whereby the degree of deflection is proportional to the temperature difference. This is due to an electrical field that is created by the temperature gradient on the conductors.

In 1834, the French scientist Jean Peltier discovered that this effect can be reversed and used as a heat pump: if a current is connected to the interconnected conductors, a temperature gradient is created at the junctions. Thermal energy is transported from one junction to the other. The so-called Peltier effect can be used for heating or cooling. The maximum possible yield when heat is thermoelectrically converted into electrical energy is physically limited by the efficiency of the Carnot cycle process.

1.1.1 Figure of Merit

In 1909 and 1911, Edmund Altenkirch introduced a constant property model to derive the maximum efficiency of a thermoelectric (TE) generator as well as the performance of a cooler, when the design and operating conditions where fully optimized [2]. This relationship, later developed into the 'figure of merit' ZT, and revealed that good thermoelectric materials should possess large Seebeck coefficients (S), high electrical conductivity (σ) and low thermal conductivity (λ). The mathematical relation is shown in Eq. 1. Along with reproducibility and reliability, ZT has been the main driver of thermoelectric materials development in recent history.

C. Junior et al. (eds.), *Energy and Thermal Management, Air Conditioning, Waste Heat Recovery*,
DOI 10.1007/978-3-319-47196-9_10

$$ZT = \frac{S^2\sigma}{\lambda}T \tag{1}$$

Various TE material classes with high ZT values are known and recognised as suitable for the conversion of waste heat into electrical energy. The maximum ZT value (ZT_{max}) is attained at different temperatures depending on the material class and the exact composition. However, the average ZT value (ZT_{av}) across a specific temperature range is required to determine the material efficiency for a certain temperature combination (Eq. 2),

$$\eta = \frac{\sqrt{1+ZT_{av}}-1}{\sqrt{1+ZT_{av}}+\frac{T_c}{T_h}} \cdot \eta_{Carnot} \quad \text{with} \quad \eta_{Carnot} = \frac{T_h - T_c}{T_h} \tag{2}$$

with T_c: cold side temperature (heat sink) and T_h: hot side temperature (heat source).

Figure 1 shows the conversion efficiency of TE converters, as derived from their material property ZT versus the Carnot efficiency. State-of-art converters exhibit a peak ZT value of approximately 0.8–1.0 and reach efficiencies in the range from 5–10%.

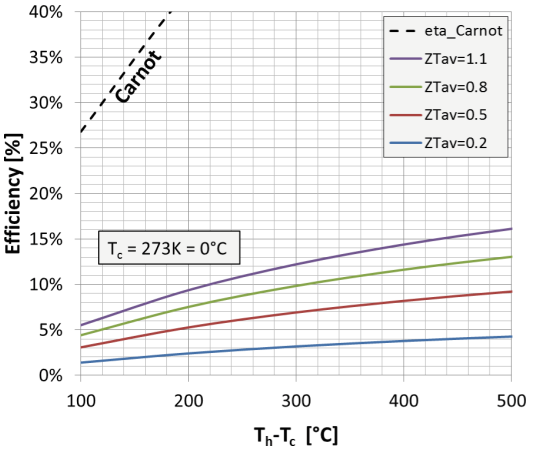

Fig. 1. Conversion efficiency at certain ZT values vs. Carnot efficiency

1.2 System Design Aspects

In a system design, the TE material is typically applied in the form of TE modules which consists of n- and p-type TE materials (legs) that are connected thermally parallel and electrically in series (see Fig. 2). Waste heat is converted by means of a heat flow through the TE module which generates an electrical current in the module. The electrical connection between the TE legs is realized in most cases by bonding the legs onto a contact material, usually a metallic strip. The contact resistance between the TE legs and the contact material should be very low in order to reduce losses caused by

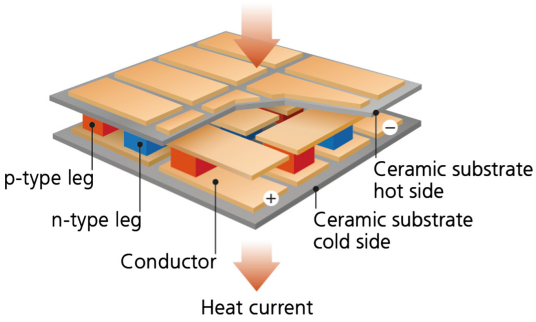

Fig. 2. Schematic view of a thermoelectric module.

Joule heating. The backbones of the TE module are two thin and thermally high conductive but electrically isolating substrates, most commonly ceramic plates. The numbers and dimensions of the TE legs differ according to the intended application of the module.

The thermoelectric modules are placed between a hot source, e.g. an exhaust gas heat exchanger, and a cold sink, e.g. a fluid cooler/heat exchanger. In combination this arrangement forms a thermoelectric generator (TEG). When designing the TEG the thermal resistance of the modules as well as the electrical load resistance of the system have to be carefully balanced in order to obtain the maximum power output [3, 4]. Due to design fundamentals, the system efficiency is typically less than 50% of the conversion efficiency of the thermoelectric material.

2 High Temperature Module Manufacturing

2.1 The Half-Heusler Alloys

Among the numerous materials studied at the Fraunhofer IPM (skutterudites, silicides, chalcogenides, …), the half-Heusler alloys have emerged to be the most reliable and most durable material class for high temperature TE applications. It allows for a usage range of up to 600 °C for its active material temperature. This high working temperature yields high conversion efficiencies in applications that are currently not accessible with commercial Bi_2Te_3 materials due to thermal limitations at above 250 °C.

After a successful scale up of powder and bulk material production in the public funded project “thermoHEUSLER” [5, 6], the developments at Fraunhofer IPM continued towards a semi-automated module production line.

Figure 3 shows the half-Heusler material properties that have been obtained by the developing partners Isabellenhütte-Heusler GmbH & Co.KG and Vacuumschmelze GmbH & Co.KG.

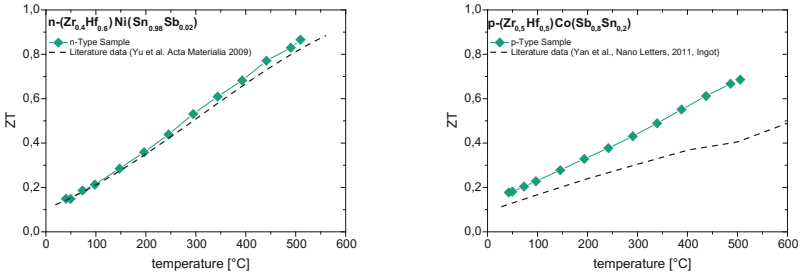

Fig. 3. Material properties obtained by Isabellenhütte Heusler GmbH & Co.KG (n-type, left) and Vacuumschmelze GmbH & Co.KG. (p-type, right) [7].

2.2 Module Manufacturing Process

The production of TE modules can be described with the following process steps (Fig. 4):

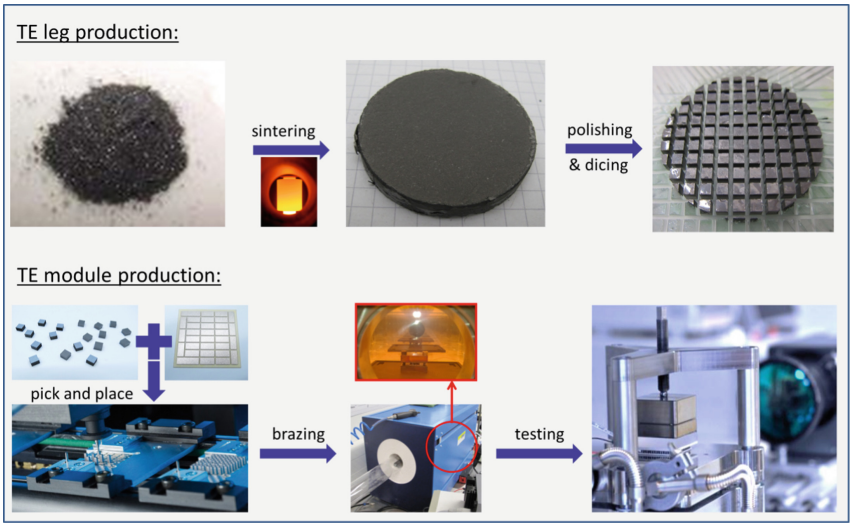

Fig. 4. TE leg and module production steps at Fraunhofer IPM.

TE leg production

- Sintering of powders: N- and p-type semiconductor pucks are compacted and sintered from powder to optimize the TE properties.
- Polishing: During the polishing step the TE leg height and surface quality are adjusted.
- Dicing: The legs are cut into their final shape.

TE module assembly

- Pick and place: N- and p-type legs are arranged on a metallized substrate ceramic (usually Al_2O_3).
- Brazing: The substrate and legs are joined using high temperature brazing process.
- Wiring/interconnection: Lead wires are attached to the module.
- Final Quality Check: Key characteristics are validated.

A cost effective and reliable module production process is essential for the industrialization of thermoelectric materials in waste heat recovery.

2.3 Recent Breakthrough

In July 2016 a new semi-automated production line has been put into operation at Fraunhofer IPM. With the new pilot-line, it is now possible to reduce the module production costs by a factor of 10. This allows moving a significant step closer towards the industrialization of the technology and opening the possibility of small series production.

2.4 Module Performance

The current top-selling module design exhibits a thermal contact area of 16 × 16 mm^2 and involves 7 p-n couples (Fig. 5). With a demonstrated power density of up to 1.1 W/cm^2, the module has achieved conversion efficiencies of up to 5.2% (both at ΔT = 530 K, T_{cold} = 20 °C). By scaling the leg geometry the module can be individually matched to meet the application.

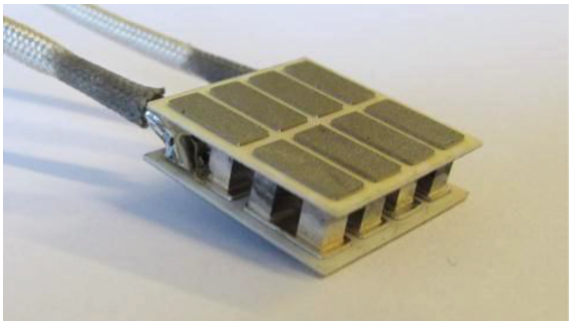

Fig. 5. Half-Heusler module made by Fraunhofer IPM.

2.5 Manufacturing Reproducibility

During module production, manufacturing reproducibility is ensured by both in-line and offline measurements. Identified key characteristic parameters which are checked

are the module height and the module internal resistance at room temperature. Reasonable reproducibility values have been achieved for both:

$$\begin{aligned} \text{Module height deviation :} \quad & < 1\% \quad \text{(out of 160 samples)} \\ \text{Module internal resistance deviation :} \quad & < 6\% \quad \text{(out of 160 samples)} \end{aligned}$$

2.6 Reliability

Thermal cycling tests performed by Faurecia Emission Control Technologies, Germany GmbH in Augsburg have confirmed that the TE modules are durable enough to withstand 1,000 thermal shock cycles between 20 °C and 550 °C exhaust gas temperatures, even when being operated in air. During and after the test no significant degradation was observed. Figure 6 shows the applied test cycle and the test fixture. During the test the module's cold side temperature was maintained constant.

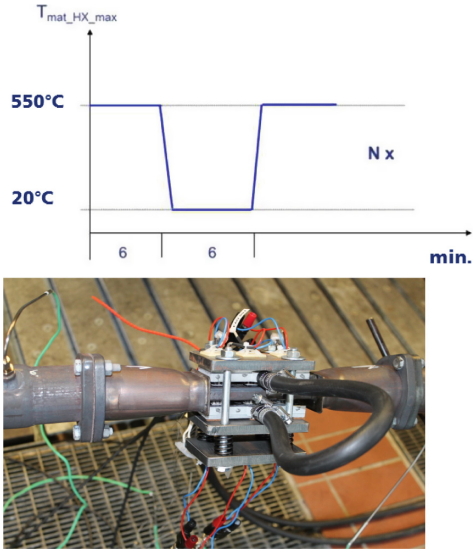

Fig. 6. Thermal cycle and test fixture.

2.7 Outlook and Future Challenges

The future of high temperature modules is tied to the identification of the right application. Today three major scenarios are considered: Automotive exhaust heat recovery, industrial waste heat recovery and combined heat and power systems (both industrial and residential). All applications inherit their need of a sufficient amount of prototypes and demonstrators to develop the system architecture and to assess economical and technical feasibility.

Despite the application, several challenges remain that need to be addressed by various means. Some of them and possible solution strategies are listed

Achieve a module cost reduction by …

- Fully automated, lean production with new and innovative production technologies
- Optimization of material usage (TE module downsizing), new and improved module designs
- Substitution or reduction of rare elements (like Hafnium)

Achieve a module performance improvement by …

- Continuous design improvements
- Advancements in TE material development

Achieve a module reliability improvement by …

- Advanced design methodologies and new module designs
- Process optimization and advanced in-line inspection technologies
- Extensive testing of modules designed for serial manufacturing

2.8 Summary

With its new semi-automated production line and advanced module manufacturing technology, Fraunhofer IPM has demonstrated that cost reduction, reproducibility and reliability are possible for high-temperature thermoelectric modules. We are ready to supply custom designed TE modules for thermoelectric generator applications ranging from automotive exhaust heat recovery to combine heat and power plants to industrial waste heat recovery.

References

1. König, J., et al.: Thermoelectrics: Power from waste heat, BINE Themeninfo I/2016, www.bine.info, FIZ Karlsruhe (2016). ISSN 1610-8302
2. Altenkirch, E.: Physikalische Zeitschrift **10**, 560–580 (1909); Physikalische Zeitschrift **12**, 920 (1911)
3. Rosenberger, M., et al.: Fahrzeugintegration eines thermoelektrischen Generators, Motor-technische Zeitschrift: MTZ 77, No.4, pp. 38–45 (2016). ISSN 0024-8525
4. Snyder, G.J., Ursell, T.S.: Thermoelectric efficiency and compatibility. Phys. Rev. Lett. **91** (14), 2003 (2003). doi:10.1103/PhysRevLett.91.148301
5. Bartholome, K., et al.: Thermoelectric modules based on half-heusler materials produced in large quantities. J. Electric Mater. **43**, 1775 (2014). doi:10.1007/s11664-013-2863-x
6. Abschlussbericht zum BMWI-Verbundprojekt thermoHeusler: CO2-Einsparung durch Entwicklung von preiswerten, thermoelektrischen Materialien und Modulen auf Basis von Halb-Heusler-Legierungen; FKZ 0327876, TIB Leipzig (2014)
7. Tarantik, K., et al.: Reproducibility and reliability in manufacturing thermoelectric modules based on half-heusler compounds. In: 35th International Conference & 1st Asian Conference on Thermoelectrics (ICT/ACT 2016), Wuhan, China (2016)

Thermoelectrics – An Opportunity for the Automotive Industry?

Daniel Jänsch(✉), Jens Lauterbach, Markus Pohle, and Peter Steinberg

IAV GmbH, Berlin, Germany
Daniel.Jaensch@iav.de

Abstract. The paper looks at the key issues in terms of what thermoelectrics (TE) can and must do for the automotive industry through to 2020+.

A brief introduction to the topic of waste heat recuperation and thermoelectric generators (TEG) is followed in the first section of the paper by an illustration of the potential offered by a fictive TEG ideally rated for use in the exhaust system of a passenger car with conventional powertrain, with an estimate of possible benefits and costs. This begins by asking which minimum contribution a new technology has to provide for it to be included by the automotive industry in the package of measures needed to achieve future CO_2 targets. A proposal is presented as the basis for the subsequent observations. The paper then looks at the necessary material/module efficiency and the required mean ZT value as well as availability.

This is followed by a brief description of the objective, consortium, job split, contents and scope together with a summary of selected results obtained with the consortium project TEG2020 funded by the BMBF (German Federal Ministry of Education and Research).

The very general theoretical observations in the first section are then compared in the second section with selected results obtained in test bench and vehicle measurements using the laboratory generator developed in the project. The focus here is not on the generator itself but on the impact of the conventional generator, the additional mass of the TEG and its exhaust gas backpressure, auxiliary power consumption and the necessary recooling.

The project results show that it is possible to realize the fictive TEG featured in the estimate of potential using the existing possibilities.

1 Introduction

Today and in the foreseeable future, most vehicles will be driven by fossil fuels. Reserves of fossil fuels are finite. Their extraction and utilization place a considerable burden on health, the environment and climate. Even so, it is still generally accepted that only a very small part of the energy contained in the fuel is used to actually propel the vehicle (Fig. 1). More than half of the fuel energy is still lost to the environment unused as waste heat, with considerable costs and consequences [1]. However, waste heat recuperation could help to achieve future CO_2 limits. The aim must therefore be to make use of this lost energy on the basis of economically viable technologies.

C. Junior et al. (eds.), *Energy and Thermal Management, Air Conditioning, Waste Heat Recovery*,
DOI 10.1007/978-3-319-47196-9_11

This is where thermoelectric converters come in. They convert heat directly into electrical energy for the vehicle electrical system; by relieving the pressure on the mechanically driven generator, they make it very easy to save fuel and reduce CO_2 emissions. Their unique properties are based on their solid-state-physical principle of operation. They therefore need neither chemical nor mechanical processes. However, a poor cost/benefit ratio and the critical availability of TE materials and modules have so far prevented the widespread industrial use of this technology. But many research teams throughout the world are being driven by the attractive prospects in combination with the huge technical and economic potential of the technology in order to solve the remaining challenges. For years now, there has been a growing number of scientific publications to this effect in renowned journals and papers presented at international energy, material and thermoelectrics conferences. More and more companies are announcing promising second-generation TE materials and modules in interesting quantities, or are even capable of supplying the same already today. We can therefore expect to see adequate volumes of TE materials and modules being made available in the next few years that also meet the special requirements of the automotive industry in terms of efficiency, quality, quantity and price. This would then also fulfill a significant prerequisite for the automotive industry to get involved in TEG development. Another particular challenge, especially for automotive use of this technology, consists in the need for high efficiency paired with the low energy supply in the urban cycle as well as resistance to high temperatures and alternating loads, in order to achieve CO_2 reductions in the test cycle in a relevant magnitude.

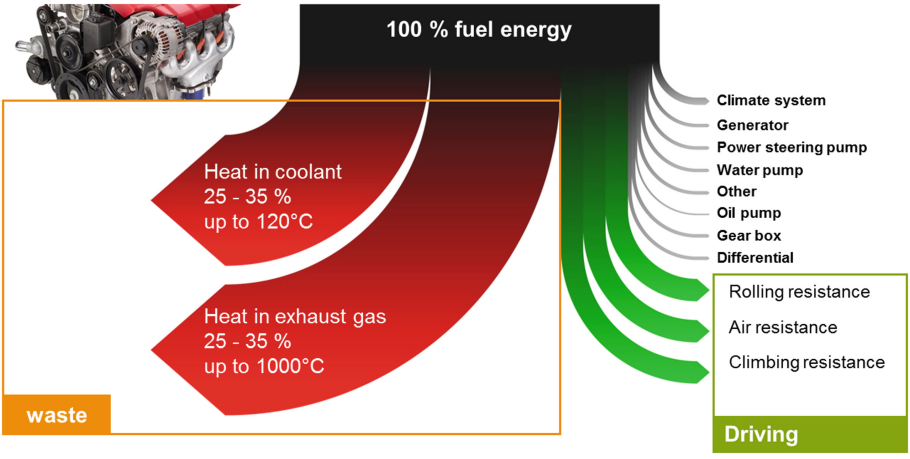

Fig. 1. Energy utilization of a passenger car engine

2 Benefits, Costs, Potential, Requirements and Availability

Before users will take a technology seriously, a reliable estimate is required of its potential contribution to achieving the set goals. New technologies in particular must provide early evidence of what they can offer when first introduced and which costs would be involved or acceptable. The central question for concepts looking at waste heat recuperation is: Which fuel savings or CO_2 reductions will be possible at which price?

2.1 Minimum Savings

Fuel savings of just one percent can already make a concept interesting, depending on its maturity and potential, and the costs involved in development and integration. In light of the economic aspects involved (e.g. costs for saving 1 % fuel or reducing 1 g CO_2, necessary mileage for reaching the payback point), TEGs will have to provide at least two to three percent in the **WLTC** (Worldwide Harmonized Light-Duty Vehicles Test Cycle) before they can be included in the industry's package of measures to cope with future CO_2 targets. For the vehicles described in the following potential estimate, this would mean a reduction of a good three, five and eight grams of CO_2 per kilometer in the **WLTC** in the standard/customer configuration, i.e. with corresponding load on generator and A/C compressor. Supercharged gasoline engines need to relieve the generator by about 50 W in the **WLTC** per gram of CO_2 reduction (see also Fig. 8). Accordingly, TEGS will have to supply approx. 150, 250 and 400 W into the vehicle electrical system on average throughout the **WLTC** in order to achieve the CO_2 targets.

2.2 Estimate

To get an idea of the potential offered by the technology and thus of its possible benefit, this paper estimates the possible CO_2 reduction that can be achieved with a TEG in the best case in the homologation and customer cycle. A simple method but one that it is accurate enough for the purpose involved here consists in roughly estimating the fuel consumption and thermal energy in the exhaust gas in relevant operating states for representative reference vehicles, in this case with conventional standard gasoline engine drives. The thermal energy available in the exhaust gas is used to derive the electrical energy or power that can be supplied to the vehicle electrical system on average by an ideally rated fictive reference TEG. It is then possible to obtain the potential fuel savings or CO_2 reductions in the cycle. The estimate takes account of all power consumption and consumption-enhancing effects of the TEG. It is also presumed that the power supplied is absorbed completely thanks to corresponding energy management and is used in a suitable way to relieve the combustion engine. Consideration is given to the following variants to obtain a field of potential that describes reality as generally as possible:

- Three reference vehicles with two auxiliary drive configurations
- Various fictive reference TEGs in a close-coupled position and away from the engine
- 80 driving profiles, including five real "customer journeys" with different driver types.

2.3 Reference Vehicles

The reference vehicles are defined by their rolling resistance levels and drive systems based on corresponding data. They represent the following segments: C/D (mid-range class) with 5.0 l/100 km, E/F (upper/luxury class) with 7.5 l/100 km and M/J (multi-van, SUV, utilities) with 10 l/100 km mean consumption in the **NEDC** (New European Driving Cycle), without generator and A/C compressor load (homologation configuration). Consumption in the normal configuration is about 20 % higher than the homologation configuration. It should reflect real average operation on the roads [2].

2.4 Fuel Savings

The graph shows possible fuel savings for a fictive TEG installed away from the engine in the cycle, on the highway and on a customer journey as well as cruising at constant speed (on the right) for the three vehicle segments. A TEG with ideal rating for the specific operation is scarcely capable of achieving targets values in excess of 2 % (yellow area, dotted lines) in the current **NEDC** homologation cycle. In the future **WLTC** homologation cycle and with a normal configuration, fuel savings of a good 2 % to 3 % are possible (green area, continuous lines), depending on the vehicle segment. Savings of more than 3 % and up to 5 % can be achieved in the customer and highway cycle respectively (Fig. 2).

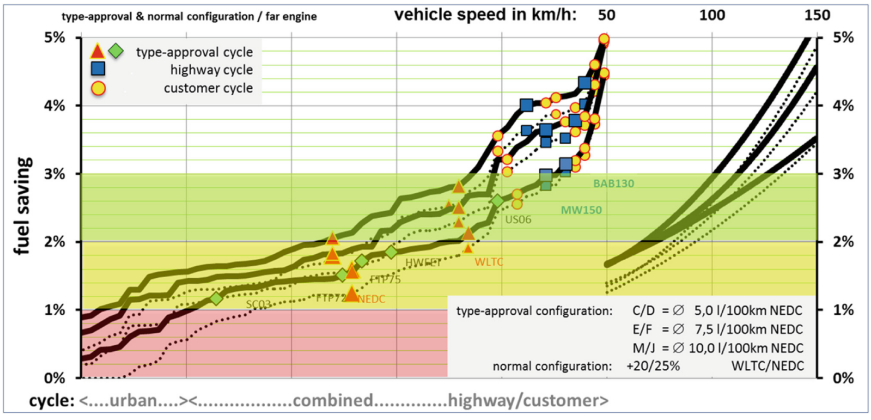

Fig. 2. Possible fuel savings for urban, combined and highway cycles and for customer driving and constant-speed cruising (on the right) in three vehicle segments

2.5 TEG Power

The corresponding electrical TEG power is shown here in Fig. 3. Accordingly, no effective power is possible for the reference vehicles in the urban/off-highway cycle for **NEDC** homologation configuration, and less than 150 W is possible in the **NEDC**. However, on average, power of between 200 W and > 1000 W is possible in the customer and highway cycle. Average TEG power of at least 150/250/400 W defined as being target-relevant is possible for the future **WLTC** homologation cycle for reference vehicles with normal configuration.

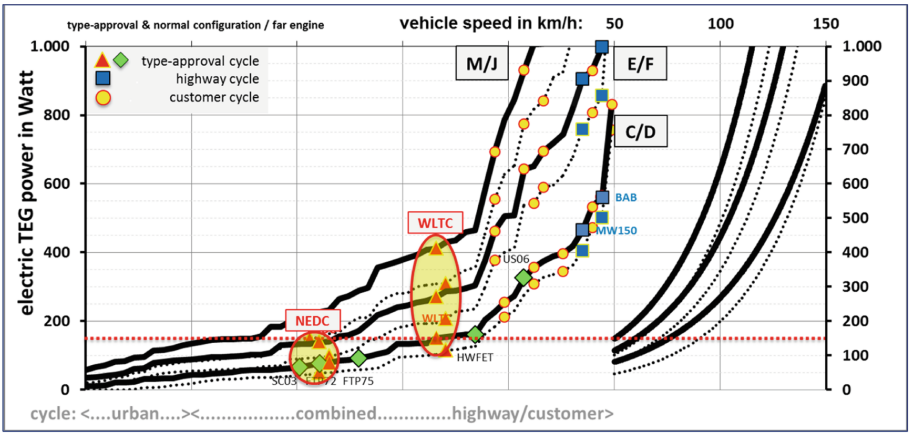

Fig. 3. Possible TEG power for urban, combined and highway cycles and for customer driving and cruising at constant speed (on the right) in three vehicle segments

3 CO_2 Reduction

Figure 4 shows the possible CO_2 reduction for all driving cycles und review and for cruising at between 50 and 150 km/h:

- For the urban cycle, only the upper segment shows relevant CO_2 reduction
- For the homologation configuration in the **NEDC**, CO_2 emissions are reduced by 1.5 respectively 2.8 and 4.2 grams per kilometer
- The reduction for highway and customer cycle and cruising at constant speed exceeds 12 g CO_2/km
- For the normal configuration in the **WLTC**, CO_2 emissions are reduced by 3.2 respectively 5.6 and 8.5 grams per kilometer
- For the urban cycle, the reduction is 2 to 5 g CO_2/km for the upper segments
- The reduction for highway and customer cycle and cruising at constant speeds amounts to up to 16 g CO_2/km

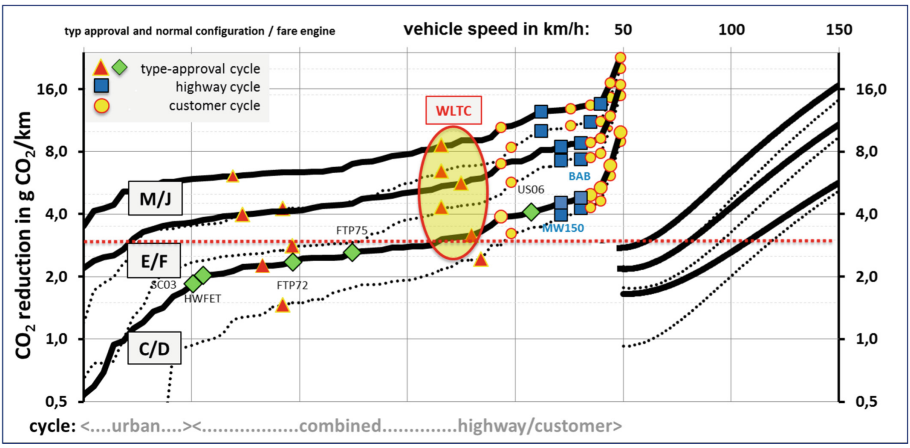

Fig. 4. CO_2 reduction of a TEG after EAT in cycle mode and cruising at constant speed for reference vehicles in homologation and normal configuration

Moving the TEG from the thermally less favorable position downstream of the EAT (**E**xhaust gas **A**fter-**T**reatment system) to a close-coupled position clearly increases the TEG power on account of the higher exhaust gas temperatures. The increase amounts to approx. 50 % for the single-flow system analyzed here. Although just a rough indication, this value clearly shows that close-coupled concepts are definitely worth checking and also pursuing, even if these are far more complex.

3.1 Material and Module Efficiency

That leaves the question as to what a TEG has to be like in order to achieve the intended target power. To start with, TEG power is greatly influenced by the heat supply, i.e. exhaust gas mass flow and temperature. This depends primarily on the vehicle and its drive and mode of operation. Anything that improves the heat supply or ensures that this is not used up before reaching the TEG is helpful, including in particular making adjustments to the position of the TEG (close-coupled position or away from the engine). Insulating the exhaust gas system up to the TEG also makes sense, where possible and permissible. Only two aspects of the TEG itself will be considered here.

For a constant heat supply, prime responsibility for the power lies with the efficiency of the heat exchanger systems and the modules. An estimate has been given of the module/material efficiency necessary for the target power. Figure 5 shows the average material/module efficiency required for the vehicle segments for three different heat exchanger systems with 50/66/75 % heat utilization in a position away from the engine (black) and a close-coupled position (red). The target power can be achieved with a good 8 %, or even less than 5 % with excellent heat exchangers in a close-coupled position.

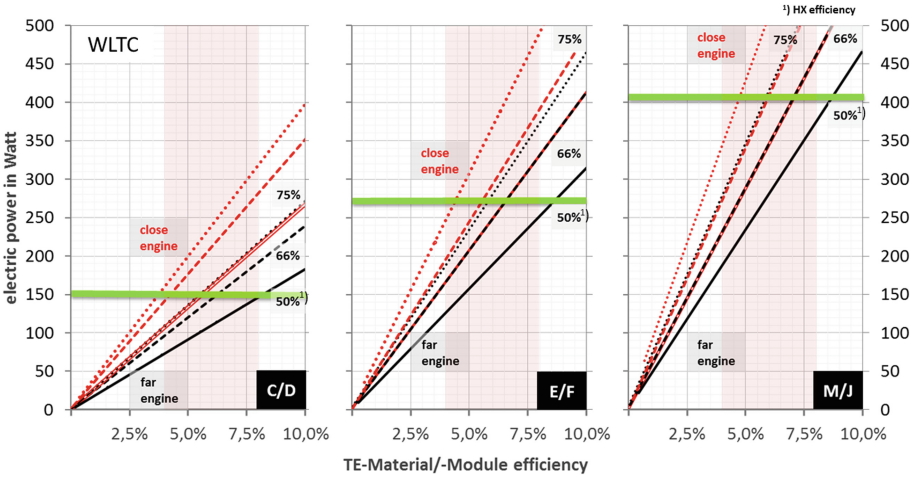

Fig. 5. Necessary material/module efficiency

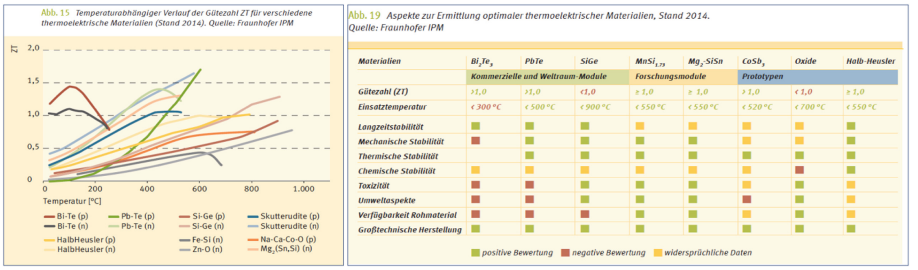

Fig. 6. ZT curve and development status of promising TE materials [3]

Table 1. ZT_{avg}, ZT_{peak} und material efficiency η for TE-Material of Fig. 6

	Bi-Te(p)			Pb-Te(p)			Skutterudite(p)			HalbHeusler(p)			Na-Ca-Co-O(p)		
T_{cold} / T_{hot}	ZTavg	ZTpeak	η	ZTavg	ZTpeak	η	ZTavg	ZTpeak	η	ZTavg	ZTpeak	η	ZTavg	ZTpeak	η
[°C] / [°C]	[-]	[-]	[%]	[-]	[-]	[%]	[-]	[-]	[%]	[-]	[-]	[%]	[-]	[-]	[%]
25 / 250	1,23	1,46	10,3%	0,09	1,65	1,2%	0,44	1,06	4,9%	0,29	0,86	3,4%	0,16	0,71	2,0%
50 / 250	1,21	1,46	8,9%	0,10	1,65	1,1%	0,47	1,06	4,4%	0,30	0,86	3,1%	0,17	0,71	1,8%
50 / 500				0,41	1,65	6,8%	0,72	1,06	10,5%	0,45	0,86	7,3%	0,31	0,71	5,4%
100 / 500				0,45	1,65	6,3%	0,77	1,06	9,4%	0,48	0,86	6,6%	0,33	0,71	4,9%
100 / 600				0,65	1,65	9,5%	0,82	1,06	11,2%	0,54	0,86	8,3%	0,40	0,71	6,5%
150 / 600				0,71	1,65	8,9%	0,86	1,06	10,2%	0,57	0,86	7,5%	0,43	0,71	6,0%
	Bi-Te(p)			Pb-Te(n)			Skutterudite(n)			HalbHeusler(n)			Mg2(Sn,Si)(n)		
25 / 250	1,01	1,09	9,1%	0,51	1,41	5,5%	0,64	1,67	6,5%	0,34	0,98	3,9%	0,53	1,31	5,7%
50 / 250	1,00	1,09	7,8%	0,54	1,41	5,0%	0,67	1,67	5,8%	0,35	0,98	3,5%	0,56	1,31	5,1%
50 / 500				0,92	1,41	12,4%	0,96	1,67	12,8%	0,56	0,98	8,7%	0,84	1,31	11,6%
100 / 500				0,99	1,41	11,2%	1,01	1,67	11,4%	0,60	0,98	7,9%	0,89	1,31	10,4%
100 / 600				1,00	1,41	12,9%	1,12	1,67	13,9%	0,67	0,98	9,7%	0,97	1,31	12,6%
150 / 600				1,06	1,41	11,7%	1,18	1,67	12,5%	0,71	0,98	8,9%	1,02	1,31	11,4%
	Bi-Te(p)			**Pb-Te(p)(n)**			**Skutterudite(p)(n)**			**HalbHeusler(p)(n)**			**Na-Ca-Co-O /Mg2(Sn,Si) (p)(n)**		
25 / 250	**1,12**	**1,27**	**9,7%**	**0,30**	**1,29**	**3,6%**	**0,54**	**1,31**	**5,7%**	**0,31**	**0,92**	**3,7%**	**0,35**	**1,01**	**4,0%**
50 / 250	**1,11**	**1,27**	**8,4%**	**0,32**	**1,29**	**3,2%**	**0,57**	**1,31**	**5,1%**	**0,33**	**0,92**	**3,3%**	**0,36**	**1,01**	**3,6%**
50 / 500				**0,66**	**1,29**	**9,9%**	**0,84**	**1,31**	**11,7%**	**0,51**	**0,92**	**8,0%**	**0,57**	**1,01**	**8,8%**
100 / 500				**0,72**	**1,29**	**9,0%**	**0,89**	**1,31**	**10,4%**	**0,54**	**0,92**	**7,2%**	**0,61**	**1,01**	**8,0%**
100 / 600				**0,83**	**1,29**	**11,3%**	**0,97**	**1,31**	**12,6%**	**0,61**	**0,92**	**9,0%**	**0,69**	**1,01**	**9,9%**
150 / 600				**0,89**	**1,29**	**10,4%**	**1,02**	**1,31**	**11,4%**	**0,64**	**0,92**	**8,2%**	**0,73**	**1,01**	**9,0%**

It is also possible to roughly ascertain the average necessary ZT values for the **WLTC**: ZT_{max} values $\leq$ 1.2 or ZT_{avg} values $\leq$ 1.0 would be sufficient. TE material is usually described by means of its ZT_{peak}. However, without knowing the temperature-dependent ZT curve (Fig. 6), this value gives very little indication of the practical suitability of the TE material as shown in Table 1.

3.2 Availability

Thermoelectrics are increasingly becoming suitable for large-scale use [3]. At the moment, researchers are investigating promising materials and synthesis methods which already achieve figures of merit of ZT_{peak} = 1.5 to 2.5 in the laboratory. Materials with ZT_{peak} values of up to 1.5 are already suitable for use. TE materials with ZT_{peak} values of around 1.0 are commercially available. Together with the three classic examples Bi_2Te_3, PbTe and SiGe, the preferred materials include silicide, skutterudite or half-Heusler materials. There is currently no knowing which material will win the race. In the end, the choice of material will depend on the requirements (costs, efficiency, weight etc.) of the specific application. Such materials and corresponding modules have been available as prototypes for some time now, although scarcely on the free market. Today it is possible to produce silicides by the kilo, half-Heusler and PbTe materials on a multi-kilo scale and some skutterudites and Bi_2Te_3 by the ton. Current developments focus particularly on material and production costs.

[4] looks in detail at the "availability and maturity of thermoelectric materials for use" (as of 2014). The Austrian company Treibacher Industrie AG is featured as an example, offering powdered skutterudite material with *ZT* values > 1 on a multi-kilo scale for some time now. Half-Heusler modules should be available in small-scale production as from 2017. As part of the thermoHeusler^2 consortium project funded by the German Federal Ministry for Economic Affairs and Energy (BMWi) [5], Vacuumschmelze GmbH & Co. KG is looking at further development of a powder metallurgy process for manufacturing half-Heusler compounds, while Isabellenhütte is investigating further development of a smelting metallurgy process to the same end. The project aims to "develop material and module production suitable for volume production, together with a near-production manufacturing and installation concept for the TEG that boost cost efficiency to such an extent as to permit standard use of this technology in the medium term" [6, 7]. The Fraunhofer Institute for Physical Measurement Techniques (IPM) in Freiburg "has now developed and commissioned the world's only pilot production line for thermoelectric high-temperature modules" [8]. The semi-automatic production line produces large quantities of thermoelectric modules for up to 600 °C operating temperature at far lower costs than hitherto possible.

Finally it is also worth mentioning that module efficiency levels of 4 to 8 % depending on TE material have been reported in numerous publications for a long time now, e.g. [6, 9, 10].

3.3 Costs

The costs of innovative technologies are initially borne by the vehicle manufacturers, who then pass on the additional costs to their customers. Even if customers do not see the costs of measures reducing fuel consumption and emissions, because they are incorporated in the overall vehicle costs, each one must be economically viable in itself.

For customers buying new cars, lower operating costs and low fuel consumption are the most important purchasing criteria. More than half of new vehicles are used in the business customer segment (in Germany). Here as well as with commercial vehicles, economic rationale is almost exclusively decisive for the adoption of technical innovations. Technologies only prevail in the market if the higher acquisition costs are balanced out by lower operating costs.

The question as to what a TEG may cost needs to be answered by customers and manufacturers.

Various publications have indicated that manufacturers must invest up to € 50 for every gram of CO_2 saved per vehicle [11]. Accordingly, a TEG should not cost more than € 158 (C/D), € 280 (EF) or € 427 (M/J) referred to the **WLTC** in order to be included in the package of measures of the OEMs. Given that the respective mean net electrical power capacities are nearly identical in terms of amount, the costs referred to electrical power are almost exactly equal to the initial target of € 1 per watt indicated in many publications. However, it is also clear that the costs per gram of CO_2 and TEG efficiency can increase further going beyond 2020, so that even higher system costs will be acceptable in future. And the threat of penalties also means that new technologies in future will certainly offer better value for money.

Comments often say that the € 95/g excess emissions penalty would actually then be applicable. However, that would only be true once the automotive industry will have exhausted all measures that are "cheaper" than € 95/g and the fleet objectives are still not reached.

3.4 Payback Point

As far as the customer is concerned, the extra costs for a TEG would reach payback point "at the fuel pump" after about 77,000 km of mileage, depending on driving style, based on a price of € 1.50 per liter of gasoline fuel in the **WLTC**. In terms of appropriate payback periods, this is a challenge for customers with comparatively low mileage. However, the payback period will be far shorter in real customer cycles with **WLTC**-based costs, and may even be halved, depending on vehicle use.

3.5 Summary

To summarize the benefits of a suitably rated TEG in a passenger car, it can be said that depending on the vehicle and driving style, relative fuel savings and CO_2 reductions of two to three percent are possible on average in the combined cycle and up to five percent in the customer and highway cycle. The technology offers scarcely any improvement in the purely urban cycle on account of the low heat supply and the great

influence of cold starts. Higher relative savings are possible with higher energy supplies and higher exhaust gas temperatures (close-coupled positions!) or more efficient TEGs. It can be presumed that such TEGs can fulfill the initial conditions for many vehicle manufacturers, particularly for large and heavy vehicles. In our opinion, such generators could certainly be ready for volume production using materials and modules that are currently in development by 2020. For the most part, the prerequisites have been established in recent years. Prototypes of corresponding TE materials and modules are available. At the moment, global developments focus on industrialization, availability, costs, quality and durability.

4 Funding Project TEG2020

Making this outstanding technology accessible to the mass market was the motivation behind the consortium project TEG2020 (03X3552A) funded by the German Federal Ministry of Education and Research **(BMBF)** in the framework of the WING program - Material Innovations for Industry and Society.

The aim of this research project was to develop highly efficient, economical concepts and systems for thermoelectric generators (TEG) suitable for volume production that have been validated in theory and by experiments for recuperating heat lost from transport, propulsion, work and energy systems. An innovative, flexible modular concept should offer possibilities for adapting the TEG to different applications, target systems and output classes.

In the interests of high system efficiency, new installation and connection technologies have been pursued together with innovative approaches to integration and energy management which can be applied to a broad range of thermoelectric (TE) materials.

A flexible demonstrator system was produced by developing a suitable installation and connection technology, working with established bismuth and lead-telluride material systems. At the same time, attention also focused on half-Heusler materials as a suitable substitute for lead telluride on the high-temperature side. The key issue was to obtain a positive substance bond between the TE material and the heat exchange media, both on the cold and on the hot side. To this end, unimpeded contact should be warranted between the heat exchanger and the TE material to the greatest possible extent. Special measures took account of thermomechanical effects. The concept was also extended for friction-locked installation to allow for the use of TE modules currently on the market.

The individual components and the complete demonstrator system were operated and analyzed virtually by simulation and in real terms on a laboratory and engine test bench as well as in the project vehicle.

These demanding project targets can only be achieved with a consortium that offers interdisciplinary skills covering all necessary work steps from material development via connection technologies and module production through to system production and integration. The project includes seven partners from science and industry (see Sect. 3.3) who had already been intensively involved with the issue of waste heat recuperation before the project began. The partner were responsible for their particular

section of the development scope according to their core expertise and technological know-how.

This paper presents some of the project's simulation and test results. Rather than concentrating on the TEG itself, attention instead focused not just on the opportunities, benefits and potential but primarily on the known drawbacks of the technology, such as costs, weight, exhaust gas backpressure, auxiliary power consumption and recooling. Experience gained during the project shows that it is possible to reduce the potential weaknesses to an acceptable level with an optimum strategy, layout and design of the TEG, thus clearing the way forward onto the automotive volume market.

The test vehicle for investigating the impact factors of a TEG on fuel consumption consisted of a VW Golf GTI with 2.0 l displacement and an output of 147 kW. All curves and values presented below are mean values obtained from several tests in each case. The following changes to the standard vehicle were examined during the project:

- Increasing vehicle mass by +100 kg
- Narrowing the flow cross-section of the exhaust gas system to about 20 %
- Additional load of +900 W on the conventional generator
- Integration of a self-sufficient cooling system
- Operation without (standard) and with TEG

5 Conventional Generator

In contrast to commercial vehicles, passenger cars use a considerable share of their drive power output as supply for the vehicle electrical system. Constantly growing electrification of the vehicles will increase this share even further, despite greater efficiency of future mechanical generators and electrical vehicle components. TEGs supply electricity from heat. They boost efficiency directly via the electrical path without additional conversion subject to losses (Fig. 7). Only the voltage needs to be adjusted. Further conversion into mechanical energy is conceivable, but is put into second place by the conversion losses. This is appropriate if the electrical energy supplied by the TEG can no longer be absorbed because of insufficient demand from the vehicle electrical system and when the accumulator is full. The prime aim for using TEGs is to relieve the pressure on the mechanical generator powered by the combustion engine. Furthermore, additional beneficial effects can be obtained by TEGs working in combination with other vehicle systems.

Power generation in the vehicle is actually rather inefficient because of the need for double conversion; the efficiency achieved depends greatly on the operating point of the combustion engine and the claw-pole generator. On average, it is between 22 % and 35 %, depending on engine speed and load, and can be far lower under unfavorable operating conditions [12]. Power generation can easily account for more than 10 % of engine output. In [13, 14], the additional fuel consumption from the added generator load is put at 1 l/100 km for 1 kW generator load. Figure 8 gives a numerical estimation for the additional fuel consumption in l/100 km and the relevant CO_2 emissions in g/km; this is then visualized on the basis of the additional fuel consumption according to [15, 16] as a function of average vehicle speed and generator load.

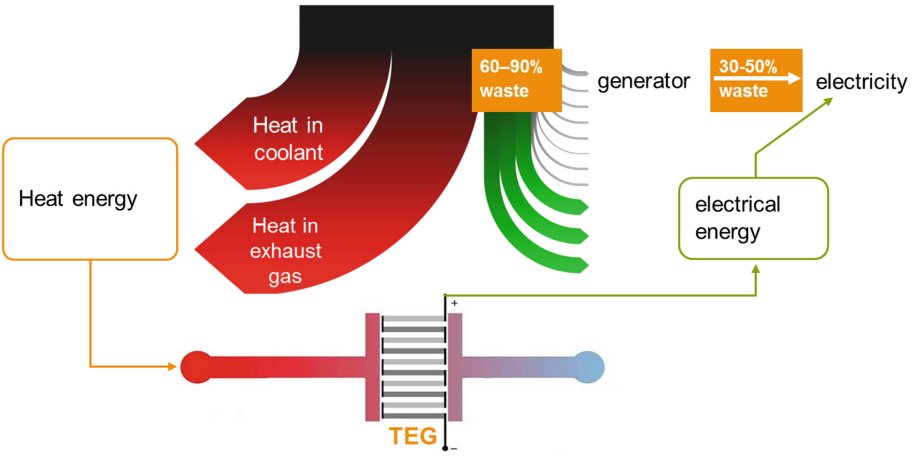

Fig. 7. TEGs in the vehicle electrical system

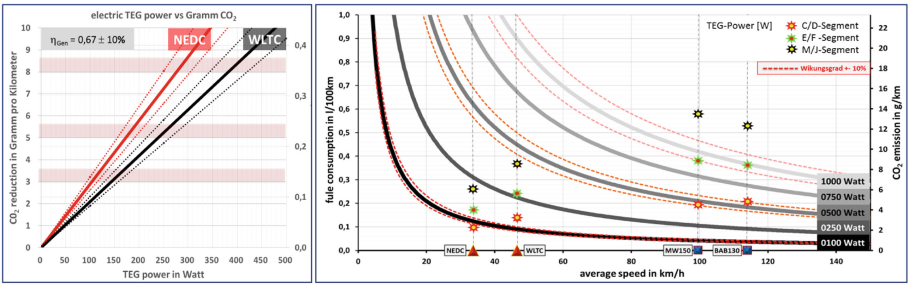

Fig. 8. Additional fuel consumption/CO_2 emissions as a function of average vehicle speed and generator load

The four comparison cycles are marked according to their average vehicle speeds. Many publications (see e.g. [17]) state as a general principle that power demand from the vehicle electrical system is essentially independent from the cycle so that the consumption effect should be evaluated in liters per second. For supercharged gasoline engines, this is approximately 0.4 l/h for one kW electrical power. The route-related consumption or CO_2 reduction effect therefore decreases with increasing average vehicle speed of the driving cycle, as shown in Fig. 8.

To gain a real impression of basic and normal load together with the maximum load of the vehicle electrical system, preliminary tests were carried out with the standard vehicle at two different operating points shown to Table 2.

No electrical consumers were switched on in the vehicle during the base load tests. During the journey, the generator only had to provide the electrical power needed to operate the engine. Typical electrical consumers were switched on for normal operation, while all the test vehicle's electrical consumers were switched on for the maximum possible load on the vehicle electrical system.

Table 2. Generator power at two operating points using various consumers in the test vehicle

	Basic load [W]	Normal load [W]	Maximum load [W]
Idling	162	359	999
125 km/h in 6th gear	198	401	1137

Table 3 shows the additional consumption for adding +900 W to the base load. As explained above, the higher generator load has a far greater impact on fuel consumption in the **WLTC** than in the **MW150** (Artemis Motorway 150) and fits in well with the estimate given in Fig. 8.

Table 3. Additional fuel consumption for (max.) load on the vehicle electrical system in two different cycles (**WLTC** and **MW150**)

	Additional load [W]	Additional consumption [l/100 km]
WLTP (∅v ~ 047 km/h)	900	0.90
MW150 (∅v ~ 100 km/h)	900	0.47

As already mentioned above, the prime aim of a TEG is to relieve the mechanical generator in order to save fuel and reduce CO_2 emissions. Considerable potential is seen particularly at low vehicle speeds and high power demand. This depends on the TEG being offered adequate thermal energy with sufficiently efficient subsequent conversion into electrical energy. However, this is not the case in the two EU homologation cycles **NEDC** and **WLTC**, as clearly illustrated in Fig. 8. The mean electrical power is relatively low here. To a limited extent, this can be counteracted by optimum layout of the TEG for the respective cycle and with a corresponding energy management system which decouples power generation and consumption in terms of time. In this way, TEGs can make an important contribution to achieving the target with kinetic and thermal recuperation covering all the vehicle's electrical energy demands for all conceivable modes of operation, using the combustion engine to supply electrical power only as a reliable redundancy solution. Such solutions are possible with hybrid drives.

6 Thermoelectric Generator

During the project, a modular TEG concept was devised among others and investigate in the test vehicle. A diagram of the concept is shown in Fig. 9.

The TEG consisted of altogether ten modules, in two rows of five facing each other. Two separately actuated servomotors controlled the flaps constantly as a function of defined component temperatures and exhaust gas pressure loss.

Figure 10 shows the TEG fitted in the test vehicle. Commercially available modules were used in each case (oxides and chalcogenides). Each module was fitted with temperature sensors on both the cold and the hot side to monitor the component temperatures and to use the real module temperatures as input variables for parallel

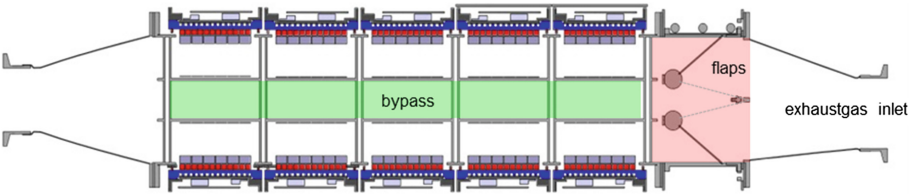

Fig. 9. Schematic set-up of the TEG

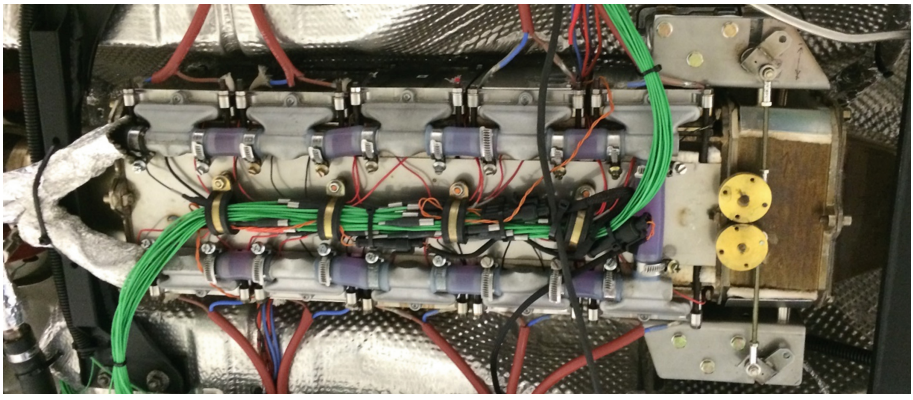

Fig. 10. TEG fitted on the underfloor of the test vehicle

hardware-in-the-loop simulations. A self-sufficient cooling system was responsible for recooling.

Figure 11 shows selected measurement variables for assessing TEG system behavior compared to the standard vehicle for the **WLTC**. It is apparent that the temperature difference over the TEG is higher than in the standard state already shortly after starting the engine (max. 400 K). Even so, pressure loss over the TEG is almost the same as the standard state. The bypass flaps only have to open in the last segment of the **WLTC**. However, this is in order not to exceed the maximum surface temperature of the modules, rather than as a result of elevated backpressure. Among others, two effects are responsible for this positive behavior in terms of pressure losses. Firstly, the flow rate is altogether on a low level, and secondly, the decrease in temperature over the TEG reduces the pressure losses in the downstream parts of the exhaust gas system, cf. [18]. This effect compensates for part of the anticipated higher pressure losses.

In the same fashion as Figs. 11 and 12 shows the measurement variables for the **MW150**. The vehicle speed profile is clearly increased compared to the **WLTC** so that the components heat up more quickly, while the temperature difference over the TEG section is also clearly above the standard state (max. 480 K).

The additional flow resistance caused by the TEG also has a clear effect on pressure losses at times, compared to the standard state. Compensating pressure losses by reducing the temperature is only possible here to a limited extent. The bypass flaps also

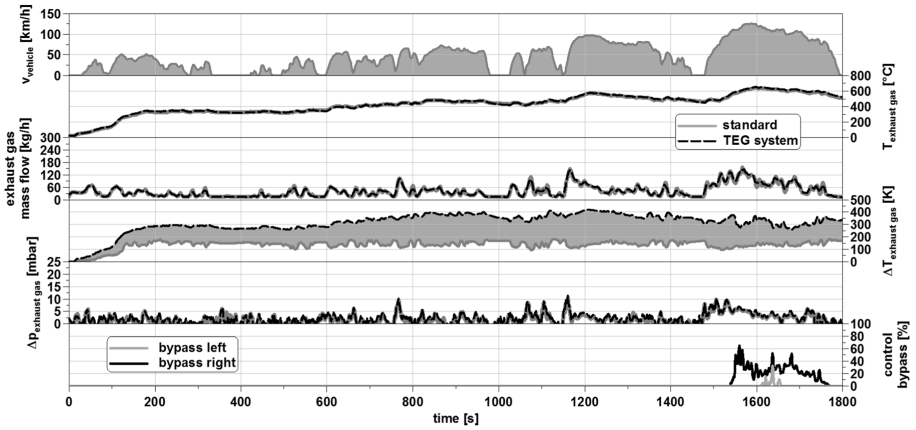

Fig. 11. Selected TEG measurement variables in the **WLTC** compared to the production vehicle

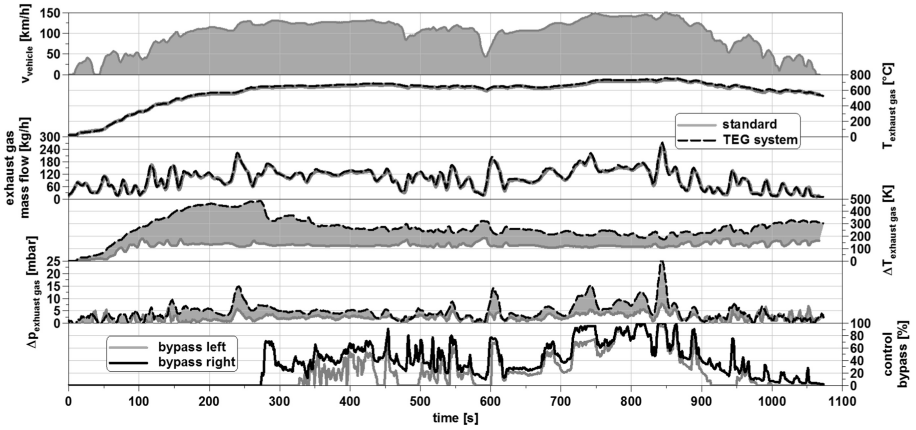

Fig. 12. Selected TEG measurement variables in the **MW150** compared to the production vehicle

have to open relatively early to protect the modules from excessive temperature. The opening of the bypass channel is clearly indicated by the marked decrease in exhaust gas temperature difference.

However, the total accumulation effect caused by the TEG exceeds 10 mbar only briefly in strong acceleration phases and does not exceed this level at all for most of the **MW150**. As indicated in Sect. 2.5 below, an increase in exhaust gas backpressure in this magnitude is not seen to influence fuel consumption.

Figure 13 shows the HiL simulation results obtained during the vehicle trials for virtual TE modules with PbTe ($ZT \sim 1$). It presents the curves for electrical TEG power computed from the process data after deducting DC/DC conversion losses.

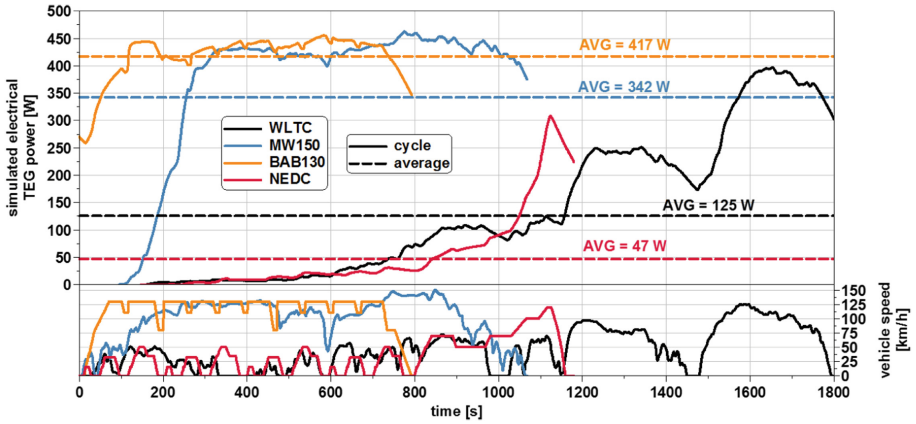

Fig. 13. Simulated electrical TEG power in various cycles

In the **NEDC,** the maximum simulated TEG power increases to about 300 W in the interurban segment, with mean power of approx. 47 W. The limited exhaust energy available in the four urban phases of the **NEDC** results in only slow increases in component temperatures. The first two phases of the **WLTC** (low and middle) show similar behavior to the **NEDC**. In the last two phases of the **WLTC** (high and extra high), there is a clear increase in the TEG power computed for PbTe, which is ascribed to the higher energy available in the exhaust gas. The maximum value for electrical power increases to about 400 W in the phase with the highest vehicle speed, with a mean of about 125 W. In contrast to the **NEDC**, in the **WLTC** the temperature control opens the bypass at the end of the cycle.

Driving cycles with higher average vehicle speeds, e.g. the **MW150** or the **BAB130** (ADAC Highway Cycle), offer greater heat, generating an adequate temperature difference at the TEG module. The maximum power output in the **MW150** thus exceeds 460 W with a mean value of approx. 342 W. Actuating the bypass flaps limits the component temperature of the modules at position 4 and 5 (Bi_2Te_3!), resulting in lower power output. Without activating the temperature control, there would be more than 500 W of power here.

The **BAB130** was always carried out as a warm start so that the simulated TEG power exceeded 250 W already at the start. Electrical power during the cycle ranged from 400 to 450 W, limited by controlling the maximum component temperature of the last TEG modules. The lack of a cold start in the **BAB130** results in a higher mean power output of 417 W.

To summarize, it can be said that it was possible to verify the function of the examined laboratory TEG and the implemented system concept. The TEG completed a large number of operating hours in many different cycles and operating points, also including high thermal loads. The measurement and simulation results have shown that the electrical power to be gained with the TEG mainly depends on the TEG heating up quickly and on the energy available in the exhaust gas. The thermal mass must be kept as low as possible to quickly achieve an adequate temperature gradient over the TE

modules, particularly in the homologation cycles. To a certain extent, the reduction in temperature over the TEG can compensate for the just slightly higher flow resistance. This depends on the operating point of the engine and the position of the bypass flaps. Using suitable high-temperature modules would result in much later bypass control, if at all. In this case, the bypass flap would only have to open briefly, e.g. to deal with excessive backpressures or cooling loads. This would allow for simple design of the bypass flap and its control, e.g. just as a single flap open/close solution.

The HiL simulation results obtained during the vehicle tests for virtual TE modules with PbTe (ZT $\sim$ 1) also confirm the good potential estimate for vehicles in the C/D segment, which is where the test vehicle belongs. The achieved 125 W is only 17 % below the target of 150 W for a C/D vehicle in the **WLTC**, thus confirming its feasibility, especially in view of the fact that the laboratory TEG used in the project is not optimized for the **WLTC**, particularly in terms of thermal mass. The mean power output achieved in the **MW150** is only 342 W instead of 465 W, due to the massive intervention of the bypass control to protect the module, which is necessary.

7 Weight

The prime drawback of TEGs is that they make it very difficult to avoid an increase in weight. Consistent lightweight design is the only chance for minimizing the additional weight, with the TEG integrated in existing parts of the exhaust gas system or even substituting for them. A rough overview shows that system weights of between 5 and 25 kilograms must be expected for cars, depending on the configuration concept, design and power output.

Both theory and practice show that every additional weight in the vehicle increases fuel consumption. The mass of the vehicle impacts on three of the four rolling resistances, see Fig. 14.

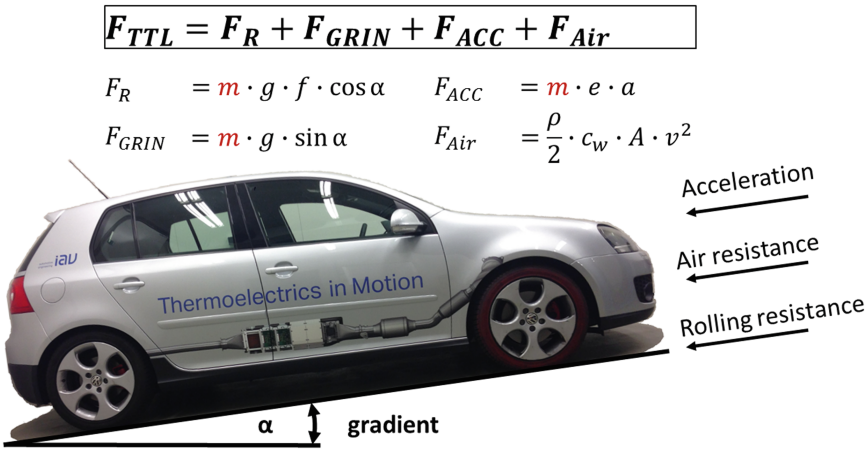

Fig. 14. The influence of mass on rolling resistances of the project vehicle [20]

Mass-related acceleration resistance is one of the biggest problems, given its dominant influence on consumption. Literature gives various indications and general rules for additional fuel consumption caused by added vehicle weight. According to [19] for example, 100 kg of additional vehicle weight increases fuel consumption by 0.4 l/100 km. According to [15], published values indicate between 0.3 and 0.7 l/100 km for 100 kg. In many cases, these values are just estimated. There is no physical derivation, nor is anything said about the mode of operation or driving profile. Strict attention must be paid to the boundary conditions for such "indicative values" in view of the significant impact of mass on fuel consumption.

According to [21, 22], the computed additional consumption for 100 kg of added weight in the **NEDC**, for example, is only about 0.137 l/100 km. In [15], a value of 0.15 l/100 km is obtained for a vehicle with supercharged gasoline engine and 1300 kg in the **NEDC**, and 0.23 l/100 km for a modified, more dynamic **NEDC**. This underlines the great impact of driving dynamics in terms of the frequency, duration and amount of vehicle speed changes.

The dynamics factor of a driving cycle as explained in [23] provides a very helpful description of the dynamics of driving maneuvers, showing that consumption due to added vehicle weight increases with driving dynamics. Figure 15 illustrates this relationship for constant alternator efficiency. It shows the additional consumption for a reference vehicle together with the increase in CO_2 emissions caused by 10 resp. 25 kg added vehicle weight (future TEGs will probably be within this weight range) based on the dynamics factor of a dozen scientific and homologation-relevant cycles as well as five customer cycles. The four cycles always used for comparison and assessment in the TEG2020 project are marked. According to Fig. 15 for example, a TEG with 10 kg added weight causes additional consumption of 0.018 l/100 km with emissions of approx. 0.42 g CO_2 per kilometer in the **WLTC**, corresponding to a weight factor of 0.042 g CO_2/km per kilogram.

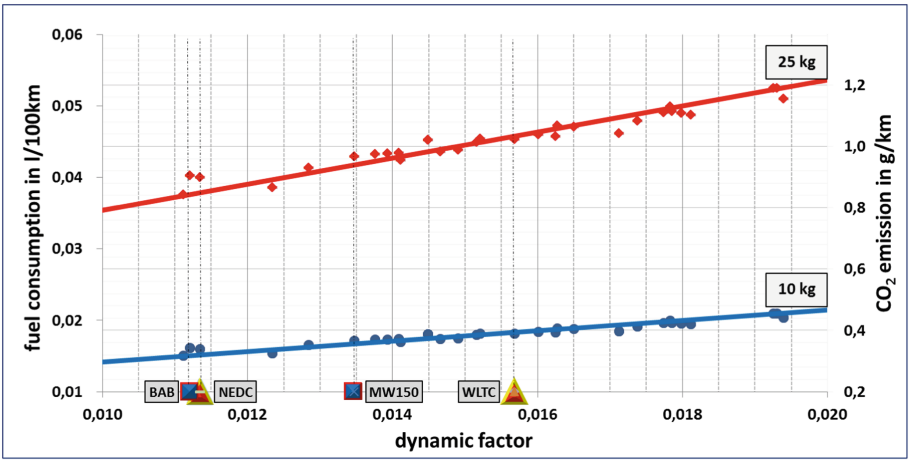

Fig. 15. Fuel consumption and CO_2 emissions in relation to the dynamics factor according to Prof. Helling [23] in the viewed cycles for 10 and 25 kg additional weight

From 2020 onwards, the permissible CO_2 emissions of a manufacturer's fleet of new vehicles must be calculated using the formula [24]

$$CO_2|_{specified} = 95 + 0.0333 \cdot (m - m_0) \quad (1)$$

whereby m is the vehicle mass and m_0 the average mass of new passenger cars in the last three years. Here the weighting factor is chosen so that 1 kg of additional weight increases the limit value by 0.0333 g CO_2/km (up to 2020: by 0.0457 g CO_2/km). According to [16], the weight factor Δm used to define the CO_2 correction amount in g CO_2/km obtained from the mass change of a vehicle after installing a system in the context of ecological innovation is calculated with the formula used there

$$\Delta CO_2|_{correctionamount} = 0.0277 \cdot \Delta m \quad (2)$$

to obtain a value of just 0.0277 g CO_2/km per 1 kg additional weight for vehicles with gasoline engine.

Measurements on the roller dynamometer in the WLTC resulted in additional fuel consumption of 0.28 l/100 km for 100 kg added weight. The real values are above the computed values, which is ascribed mainly to the real-life additional consumption of the respective engine in l/kWh.

In any case, the success of a measure depends significantly on the lightest possible design and a sophisticated integration concept, minimizing extra weight as far as possible. In the **WLTC**, every kilogram of additional weight has to be compensated by a good 2 W generator relief.

8 Exhaust Gas Backpressure

The relief for the conventional generator that can be achieved with the TEG depends on how effectively the hot side of the TEG is connected to the heat source. The exhaust system has to be fitted with a heat exchanger that is rated to withdraw a sufficiently large heat flow from the exhaust gas to convey it over the TE modules. The heat exchanger must be designed for transferring a large quantity of heat, as well as minimizing pressure losses in the exhaust gas system. A heat exchanger with a large effective surface improves heat transfer to the TEG but also increases the backpressure level. On the other hand, a small heat exchanger surface reduces repercussions on the charge cycle processes in the combustion engine, but has only a small heat flow to be withdrawn from the exhaust gas. This trade-off is solved by an effective exhaust gas heat exchanger that withdraws the necessary amount of heat from the exhaust gas while minimizing the increase in exhaust gas backpressure.

A TEG with its necessary heat transfer structure constitutes an additional flow resistance in the exhaust gas system. Pushing the exhaust gas out of the cylinder against a higher level of pressure has a negative impact on the charge cycle; the higher residual gas level in the combustion chamber leads to increased fuel consumption if the same effective power output is to be produced [25–27] indicate that if there is only a slight increase in the exhaust gas backpressure, it is not possible to say anything reliable

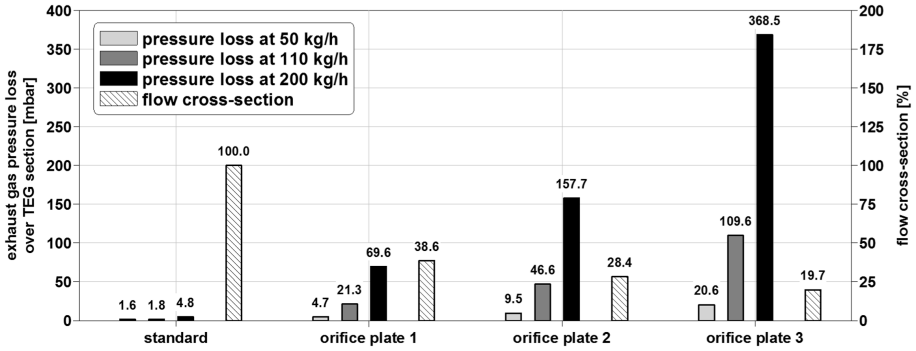

Fig. 16. Percentage change of flow cross section and exhaust gas pressure losses over the TEG segment with the throttles in constant operating points

about the relationship between increased pressure level and fuel consumption. It is only possible to make a rather general statement at engine operating points with high exhaust mass flows and backpressure increases above 250 mbar.

In order to assess the impact on fuel consumption of an additional throttling point, the original diameter of the exhaust pipe (56.3 mm) was reduced to 35, 30 and 25 mm (throttles 1 to 3). As a general rule, the higher the engine operating point and thus the mass flow and temperature of the exhaust gas, the greater also the pressure losses over a defined segment. Figure 16 shows this behavior in real measurements. The pressure losses are indicated both in the standard state and also for the three throttles in three different constant exhaust gas mass flows.

Figure 17 shows the measurement results for the three exhaust throttles in the **WLTC**. The **WLTC** with its mainly lower engine operating points and therefore lower exhaust gas mass flows has comparatively low pressure losses, mainly below 50 mbar.

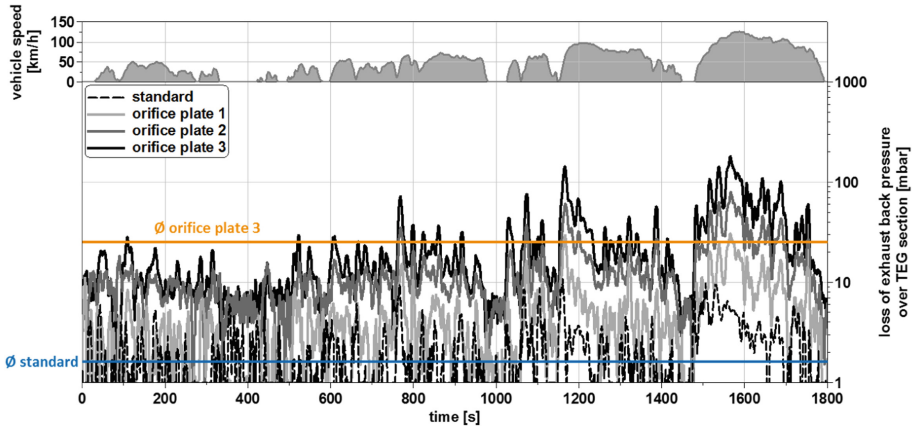

Fig. 17. Comparison of pressure losses over the TEG segment with the different throttles in the **WLTC**

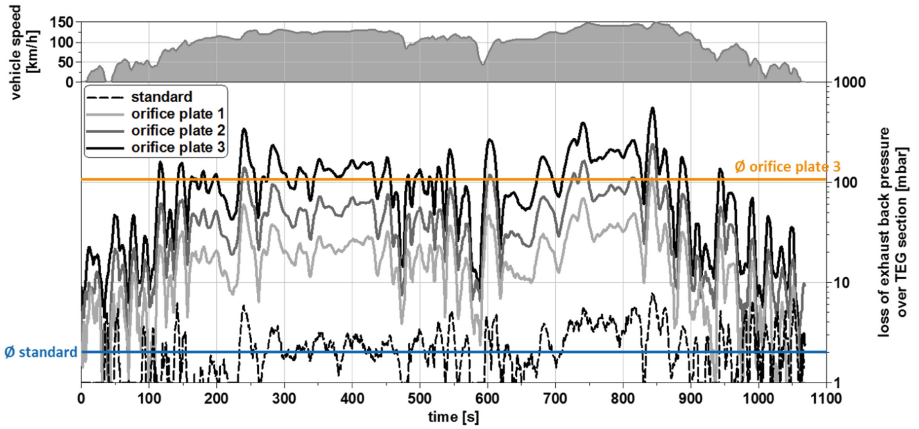

Fig. 18. Comparison of pressure losses over the TEG segment with the different throttles in the **MW150**

It is only in the strong acceleration phases and the last segment of the **WLTC** that the exhaust gas pressure loss over the TEG segment with throttle 3 comes close to or briefly exceeds a value of 100 mbar. The maximum value is about 180 mbar.

The higher speeds in the **MW150** also result in higher engine load points, reflected in higher mass flows and higher exhaust gas temperatures with far larger pressure losses. The measurement results with the three throttles are shown in Fig. 18. When throttle 3 is used, pressure losses exceed 100 mbar for an extensive part of the driving cycle and reach a maximum value of approx. 620 mbar.

Table 4 shows the relative additional consumption rates compared to the production vehicle and the mean pressure losses over the TEG segment in the **WLTC** and **MW150** when using throttle 3. The very slight consumption increase of 0.2 % in the **WLTC** clearly shows that even when the smallest throttle is used, there is no clear influence on fuel consumption. By contrast, in the **MW150** the additional consumption is clearly visible with 2.9 %.

Table 4. Relative additional consumption compared to the production vehicle and mean exhaust gas pressure loss over the TEG segment in the **WLTC** and **MW150** with exhaust throttle 3

	Additional consumption [%]	Mean pressure loss [mbar]
WLTC	0.2	24
MW150	2.9	102

To summarize, it can be said that only a drastic reduction in the cross section results in a significant increase in fuel consumption. However, the measurements obtained with the TEG used in the project indicated that it is possible to minimize the pressure increase with a suitably rated module which therefore also has only a very low impact on fuel consumption.

9 Auxiliary Power Consumption

In order to be able to make a reliable statement about the real benefit of a TEG and to produce an energy balance, due consideration has to be given not just to all effects on engine and vehicle but also to all additional consumers needed to operate the TEG, such as water pump, exhaust flap actuator and voltage converters. The additional power needed by these components depends greatly on the overall concept and the respective mode of operation, so that the following calculation is only intended to give a qualitative overview. The electrical consumers are estimated with reference to the TEG used in the TEG2020 project. Here the focus was on functional capability and safety with the greatest possible variability in the overall system, and not on optimizing the cooling system or each individual consumer. However, the holistic design of a TEG for a target system must presume various potential optimizations for minimizing "power consumption".

A look at the overall progression of the **WLTC** shows that with consistent, optimized layout of the system, the additional consumers such as servomotors or water pump only need to be used when absolutely necessary, thus minimizing their ON times. Minimum coolant circulation is sufficient during the cold start and in the urban and interurban cycle. A constant increase in pump power to 100 % is only necessary for higher loads. The same strategy also applies to the servomotors. They are only needed briefly to deal with a high heat supply and when the system exceeds the limits for module temperature, exhaust gas backpressure and cooling system load. Otherwise they remain inactive and de-energized. Their power consumption is irrelevant in terms of energy balance.

The efficiency of the power converters depends on the operating range of the TEG as a function of the transient heat supply from the consumption engine. A high conversion rate therefore depends on optimum rating of the system layout according to the anticipated range. (The efficiency of the DC/DC converters is taken into account in the results shown in Fig. 13!)

In Fig. 19, the real pump power (taking account of efficiency) from vehicle measurements is entered for the coolant temperature range 25 °C (left edge) to 60 °C (right edge). This shows the necessary pump power for the overall system and also proportionately for the TEG itself. The TEG is clearly seen to account only for a small share of the required pumping capacity. The remaining cooling circuit with hoses, recooler and various sensors has a far greater impact. The required power can certainly be halved in the range of 20 to 25 V by intelligently connecting the TEG coolant circuit to the engine coolant circuit, or at least by optimizing the separate coolant circuit. The required power is reduced by giving due consideration to the fact that the water pump is only on for about half the time.

Finally, it can be said that while the additional electrical consumers reduce the power obtained, this is to a far lesser extent than often presumed. With intelligent rating and usage of existing resources as well an ideally calibrated DC/DC converter, a potential estimate can work on the basis of auxiliary power consumption in the TEG between 10 % and maximum 15 % of the converted electrical power, referred to the mean electrical power in the WLTC.

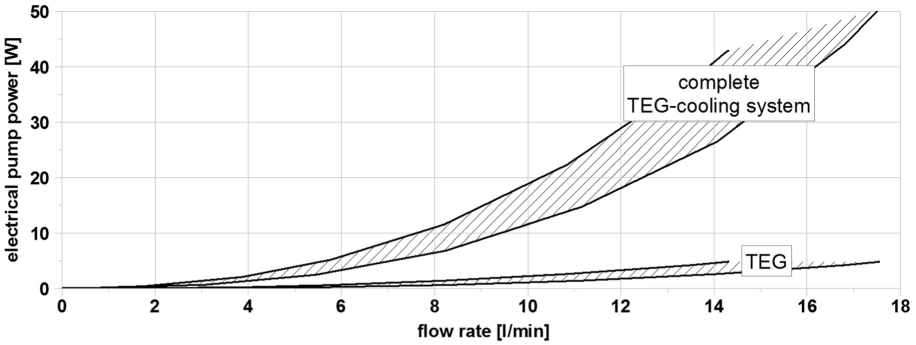

Fig. 19. Electrical pump power at 25 °C and 60 °C coolant temperature for the entire cooling circuit and proportionally for the TEG

10 Recooling

Besides the quality of the TE material's thermoelectric characteristics, it is also necessary to have a sufficiently large temperature gradient between the hot and the cold side in order to drive corresponding electrical power with the TE modules. The vehicle's exhaust gas acts as heat source. The heat sink in the vehicle consists, for example, of the separate, possibly available low-temperature cooling circuit or the engine cooling system, which absorbs the heat flow over the TEG and dissipates it via corresponding radiators back to the surroundings.

Depending on the TE material being used, the application and the possibilities in the vehicle, it is necessary to estimate to what extent reducing the coolant temperature will generate a further economic advantage in the overall system. Not every temperature reduction will always generate the desired effect. Usually it will be sufficient to "simply" connect the cold side of the TEG to the engine cooling system. Table 5 shows the gained power of the TEG as a function of coolant temperature for Bi_2Te_3 and PbTe, based on 90 °C coolant.

Table 5. Influence of coolant temperature on the power generated by the TEG

Coolant temperature	Power gain Bi_2Te_3	Power gain PbTe
10 °C	+88 %	+23 %
50 °C	+45 %	+11 %
90 °C	0 %	0 %

If the temperature level of the engine cooling system is adequate, the question arises whether this can absorb or recool the additional heat input from the TEG. According to [28], the maximum cooling capacity of modern cooling systems is rated for representative operating states. These include driving states with high heat input into the cooling system, such as long highway journeys at top speed or driving uphill with maximum payload and towed weight. Rating the cooling system to this high cooling demand means that it will be over-dimensioned for the predominant driving states, depending on the layout strategy pursued by the OEMs.

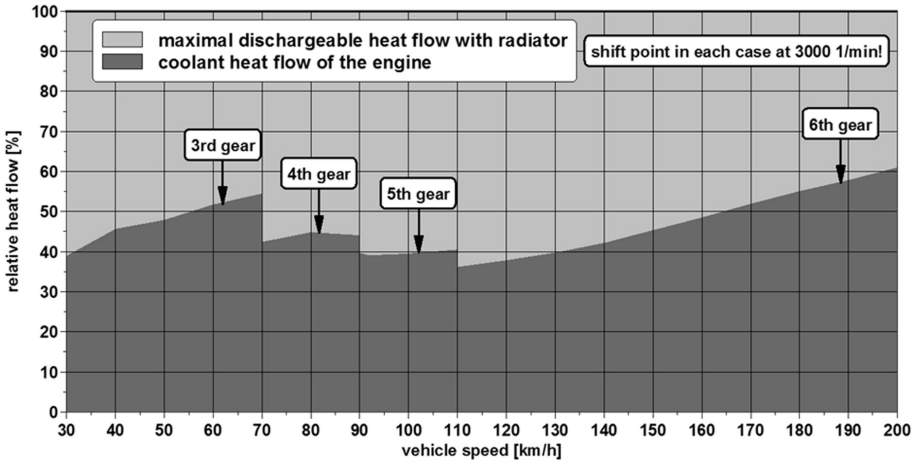

Fig. 20. Coolant heat flow of an engine relative to the maximum possible heat flow of the radiator (road part-load in 3rd to 6th gear on the flat at inlet temperature difference = 70 K)

Figure 20 shows the ratio of engine cooling demand to maximum possible cooling capacity of the vehicle radiator, illustrated with a mid-range vehicle. The values were defined for road part-load points when driving on the flat in 3rd to 6th gear and up to a speed of 200 km/h. It can be clearly seen that when driving on the flat up to 160 km/h, the cooling system of the example vehicle is only operating at up to approx. 50 % of its maximum capacity. With a corresponding layout strategy, the standard cooling system can therefore certainly cope with the additional heat input from the TEG. At operating points with high cooling demand, the TEG system has to be bypassed on the exhaust side to minimize the additional heat input and prevent overload on the cooling system. Taking the TEG system into account at an early point in the vehicle development is therefore an advantage.

Figure 21 shows the ratio of the heat flows in the project vehicle at various constant-speed driving points. On the one hand, it features the heat flow dissipated via the vehicle radiator to the surroundings. On the other hand, it also indicates the heat flow entering the separate cooling circuit from the TEG, with values at various vehicle speeds in 6th gear.

The higher cooling demand from the engine triggered by the road resistance that increases with speed can be clearly seen in the diagram. The higher engine operating point also increases the energy supply in the exhaust gas, so that there is a greater heat input from the TEG into the separate cooling system. As soon as the bypass control intervenes so that part of the exhaust gas mass flow bypasses the TEG, the coolant heat flow stagnates with practically no further increase. For the project vehicle with the examined TEG concept, the TEG results in additional cooling capacity demand of up to 25 % of the engine cooling demand, with the maximum value at low load points where the bypass is still completely closed. At higher load points, the TEG heat flow decreases continuously in relation to the overall cooling demand of the engine.

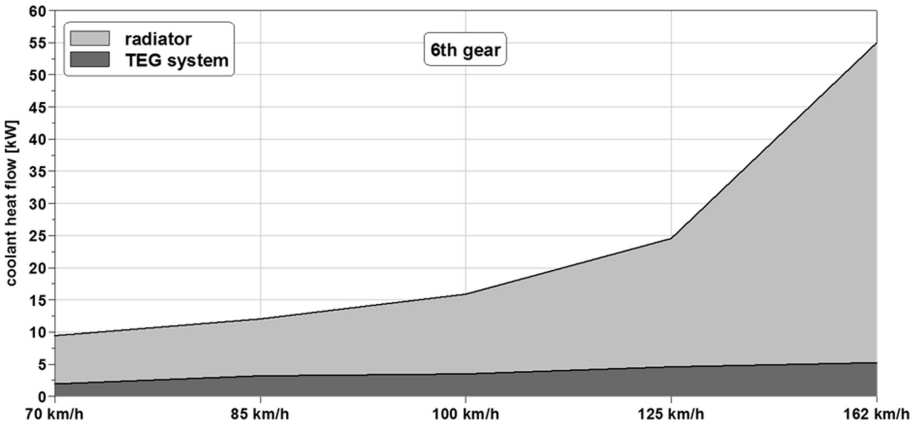

Fig. 21. Coolant heat flows over engine radiator and TEG system in the test vehicle

Comparing these values with the findings from Fig. 20 leads to the conclusion that the production cooling system is definitely capable of coping with the additional heat input from the TEG into the coolant in most driving states. This depends on optimum integration of the TEG in the cooling system, which can be achieved by including the TEG early on in the development process of a new vehicle.

11 Summary

A TEG that feeds mean net electrical power of 150/250/400 W (depending on the reference vehicle) into the vehicle electrical system, thus relieving the conventional generator, is capable of achieving 2 to 3 % fuel savings in the WLTC. With savings in this magnitude, the technology offers vehicle manufacturers a successful means of coping with their CO_2 deficits.

Although devised as a laboratory generator that has not been designed specifically for the **WLTC** and assessed only with provisional material (PbTe), the project TEG in the project vehicle (C/D) already produces 125 W. When rated accordingly for the **WLTC** with current or future TE materials, configuration and connection technologies respectively TE modules in suitably optimized concepts and designs, TEGs in vehicle quality will achieve the necessary conversion rates by 2020.

The challenges still posed by the technology are also manageable. **Costs** of less than € 50 for every gram of CO_2 saved per kilometer and vehicle, respectively less than € 1 per watt of net electrical TEG power should be sufficient to clear the way ahead for this technology into the automotive world. Without doubt, these cost targets are a huge challenge for many manufacturers of TE materials, modules and components. However, they are the entrance ticket to the mass market of the automotive industry and there are many different possibilities of achieving them.

Payback directly at the fuel pump is still unsatisfactory for the normal user, but certainly achievable for frequent drivers and commercial users. The **weight** has a

critical impact because of its inevitability. On the other hand, this can be managed with consistent lightweight design and intelligent installation concepts. No drawbacks are anticipated from the **exhaust gas backpressure**, as long as the system uses an exhaust gas heat exchanger with a suitable, optimized design. A suitable heat exchanger design in a system with intelligent coolant and exhaust gas management also keeps **auxiliary power consumption** low. Voltage adaptation with a DC/DC converter is necessary on account of the TEG's characteristics, and reduces the net power. However, suitably designed converters will keep this in the single-figure percentage range. In a correctly devised and rated system, **cooling** is not a critical aspect. There are many options here which in some cases even offer secondary effects that compensate for the negative impact on the vehicle as a whole.

Acknowledgements. The TEG2020 project was funded by the Federal Ministry of Education and Research **(BMBF)** in the framework of the WING program – Material Innovations for Industry and Society (**03X3552A**). We would like to express our gratitude for constructive, successful cooperation to the Project Administration at Forschungszentrum Jülich GmbH **(FZJ)** and the partners in the consortium project:

- BASF SE
- Benteler Automobiltechnik GmbH
- Fraunhofer Institute for Physical Measurement Techniques
- Berlin University of Technology, Institute of Energy Technology, Mechanical and Systems Engineering Faculty
- Berlin University of Technology, Institute of Energy and Automation Technology, Electronic Measurement and Diagnostic Technology Faculty

References

1. Steinberg, P., Briesemann, S., Goßlau, D.: Der Fahrzeugmotor als Energielieferant für Wärmenutzungskonzepte, Thermoelektrik – Eine Chance für die Automobilindustrie. Expert verlag, Renningen (2009)
2. Spiegel Online Auto; Studie zum Spritbedarf von Autos: Die große Verbrauchslüge. http://www.spiegel.de/auto/aktuell/studie-des-icct-zum-realen-spritverbrauch-zu-autos-a-902224.html. Accessed Sep 2016)
3. Forschung für die optimalen Materialien; in Thermoelektrik: Strom aus Abwärme; *Thermoelektrische Generatoren machen Systeme energieautark und sparen Energie;* BINE Informationsdienst, Energieforschung kompakt, Themeninfo I/2016, pp. 10–13. http://www.bine.info/fileadmin/content/Publikationen/Themen-Infos/I_2016/themen_0116_internetx.pdf, http://www.bine.info/fileadmin/content/Publikationen/Themen-Infos/I_2016/themen_0116_engl_internetx.pdf. Accessed Sep 2016
4. Stiewe, C., Müller, E.: Anwendungspotential thermoelektrischer Generatoren in stationären Systemen, Chancen für NRW; Studie im Auftrag des Ministeriums für Innovation, Wissenschaft, Forschung des Landes Nordrhein-Westfalen, erstellt durch Deutsches Zentrum für Luft- und Raumfahrt e.V. (DLR), Institut für Werkstoff-Forschung, Cologne
5. thermoHEUSLER^2 - Systemintegration thermoelektrischer Abgaswärmeenergierückgewinnung; Projektbeschreibung; TÜV Reinland. http://www.tuvpt.de/index.php?id=foerderung0001000000114. Accessed Sep 2016

6. Rosenberger, M., Dellner, M., Kluge, M., Tarantik, K.R.: Fahrzeugintegration eines thermoelektrischen Generators. MTZ - Motortechnische Zeitschrift **77**, 38–45 (2016)
7. Fraunhofer IPM; Kraftstoff sparen im realen Verbrauch dank Thermoelektrik; press release published on 08 Oct 2015. http://www.ipm.fraunhofer.de/de/presse_publikationen/Presse-informationen/thermoHEUSLER2.html. Accessed Sep 2016
8. Fraunhofer IPM; Neue Pilot-Fertigung für thermoelektrische Module; press release published on 28 July 2016. http://www.ipm.fraunhofer.de/de/presse_publikationen/Presse-informationen/fertigung-thermoelektrische-module.html. Accessed Sep 2016
9. Kober, M., Heuer, J.: DLR, Institut für Fahrzeugkonzepte und Fraunhofer IPM; Elektromobilität – Projekt „REXTEG" Thermoelektrische Generatoren für effiziente Range-Extender. http://www.dlr.de/fk/Portaldata/40/Resources//2015_RExTEG_Kurzbericht.pdf. Accessed Sep 2016
10. Tarantik, K., Bartholomé, K., Heuer, J., Horzella, M., Jägle, M., König, J.: Survey of thermoelectric modules for waste heat recovery and opportunities due to thermoelectric downsizing. In: ICT/ECT 2015, Dresden (2015)
11. MOTOR-TALK; Zetsche und Winterkorn nennen CO2-Kosten - JEDES GRAMM KOSTET EXTRA. http://www.motor-talk.de/news/jedes-gramm-kostet-extra-t5073071.html. Accessed 17 Apr 2016
12. Büchner, S.: Energiemanagement-Strategien für elektrische Energiebordnetze in Kraftfahrzeugen, Dissertation 2008, Dresden University of Technology. Cuvillier Verlag, Göttingen (2008). ISBN: 978-3-86727-803-4
13. Lunanova, M.: Optimierung von Nebenaggregaten – Maßnahmen zur Senkung der CO_2-Emission von Kraftfahrzeugen, 1st edn. Vieweg + Teubner, Wiesbaden (2009)
14. Woll, T., Kapitel Verbrauch und Fahrleistungen. In: Schütz, T. (ed.) Hucho – Aerodynamik des Automobils – Strömungsmechanik, Wärmetechnik, Fahrdynamik, Komfort, 6th edn. Springer, Wiesbaden (2013)
15. Rohde-Brandenburger, K.: Was bringen 100 kg Gewichtsreduzierung im Verbrauch? – Eine physikalische Berechnung, ATZ 07-08 2013, vol. 115, pp. 584–591 (2013)
16. Official Journal of the European Union L 332/34 (2014/806/EU), 19.11.2014, COMMISSION IMPLEMENTING DECISION of 18 November 2014 on the approval of the battery charging Webasto solar roof as an innovative technology for reducing CO_2 emissions from passenger cars pursuant to Regulation (EC) No. 443/2009 of the European Parliament and of the Council
17. Breitling, T., Siegert, R., Steffens, D., Baumgärtner, W.: Potenziale des Energiemanagement für den Realverbrauch, Thermoelektrik – Eine Chance für die Automobilindustrie. Expert verlag, Renningen (2009)
18. Kühn, R., Koeppen, O., Kitte, J.: Influence of an optimized thermoelectric generator on the back pressure of the subsequent exhaust gas system of a vehicle. J. Elektronic Mat. **43**(6), 1521–1526 (2014)
19. Dudenhöffer, F., John, E.M.: EU-Normen für Verbrauchsangaben von Autos: Mehr als ein Ärgernis für Autokäufer, ifo Schnelldienst 13/2009, vol. 62; pp. 14–17 (2009)
20. Köpf, P., Schwab, M.: Kapitel triebstrang. In: GmbH, R.B. (ed.) Kraftfahrtechnisches Taschenbuch, 23rd edn. Vieweg, Wiesbaden 1999
21. Diegelmann, C.: Potenzial einer SOFC-APU bei der Verbrauchsoptimierung von Kraftfahrzeugen, Munich University of Technology, Institute for Energy Economy and Application Technology, Dissertation, Munich (2008)
22. Eberle, R.: Methodik zur ganzheitlichen Bilanzierung im Automobilbau, Berlin University of Technology, Schriftenreihe B – Fahrzeugtechnik – des Institutes für Straßen- und Schienenverkehr, Dissertation, Berlin (2000)
23. Helling, J.: Lecture script "Kraftfahrzeuge I". RWTH Aachen University, Aachen (1978)

24. Official Journal of the European Union L 103/15, 05.04.2014, Regulation (EU) No. 333/2014 of the European Parliament and of the Council of 11 March 2014 amending Regulation (EC) No 443/2009 to define the modalities for reaching the 2020 target to reduce CO_2 emissions from new passenger cars
25. van Basshuysen, R., Schäfer, F.: Handbuch Verbrennungsmotor: Grundlagen, Komponenten, Systeme, Perspektiven, 5th edn. Vieweg + Teubner, Wiesbaden (2010)
26. Häfele, C., Schier, M., Hahn, S., Weiler, T., Friedrich, H.: Experimentelle Fahrzeug-Untersuchungen im Hinblick auf exergetische Potentiale und Gesamtsystemrückwirkungen bei der Integration Thermoelektrischer Generatoren. In: Thermoelectrics Goes Automotive. Expert Verlag, Renningen (2011)
27. Cloos, L.K., Glahn, C., Hermann, I., Schäfer, J., Bier, W.: Einfluss der Motorintegration beim aufgeladenen Ottomotor – Beurteilung der Auswirkungen auf RDE-Anforderungen. In: International Engine Congress 2015. Springer Vieweg, Wiesbaden (2015)
28. Neuendorf, R., Zuck, B.: Kapitel Kühlung und Durchströmung. In: Schütz, T. (ed.) Hucho – Aerodynamik des Automobils – Strömungsmechanik, Wärmetechnik, Fahrdynamik, Komfort, 6th edn. Springer, Wiesbaden (2013)

Energy Management, Ventilation

Monitoring the Fresh-Air Flow Rate for Energy-Efficient Bus Ventilation

Kemal-Edip Yildirim[1(✉)], Matthias Finkenrath[2], Mehmet Gökoglu[3], and Frank Seidel[1]

[1] MAN Truck and Bus AG, Munich, Germany
{kemal-edip.yildirim, frank.seidel.a}@man.eu
[2] Institute of Energy and Propulsion Technologies, Kempten University of Applied Sciences, Kempten, Germany
matthias.finkenrath@hs-kempten.de
[3] Diploma Thesis at MAN Truck and Bus AG, Munich, Germany
mehmet.goekoglu@web.de

Abstract. City busses and coaches are typically ventilated with high fresh air rates without monitoring of air quality according to recommendations and requirements of associations of public transport companies. The air quality of cabin air regarding humidity and CO_2-concentration depends however on the number of passengers. Hence the air quality of the ambient air could be monitored and air conditioning units could be switched on re-circulation air, which is called here "*monitored fresh air rate*". Average occupancy of city busses is 30 %. This means the cabin will be ventilated with a surplus of about 70 % of the required fresh air. This causes a high energy consumption which could be saved. The aim of this work is the monitoring of the cabin air quality with the help of sensors and development of appropriate control algorithms that could reduce energy consumption without any impairment of safety, comfort, stress and health.

Keywords: Busses · Fresh air rate · Air quality · Cabin humidity · CO_2-concentration · Control algorithms

1 Current Situation

The air quality in busses influences passenger comfort and health conditions. Furthermore, air quality also affects safety aspects such as fogging of wind shield and increased driver's stress at uncomfortable conditions.

Therefore high air exchange rates are recommended or requested for cabin air by VDV (Association of German Transport Companies) [2] for city busses, with 15 m^3/h per passenger, and by GBK (Quality Association of Bus Comfort) [3], with a 75-times per hour air exchange for parked coaches for quality levels 3–5.

Based on these overall requirements current ventilation of busses is carried out independently of the number of passengers, assuming instead full occupancy. The number of transported passengers varies very widely in the course of the day, with average occupancy of 30 % in city busses. This means, in most times energy is wasted with heating and cooling fresh air that actually is not needed to desired temperatures.

C. Junior et al. (eds.), *Energy and Thermal Management, Air Conditioning, Waste Heat Recovery*,
DOI 10.1007/978-3-319-47196-9_12

2 Motivation and Objectives

Increased requests of customers to reduce fuel consumption and also the European commission's communication COM(2014) 285 "Strategy for reducing Heavy-Duty Vehicles' fuel consumption and CO_2-emissions" [4] make it necessary to develop solutions for commercial vehicles with reduced fuel consumption and thus reduced CO_2-emissions.

Besides optimization of the primary power train, fuel consumption reduction of the secondary consumers is getting increasingly attractive. Here aggregates for heating and air conditioning of passenger compartments are the largest secondary consumers.

There are different known concepts to improve the cooling and heating performance. Reducing the fresh air rate in to the vehicle cabin depending on the number of passengers (and hence the air quality) is a possibility with a performance improvement high potential.

The actual thermal load by external and internal effects can be controlled also by re-circulating air, if the quality of cabin air is controlled simultaneously.

City busses are particular interesting for energy efficient ventilation because their occupancy widely varies between 0–100 % throughout the day, and with an average occupancy of about 30 % included rush hours. Besides different level of occupancy, door opening phases can are influencing cabin air conditions significantly. Moreover, external conditions can change very quickly due to mobility of the bus, and these can influence cabin air conditions. Energy efficiency of city busses is besides environmental aspects a specific requirement of public transport companies.

3 Monitoring Parameter and Control Algorithms

The most relevant monitoring parameters of air quality are the air humidity and the CO_2-concentration of the air. The concentration of harmful gases from ambient air, e.g. exhaust gases, hydrocarbons, etc. will be detected by external air quality sensors and the gases will be refrained from the vehicle cabin by filters or by flap switching to re-circulation air. The cabin humidity content and CO_2-concentration is hence directly influenced by number of passengers. The CO_2-concentration is also a good indicator for estimating bus occupancy, since passengers are generally the sole source of CO_2-emissions within the bus [14].

Every passenger breathes out a CO_2-volume flow of 12–20 l/h depending on the level of activity, and water vapor up to 65 g/h depending on the temperature [9, 13] (see Fig. 1). Additional humidity is added to the cabin by clothes, etc. This needs to be removed from the cabin or reconditioned in order to maintain the acceptable limits of comfort, health and safety and to meet legally required maximum limits.

With a concentration about 400 ppm CO_2 is a natural content of ambient air [14]. A rising CO_2-concentration increases the discontent of passengers. Even at an allowed CO_2-concentration about 2000 ppm the discontent increases to over 40 % [8] (see Fig. 2).

High CO_2-concentrations in vehicle cabins can cause health issues from indisposition up to critical state of health like sickness, headache and difficulties in

Cabin air temperature in °C	18	20	22	24	26
Heat loss, convection and radiation in W	100	95	90	75	70
Moisture emission in W	25	25	30	40	45
Total performance in W	125	120	120	115	115
Moisture emission in g/h	35	35	40	60	65

Fig. 1. Human heat and moisture exhalation at rest without solar radiation [9]

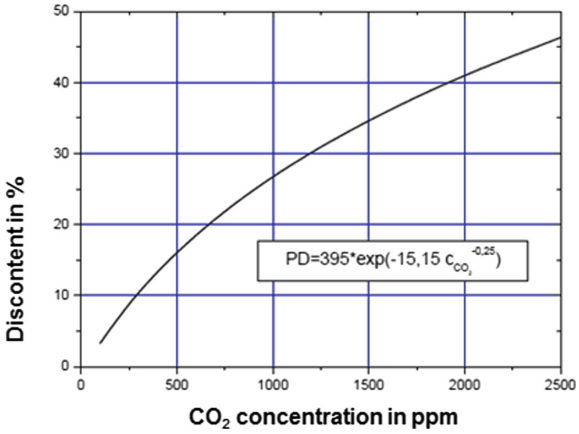

Fig. 2. Discontent depending on CO_2-concentration above ambient air concentration [8]

concentrating and – even up to unconsciousness. Therefor there have been CO_2-limits defined by Pettenkofer, DIN EN 13779 and ASHRAE 62-2001. According to Pettenkofer, the air quality in living spaces is excellent up to 1000 ppm. This limit cannot be transferred readily to vehicles due to specific differences. DIN EN 13779 requires a limit about 1500 ppm. According ASHRAE 62-2001, a CO_2-concentration of 2000 ppm is allowed at working places for 8 h [5–7, 12] (see Fig. 3).

Fogging on the wind shield due to high moisture content is safety relevant. In addition, humidity affects passenger comfort in the cabin. The higher the air temperature, the lower is the upper threshold for relative humidity with respect to comfort [2] (see Fig. 4).

Ambient conditions of a vehicle can change very quickly due to its mobility and hence the comfort level in the vehicle cabin, e.g. after entering a tunnel from a sunny ambient, or due to changing solar radiation because of shadowing or by changing of driving direction, which can change the temperatures of vehicle glasses, as well as the relative humidity in the cabin.

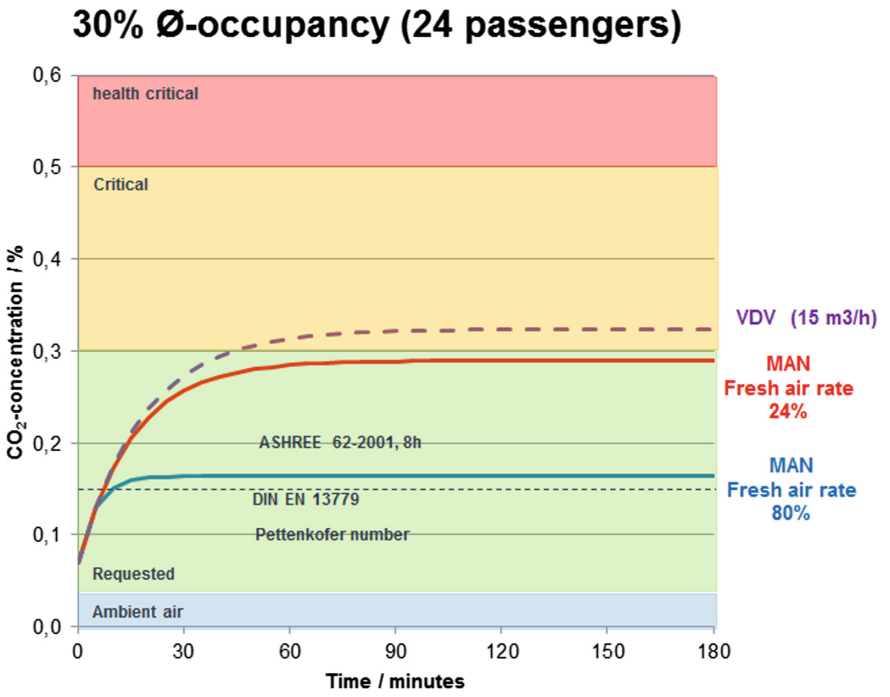

Fig. 3. CO_2-concentration depending on fresh air rate and compared to different standards [5–7]

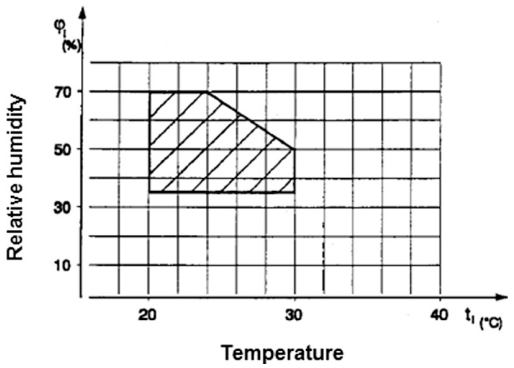

Fig. 4. Comfort zone depending on temperature and relative humidity [2]

4 Control Algorithms

While the CO_2-concentration in a bus cabin - according to the state of art - can only be influenced by controlling the amount of fresh air [11], the humidity of the cabin air can be effected by both fresh air ratio or reheat. Reheat is used in combination with low air volume flows and energy-intensive condensation of water vapor of the air. Instead, if

pure fresh air is used for controlling air humidity, high air volume flows are required and condensation does not take place.

Therefore, control algorithms for energy-efficient monitoring of the fresh air rate are required, which account for conditions within and outside of the cabin. In this work ambient temperatures are split into four characteristic ranges (see Fig. 5). For these control algorithms differ considerably due to the differences in external conditions.

Ambient temperature range	Characteristic	Parameters to control fresh air rate
Winter < 3 °C	Dry air $T_{ambient} << T_{windshield} << T_{cabin}$	• CO_2 concentration • Relative humidity at wind shield (fresh air against fogging)
Transitional season 3- 18 °C	Partly high air relative humidity $T_{ambient} < T_{windshield} < T_{cabin}$	• CO_2 concentration • Relative humidity at wind shield (fresh air / reheat against fogging)
Only ventilation 18-22 °C	$T_{ambient} \approx T_{windshield} \approx T_{cabin}$	
Summer > 20 °C	$T_{ambient} > T_{windshield} > T_{cabin}$	• CO_2 concentration • Relative humidity compatible to comfort range

Fig. 5. Temperature ranges

In cold seasons with temperatures below 3 °C the humidity and CO_2-concentration is advantageously controlled by monitoring the fresh air rate, since reheat thermodynamically and due to icing risk of the evaporator is not attractive in this operating regime.

In transitional seasons (spring and autumn) at temperatures between 3 °C and 18 °C the air can contain high humidity, which could be insufficient dehumidifying the cabin air. In these cases and at sudden fogging of the wind shield, e.g. due to quick changes of conditions as a result of mobility, a reheat-operation could be needed inevitably. Additionally the CO_2-concentration of the cabin air needs to be considered. This temperature range is most interesting for energy optimization.

In the temperature range of 18–22 °C pure ventilation can be sufficient, if the internal and external thermal load can be balanced with this and the fresh air rate can be adjusted up to maximum. Therefore this range is not very relevant for an energetic optimization by controlling the fresh air rate.

In warm seasons over 20 °C the fresh air rate will be controlled depending on comfort considerations related to cabin humidity and CO_2-concentration, while fogging of the wind shield is not relevant.

In cooperation with Kempten University of Applied Sciences within a diploma thesis [1] (see Fig. 6), control algorithms for energy-efficient control of fresh air rates have been derived from process simulation depending on changing internal and external air conditions. By using of these simulations, fuel consumption was analyzed under realistic operating scenarios. The results show a high fuel consumption reduction potential by applying fresh air control strategies.

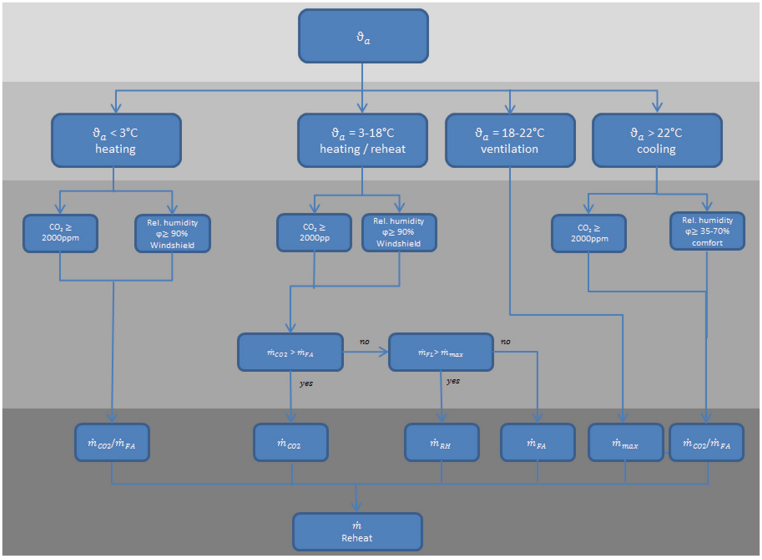

Fig. 6. Temperature ranges and control algorithms [1]

5 Comparison and Energy-Efficiency

Because of manifold factors which can impact ambient air conditions, especially in city busses, fuel consumption reduction by controlling fresh air rates can be reliable determined only by real measurements. For this purpose, MAN Truck & Bus AG has provided a customer bus with related sensors for field monitoring to determine the effect of different operating conditions like school holidays, weekends, rush hours, early and late drive services, different ambient conditions and other external influences like shadowing, tunnel driving, etc.

The city busses operate 20 h from 5:00 o'clock in the morning until 1:00 o'clock in the night with an annual mileage of about 60,000 km and an average speed of 16 km/h, whereby an average distance between two stops is 450 m and the average driving distance of passenger is about 4.5 km [10].

For this work representative data of three temperature ranges of weekdays were for further analysis. Presently MAN controls the fresh air rate only depending on ambient temperature, whereby the fresh air rate is reduced at extremely low and high temperatures in order to reach the desired temperature. Instead the new control strategy is controlling the fresh air rate by monitoring air qualities.

Fundamental the energy consumption will be determined by the internal load, solar radiation and the ambient temperature (thermal load and conditioning of fresh air), and by this the amount of fresh air.

The first case (see Fig. 7) investigates operation of a city bus during warm seasons (summer) within temperature ranges between 25 °C and 33 °C. During the day the temperatures increases up to 33 °C, while the ambient relative humidity changes little. Between 14:00–18:00 o'clock at high ambient temperatures the current control unit

reduces the fresh air rate to reach the desired temperature of the cabin. Nevertheless the energy consumption is high due to high ambient temperatures. Both the current and new (monitored) control strategies have most similar fuel consumption in phases of high occupancies (about 8:00 o'clock and 18:00 o'clock). On the typical summer day shown, the potential of fuel consumption reduction is on average about 0.68 l/h which is comparably high, whereby the COP-values of the air conditioning unit are in average about 2.5.

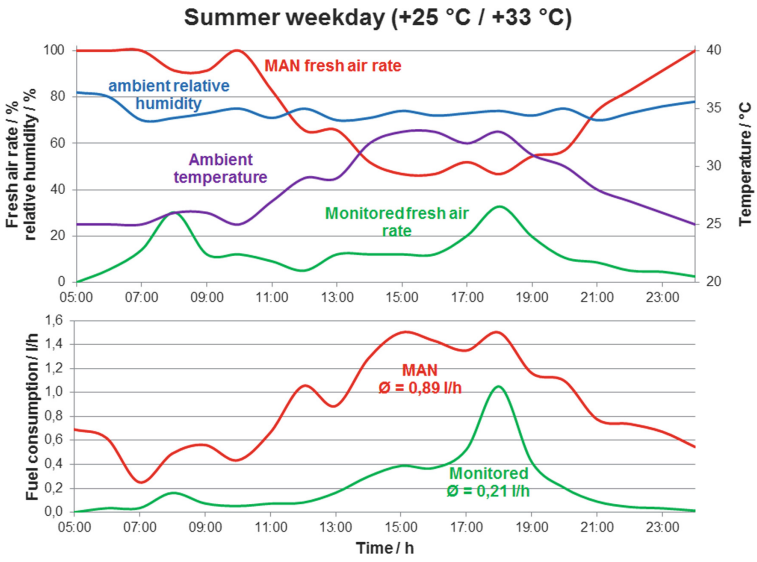

Fig. 7. Summer case

The second case (see Fig. 8) analyses operation during transitional season (spring and autumn) with a temperature range between 9 °C and 19 °C. The current control unit does not reduce the fresh air rate due to moderate temperatures. Nevertheless the fuel consumption is comparatively low, but with a high potential for fuel consumption reduction of on average 0.35 l/h, which is proportionally high due to a low COP of about 0.8 of the auxiliary heater.

The third and last case (see Fig. 9) represents a cold season (winter) with a temperature range between −14 °C and −6 °C with relative harsh ambient conditions. The current control unit de-throttles the fresh air rate with increased ambient temperatures. In early hours the controlled (monitored) fuel consumption gets close to those of the current control unit due to high occupancy of the city bus and high throttling of fresh air rates by the current control unit. At such a winter day the potential for fuel consumption reduction is on average 1.09 l/h, which is highest due to a low COP of auxiliary heater of 0.8 and due to big temperature differences between ambient and cabin temperatures.

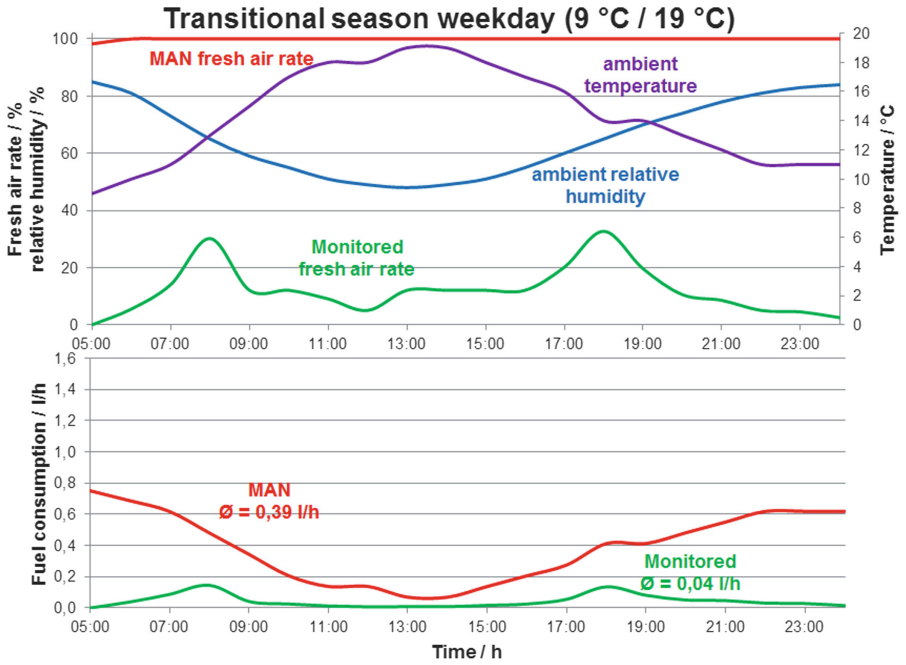

Fig. 8. Transitional season case

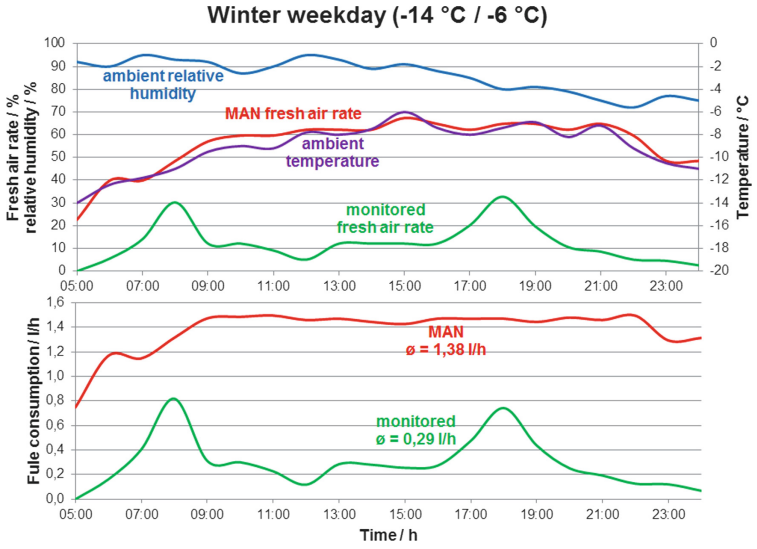

Fig. 9. Winter case

6 Annual Consideration

For estimating the potential for fuel consumption reduction different vehicles types need to be considered: diesel, hybrid and battery. The mixed type hybrid is however not considered in this investigation.

The most significant difference of potentials between of diesel and battery busses is in the temperature range of 10–18 °C, because heat demand is satisfied by engine heat for the diesel busses, while the battery busses need extra energy of their batteries.

The highest potential of fuel consumption reduction is at temperatures below18 °C: In winter below 3 °C due to big temperature differences of 17 K or more between ambient and cabin temperatures, and during transitional season of 3–18 °C due to the high occurrence of these temperatures with 60.9 % (see Fig. 10). The effect is increased by the low COP of the auxiliary heater of 0.8.

	Fuel consumption reduction		
	Diesel	Battery	Ratio
Summer cooling >22 °C	0.03 l/h		8.6%
Only ventilation 18 °C – 22 °C	0.00 l/h		15.1%
Heating by engine / battery 10 °C – 18 °C	0.00 l/h	0.26 l/h	43.5%
Transitional heating 3 °C – 10 °C	0.97 l/h		17.4%
Winter heating <3°C	1.12 l/h		15.4%
Fuel consumption reduction full year	0.35 l/h	0.46 l/h	
	3.4%	4.6%	

Fig. 10. Fuel consumption reduction

The results show the potential for fuel consumption reduction of about 3.4 % for diesel-city busses and of 4.6 % for battery-city busses.

This could be translated into a reduction of the annual fuel consumption of 750–1000 l depending on the bus type.

7 Summary and Outlook

The results show the high potential for fuel consumption reduction by controlling the fresh air rate, especially in city busses with an average occupancy about of 30 %.

The reduction of energy consumption in seasons with heating demand is highly relevant especially for electrified vehicles (battery-city busses) because of the impact on driving range and battery capacity.

If a heat pump is used for heating, the potential for fuel consumption below 18 °C is reduced correspondingly.

The position of the CO_2-sensor is important for determining the correct CO_2-concentration and hence the energy reduction potential, which can be relevant for

future further investigations. There are spots within the bus with low air exchange und correspondingly high air aging. A CO_2-sensor placed in the recirculation air measures average CO_2-concentrations risking that not allowed high CO_2-concentrations in bus areas with high air aging are insufficiently detected.

These potentials for fuel consumption reduction could be further improved by individual or zonal air conditioning with corresponded sensors.

The monitoring and controlling of fresh air rates is also compatible with the latest recommendation of VDV, which is valid from 2017. Furthermore it is able to fulfill the expected directions of the European Commission with respect to future regarding CO_2-emission.

References

1. Gökoglu, M.: Diplomarbeit: Untersuchung zum Verbrauchseffekt des Frischluftanteils bei der Busbelüftung, Unveröffentlicht, June 2016
2. VDV-Schrift 236: Klimatisierung von Linienbussen der Zulassungsklassen I und II, für konventionell angetriebene Diesel- und Gasbusse sowie für Hybrid-, Brennstoffzellen- und Elektrobusse. VDV-Verlag, Köln, 6 Juni 2015
3. Gütesicherung RAL-GZ 791: Buskomfort. Beuth-Verlag GmbH, Berlin, May 2007
4. COM(2014) 285: Strategy for reducing Heavy-Duty Vehicles‘ fuel consumption and CO_2-emissions
5. ASHRAE Standard 62-2001: Indoor Air Quality (2002)
6. DIN EN 13779: Ventilation for non-residential buildings - Performance requirements for ventilation and room-conditioning systems. Beuth Verlag GmbH, Berlin, September 2007
7. Pettenkofer: Besprechung Allgemeiner auf die Ventilation bezüglicher Fragen. Über den Luftwechsel in Wohngebäuden. J.G. Cottaísche Buchhandlung, München (1858)
8. Fritzner, K., Finke, U.: Lüftungsregeln für freie Lüftung, Bundesanstalt für Arbeitsschutz und Medizintechnik (2012)
9. VDI 2078: Berechnung der thermischen Lasten und Raumtemperaturen. Beuth Verlag GmbH, Berlin, 2015
10. Leuthardt, H.: Die Wirtschaftlichkeit von Gelenkbussen und Buszügen, Der Nahverkehr, May 2010
11. Dougan, D.S., Damiano, L.: CO_2-based demand control ventilation. ASHREA J., October 2004
12. SIEMENS: Demand-controlled ventilation, control strategy and application for energy-efficient operation (2010)
13. Müller, R.: Atmung, Stoffwechsel und Blutkreislauf, Universität München
14. Umweltbundesamt: Gesundheitliche Bewertung von Kohlendioxid in der Innenraumluft. Springer Medizin Verlag (2008)

Air-Conditioning, Approaches to Optimization

Amelioration of Energy Efficiency for Refrigeration Cycles by Means of Ejectors

Ahrendts Fabian[1(✉)], Thoma Werner[2], and Köhler Jürgen[1]

[1] Institut für Thermodynamik, TU Braunschweig, Brunswick, Germany
fabian.ahrendts@tu-bs.de
[2] Daimler AG, Sindelfingen, Germany

Abstract. In this paper is explained how the efficiency of refrigeration cycles and in particular those with carbon dioxide (CO_2, R744) as refrigerant can be augmented by use of an ejector. Special emphasis is put on the exposure of CO_2 as a safe and environmental friendly working fluid – making it a promising candidate to replace today's standard refrigerant in the automotive field tetrafluoroethane (R134a), which is about to be banned within the European Union for mobile applications.

The working principle of ejectors as well as their operational behaviour is described. Furthermore an approach to quantify ejector efficiency is presented. Different classes of refrigeration cycles with ejectors are introduced and an automotive application example from an ongoing research project is described in detail: It is shown how an ejector can be fruitfully put into place in charge air cooling.

Keywords: CO_2 · R744 · Ejector · Refrigeration cycle · Charge air cooling

1 Introduction

Refrigeration systems are mayor contributors to both direct and indirect greenhouse gas emissions. Direct emissions are linked to leakage whereas indirect emission arise from the provision of driving energy for the system. In order to lower the greenhouse gas emissions both emission types have to be taken into account.

Direct emissions can be reduced by minimising leakage or by using refrigerants with a low GWP (Global Warming Potential). In this regard the natural refrigerant CO_2 is a good choice. It has a low GWP of one and is furthermore nontoxic as well as non-flammable in contrast to other natural refrigerants like ammonia or propane. Its rather high evaporation enthalpy makes it an interesting choice for mobile applications. Pipe cross-sectional areas can be chosen smaller in comparison to cycles with refrigerants with higher evaporation enthalpy. One mayor shortcoming of CO_2 systems is however the low exergetic efficiency at high ambient temperatures due to higher expansion losses in the throttling valve of conventional refrigeration cycles in comparison to other refrigerants. Lucas (2015) has shown that the specific expansion losses with respect to the compression work for a conventional refrigeration cycle with CO_2 as working fluid can reach 35% in dependence of the inlet temperature of the expansion valve. Those losses are about 10% lower for an R134a cycle, while the other specific

C. Junior et al. (eds.), *Energy and Thermal Management, Air Conditioning, Waste Heat Recovery*,
DOI 10.1007/978-3-319-47196-9_13

cycle losses are more or less of the same order. Hence a reduction of the expansion losses is desirable and key to the competitiveness of CO_2 refrigeration systems. The expansion losses can be recovered and thus the system efficiency ameliorated by means of ejectors. A refrigeration cycle with an ejector is shown in Fig. 1. The ejector has a high and a low pressure inlet for the working fluid which is mixed and then decelerated in order to achieve a pressure rise at the outlet and to relief the compressor as a consequence.

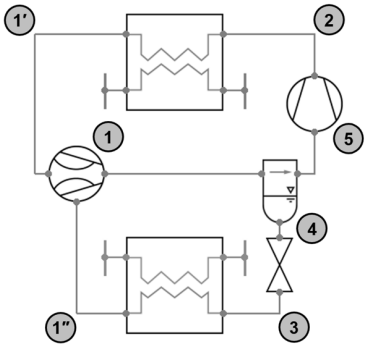

Fig. 1. Refrigeration cycle with ejector

The potential benefit of the application of ejectors in refrigeration systems has been subject to extensive research. Major improvements of the system efficiency which is characterised by the COP (Coefficient of Performance) were shown numerically among others by Fiorenzano (2011) and Jeong et al. (2004). Elbel et al. (2012) derived numerically form experimental data a COP increase of up to 7% compared to an expansion valve refrigeration system including an Internal Heat Exchanger (IHX). Lucas and Koehler (2012) were able to demonstrate experimentally a COP increases of up to 17% for an ejector refrigeration cycle compared to an expansion valve refrigeration cycle.

2 Ejector Devices

Before reviewing ejector devices it is important to notice that ejectors were initially not developed for pressure recuperation in refrigeration cycles. The first ejector invented and patented by Henry Giffard was intended to pump liquid water to the reservoir of steam engine boilers. This was achieved by condensing the high pressure steam and using the created vacuum to suck water. Other applications described by different authors were comprehensively collated by Elbel (2009) among them a gas-liquid reactor to mix two different fluid streams reported by Elgozali et al. (2002).

As a result one finds many alternative expressions for the term ejector such the term injector, eductor, diffusion pump, aspirator, or jet pump depending on the application. If one restricts oneself to single fluid ejectors, they can be classified according to a proposal of Elbel (2007) like in Table 1.

Table 1. Classification of ejectors according to Elbel (2007)

Type	Driving flow	Driven flow	Exit flow	Remarks
Vapor jet	Vapor	Vapor	Vapor	Two-phase flow can occur, shock waves possible
Liquid jet	Liquid	Liquid	Liquid	Single-phase flow without shock waves
Condensing	Vapor	Liquid	Liquid	Two-phase flow with condensation of driving vapor, strong shock waves
Two-phase	Liquid	Vapor	Two-phase	Two-phase flow can occur, shock waves possible

The vapour jet ejector and the two-phase ejector can be encountered in refrigeration cycles. The first ejector for refrigeration purposes was according to Elbel (2009) a vapour jet ejector proposed by Leblanc in 1910. Because of the vast availability of steam at the time the so-called steam jet refrigeration systems spread widely for the climatisation of large buildings and railroad cars. The first two-phase ejector was introduced by Gay (1931) in order to achieve indeed the aforementioned reduction of throttling losses.

The idea of using CO_2 as refrigerant goes as way back as the ejector itself as Elbel (2007) elaborates. The use of CO_2 as refrigerant was first patented by Alexander Twining in 1850. Its application in refrigeration systems for ice production was patented by Thaddeus Lowe in 1867. Refrigeration with CO_2 remained of importance in ice production, beer breweries, and in cargo ship refrigeration until the beginning of the 20th century. The refrigerant CO_2 was then outed by synthetic refrigerants such as R134a and only rediscovered in the late 1980s in the context of transcritical air-conditioning systems including ejectors along with the emerge of environmental awareness.

2.1 Working Principle

The basic four components of an ejector are equal for all ejectors types given in Table 1: They consists of a motive nozzle and a suction nozzle, a mixing chamber and a diffuser as shown in Fig. 2.

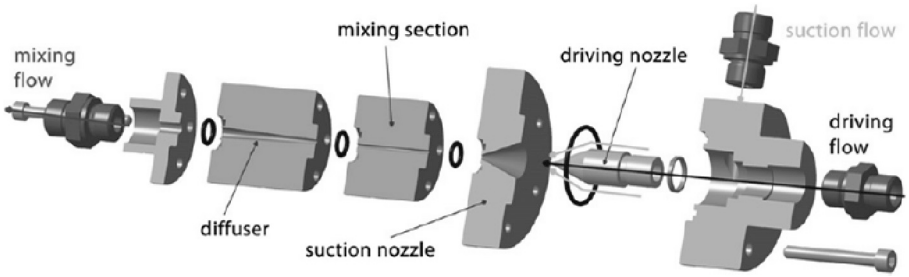

Fig. 2. Ejector components, Tischendorf et al. (2010)

In the motive nozzle the pressure energy of the driving flow is converted into kinetic energy. In case of gaseous or vaporous fluid at the inlet the motive nozzle is often realized as a converging-diverging nozzle allowing supersonic discharge velocities. As far as two-phase ejector are concerned the phase change of the primary flow inside the nozzle might be delayed due to thermodynamic and hydrodynamic non-equilibrium effects leading to flash vaporisation downstream.

The sucked fluid is accelerated and directed inside the suction nozzle which both contributes to the reduction of hydrodynamic losses. Large velocity differences between the driving and the driven flow cause shearing losses whereas a too steep angle of the sucked flow with respect to the driving flow are connected with losses due to deflexion and areas of recirculation in the mixing chamber.

When entering the mixing chamber the driving flow post-expands and entrains the sucked flow by transferring momentum. The mixing chamber can either be designed with constant cross-sectional area or conical geometry in order to achieve mixing at constant pressure. The expansion of the driving flow can be connected with the creation of a fluidic throat in which the sucked flow is further accelerated to sonic velocity. Within the mixing chamber one can usually observe shock waves that lead to a significant first pressure rise and the deceleration of the flow to subsonic velocity.

A further deceleration and pressure rise respectively is achieved by means of the subsonic diffuser. The pressure at the outlet of the diffuser lies in general in between those of the driving and the driven flow. Though there are designs and operating conditions under which the pressure at the outlet rises above the pressure of both inlets.

2.2 Operational Behaviour and Efficiency

The operational behaviour of an ejector is mainly characterized by the recuperated pressure Δp_{Rec} or the suction pressure ratio Π and the mass entrainment ratio ϕ. The recuperated pressure is the difference between the pressure at the diffuser exit and the pressure of the suction flow entering the ejector

$$\Delta p_{Rec} = p_e - p_s, \tag{1}$$

whereas the suction pressure ratio is defined as the pressure ratio at the diffuser exit pressure to the pressure of the suction flow entering the ejector

$$\Pi = \frac{p_e}{p_s} = \frac{\Delta p_{Rec}}{p_s} + 1. \tag{2}$$

As is derived in Eq. (2) both expressions (1) and (2) contain the same information and can therefore be exchanged. The recuperated pressure is dependent on the entrainment ratio which is defined as the ratio between the entrained and the driving mass flow

$$\phi = \frac{\dot{m}_s}{\dot{m}_d}. \tag{3}$$

Augmenting the driving mass flow results in lower entrainment but better pressure recuperation, while diminishing it results in low pressure change. This dependency has a linear characteristic over a wide range of operating conditions and especially around the point of maximum efficiency as has been show by Lucas (2015).

The efficiency value of an ejector is subject to its definition. In the following the definition of ejector efficiency by Köhler et al. (2007) is presented. Ebel and Harnjak (2008) presented later a similar definition which was derived in a different way.

The working principle of an ejector can be described by an equivalent model of a turbine driving a compressor as shown in Fig. 3. The maximum power in order to drive the compressor can be extracted from the driving mass flow by an isentropic expansion to the diffuser exit pressure in the turbine. The highest possible pressure rise in the compressor is achieved via an isentropic compression of the sucked mass flow to the diffuser exit pressure.

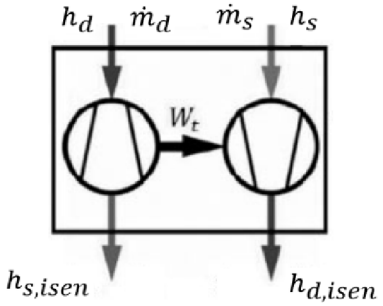

Fig. 3. Equivalent model of an ejector

The ejector efficiency has been defined by Köhler as the ratio between recuperated power and maximum recuperated power which corresponds to the product of the entrainment ratio and the ratio of the enthalpy differences of the isentropic compression and expansion

$$\eta = \frac{\dot{W}_{Rec}}{\dot{W}_{Rec,max}} = \phi \cdot \frac{h_{s,isen} - h_s}{h_d - h_{d,isen}}. \tag{4}$$

This definition has the advantage in comparison to others that it is determined with external parameters and that it is independent of the working fluid or the ambient condition. According to this definition Lucas (2015) has reported experimentally measured ejector efficiencies of up to 35%.

3 Ejector Cycles

The goal of the application of the ejector is to improve the overall efficiency of the refrigeration cycle it is integrated in. It is important to understand that the efficiency of the ejector component is only one factor among others that determine the COP. The intrinsic efficiencies of the cycle components play a role as well as their interaction for example the one of the ejector and the separator which splits liquid and gas. Due to the mass conservation of the two phases there is a dependency between the steam content at the separator inlet and the entrainment ratio. Within the cycle it is no longer a free variable. Therefore it makes sense to characterise ejectors not only at component but also at system level.

3.1 Classification of Ejector Cycles

According to a proposal by Bergander (2015) three basic types of refrigeration cycles with ejectors can be distinguished in dependence on the pressure recuperation with respect to the compressor. Typical vapour compression cycles consist of a gascooler, an expansion valve, an evaporator and a compressor. The supply of the compressor with electrical energy is effort with respect to the cycle balance. This effort can be reduced by means of an ejector as the pressure recuperation relieves the compressor. This relief can either be realized as pre- or post-compression. An ejector can also replace the compressor and take over the entire vapour compression.

In the ideal vapour refrigeration cycle also known as Evans-Perkins- or Plank-process, vaporous refrigerant is fully evaporated, isobarically superheated, isentropically compressed, isobarically cooled, condensed, isobarically supercooled and finally isenthalpically throttled. The throttling is connected with losses as the pressure energy transformed into kinetic energy is dissipated. The ejector cycle shown in Fig. 1 makes use of the device as replacement for the expansion valve and as a pre-compressor. Examples of refrigeration cycles with an ejector as post compressor and an ejector as a replacement for the compressor are shown in Fig. 4.

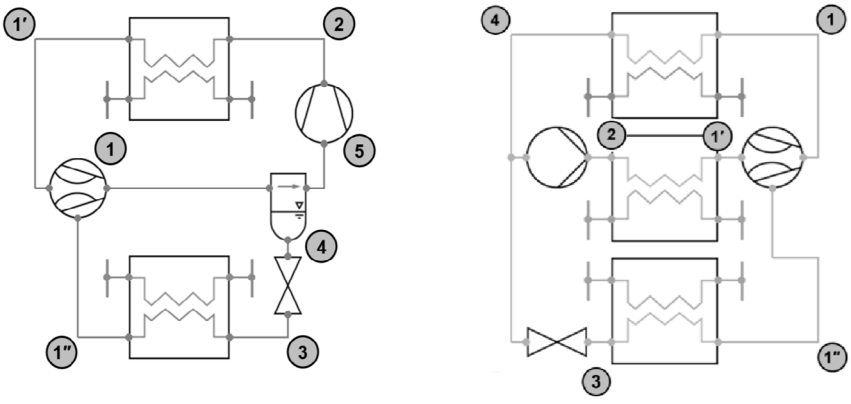

Fig. 4. Ejector as post-compressor and as replacement for the compressor

3.2 Application Example: Charge Air Cooling

A new application of ejectors is charge air cooling for automotive applications. The basic concept for this applications is outlined in Fig. 5. The hot exhaust heats up isobarically the already gaseous working fluid in heat exchanger 1 (HX 1) which is used to drive the ejector. The ejector sucks form the outlet of the charge air cooler also gaseous working fluid. The two flows are mixed inside the ejector. The mixed flow out of the ejector is isobarically cooled in HX 2 and separated. One portion of the flow delivered to the compressor which is connected to HX 1. The other portion of the working the fluid is throttled in the expansion valve (XV) and feeds the charge air cooler. With respect to the classification above the ejector is used as a pre-compressor in the cycle.

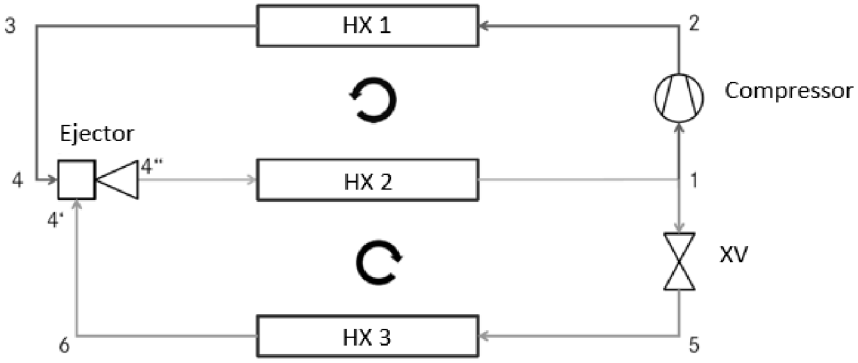

Fig. 5. Basic cycle for charge air cooling with ejector

The application of the cycle in the automotive flied is connected with particularly challenging requirements regarding performance and weight. Therefore the cycle has further been optimized as shown in Fig. 6. Two recuperators (R) have been added. The first recuperator reduces the amount of heat released while the second recuperator cools the working before entering HX 3. It reduces the mass flow necessary to achieve the same cooling effect that would have been realized without the recuperator. The cycle point 6 is defined by the charge air temperature and the dew point of the working fluid. Within this cycle the pressure and temperature levels can be chosen freely apart from cycle point 1 as the ambient is the heat sink. Cycle point 3 is dependent on the heat transfer from the exhaust.

It was possible to show that the target figures of mass flow, the pipe cross-sectional area, the heat release and the compressor power are dependent on four characteristic values. They are dependent on the values for the high and intermediate pressure as well as the temperatures at cycle points 1 and 3. An optimal operating condition was determined by optimizing the object figures with respect to the parameters named. The possible improvements by the application of the recuperators and the described optimization process led to 28% less compression power, 20% less cross-sectional area, 58% less required mass flow, 76% less released heat and 28% COP increase in comparison to the initial cycle design.

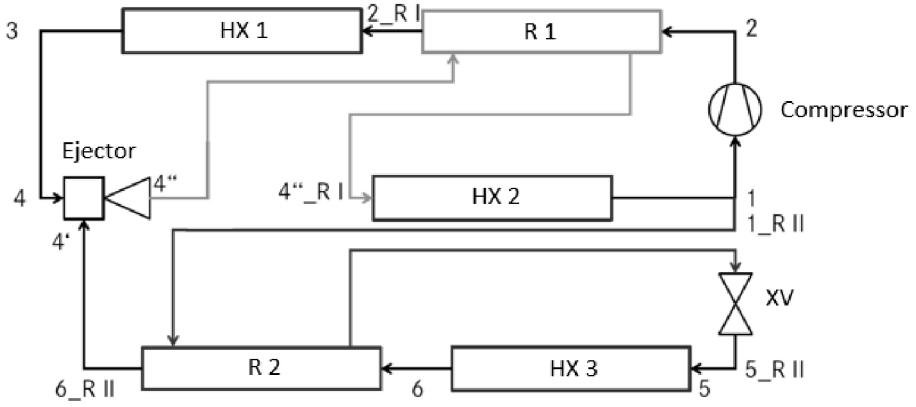

Fig. 6. Cycle for charge air cooling with ejector and recuperators

4 Summary

Due regulation new refrigerants with low GWP will be required. CO_2 is a promising option being both environmentally friendly and safe. Its relative high evaporation enthalpy makes it an interesting option especially for mobile refrigeration systems. Anyhow the low exergetic efficiency at high ambient temperatures is challenging. The component with the highest specific losses in classic refrigeration cycles with CO_2 as working fluid is the expansion valve. The application of ejectors in order to recuperate pressure and to relief the compressor is a promising solution. In dependence on the definition device efficiencies of up 35% have been reported.

A refrigeration cycle with a ejector as a pre-compressor has been presented for charge cooling. It has been shown how the basic design for the cycle can further be improved by means of recuperators and an optimization of some characteristic parameters with respect to the target figures of mass flow, pipe cross-sectional area, heat release and compressor power leading to possible COP improvements of 28% in comparison to the initial design.

References

Bergangder, M.J.: Ejector refrigeration cycles. In: Gaspar, P.D., da Silva, P.D. (eds.) Handbook of Research on Advances and Applications in Refigeration Systems and Technologies (2015)

Elbel, S., Reichle, M., Bowers, C., Hrnjak, P.: Integration of a two-phase ejector into a compact, lightweight unitary-type air-conditioner using R744 for energy efficient operation in hot climates. In: Proceedings of 10th IIR Gustav-Lorentzen Conference (2012)

Elbel, S.: Experimental and analytical investigation of a two-phase ejector used for expansion work recovery in a transcritical R744 air-conditioning system. Ph.D. thesis, University of Illinois at Urbana-Champaign (2007)

Elbel, S.: Historical and present developments of ejector refrigeration systems with emphasis on transcritical carbon dioxide air-conditioning applications. In: International Seminar on Ejector/Jet-pump Technology and Applications, Louvain-la-Neuve, Belgium, 7–9 September 2009

Elbel, S., Hrnjak, P.: Experimental validation of a prototype ejector designed to reduce throttling losses encountered in transcritical R744 system operation. Intl. J. Refrigeration **31**(3), 411–422 (2008)

Elgozali, A., Linek, V., Fialová, M., Wein, O., Zahradník, J.: Influence of viscosity and surface tension on performance of gas-liquid contactors with ejector type gas distributor. Chem. Eng. Sci. **7**(15), 2987–2994 (2002)

Fiorenzano, R.: Untersuchung von Ejektor-Kälteanlagen beim Einsatz in tropischen Gebieten, Ph.D. thesis, Technische Universität Braunschweig, Germany (2011)

Gay, N.H.: Refrigerating system, U.S. Patent 1,836,318 (1931)

Köhler, J., Richter, C., Tegethoff, W., Tischendorf, C.: Experimental and theoretical study of a CO2 ejector refrigeration cycle. In: VDA Winter Meeting Saalfelden (2007)

Lucas, C., Koehler, J.: Experimental investigation of the COP improvement of a refrigeration cycle by use of an ejector. Intl. J. Refrigeration **35**(6) 1595–1603 (2012)

Lucas, C.: Untersuchung der Betriebscharakteristik von zweiphasigen CO_2 Ejektoren. Ph.D. thesis, Technische Universität Braunschweig, Germany (2015)

Jeong, J., Saito, K., Kawai, S.: Efficiency enhancement of vapor compression refrigerator using natural working fluids with two-phase flow ejector. In: Proceedings of 6th IIR Gustav Lorentzen Conference on Natural Working Fluids, Glasgow, United Kingdom (2004)

Tischendorf, C., Lucas, C., Koehler, J., Tegethoff, W.: Visual investigation of an ejector motive nozzle. In: Proceedings of the ASME 2010 International Mechanical Engineering Congress & Exposition, Vancouver, Canada (2010)

Performance Control of Refrigeration Cycles by Adjustment of the Composition of the Working Fluid

T. Tokan(✉), E. Aeini, and S. Kabelac

Institute for Thermodynamics, Leibniz University of Hannover,
Callinstr. 36, 30167 Hannover, Germany
tokan@ift.uni-hannover.de

Abstract. A control strategy for a machine must take care of different operation situations. A machine is typically confronted with different boundary conditions during operation. The control of this machine must find adequate settings for the actuators within the machine to adjust to each specific operation situation. In vapor compression cycles, which are used for refrigeration and heat pump machines, there are multiple actuators to adjust the cycle performance to the requirements, for example the expansion device, the compressor and possibly some actuators within the heat exchangers. An additional way to adjust a cycle to varying operation requirements is a dedicated shift of the composition in the working fluid of the cycle. Of course this option is only available to vapor compression cycles which have a mixture as a working fluid. This situation is encountered quite often nowadays as pure refrigerants, for example, are not in line with international regulations. This contribution analyses the options for control strategies of vapor compression cycles in part-load situations. In the first part of the paper, the variable speed control for the compressor, the variable speed control of the air-side ventilation fans of the evaporator and the condenser and the expansion valve are taken as possible actuators. Experimental and theoretical results are presented to show the manifold possibilities in parameter setting, of which only one setting will result in an optimal COP efficiency value.

In the second part of the contribution the benefits of a possible shift in the composition of the working fluid mixture are discussed. The composition shift can be achieved during operation by means of a rectificator. This part is on a theoretical level only, so far.

1 Introduction

The vapor compression cycle is by far the most common concept in refrigeration, air conditioning and heat pump applications. As it is operating in millions of machines, even small improvements within such cycles will have an impact on the overall consumption of electric energy needed to drive all these machines. One of the challenges in the design of a vapor compression cycle is the part-load behavior. Most devices, especially small ones, operate with a simple on/off control, which is not the most favorable solution. Vapor compression machines have a nominal design point, which is defined by a temperature lift ΔT_{lift} and a thermal load $\dot{Q}_0$. The temperature lift is the

C. Junior et al. (eds.), *Energy and Thermal Management, Air Conditioning, Waste Heat Recovery*,
DOI 10.1007/978-3-319-47196-9_14

difference between the upper mean cycle temperature $T_{0,m}$ and the lower mean cycle temperature $T_{u,m}$, i.e. $\Delta T_{lift} = T_{0,m} - T_{u,m}$. In some cases these mean thermodynamic temperatures address the inside temperatures of the working fluid. In our case these are the temperatures of the heat sink and the heat source, as for example, the ambient air and the cold room air. The thermal load $\dot{Q}_0$ is, in our definition, the thermal load of the evaporator, see Fig. 1. Most of the vapor compression cycles are not operated at their nominal design point, but at some other operating condition. This can be a deviating ΔT_{lift} and/or a different thermal load. The temperature lift may be lower or, in some cases, a little higher than the nominal design value, the thermal load is typically smaller in part load. The control strategy of the vapor compression cycle must be able to adjust in a smart way to part load operation. If the temperature lift ΔT_{lift} is changed, the upper and lower pressure of the working fluid must be adjusted to give new saturation temperatures within the evaporator and the condenser. If the thermal load changes, the mass flux of the working fluid must be adjusted. Unfortunately, adjusting the compressor performance and/or the expansion valve changes pressure difference and mass flux simultaneously. The simplest way of control is the temperature guided on/off control, as is done, for example, in most domestic refrigerators. Nowadays electronical controlled devices become better available at affordable prices, so the speed-controlled compressor, the electronic expansion valve and speed-controlled fans at the condenser and the evaporator are encountered in real machines more frequently now [1]. These electronical controlled devices offer a great chance in enabling an efficient part load operation, but they call for a predictive model based control strategy to find the optimum operation mode [2, 3]. This problem of predictive model strategy will be discussed in the first part of the paper. The second part of the paper will be devoted to an additional tool that could be used for further optimization of the energy efficiency of a given cycle during operation. This additional tool aims for a shift in composition of the working fluid within the machine. If the working fluid, the refrigerant is a mixture, the concentration of the components of this mixture determines the thermophysical properties of the working fluid and thus will have an influence on the operation performance of the cycle. The questions about why to shift the composition and how to shift the composition as an additional measure of control will be discussed in the later part, Sects. 3 and 4.

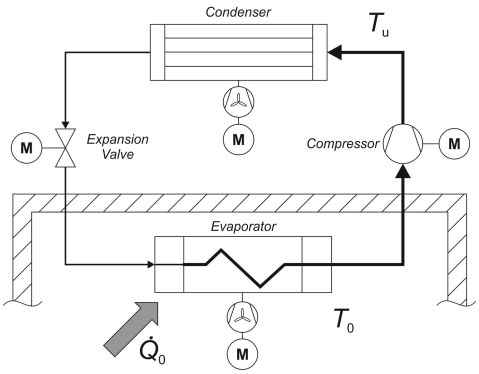

Fig. 1. A simple vapor compression cycle, working as a refrigerator

A shift in composition during operation of a vapor compression cycle as an additional control option has, to our knowledge, not yet been addressed in the literature. The model-based predictive control (MPC) has been discussed in recent years, as variable speed drives and electronic components became better available [1]. Jakobsen and Rasmussen [2] have shown for a single-stage vapor compression cycle an improvement in energy efficiency of 10% using MPC. The cycle consisted of an air-cooled evaporator and an air-cooled condenser, where the fans were controlled by variable speed motor drives. The compressor also had a variable speed. An optimal setting for each component in different part-load situations has increased the COP-value by about 10% for a specific part load situation. Leducq, Guilpart and Trystram [3] have presented a non-linear predictive control algorithm to optimize the operation of a laboratory-scale refrigerating plant. They have included optimality criteria and technological constraints into the reduced model for the vapor compression cycle. The energy benefits they have seen both theoretical and experimental were between 8% and 20%, depending on the number of actuators available for optimization. An overview on possible advanced control strategies for vapor compression cycles used for electronics cooling is given in a Ph.D. thesis by J. Catano in 2011 [4].

2 Optimum Operation Modes in Part Load

In a first step, the possible benefits of a model-based predictive control without composition shift have been analyzed both theoretically and experimentally. The single stage vapor cycle, which has been considered for this analysis, is shown in Fig. 1. This cycle is equipped with four electronic actuators, i.e., the variable speed drives for the compressor and for the fans of the air cooled evaporator and condenser as well as the electronic expansion valve. The nominal design values for this cycle are a thermal load of $\dot{Q}_{0,n} = 8\text{kW}$ and a temperature lift $\Delta T_{lift,n} = 40\,\text{K}$. In this nominal design point, the rotational speed of the electric drives and the valve opening are marked to be at 100%. In a first step the thermal load $\dot{Q}_0$ is lowered to a part load situation, keeping a constant temperature lift of $\Delta T_{lift,n} = 40\,\text{K}$. Several settings of the electronic actuators are possible to operate the cycle in such a specific part load mode. One option is to operate the fans ventilating the air side of the heat exchangers at a lower speed, saving electric energy for the fan electric drive, but of course giving lower heat transfer values on the air side of both heat exchangers. This will result in a larger temperature difference between refrigerant and air in the evaporator ΔT_{ev} and in the condenser ΔT_{con}. This is called 'case A' in Fig. 2, these temperature differences are also shown in Fig. 2. Such large temperature differences will call for a higher pressure of the working fluid in the condenser and lower pressure of the refrigerant in the evaporator, as the ambient temperature T_{amb} and the cold room temperature T_o are fixed. This enlarged pressure difference of the refrigerant between hot and cold side provokes an enlarged energy consumption of the compressor drive.

Another possible setting of the electronic actuators for the very same part load setting could be full power to the fans ventilating evaporator and condenser, giving high heat transfer rates, thus lower temperature differences ΔT_{ev} and ΔT_{con} and thus

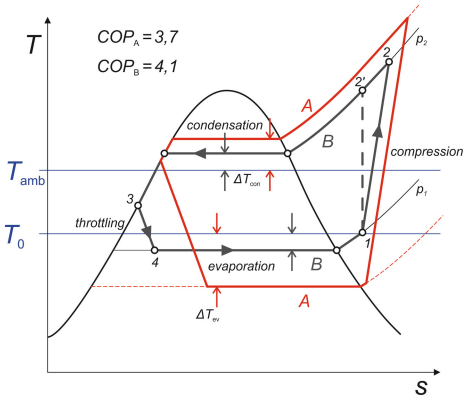

Fig. 2. A temperature entropy diagram of a vapor compression cycle showing two different operation modes for the same part-load situation. Case A: low fan speed, high compressor load; Case B: high fan speed, lower compression load

less pressure difference on the hot and cold side of the refrigerant. This will see a decreased electric energy consumption of the compressor, but an increased energy consumption of the fans. So different settings for the speed control enable the very same operating condition, but end up in different values for the overall consumption of electric energy. This results in different values of the COP at the same temperature lift and the same thermal load. This is seen in Fig. 2, where only two different settings are compared, as described above, and also in Fig. 3. This graph summarizes experimental data gained from a setup shown in Fig. 4 and, schematically, in Fig. 5. Here it becomes clear again that different settings of the fan speed, the compressor speed and the expansion valve opening give the same values $\dot{Q}_0$ and T_{lift}, but at different COP's.

The COP-surface shown in Fig. 3a has multiple local maxima, so a predictive model-based control strategy is needed to adjust the machine to the most energy efficient operation in each specific operation demand mode. This MPC must be fast enough to perform in real time, it must also be able to incorporate external parameters

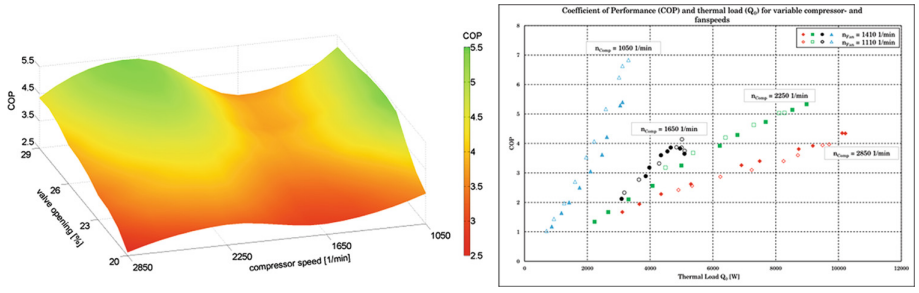

Fig. 3. (**a**) The COP-value of the cycle as a function of valve-opening and rotational speed of compression (**b**) COP-value of the cycle as a function of thermal load. Different actuator settings are possible.

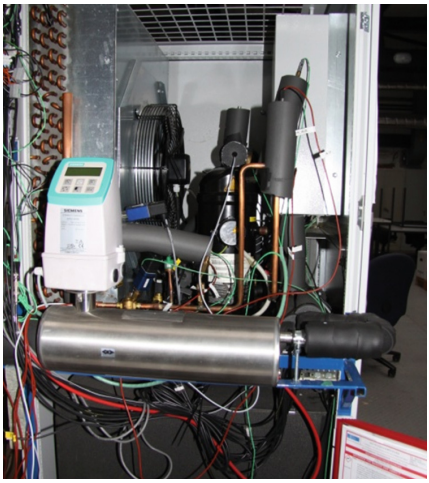

Fig. 4. Photo of the experimental setup

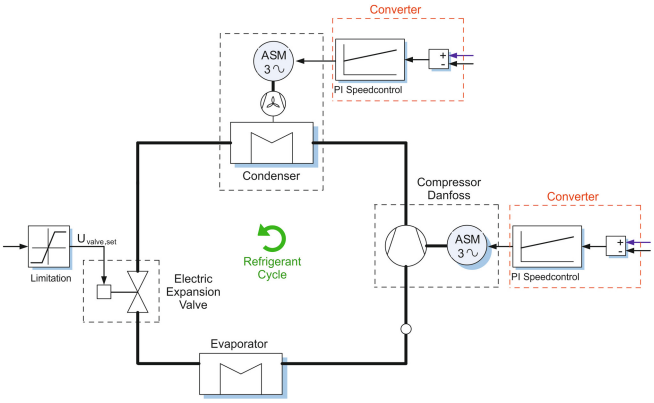

Fig. 5. Schematic diagram of the setup

which influence the thermal load and the temperature lift needed in a specific situation. The Ph.D. thesis of M. Bianchi [5], for example, describes a MPC for a domestic heat pump driven heating system, which also takes into account a weather forecast and a user profile of the heating demand.

This MPC must not necessarily be based on a dynamic model, a quasi-static description of the cycle is sufficient. The physical dynamic models of a vapor compression cycle typically result in a system of non-linear differential equations. These equations cannot be solved fast enough in an affordable microcontroller system, so simpler and faster approaches have to be considered. We are currently working on an artificial neural network approach to enable the MPC within an ASIC-microcontroller.

3 Composition Shift Control

In the preceding section the increasing complexity in the control strategy was discussed, which appears when more adjustable cycle parameters become available. If there are only two output values, the temperature lift ΔT_{lift} and the thermal load Q_o, to be adjusted to an application situation, four tunable parameters, variational speed of the compressor, the fans and the expansion valve opening, should be sufficient. So why is there a need of an additional control parameter as composition shift? To answer this question, the features accessible by a composition shift are introduced first.

3.1 What Is a Composition Shift?

The composition shift addresses vapor compression cycles, which have a binary or ternary mixture as a working fluid. To show the basic features of a shift in a composition, a binary working fluid showing azeotropic behavior is assumed. The temperature composition phase diagram of such a working fluid is shown in Fig. 6. In the following two operation modes will be discussed, one mode is marked A and uses the mole fraction x_A very close to the azeotropic point as the composition of working fluid. The second mode uses a composition with mole fraction x_B, where the working fluid shows a zeotropic behavior with a temperature glide ΔT_{glide} during an isobaric phase change, see Fig. 6. The shift in composition is achieved during operation by means of a so-called rectification unit. This unit is included into the vapor compression cycle, it connects the cycle with a small reservoir tank. This feature is shown schematically in Fig. 7.

The rectification unit is a thermal separation device which separates, for example, the low boiling component from the mixture. It will be operated for some minutes only to fill the reservoir with the low boiling component, so that the working fluid mixture sees a shift in composition resulting in a lower mol fraction x_B of the lower boiling

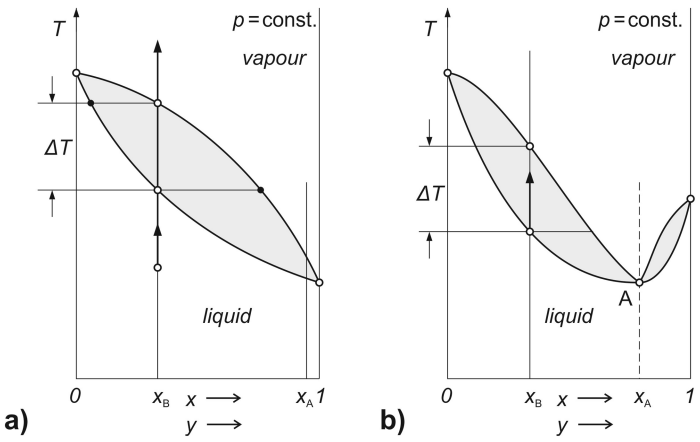

Fig. 6. Two possible phase diagrams of a binary working fluid mixture. (a) zeotropic mixture, (b) azeotropic mixture

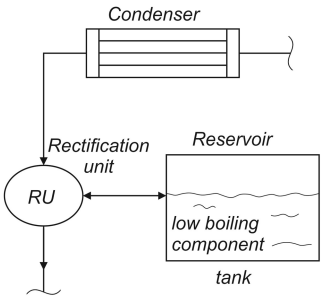

Fig. 7. The schematic rectification unit and the reservoir tank as additional components in a cycle featuring a composition shift.

component. If the operation conditions are favorable again for the original composition x_A, the contents of the reservoir will be re-injected into the vapor compression cycle to restore the original composition x_A. The composition shift shall not be performed frequently, it is more like a two-wheel or a four-wheel drive when going off-road with a car. The model based predictive control must take care of identifying appropriate time periods to govern reasonable shifting of composition.

3.2 What Is the Benefit of a Composition Shift?

The thermodynamic and thermophysical properties of the vapor compression cycle have a well-known influence on the cycle efficiency. This is, on one side, the adjustment of the characteristic curves of the compressor and the expansion device. On the other side, the heat transfer coefficients of the working fluid in the evaporator and the condenser are influenced [6]. The main benefit of a composition shift results from the temperature profiles in the heat exchangers. The local temperature difference ΔT between the two fluids within a heat exchanger, i.e., in the condenser the ΔT between the high pressure working fluid and the fluid of the heat sink, in the evaporator the ΔT between the low pressure working fluid and the fluid of the heat source, causes an entropy production rate $\dot{S}_{irr}$. Following Bejan [7], this entropy production is strongly dependent on the local temperature difference $\Delta T = T_{cold} - T_{hot}$, where T_{cold} could be the local temperature of the air in the chilled room, T_{hot} could be the local temperature of the working fluid at this position:

$$d\dot{S}_{irr,T} = \frac{T_{hot} - T_{cold}}{T_{hot} \cdot T_{cold}} \cdot d\dot{Q} = \frac{U(T_{hot} - T_{cold})^2}{T_{hot} \cdot T_{cold}} \cdot dA$$

Here U is the overall heat transfer coefficient and dA is the local heat transfer area. Each entropy production $\dot{S}_{irr}$ is connected to an exergy destruction $\dot{E}x_{lost} = T_{amb} \cdot \dot{S}_{irr}$, where the entropy production due to the pressure losses has not yet been included. A reduction of the exergy destruction is beneficial to the overall exergetic efficiency, which typically results in more favorable exit temperatures of the cooling fluids.

Figure 8 underlines this expectation. We fixed the heat source and the heat sink to be single phase fluids (air) with the temperature profiles shown in Fig. 8. The benefit of the composition shift of the working fluid would be to fit the temperature profile within the evaporator (heat source) and the condenser (heat sink) to the given temperature profile of the external single phase fluids, so to keep the temperature differences $\Delta T_{heatsource}$ and $\Delta T_{heatsink}$ as small as possible. A temperature difference of 3–5 K would be fine, which calls for well-designed evaporators and condensers. Using plate heat exchangers such tight temperature gradients could be realized [8].

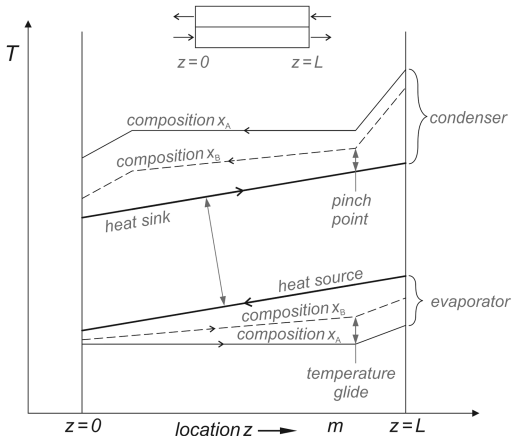

Fig. 8. The temperature location plot for the evaporator and the condenser. The working fluid composition x_B allows for smaller ΔT and thus less entropy production as compared to composition x_A

In summary, the energy and exergy efficiency of a vapor compression cycle can be optimized if the temperature differences in the condenser and in the evaporator can be minimized by a shift in composition of the working fluid, as seen by comparison of case A and case B in Fig. 8. This benefit seems to be minor at first sight, but an example calculation shows that such an optimization can give additional up to 5% increase in efficiency. In case of large industrial heat pumps, where an ammonia/water mixture is used as a working fluid, the benefit of such a composition shift could be even more.

3.3 How Can a Composition Shift Be Realized?

The basic scheme of a technical component which will be able to implement a shift in the composition of a working fluid mixture was shown in Fig. 7. This apparatus consists of a so-called ‘rectificator’ and a storage tank. The ‘rectificator’ is a distillation column, which can separate a low boiling component from a mixture. In our case it is not necessary to achieve any specific purities. Such a column needs a heat source for the evaporation and a cooling fluid (heat sink) at the head of the column for condensation of the reflux and distillate (Fig. 9). This ‘rectificator’ is not designed in detail yet,

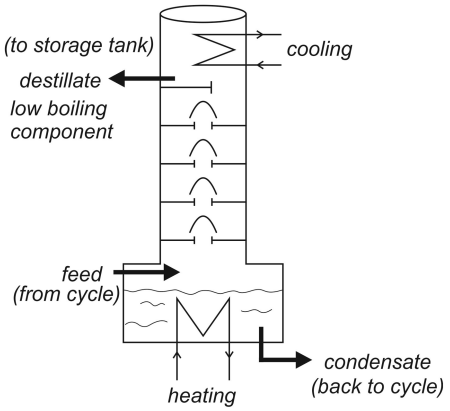

Fig. 9. A possible design for a rectification unit

it calls for a smart integration into the overall cycle. It must be remembered that this composition shift device will be in operation for some minutes only during a day, so price and effectiveness must be well balanced.

4 Conclusion

The part load operation of vapor compression cycles, i.e., refrigerators, heat pumps and air conditioners, offer a significant potential in energy saving. For a standard vapor compression cycle, the components can be electronic activators, which can adjust the operation mode of a cycle to an energetic optimum, in principle. These actuators are the compressor with a rotational speed regulated drive, the electronic expansion valve and fans for the air side of the evaporator and the condenser. To find such an optimum operation mode for each individual part load situation, a predictive smart control scheme must be found. In the first part of this contribution, results are shown for a simple refrigeration cycle in different part load operations.

The second part of the paper deals with a possible shift in composition, given a mixture as the working fluid. The benefits of such a composition shift are discussed, and a possible realization of this feature is presented.

References

1. Handbuch der Kältetechnik (VDE)
2. Jakobsen, A., Rasmussen, B.: Energy-optimal speed control of fans and compressors in a refrigeration system. Eurotherm Seminar 59, Nancy, France (1998)
3. Leducq, D., Guilpart, J., Trytram, G.: Non-linear predictive control of a vapor compression cycle. Int. J. Refrigeration **29**, 761–772 (2006)

4. Catano, J.: Dynamic modelling and advanced control of vapor compression cycles for electronics cooling. Ph. D. thesis, Dep. of Mechanical, Aerospace and Nuclear Engineering, Rensselaer Polytechnic Institute (2011)
5. Bianchi, M.: Adaptive Modellbasierte Prädiktive Regelung einer Kleinwärmepumpenanlage. Ph. D. thesis, ETH Zürich, Switzerland (in German) 2006
6. VDI Heat Atlas, Chapt. H, 2nd edn. Springer, Berlin (2010)
7. Bejan, A.: Convection Heat Transfer, 4th edn. Wiley, Chichester (2013)
8. Wang, L.: Plate Heat Exchangers. WIT-Press, Southampton (2007)

New Concept for High-Efficient Cooling Systems Based on Solid-State Caloric Materials as Refrigerant

Kilian Bartholomé(✉), T. Hess, M. Winkler, A. Mahlke, and J. König

Fraunhofer-Institut für Physikalische Messtechnik IPM,
Heidenhofstr. 8, 79110 Freiburg, Germany
kilian.bartholome@ipm.fraunhofer.de

Abstract. Caloric materials – in particular magneto-, electro- and elastocaloric materials – show a strong reversible thermal response close to a ferroic phase transition when they are exposed to their respective fields. By cyclic operation of these materials and their alternating thermal coupling to heat sink and source, efficient heat pumps can be realized where no harmful fluids are involved. In the last few years several different groups worldwide have worked on the improvement of the properties of caloric materials as well as on the development of caloric cooling systems with larger temperature span, cooling power and efficiency. Basically, all of these systems are based on a concept using a heat transfer fluid which is actively pumped through a bed of caloric material in order to transfer thermal energy from a heat source to a heat sink. Hereby, especially for magnetocalorics, several powerful systems were built, generating large temperature spans of more than 50 K while others provide large cooling capacities of several kW. However, up to now no caloric system has been built which provides large temperature span and cooling capacity while having a coefficient-of-performance (*COP*) better than standard compressor-based cooling systems.

In this work, a new concept and first experimental data of a caloric heat pump will be presented. In this concept, the heat transfer is realized by the combination of caloric material with thermal diodes which are based on latent heat transfer. Similar to thermosyphons, thermal energy is efficiently transported by condensation and evaporation processes leading to heat transfer rates which are several orders of magnitude larger than for conventional heat transfer by conduction or convection. At the same time, no additional pumps are required for transporting the heat exchange fluids, enabling systems with large temperature spans and competitive *COP*s at the same time.

1 Introduction

The technological demands on the air conditioning in vehicles are very large: The systems must be lightweight, occupy minimal space, operate reliably in very large temperature ranges and be resilient to vibration. At the same time greater demands are being placed on the efficiency and environmental sustainability of systems. The central elements of classic compressor systems are refrigerants. All of which show at least one

C. Junior et al. (eds.), *Energy and Thermal Management, Air Conditioning, Waste Heat Recovery*,
DOI 10.1007/978-3-319-47196-9_15

environmental or security-related disadvantage. Either they have a high global warming potential (such as R134a and R410a), are flammable (such as R600a and 1234yf), are toxic (R-717) or must be operated at very high pressures such as CO_2 (>100 bar).

For these reasons, there is strong interest in the development of new efficient and environmentally friendly climate systems for automotive application. Promising candidates for enabling these systems are caloric materials.

2 Caloric Cycle

Cooling systems based on caloric materials have the potential to increase the systems efficiency compared to conventional compressor-based cooling technology by 30 % [1]. The principle is schematically shown in Fig. 1. Caloric materials heat up when exposed to an external field and cool down again as soon as the field is removed [2–4]. By cyclic operation with appropriate thermal coupling a cooling system can thereby be established.

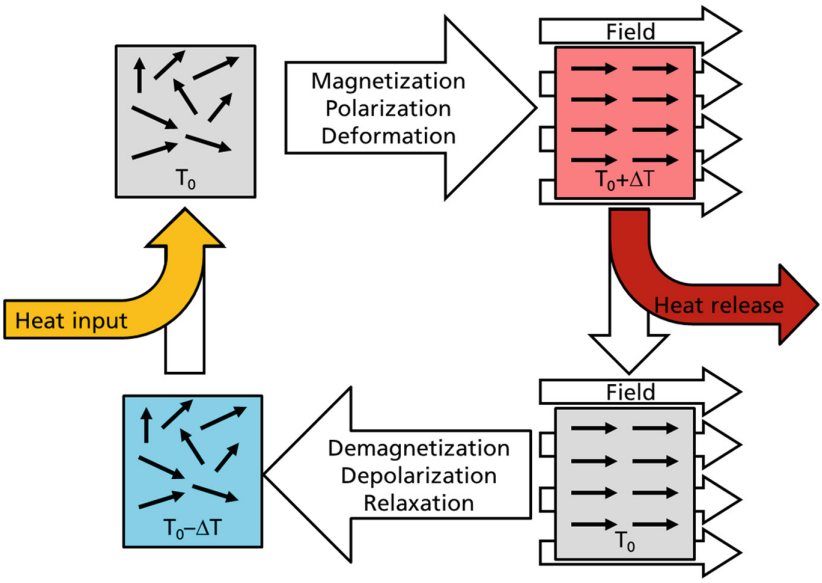

Fig. 1. Principle of caloric cooling

3 Magnetization/Polarization/Deformation

The caloric material is exposed to its respective field and heats up from temperature T_0 to $T_0 + \Delta T$.

4 Heat Release

The caloric material is connected to a heat sink, the heat produced can be dissipated, the caloric material cools down again to temperature T_0.

5 Demagnetization/Depolarization/Relaxation

If the field is removed, the caloric material cools down and is at a lower temperature $T_0 - \Delta T$ than it is at the start of the cycle.

6 Heat Input

The caloric material is now connected to the system to be cooled and can absorb heat, until it reaches temperature T_0 again.

7 Caloric Materials

The two important parameters describing the quality of caloric materials are the adiabatic temperature change ΔT and the isothermal heat change Q. The adiabatic temperature change indicates the temperature lift of the caloric material when it is exposed to an external field, while the isothermal heat is proportional to the amount of heat that is generated and that can be absorbed by the caloric material.

Figure 2 shows an overview of these two parameters for different caloric materials. It can be seen that the largest adiabatic temperature changes and isothermal heat can be generated by thin film electrocaloric materials (EC). Very good performance is also shown by elastocaloric materials (eC), especially from Ni-Ti-alloys. Magnetocaloric materials (MC) show moderate values, whereas bulk electrocaloric materials and barocaloric materials (BC) show the smallest effect.

Besides the provision of large adiabatic temperature changes and isothermal heat, several other parameters are important for caloric materials in order to fulfill requirements for caloric heat pumps:

- Adjustable Curie-Temperature
  The origin for the caloric effect of the materials is a phase-transition generated by the application of an external field. This phase-transition is associated with a temperature, the Curie-Temperature T_C. Around the vicinity of the Curie-Temperature the caloric effect is strongest. In order to be able to build a heat-pump capable of generating a temperature lift of several 10 K, it might be necessary to cascade several materials with different Curie-Temperatures in a system, depending on the size of the adiabatic temperature change. This in turn requires the Curie-Temperature to be adjustable for the caloric material.

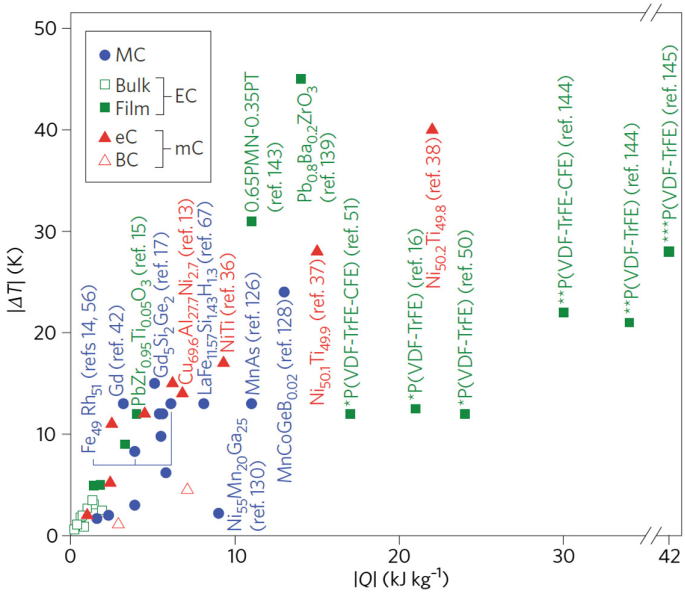

Fig. 2. Adiabatic temperature change and isothermal heat for different caloric materials, taken from [3]. MC: Magnetocaloric materials; EC: Electrocaloric materials; mC: Mechanocaloric materials; eC: Elastocaloric materials; BC: Barocaloric materials.

- Wide temperature range of caloric effect:
  In order to generate a certain temperature lift with the heat-pump, a certain amount of caloric materials must be cascaded, depending on the temperature range in which the caloric material shows the caloric effect. The larger this temperature range is, the fewer caloric materials with different Curie-Temperatures are required and the simpler the final system will be.
- Minimal dissipative losses
  For every caloric material which undergoes a caloric cycle, a certain amount of generated heat is not reversible, i.e. dissipative. These dissipative losses can occur due to internal friction or hysteresis losses. In order to be able to realize an efficient heat pump, these dissipative losses must be much smaller than the reversible caloric effect.
- Long-term stability
  The requirements on the lifetime of a heat pump are very demanding. A household refrigerator for example should run for at least ten years, usually even much longer. Assuming a cycle frequency of 10 Hz for the caloric cycle and a lifetime of 10 years, the caloric materials need to encounter more than $3 \cdot 10^9$ cycles, in which their performance should not significantly be altered.
- Abundance, economic feasibility and eco-friendliness
  In order to have a chance be economically competitive, the elements needed for the caloric materials as well as for the field source need to be abundant and the production must be affordable. At the same time the materials need to be ecologically harmless.

Table 1. (Incomplete) overview of the state of the art of the different properties of caloric materials: Adiabatic temperature change (ΔT), isothermal heat (ΔQ), adjustable range of Curie-Temperature (T_c), temperature range of caloric effect (TR), dissipative losses (DL), long term stability (Stab.), abundance, economic feasibility and eco-friendliness (AEE).

	ΔT [K]	ΔQ [kJ/(kg)]	T_c [K]	TR[K]	DL	Stab.	AEE
Electrocaloric – Film	10 – 40	1-40	?	?	?	?	+
Electrocaloric – Bulk	1 – 6	0.5-2	?	?	?	?	-
Magnetocaloric	3-10	3-10	200-400	~3	small	~10^6 cycles	0
Mechanocaloric	10 – 40	1-15	200-400	50	?	~10^7 cycles	+

In Table 1, a comparison of these different parameters for the different caloric materials is shown.

8 Caloric Systems

Most caloric cooling systems have been built using magnetocaloric materials. Worldwide several dozens of different prototypes have been built. A very good overview of these prototypes is given in Kitanovski et al. [1] and Yu et al. [5].

For elastocaloric materials, only a handful of prototypes have been published yet. The most advanced system has been built by Qian et al. [6, 7], generating a maximum temperature span of 25 K and maximum cooling power of 139 W at 10 K ΔT. Nevertheless in the last couple of years, interest in elastocaloric materials has strongly increased mainly due to the very large temperature spans which can be generated from one material only [8, 9].

For electrocalorics, up to now only a handful of systems been built and characterized [10, 11]. They achieve an unsatisfactory maximum temperature difference of only about 6.6 K. A major challenge when designing electrocaloric cooling systems results from the fact that good electrocaloric materials with large values of ΔT are only available in thin films, and therefore the need to implement an efficient heat transfer mechanism from the electrocaloric material to the heat sink and source, respectively. However, recently bulk electrocaloric materials exhibiting $\Delta T > 4$ K have been presented, opening the perspective to electrocaloric heat pumps with enhanced performances [12].

Table 2 shows a collection of the best prototypes for magnetocaloric cooling systems with respect for maximum cooling power and maximum temperature span respectively. The data show, that the systems reaching the largest maximum cooling power do not generate a large ΔT and vice versa. At the same time, hardly any COP-values have been reported, and no caloric system was so far able to attain performance values that conventional compressor systems reach.

The main reason for this is based on the challenge to cyclically couple the caloric material to heat sink and source. For efficient caloric heat pumps this coupling should be very fast and at the same time have a very small thermal resistance. Currently, for

Table 2. Collection of best prototypes for magnetocaloric cooling systems with respect for maximum cooling power and maximum temperature span respectively. Table taken from Langebach et al. [13].

Demonstrator	Max. cooling power	Mass of material	Max. temperature span
Max. cooling Power			
Okamura et al. (2007)	**540 W**	4000 g	8 K
Engelbrecht et al. (2012)	**1010 W**	2800 g	19 K
Jacobs et al. (2013)	**3042 W**	1520 g	20 K
Max. temperature span			
Arnold et al. (2011)	31 W	136 g	**30 K**
Arnold et al. (2013)	96 W	650 g	**33 K**
Arnold et al. (2011)	42 W	170 g	**42 K**

most prototypes this is done using the active regenerator concept (Fig. 3). Here a heat transfer fluid is actively pumped through a magnetocaloric regenerator (porous structure of magnetocaloric material). When the magnet has magnetized the material, the heat transfer fluid is heated by the material and thereby transfers the thermal energy to a heat sink. After turning off the magnetic field by shifting the magnet, the heat transfer fluid is pumped in the opposite direction through the magnetocaloric regenerator and is cooled down. Now it can pick up thermal energy from the heat source and the cycle can start again from the beginning.

Conceptually, the larger the magnetocaloric regenerator, the larger the potential maximum temperature lift. At the same time, in order to increase the pumping power of the heat pump, the operation frequency must be increased [1]. However, both factors, an increase in regenerator length and an increase in cycle frequency also increase the friction of the heat transfer fluid in the magnetocaloric regenerator. Therefore, it is extremely difficult to realize a caloric heat pump based on the AMR-concept which has a high temperature lift, a large cooling power and COP at the same time. This is also reflected by the fact that currently many research groups are working on the

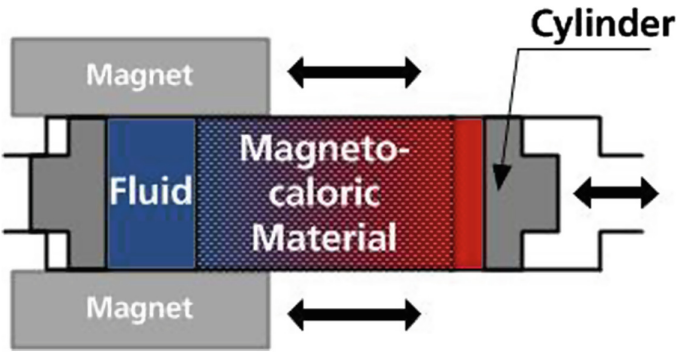

Fig. 3. Sketch of the active magnetic regeneration (AMR) concept.

optimization of the magnetocaloric regenerator in order to enhance thermal transfer and thereby reduce internal friction.

9 Alternative System Approach

In order to account for these challenges, an alternate system approach based on thermal diodes and latent heat transfer, the active magnetocaloric heat pipe (AMH), see Figs. 4 and 5.

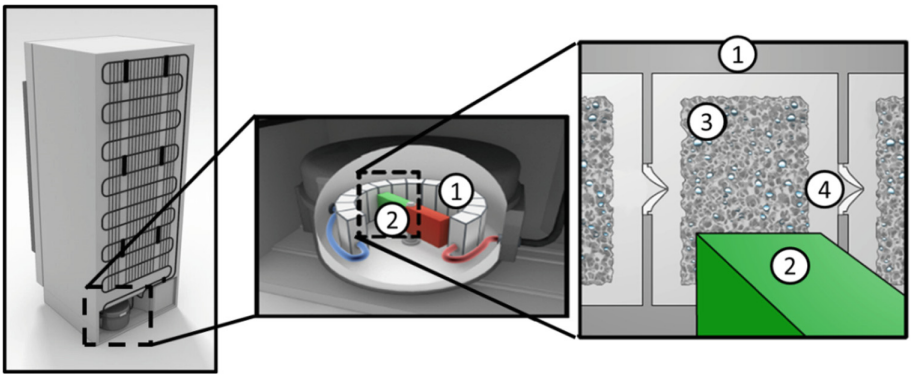

Fig. 4. Conceptual sketch of active magnetocaloric heat pipe (AMH). Left: magnetocaloric cooling unit replaces compressor in refrigerator. Middle: magnetocaloric cooling unit consisting of magnetocaloric segments and magnetic system (2). Right: magnetocaloric segments consisting of magnetocaloric heat exchanger (3) and pressure relief valve (4).

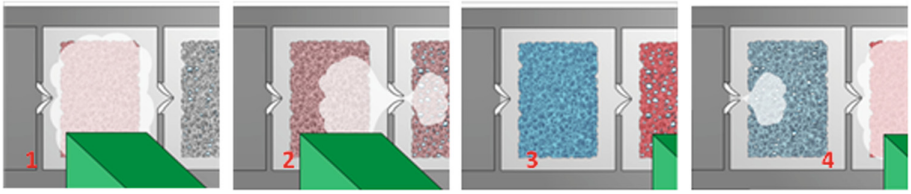

Fig. 5. Operational mode of magnetocaloric segments. The heat is » driven forward « in only one direction according to the principle of a thermal diode: The heat generated by the magnetic field causes the fluid in the MC material to evaporate (1), increasing the pressure in the segment. The pressure relief valve opens, allowing the vapor to flow into the adjoining element (2). Note that due to the unidirectional flow direction of the valves, the vapor cannot flow back into the previous element. Once the magnet has been switched off (by moving the magnet away from the segment), the MC material cools down below the starting temperature (3) and the vapor pressure drops. The vapor pressure is now lower than in the previous segment. Gaseous fluid flows in and heat from the previous segment is absorbed (4).

This concept for heat transfer facilitates passive heat transfer through the evaporation and condensation of a fluid in a hermetically sealed volume [14, 15]. The whole system is efficient and fast: By evaporating a fluid such as water or ethanol at the heat source and subsequently condensing it at the heat sink, it is possible to achieve heat transfer coefficients that are several orders of magnitude higher than those achieved in traditional heat transfer by means of thermal conduction or convection. Simulations have shown that transporting thermal energy from one caloric segment of only a few centimeters in size to the next occurs in a matter of milliseconds, making it fundamentally possible to establish cooling cycles with a frequency of more than 10 Hz.

The main advantages of this AMH-concept are the following:

- **Increase in systems efficiency:** For the transfer of the thermal energy from the magnetocaloric material to the heat exchanger, no additional pumps and therefore no additional energy is required, which increases the systems efficiency.
- **Larger cooling power**: Heat transfer based on latent heat is several orders of magnitude larger than heat transfer using sensible heat by pumping of fluids. This opens the possibility to realize magnetocaloric systems being capable of system frequencies >10 Hz, which results in an increase of cooling power.
- **Reduced system costs**: Due to an increase in the system frequency, the amount of magnetic as well as magnetocaloric material required to produce a specific cooling power can be significantly reduced, which in turn reduces the perspective costs of a magnetocaloric cooling system.

10 Conclusion

Efficient, refrigerant-free heat pumps based on the caloric materials have the potential to revolutionize cooling technology. A promising a new concept for caloric cooling systems based on latent heat transfer and thermal diodes has been presented making caloric cooling system with greatly enhanced COP feasible.

References

1. Kitanovski, A., Tušek, J., Tomc, U., Plaznik, U., Ozbolt, M., Poredoš, A.: Magnetocaloric Energy Conversion (2015)
2. Gschneidner Jr., K.A., Pecharsky, V.K.: International Journal of Refrigeration-Revue Internationale Du Froid **31**, 945 (2008)
3. Moya, X., Kar-Narayan, S., Mathur, N.D.: Nat. Mater. **13**, 439 (2014)
4. Pecharsky, V.K., Gschneidner, K.A.: J. Magn. Magn. Mater. **200**, 44 (1999)
5. Yu, B., Liu, M., Egolf, P.W., Kitanovski, A.: International Journal of Refrigeration-Revue Internationale Du Froid **33**, 1029 (2010)
6. Qian, S., Geng, Y., Wang, Y., Muehlbauer, J., Ling, J., Hwang, Y., Radermacher, R., Takeuchi, I.: Sci. Technol. Built Environ. (2016)
7. Takeuchi, I., Sandeman, K.: Phys. Today **68**, 48 (2015)

8. Ossmer, H., Miyazaki, S., Kohl, M.: 2015 Transducers-2015 18th International Conference on Solid-State Sensors, Actuators and Microsystems (TRANSDUCERS), p. 726. IEEE (2015)
9. Schmidt, M., Schuetze, A., Seelecke, S.: International Journal of Refrigeration-Revue Internationale Du Froid **54**, 88 (2015)
10. Jia, Y., Ju, Y.S.: Appl. Phys. Lett. **100**, 242901 (2012)
11. Sinyavsky, Y., Brodyansky, V.: Ferroelectrics **131**, 321 (1992)
12. Qian, X.S., Ye, H.J., Zhang, Y.T., Gu, H., Li, X., Randall, C., Zhang, Q.: Adv. Funct. Mater. **24**, 1300 (2014)
13. Langebach, R., Klaus, M., Haberstroh, C., Hesse, U. (2014)
14. Koenig, J., Bartholome, K. (2015)
15. Bartholome, K., Horzella, J., Mahlke, A., Koenig, J., Vergez, M. (2015)

Author Index

C. Junior et al. (eds.), *Energy and Thermal Management, Air Conditioning, Waste Heat Recovery*,
DOI 10.1007/978-3-319-47196-9